FIELD SIMULATION OF WASTE IMPOUNDMENT SEEPAGE IN THE VADOSE ZONE: GEOLOGIC AND HYDRAULIC CHARACTERIZATION OF A HETEROGENEOUS VADOSE ZONE WITH RESPECT TO FLUID TRANSPORT

by

Paula Arnet

Submitted in partial fulfillment of

the requirements for the degree of

Master of Science in Hydrology

New Mexico Institute of Mining and Technology

Socorro, New Mexico

August, 1991

Abstract

Geologic and hydraulic controls on fluid transport in a heterogeneous vadose zone were investigated on a densely instrumented field plot in central New Mexico. The 30-m by 30-m plot was located two miles west of the present day Rio Grande near the New Mexico Tech golf course, in Socorro, NM. The plot was situated on five meter thick heterogeneous alluvial fan sequence which was found to be underlain by a more homogeneous ancestral Rio Grande fluvial sand.

The hydrogeologic investigation consisted of five separate studies and concentrated on vertically characterizing the two geologic units: 1. Soil cores from 30 boreholes drilled to various depths up to 20-m deep were sampled for particle size distribution and moisture content. The results were analyzed using geostatistical techniques with a one meter vertical correlation being found within the Rio Grande fluvial sands. 2. Saturated hydraulic conductivity was investigated in the vertical direction within the Rio Grande sands employing shelby tube permeameters with hydraulic conductivity being found to be correlated with dominant grain size. 3. A disc permeameter was used to find saturated hydraulic conductivity within the individual alluvial fan beds with correlation also being found between dominant grain size and hydraulic conductivity. 4. Mapping and photography were employed to accurately complete the study of the plot. Two trenches of depths 1.5 and 5 m were excavated, mapped, and photographed to present a 2-D view of the geology beneath the plot. Detailed cross-sections of the trench walls were constructed. 5. 100 cc cores were extracted from vertically continuous shelby tubes and analyzed for hydraulic conductivity, porosity, saturated water content, bulk density, and d_{10} size. A vertical correlation length of one to two meters was found in the d_{10} size and saturated water content, which correlated with the average thickness of the Rio Grande beds.

The geologic investigation was divided into three scales. The large scale investigation concentrated on the depositional history as related to the geologic units found beneath the plot. The intermediate scale investigation focused on the formation of alluvial fans as related to the seven very distinct alluvial fan beds found in the top five meters of the site. The small scale investigation concentrated on a detailed geologic characterization of the plot. The site stratigraphy was composed of a fairly heterogeneous set of seven alluvial fan or piedmont slope units to a depth of 4 m. A mostly homogeneous ancestral Rio Grande sand facies extended from 4 m to at least 20 m. Borehole samples were used to create stratigraphic cross-sections based on the USCS soil classification system. The two trenches mentioned above were used to characterize the alluvial fan beds in detail.

Finally, the drainage results from a previous infiltration experiment were compared with the geology found at the instrumentation stations. Barriers to vertical unsaturated flow were attributed to changing grain size distributions. These changes contributed to lateral flow. Additional factors leading to lateral flow were the natural dip in the beds and differences in initial moisture content within each bed. Inadequacies and adequacies in terms of the amount of data needed to be collected were evaluated for this site characterization.

TABLE OF CONTENTS

List of Figures

List of Tables

Acknowledgements

This study was funded by the United States Geological Survey and the New Mexico Water Resources Research Institute under USGS award No. 14-08-0001-1G. I am the seventh master's student to earn a degree on this project.

I am grateful to my advisor, Dr. Robert S. Bowman, and to Dr. Daniel B. Stephens for their guidance and support during my time at the New Mexico Institute of Mining and Technology.

Many thanks are due my fellow graduate students working on the project; Ann Stark and Rolf Schmidt-Petersen. Their guidance, help, and support in the field, in the lab, and in the office are appreciated. I thank Dr. John Hawley for his guidance in "trench characterization" and for his expertise in New Mexico geology. I am grateful to Mike Stephens, Meiko Haushalter, and Nikki West, the student workers that provided many hours of field work, lab work, and data entry support. Special thanks go to Ruth Lohmann, Matt Davis, and other "hydros" for their friendship and for making my time in Socorro bearable and enjoyable.

I am grateful to the love and support that my parents have provided me through the years. Special thanks are extended to Bill for his love, patience, and belief in me during the last two years.

1. INTRODUCTION

1.1 PROJECT PURPOSE AND BACKGROUND

A long standing environmental problem encountered in the semi-arid regions of the western United States and many other parts of the world involves the understanding of the factors that govern the hydraulic transmission of leachate and liquid wastes through the unsaturated zone down to the water table. The Basin and Range of the western United States is a geologic environment composed of large sediment-filled valleys bounded by mountain ranges. Factories, mines, and dump sites are often located in these valleys or at the foot of such a mountain front. Surface impoundments such as evaporation ponds and mill tailings impoundments are often used for the disposal of liquid wastes at these sites. Until recently, most impoundments were unlined, allowing leachate to move through the vadose zone and possibly toward the water table. Current federal regulations require operators to show there will be no seepage discharge impacting aquifers from such impoundments. The current alternatives for inhibiting seepage are clay or synthetic liners and/or caps which prevent infiltration. As a result, any seepage that occurs through anticipated leakage through the liner or unexpected leaks in the liner is transported through porous material that is only partially saturated (before possibly reaching the water table).

It is understood that fluid transport is mostly dependent on the properties of the porous medium that the fluid is travelling through, such as particle size, shape, structure such

as layering, degree of compaction, and grain size distribution. For example, it has been found that permeability values increase when the median grain size diameter increases (Masch and Denny, 1966). Two related issues that need to be addressed when studying fluid flow through the unsaturated zone are; the nature of geologic structure such as how the position of different layers of material with respect to each other guide or inhibit fluid flow, and the nature of heterogeneity in geologic materials and their hydraulic properties for the purposes of predicting fluid flow characteristics. Simulation of hydraulic and geologic spatial variability has been investigated by many parties such as Byers and Stephens (1983).

In semi-arid regions the water table is often quite deep therefore causing vadose zone processes to play an important role in potential soil or groundwater contamination. Since the vadose zone often consists of stratified, partially saturated geologic materials, its hydraulic properties (Larson and Stephens, 1985) and its inherent spatial variability (Yeh and Gelhar, 1983) are difficult to characterize.

Predicting hydrologic properties from routinely measured textural and structural soil properties (ie Arya and Paris, 1981) and predicting fluid flow through layered or stratified porous media (ie McWhorter and Nelson, 1979) have been the focus of many studies. Even though it may now be possible to estimate soil water characteristics from textural and structural information, recent theories, along with field and laboratory evidence, suggest that spatial heterogeneity in hydraulic properties causes infiltration to

follow multidimensional pathways (as opposed to the many vertical one-dimensional flow models being used to model flow) through the unsaturated zone. Most studies though, have not focused on the nature of the geologic environment at hand and how its structural and textural makeup controls the direction and nature of drainage through this environment.

Multi-dimensional flow can be enhanced by anisotropy. This is supported by field studies (McCord and Stephens, 1987) where results indicate a strong lateral flow component in vadose water flow paths in the absence of apparent layers. They proposed that lateral flow is likely due to moisture dependent heterogeneity in the hydraulic conductivity. Theoretically, lateral spreading is enhanced where seepage occurs into dry material (Mualem, 1984), as seen in the laboratory by Stephens and Heerman (1988). Palmquist and Johnson (1962) conclude that pits for the disposal of nuclear waste can be operated more safely where the underlying granular materials are highly stratified and have different grain sizes. These results apply chiefly to arid regions where the deposits above the water table contain very little moisture to great depths, and to disposal pits in which the distance across the pit surface is only a few tens of feet. Other investigations which indicate the presence of significant lateral flow in the vadose zone are described by Johnson et al. (1981), Miller and Gardner (1962), and Traitwein and Daniel (1983).

Hillel (1980a) and Parsons (1988) review theory of vertical moisture movement in stratified soil. A current study (Stark, personal communication, 1991) reviews the theory

for and analyzes the drainage phase. The results presented by Stark (personal communication, 1991) are discussed in Chapter 4 of the current study. Hillel (1980) discusses the effects of internal drainage and redistribution following infiltration and Warrick and Nielsen (1980) discuss the spatial variability of soil physical properties in the field.

The purpose of this study was to find out what role the geologic framework of a vadose zone research plot has in controlling the flow of water from near the surface. The goal was achieved by characterizing the hydraulic properties of the materials that the water was flowing through, by characterizing the geologic framework, and by correlating the geologic information with drainage results from the plot. The results of the study add to the knowledge already available on unsaturated flow and are beneficial in the quest for prediction of water flow through unsaturated layered porous media.

In this study the importance lies in the heterogeneity of the stratification of the local Basin and Range valley fill material that the fluid is draining through and its role in controlling the pathways of flow. Stratification inhibits the downward movement of seepage. For example, in a fine over coarse layered system, water infiltrating into the fine layer will be impeded at the fine-coarse interface until the water pressure exceeds the critical value needed for flow through the coarse pores. As a result, laboratory studies such as those conducted by Miller and Gardner (1962) and Stephens and Heerman (1988) show significant horizontal flow along layers under unsaturated conditions. Most

studies have not tackled the problem of drainage through a multi-layered system, with each layer having different textural, structural, and hydraulic properties.

1.2 FIELD EXPERIMENT

In January 1987, a long range vadose zone experiment was started on the campus of the New Mexico Institute of Mining and Technology in Socorro, New Mexico, approximately 120 km south of Albuquerque. The experiment simulated leachate seepage from a lined impoundment into the unsaturated zone using a lined drip irrigation system. Site characterization began in the summer of 1986 and analysis is being completed during the summer of 1991.

The experimental site is located two miles west of the present day Rio Grande; just west of the New Mexico Tech golf course in an east-west trending arroyo that has been diverted to the north to prevent flooding. The geology beneath the site consists of two facies; a highly stratified alluvial fan or piedmont slope facies overlying a fairly homogeneous ancestral Rio Grande fluvial facies. The field site was not irrigated prior to the 1987 infiltration experiment, though the adjacent golf course is irrigated throughout the year. The water table is at approximately 21 m depth.

This is the final report to be presented concerning this field experiment. Six earlier reports describe related activities and are in part the basis for this study. Parsons (1988)

describes preliminary characterization of the geologic and hydraulic properties of the site using data from instrumentation borings and applies a one-dimensional analytical model to the observed moisture infiltration at the site. Mattson (1989) describes the site design and construction along with a two-dimensional analytical model simulating movement of infiltrating water. Flannigan (1989) and Grabka (1991) discuss solute transport experiments conducted at the site. Schmidt-Petersen (1991) investigates heterogeneity in hydraulic properties in the horizontal direction within the alluvial fan facies, primarily with the disc permeameter. In a current study (A. Stark, personal communication, 1991) there is analysis of a blue food dye tracer experiment, the nature of moisture content profiles during the drainage phase beneath the irrigated plot, and the nature of hydraulic conductivity during the infiltration phase. A. Stark (personal communication, 1991) also analyzes the drainage phase beneath the irrigated plot using the instantaneous profile method.

The following is a description of the site and a summary of the work performed during the field experiment:

The site was located on level ground in the northeast corner of New Mexico Tech's Physical Plant storage yard as shown in Figure 1-1. A 30 m x 30 m area was cleared to expose bare soil, (eliminate transpiration) and local runoff onto the site was eliminated by construction of a berm on the eastern and southern edges of the site. Mattson (1989) surveyed a 5 meter grid on top of the 30 m x 30 m area with $X=0, Y=0$ originating in

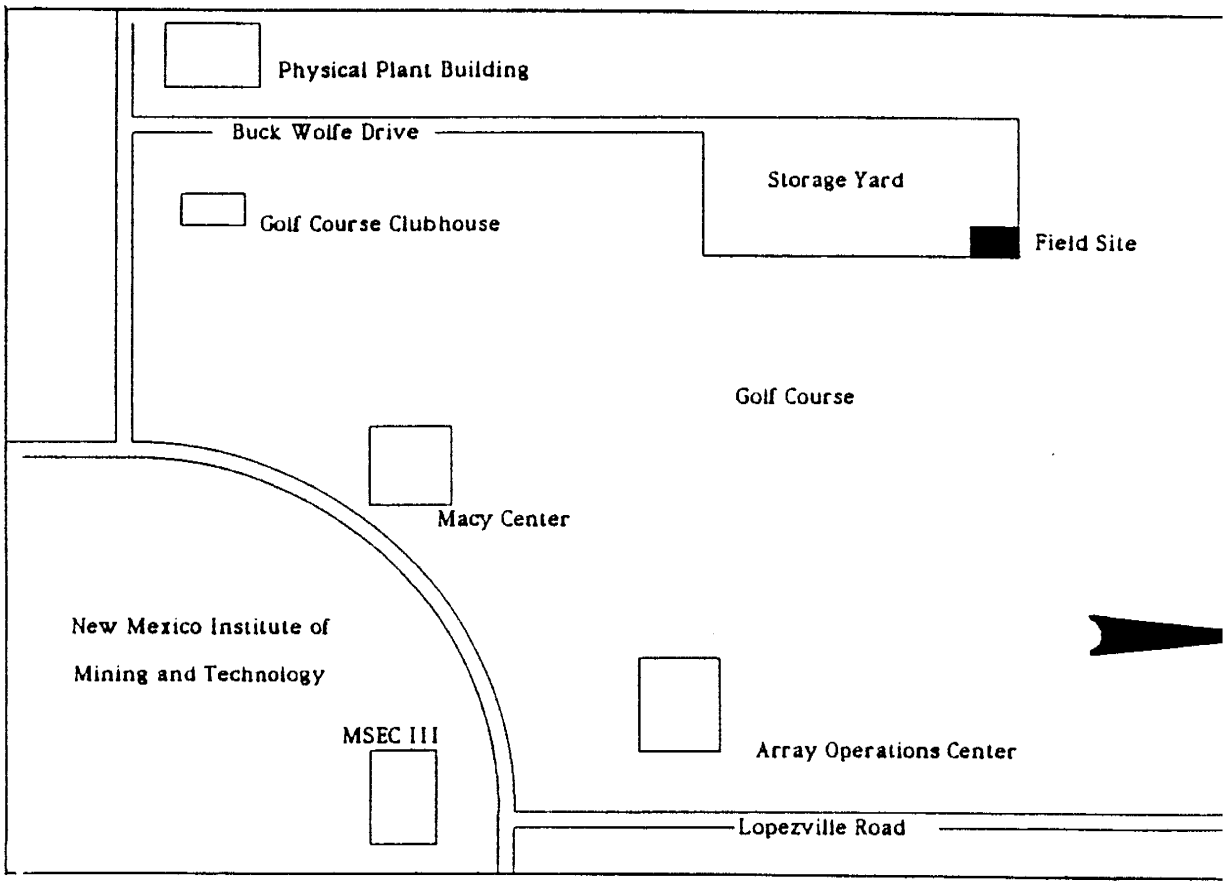

Figure 1-1 Site location map (after Flannigan, 1989).

the southwestern corner of the plot along with a datum as a horizontal line located 86 cm above the driplines (described below). The datum was at 1417.45 m above sea level and is delineated by depth = 0 on all of the stratigraphic sections and cross-sections shown in Chapters 2-4. An inside 10.5 m x 10.5 m area was prepared for the irrigation equipment. A trailer was placed south of the field site to serve as a field office and to house field equipment. Figure 1-2 shows the overall site design.

The site was equipped with a drip irrigation system for water application. Figure 1-3 shows the layout of the drip irrigation system with 21 drip lines (polyethylene, Model No. 164, Agrifirm Irrigation Inc., Fresno, CA); each with emitters spaced 50 cm apart. Hay and plastic were placed on top of the driplines to limit evaporation and to serve as insulation. A 1 cm thick layer of fine sand was placed below the emitters to ease infiltration. Fill was placed on top of this setup to just above ground surface and then covered with another plastic liner and a thin layer of soil at the surface.

Water was applied by means of a positive displacement pump (Model No. 5-BBV, Sherwood, Detroit, MI). Beginning in January 1987 water was applied at a flux rate of 1.0×10^{-5} cm/sec and in May 1989 the rate was increased by an order of magnitude. It is believed that the increased flux resulted in saturated conditions in some areas below the plot.

Parsons (1988) describes the construction of the 21 monitoring stations located on the

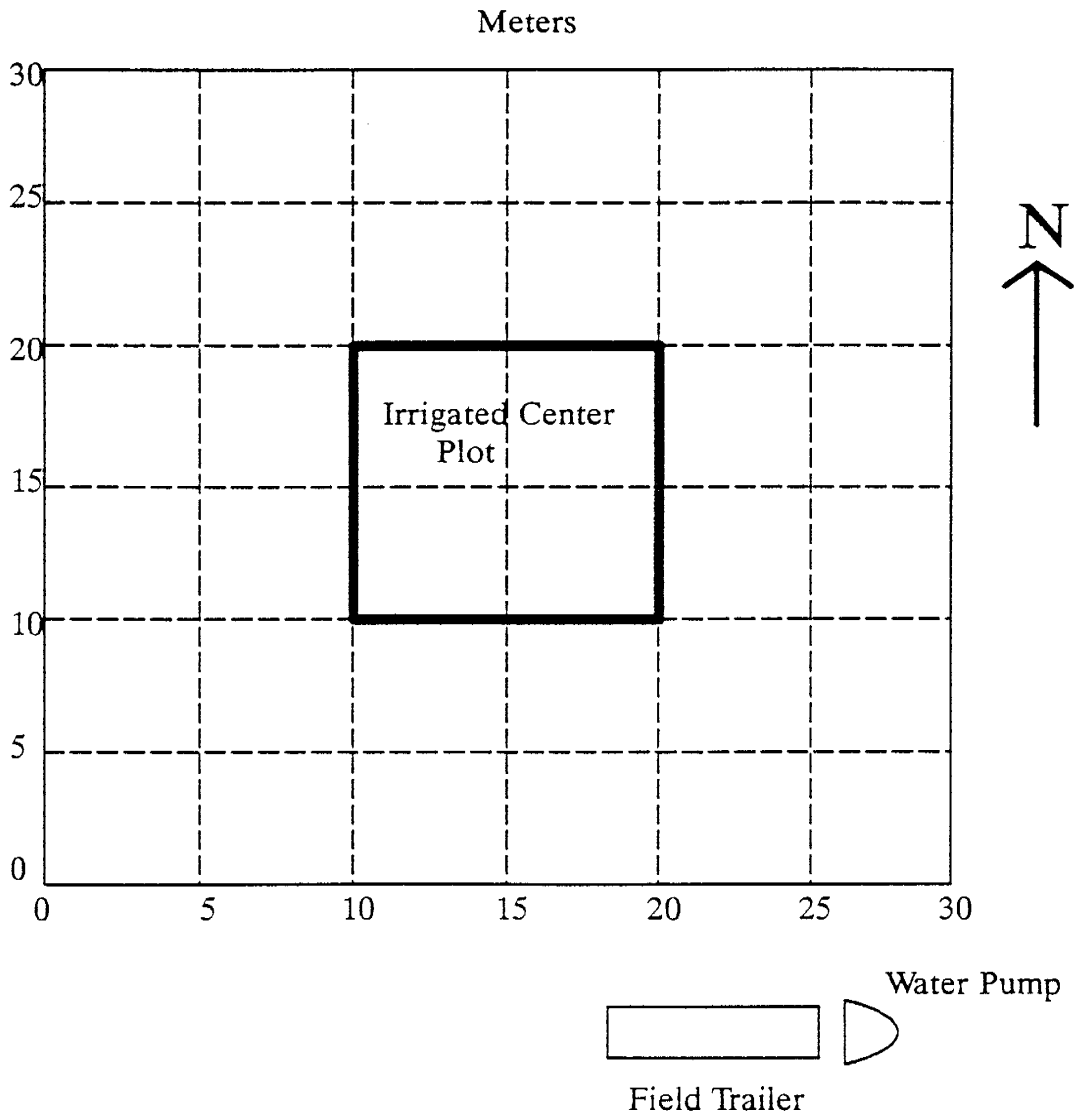

Figure 1-2 Site layout.

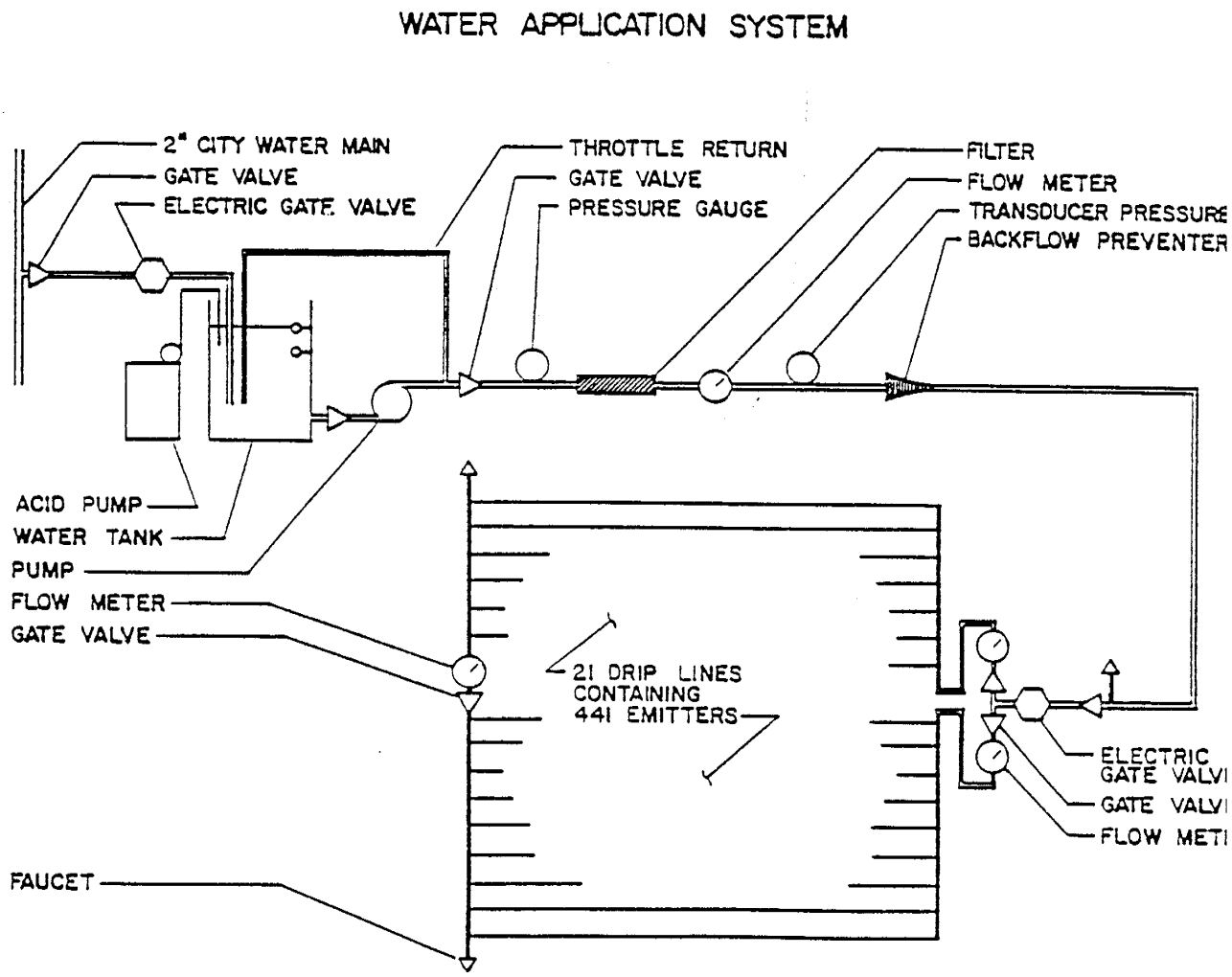

Figure 1-3 Water application system (after Mattson, 1989).

plot. They are identified by their location on the X-Y grid system. Each monitoring station consisted of a pair of tensiometer nests surrounding a neutron access tube. Infiltration and drainage were monitored using these stations. The tensiometers ranged in depth from one to five m below the site datum while neutron access tubes were up to eight meters deep. A neutron moisture probe (Model No. 503DR, CPN Corp., Martinez, CA) was used to monitor the moisture movement with depth and pressure heads were measured in multidepth tensiometer nests. A pressure transducer (Tensiometer, Soil Measurement Systems, Tucson, AZ) connected to a hypodermic needle was used to measure the pressure head through a rubber septum at the top of each tensiometer. Figure 1-4 shows such a monitoring station set up. The current study being performed (by A. Stark personal communication, 1991) describes this setup in greater detail.

Solute transport data was collected for two tracer test studies. Prior to a bromide tracer test (Flannigan, 1989) in the spring of 1988, 14 porous cup samplers or suction lysimeters were installed. Four samplers were located about six meters below and about six meters from each side of the irrigated plot. Ten other samplers were installed at various depths and locations throughout the irrigated plot. An additional 55 samplers were installed for a more involved tracer test that took place during the summer of 1989 (Grabka, 1991). Figure 1-5 shows the location of the samplers.

Subsequent to the tracer tests, a drilling project was undertaken during which the additional samplers were installed and three monitoring wells and 27 porous cup samplers

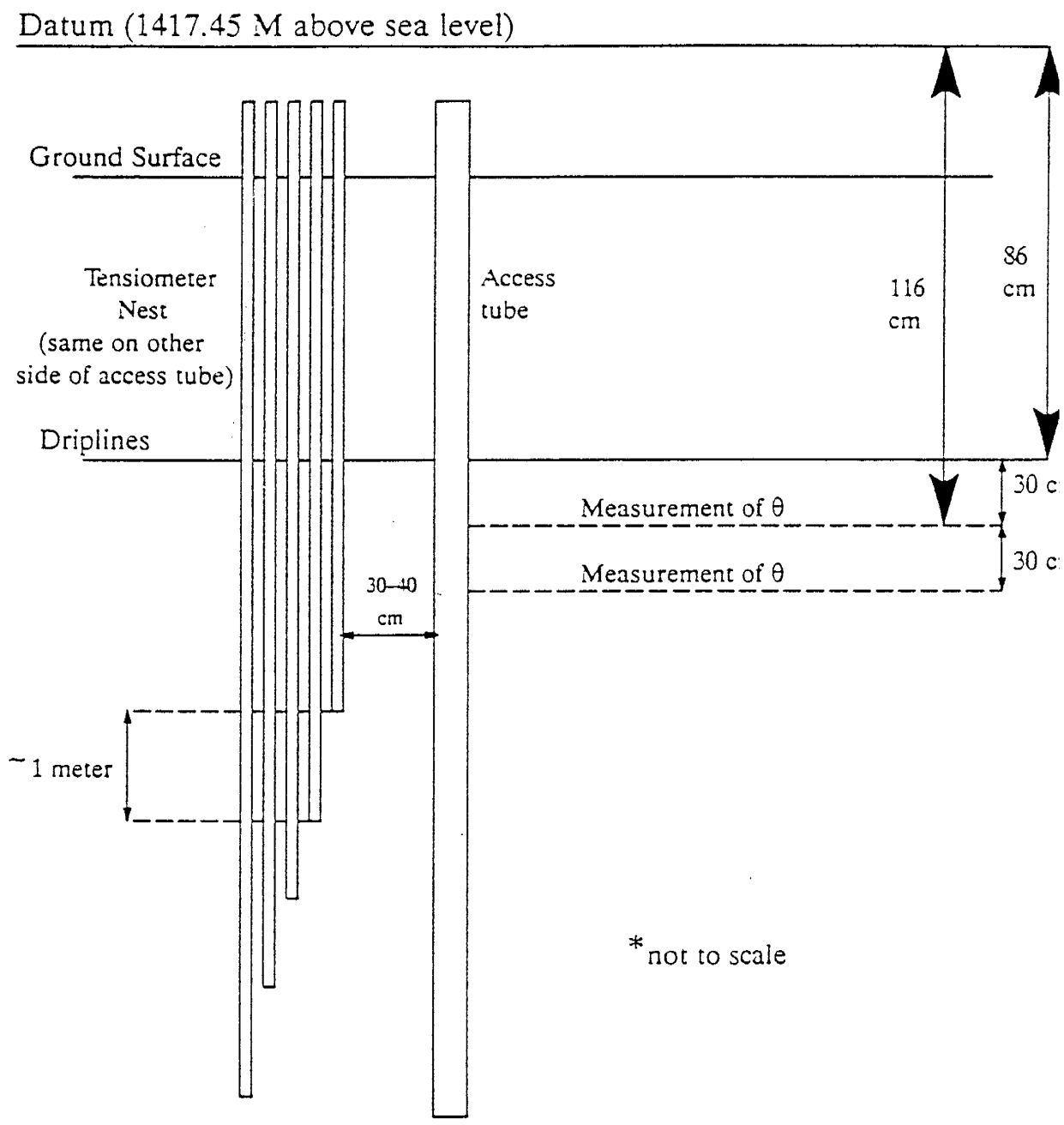

Figure 1-4 Schematic of a monitoring station (after A. Stark, 1991).

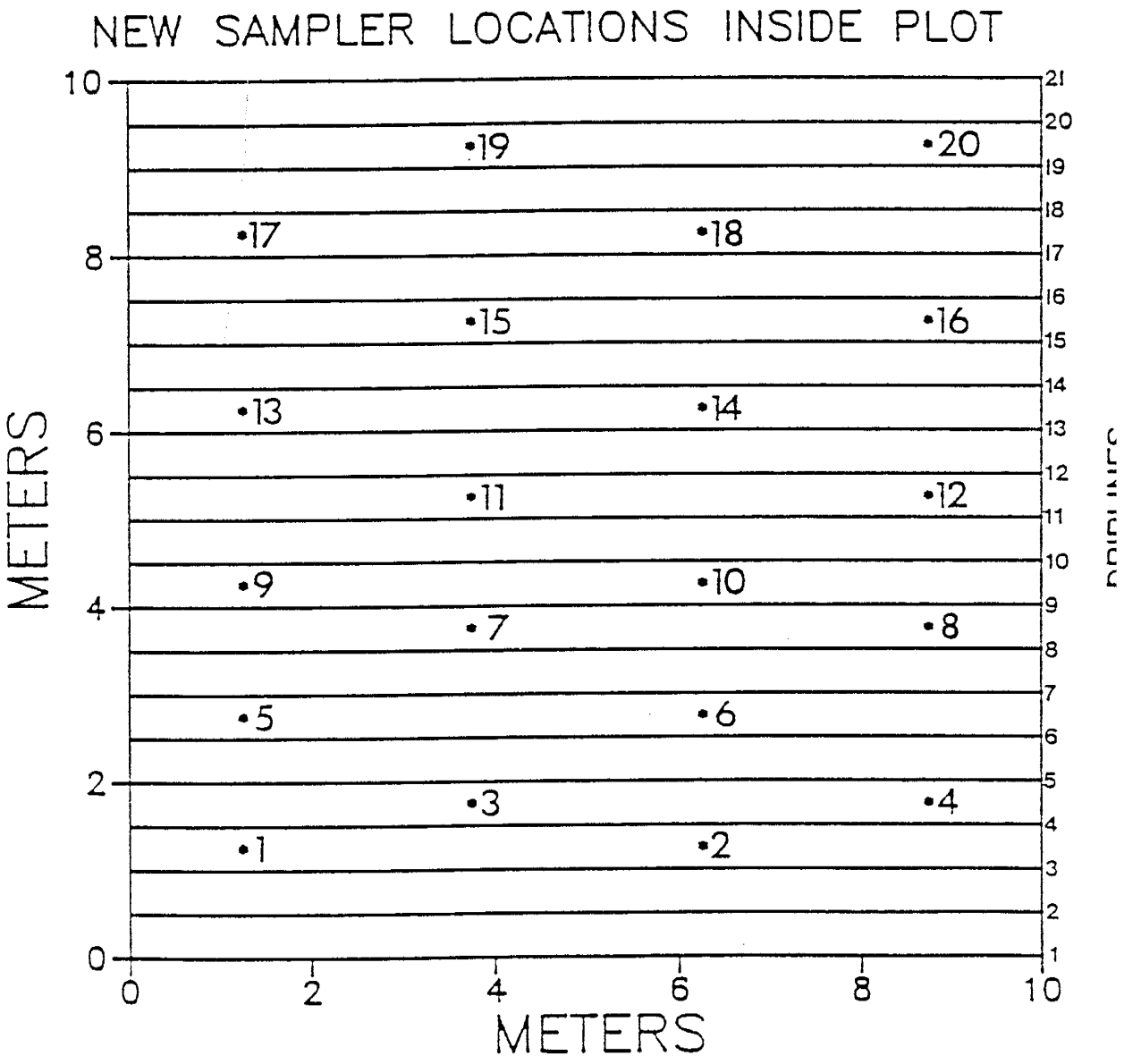

Figure 1-5 Porous cup sampler locations (after Grabka, 1991).

were installed. The shelby tube cores and split spoon samples collected during this drilling operation were analyzed for the current study. Figure 1-6 shows the well locations.

Total site instrumentation consisted of 21 neutron access tubes, 84 porous cup samplers, and 270 tensiometers. A computerized data logger (Model No. CR7, Campbell Scientific, Inc., Logan, UT) located in the field trailer, recorded precipitation, windspeed, temperature of the soil, tank water and air, barometric pressure, and humidity. Evaporation was measured weekly in a standard Class A pan located on the field site.

Irrigation ceased in September 1989 and drainage was monitored through June 1990. Blue dye was injected into the southern quarter of the irrigated plot for a period of five days just before the infiltration was discontinued. Analysis of this data and excavation of the dyed flow paths will be described by A. Stark (personal communication, 1991).

Several trenches were excavated subsequent to the cessation of infiltration. These trenches are shown in Figure 1-7. A 1.5 meter deep shallow trench was completed across the site from SE to NW in January 1990. A disc permeameter study along the floor of this trench is discussed by Schmidt-Petersen (1991) and the geology of this trench is discussed in the current study. A second five meter deep trench was completed in February 1990 across the northeast corner of the site. This trench was used to complete our understanding of the alluvial fan facies as part of the present study. A third 2.5 meter

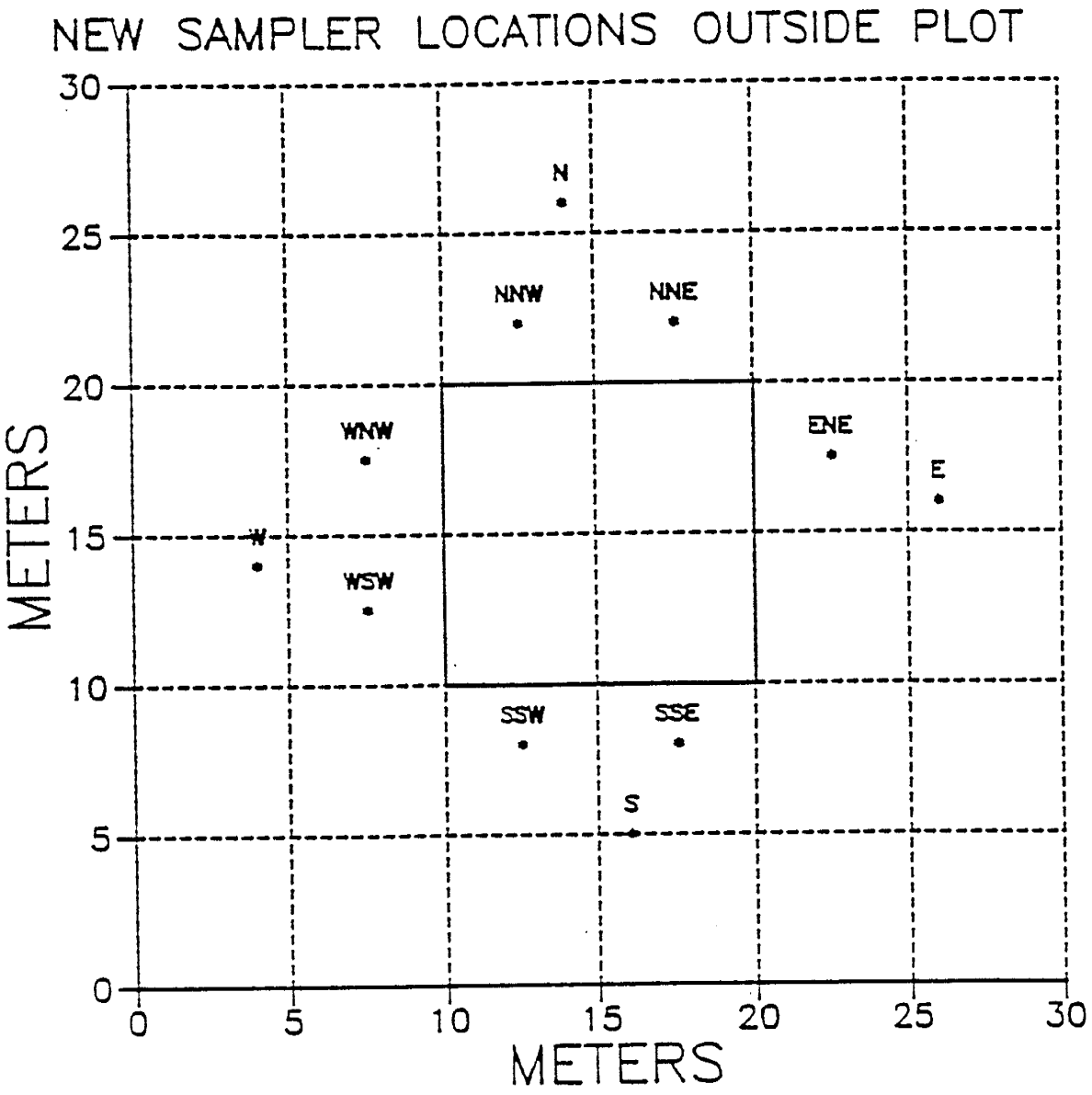

Figure 1-6 Wells and outer instrumentation stations (after Grabka, 1991).

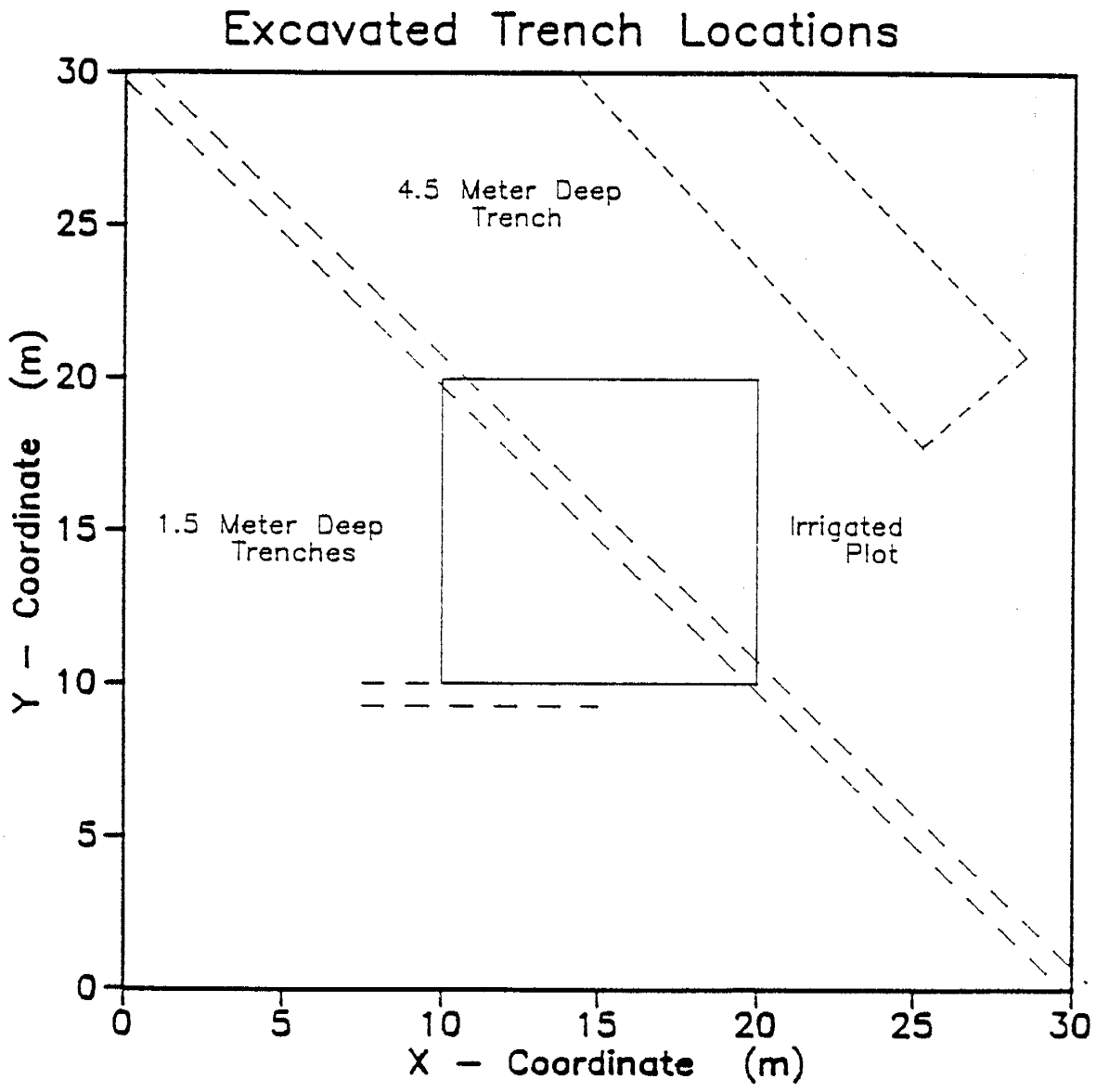

Figure 1-7 Trench locations (after A. Stark, 1991).

deep trench was excavated in the vicinity of sampler nest 12-12 to examine the relationship, if any, between dyed flow paths and instrumentation. Some piping of dye around the instrumentation was observed by A. Stark (personal communication, 1991). Laboratory studies and drainage analysis continued throughout 1989 and 1990 as part of the current study and are discussed by Schmidt-Petersen (1991) and A. Stark (personal communication, 1991), respectively.

1.3 STATEMENT OF OBJECTIVES

The objectives of the present study were to:

* Characterize the nature of vertical heterogeneity within the alluvial fan facies and the fluvial sand facies beneath the site,
* Characterize the geology beneath the plot, and
* Interpret fluid transport study results using new geologic and hydrologic knowledge.

1.4 APPROACH

In order to achieve the above objectives, studies were conducted in the field and in the laboratory. Five different studies were conducted to characterize the nature of vertical

heterogeneity beneath the plot. Particle size distribution and gravimetric moisture content were measured on split spoon samples collected from all boreholes drilled at the site, and they were also measured on samples taken at the deep trench disc permeameter locations. Saturated hydraulic conductivity (Ksat) was measured in the laboratory using continuous shelby tubes from a 20 meter deep well boring. Ksat was also measured in the alluvial fan units using a disc permeameter. Mapping and photography were employed to aid in the geologic characterization of the field site. Hydraulic properties of the fluvial sand facies were measured in the laboratory using 100 cc ring samples collected from the shelby tubes.

The geologic characterization was performed on three scales. First, the depositional history of the middle Rio Grande valley was described; second, the alluvial fan environment was studied with respect to the geology found at the site; and third, the specific small scale geology of the site was studied. The geology was studied by mapping the walls of two trenches dug across the site and by using borehole samples to create stratigraphic logs and cross-sections.

Finally, the drainage information provided by A. Stark (personal communication, 1991) was analyzed with respect to the hydrologic and geologic knowledge gained in the present study. In addition the issue of how much data is really needed for such a study is addressed.

This chapter has presented the introduction to the current study with a review of applicable theory, previous work performed on this project and a statement of current objectives. Chapter 2 discusses the hydrogeologic data collected for the purpose of characterizing vertical heterogeneity beneath the plot. The geologic characterization is described in Chapter 3. Chapter 4 includes the discussion, a presentation of the interpretation of drainage with respect to the established geologic framework and new hydrologic information on the site. Chapter 5 includes the summary and conclusions and Chapter 6 describes recommendations for future work.

2.0 HYDROGEOLOGIC DATA

To be able to understand the nature of flow through a layered section we need to understand the distribution of hydraulic properties through the section and those hydraulic differences between each of the layers that control the flow of water through them. To obtain these objectives there is a discussion of geostatistical methods used for analysis in Section 2.1. The following discussions concerning analyses of particle size distribution, gravimetric moisture content, hydraulic conductivity, mapping, photography, bulk density, porosity, and saturated water content are discussed in Sections 2.2 through 2.6. In Sections 2.2, 2.4, and 2.5 the alluvial fan facies and the fluvial Rio Grande facies are separately characterized. In Sections 2.3 and 2.6 the Rio Grande facies is characterized alone. In Sections 2.2, 2.3 and 2.6 stratigraphic sections are shown superposed with profiles of various hydraulic properties.

2.1 GEOSTATISTICAL METHODS

At this point it is necessary to briefly review spatial variability theory and background. It has been found that representative values of hydraulic and geologic parameters are necessary for both characterizing a field plot such as this and for predicting fluid flow through such a plot. Both Sections 2.2 and 2.6 present results of hydraulic and geologic parameters and their corresponding geostatistical analyses.

Many studies have used geostatistical analyses for the characterization of the spatial variability of hydraulic and geologic soil properties (see e.g. Greenholtz et al., 1988). Correlation lengths and frequency distributions have been found to be important in soil property characterization in many studies. Variogram analyses and autocorrelation functions have been used to find patterns or structures within a vertical soil profile or along a horizontal transect.

Andrews (1982) found hydraulic conductivity to be log normally distributed within a fluvial sand in central New Mexico, confirming a common finding about hydraulic conductivity (Nielsen et al., 1973, and Bakr et al., 1973). Andrews also found d10 size, median grain size, and geometric mean size to have normal distributions. Another area that has been studied to a certain degree is the dependence of hydraulic conductivity on grain size parameters. Good correlation between effective grain size (taken as the d10 size) and hydraulic conductivity was found in quite a few studies (Andrews, 1982). Byers and Stephens also found a strong correlation between log Ksat and d10. Experimental variograms have also been used for the prediction of hydrogeologic parameters (Johnson and Dreiss, 1989).

The analyses performed on the grain size and moisture content results in Section 2.2 and on the bulk density, porosity, hydraulic conductivity, saturated water content, and grain size results in Section 2.6, involved standard statistical calculations and variogram analyses. Both sets of data involve vertical structures beneath the plot. Schmidt-Petersen

(1991) discussed horizontal structure within the upper alluvial fan beds. The basic premise in geostatistics is that the spatial structure of a variable can be described with a semivariance, which is defined as the expected squared difference between pairs of data values (Journel and Huijbrets, 1978). The semivariance is considered to be independent of data locations and a function of only the direction and separation distance between points. The semivariance is defined as [γ(h)]:

$$\gamma(h) = \sum_{i=1}^{N(h)} \frac{[(z(x_i+h)-z(x_i))^2]}{2N(h)} \qquad (2.1)$$

Where 2γ(h) is the mean squared difference for two points separated by a lag distance h, z(x) is the experimental data value at point x, z(x+h) is the experimental data value at a point h distance from x, and h is the lag separation distance. The above equation is used to determine the semivariance value γ(h) at a given lag distance (h). N(h) is the number of data pairs separated by the lag distance h. All pairs of data values h distance apart in the random field z(x) are compared. Variograms show the changes in semivariance with separation distance. Variograms have different shapes according to the various properties being considered. The semivariance increases as the correlation between the observations decreases from the point of interest. At the origin four classical shapes are noted (Delhomme, 1978):

1) Parabolic shape: For a regular variable such as head in an observation well with time (Figure 2-1: a, d).

2) Nugget effect: This is a discontinuity at the origin. Nuggets can be found when dealing with ore assay data, rainfall data, or may be caused by error in sampling, handling, and analysis of data (Figure 2-1: b).

3) Pure nugget (white noise): There is no correlation between the data for a given lag distance (h). This may be seen where the sample spacing may be to large to observe the underlying structure of the soil (Figure 2-1: c).

4) Linear shape: Characteristic of the thickness of a geologic formation with distance, less regular than the parabolic shape (Figure 2-1: e).

A nested structure as shown in Figure 2-1:f indicates variogram dependence which can be separated into different components or scales within each other. At infinite lag, the semivariance can increase indefinitely or stabilize to a sill, a value equal to the variance of the field data. The range is the distance at which the sill is reached. It shows the extent of a measurement point's influence. There is no correlation beyond the range. The data need to be examined for trends, distributions, and outliers. A theoretical model is then fit to the data. These models include the nugget effect,spherical, exponential, and gaussian.

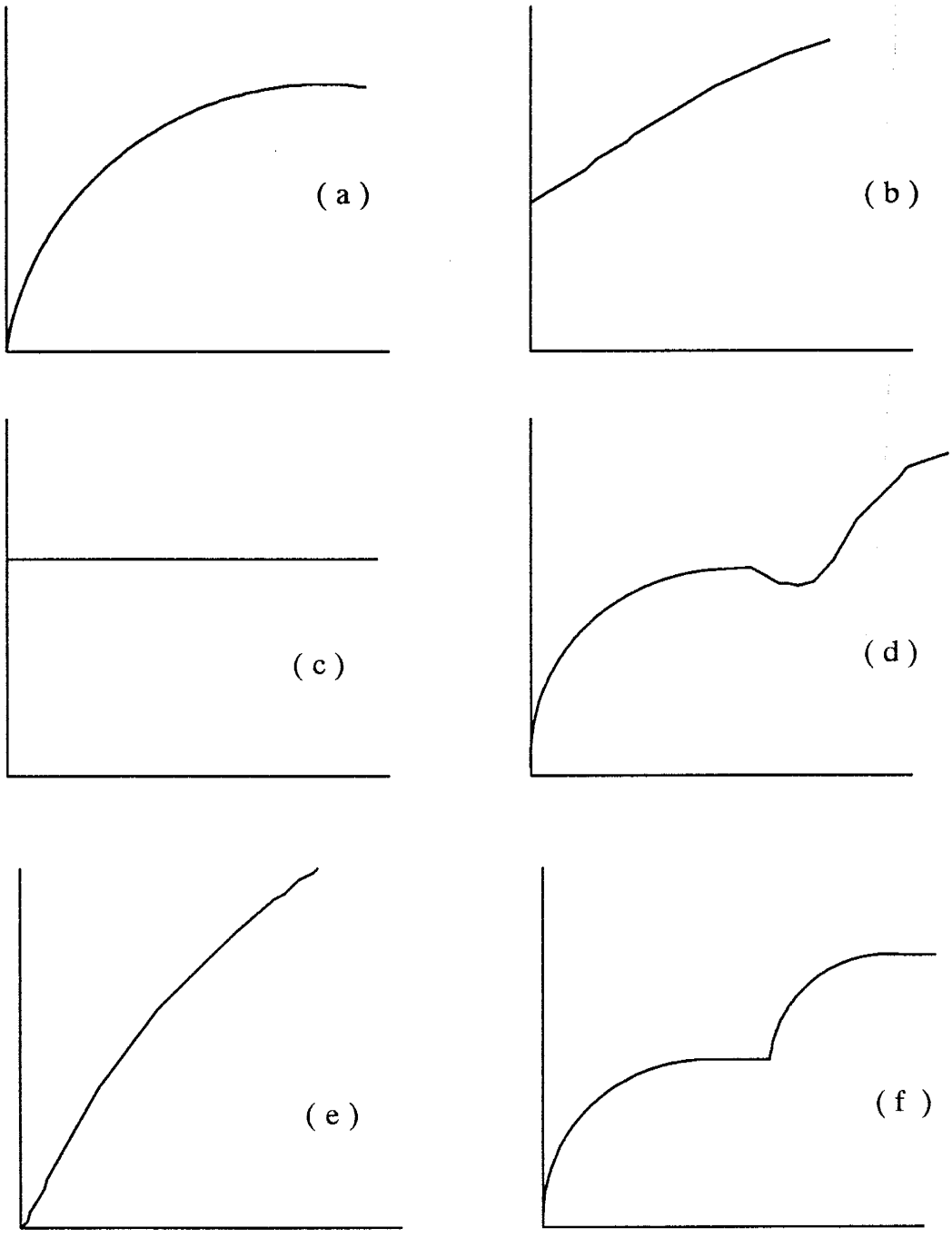

(a) Spherical model variogram
(b) Nugget effect
(c) Pure nugget (white noise)
(d) Exponential variogra with a hole effect
(e) Linear variogram (trend in the data)
(f) Nested structure

Figure 2–1 Possible shapes for isotropic variograms

2.2 PARTICLE SIZE DISTRIBUTION AND GRAVIMETRIC MOISTURE CONTENT

Two of the most important parameters that control unsaturated flow are particle size distribution and initial moisture content. It is necessary to characterize the alluvial fan facies and fluvial sand facies in terms of these parameters. Then it is necessary to see if the drainage results within the two facies could be at least partly predicted from the results of the two analyses.

The samples collected during the drilling of the porous cup sampler boreholes and the well borings were analyzed for particle size analysis and gravimetric moisture content. The samples that were collected from the deep trench and analyzed for grain size and moisture content are discussed in Section 2.4. The results of these analyses are summarized in Section 2.2.2 and are included in Appendix A.

2.2.1 Procedure

Two hundred and forty four split spoon samples were collected at regular intervals from the 4 meter deep and 8 meter deep porous cup sampler borings, and 180 samples were collected from the three 20 meter deep well borings providing nearly continuous logs of each of the 27 soil water sampler boreholes and three wells. Part of the ENE well boring

was sampled with shelby tubes as described in Section 2.3. To take a split spoon sample, auger flights were advanced with a star bit attached to the cable hammer at the bottom of the borehole to prevent soil from moving up the hollow stem. At each sampling location the star bit was raised, and the 5.08 cm (2 inch) outer diameter split spoon was lowered down the borehole. The drill hammer was used to pound the sampler into the ground for a 0.3 to 0.6 meter interval, yielding a sample core from that depth. Baskets inside the tip of the split spoon sampler prevented the soil from falling out during sample recovery.

An advantage of the split spoon sampling technique has been the ability to observe textural contacts within the recovered core, thereby giving a good approximation of contact location depths. However, soil cores obtained by split spoon sampling have been disturbed and compacted within the sampler, thus limiting their usefulness for further hydrogeologic laboratory analyses. Visual geologic descriptions of each split spoon sample were recorded in the field and in the laboratory using the Unified Soil Classification System and the Munsell (Soil Test, Inc., 1975) color chart. The above samples were analyzed for field gravimetric moisture content and for particle size distribution using standard sieve and hydrometer analyses (Lambe, 1951) in the laboratory. The sieve analysis consists of shaking the soil through a stack of wire screens with openings of known size; the definition of particle diameter for a sieve test is therefore, the side dimension of a square hole. The hydrometer method is used for the silt and clay fraction and is based on Stoke's equation for the velocity of a freely falling

sphere.

In addition, six pairs of samples from the deep trench were analyzed for particle size distribution and gravimetric moisture content. These samples were collected in conjunction with the disc permeameter operation and were collected prior to and after disc permeameter infiltration. The results of these samples are discussed in Section 2.4.

The particle size parameters measured are d_{10}, d_{30}, d_{50}, and d_{60}. These parameters indicate the percent of material by weight which is finer than the diameter given. Calculated particle size distribution parameters include the coefficient of uniformity (d_{60}/d_{10}) and the coefficient of curvature ($d_{30}^2/d_{10}*d_{60}$). In other studies it has been shown that specific yield decreased as the magnitude of the uniformity coefficient increased (Masch and Denny, 1966). A soil having a uniformity coefficient smaller than two would be considered quite "uniform" and a value of larger than five would indicate variable material. The d_{50}, or median, grain size has been shown to be a measure of representative grain diameter. It should be noted that a few studies have been performed using sorting indices to differentiate between various alluvial fan beds. The indices are based on grain size parameters and they are the trask sorting coefficient, standard deviation and quantile deviation. These indices will not be used in this study because we can not group the split spoon samples into specific matching alluvial fan units as is possible at an outcrop.

The method of analysis was to sieve the sample first and save the remaining clay portion for hydrometer analysis if necessary, to determine the percentage of silt and clay particles. The samples were first desegregated by a manual grinding technique and then sieved in the following set of American Society of Testing Methods (ASTM) standard testing sieves: 1/4, 8, 10, 16, 40, 70, 140, and 200. Those samples where the d10 parameter could not be found with sieving, were analyzed by the hydrometer method. The hydrometer method obeys Stoke's law and consists of measuring the time that it takes for the suspended fine fraction to settle in a 1000 mL cylinder.

All split spoon samples used in the geologic characterization were analyzed for in situ gravimetric content. The samples taken from the deep trench wall during the disc permeameter operation provided volumetric moisture content information through measured gravimetric moisture content values and Parsons' (1988) bulk density values. The shelby tube samples were not analyzed for gravimetric moisture content. Gravimetric moisture content and volumetric moisture content are related by the following relationship (Hillel, 1980).

$$\theta = w * \rho_b / \rho_w \qquad (2.2)$$

θ = volumetric moisture content (cm^3/cm^3)

w = gravimetric moisture content(g/g)

p_b = dry bulk density (g/cm^3)

p_w = the density of water (assumed to be 1.0 g/cm^3).

Gravimetric moisture contents are easily calculated for core samples, since theta and p_b are already measured. Volumetric moisture content is a more commonly used parameter, and can be directly compared to our neutron logging moisture content data (Parsons, 1988 and; A. Stark, personal communication,1991). To convert gravimetric moisture content of disturbed samples to a volumetric basis, the average dry bulk density for the two main geologic materials (calculated by Parsons (1988)) was used to convert the deep trench wall sample values to volumetric moisture content; 1.5 g/cm^3 was used for alluvial fan material, 1.38 g/cm^3 was used for clay, and 1.64 g/cm^3 was used for fluvial sand.

2.2.2 Results and Analysis

Tables 2.1 and 2.2 present a summary of the grain size distribution and gravimetric moisture content results for the deep and shallow boreholes. These results were grouped into a piedmont slope or alluvial fan category and a Rio Grande fluvial sand category. Standard statistical analyses were performed on the results and these are presented in Tables 2.1 and 2.2.

Table 2-1

Piedmont Slope Facies: batch statistics on grain size analyses

Variable	(mm) d10	(mm) d30	(mm) d50	(mm) d60	Cu[1]	Cc[2]	Gravimetric Moisture Content %
Arithmetic Mean	0.37	0.48	1.06	1.43	11.41	1.5	10.82
Variance	1.07	0.65	3.95	3.52	233.95	34.15	69.22
Coeff. of Variation	280.4	168.4	187.7	131.1	134.0	389.2	76.9
Skewness	12.64	5.2	7.41	2.39	4.56	10.36	4.6
Kurtosis	188.05	38.02	82.18	8.24	33.32	120.55	47.55
Number of Samples	271	271	265	263	263	260	269

[1]Cu = Coefficient of uniformity
[2]Cc = Coefficient of curvature

Table 2-2
Rio Grande Fluvial Sand Facies: Batch Statistics on grain size analyses

Variable	(mm) d10	(mm) d30	(mm) d50	(mm) d60	Cu[1]	Cc[2]	Gravimetric Moisture Content %
Arithmetic Mean	0.16	0.41	0.71	0.89	6.59	1.68	6.94
Variance	0.02	0.37	0.88	1.45	58.24	21.43	32.07
Coeff. of Variation	96.7	147.9	132.7	135.3	115.8	275.8	81.6
Skewness	6.57	6.1	3.3	3.46	3.09	9.95	2.5
Kurtosis	57.06	6.1	3.3	3.46	12.99	109.93	10.68
Number of Samples	152	153	152	151	150	148	118

[1]Cu = Coefficient of uniformity
[2]Cc = Coefficient of curvature

The mean d_{10} size was found to be 0.37 mm in the alluvial fan units and 0.16 mm in the fluvial sands. Table 2.3 shows similar analyses performed in previous studies at this field plot. In previous studies the alluvial fan material d_{10} size was .089, .049 and .067 (Schmidt-Petersen (1991) and Parsons (1988)) and the fluvial sand d_{10} size compared very similarly to the previous grain size distribution results (Parsons,1988). The average coefficient of curvature for the fluvial sands showed the most uniform material in both the present study and in Parsons' study. The alluvial fan results were more scattered, a function of their great variability.

The mean gravimetric moisture content of the alluvial fan units was 10.82% and the mean gravimetric moisture content of the fluvial sands was 6.94%. These moisture contents reflect the background moisture of the units prior to the infiltration events and indicate moisture retention in some of the alluvial fan units. These units are most likely those with the highest clay content as seen during the deep trench investigation.

The datum that was surveyed in at the site is at the 0-meter depth on all of the figures. The following is a brief description of the five different groups of geologic material shown in the stratigraphic logs. Cobble and/or gravel layers are shown with drawn cobbles. Clay/silty clay layers are shown as filled black lines and fine to medium sand layers are shown as filled light grey lines. Silty fine sand with a little gravel is shown with medium length horizontal black lines and small drawn cobbles. Fine to coarse sand with a little silty sand and a little gravel is shown in medium grey with short horizontal

Table 2-3 Particle Size Parameters from previous studies: Batch Statistics

Variable	(mm) d10	(mm) d30	(mm) d50	(mm) d60	(mm) d90	Cu[1]	Cc[2]
FINAL MOISTURE SAMPLES: Alluvial Fan Material							
(Schmidt-Petersen,1991)							
Arithmetic Mean	0.089	0.437	609	0.747	1.908	23.2	3.0
Variance	0.058	2.154	1.061	1.31	2.381	1074.6	17.6
Coeff. of Variation	272.7	336	169.05	153.16	80.9	141.8	139.3
Skewness	7.83	8.07	3.265	3.395	1.647	5.543	8.84
Kurtosis	69.7	72.73	13.18	14.43	4.38	40.98	45.7
Number of Samples	92	97	98	96	87	90	90
SOIL CORE SAMPLES: Alluvial Fan Material							
(Schmidt-Petersen,1991)							
Arithmetic Mean	0.049	0.169	0.358	0.526	1.776	18.56	2.49
Variance	0.003	0.015	0.143	0.303	1.887	232.86	4.58
Coeff. of Variation	114.72	72.75	105.7	104.7	77.36	82.2	85.8
Skewness	3.6	3.67	4.36	3.94	2.04	1.36	1.46
Kurtosis	22.71	18.8	26.04	22.63	6.237	4.103	5.29
Number of Samples	102	100	101	101	90	101	101
ALLUVIAL FAN MATERIAL (Piedmont Slope Facies)							
(Parsons, 1988)							
Arithmetic Mean	0.067	0.197	0.39	0.566	3.851	59.3	3.1
Variance	0.008	0.098	0.353	0.71	15.342	14161.4	18.3
Coeff. of Variation	134.2	158.7	152.5	149	101.7	200.8	137.2
Number of Samples	59	59	59	59	59	59	59
FLUVIAL SAND FACIES							
(Parsons, 1988)							
Arithmetic Mean	0.163	0.359	0.803	1.223	4.549	7.071	0.89
Variance	0.002	0.066	0.994	2.709	25.112	102.87	0.05
Coeff. of Variation	25	71.3	124.1	134.6	110.2	143.4	25.9
Number of Samples	21	21	21	21	21	21	21

[1]Cu = Coefficient of uniformity
[2]Cc = Coefficient of curviture

black lies and small drawn cobbles. Figures 2-2 and 2-3 present the geologic logs of SSW and NNW superposed next to the d_{10} and gravimetric moisture content profiles. The NNW profile shows the large deviations in moisture content and d_{10} at the depths of the cobble layers at four meters and at seven meters. It is also important to note that the range in grain size and moisture content diminishes below the second cobble layer at seven meters. Below this depth are only fluvial sediments as opposed to the quite heterogeneous alluvial fan sediments above. The SSW profile also shows the presence of cobbles at four meters. The profile for the third deep well boring is included in Section 2.6. Figures 2-4 and 2-5 present the coefficient of uniformity and coefficient of curvature for SSW and NNW with depth. Variogram analysis of the d_{10} size in the alluvial fan facies and in the fluvial sand facies present interesting results. Figure 2-6 shows a variogram of all of the d_{10} results between the datum and five meters below datum. Five meters are used as the cutoff depth between the two facies. The alluvial fan material is quite heterogeneous and is not correlated in the vertical direction. On the other hand the vertical variogram for all d_{10} samples taken in the fluvial sand facies shown in Figure 2-7 shows a correlation length of approximately 1.2 meters. An exponential model is fit to this variogram with a sill at 0.025 and a range of approximately 1.2 meters. The range is calculated as being 66% of the sill. An average thickness of the fluvial sand beds seen in the stratigraphic sections of ENE, SSW, and NNW is between one and two meters. Correlation is not found in the alluvial fan facies due to the particular stratigraphy of this facies as discussed in Section 3.3. Each bed within the alluvial fan facies is different from those below and above it. Each bed

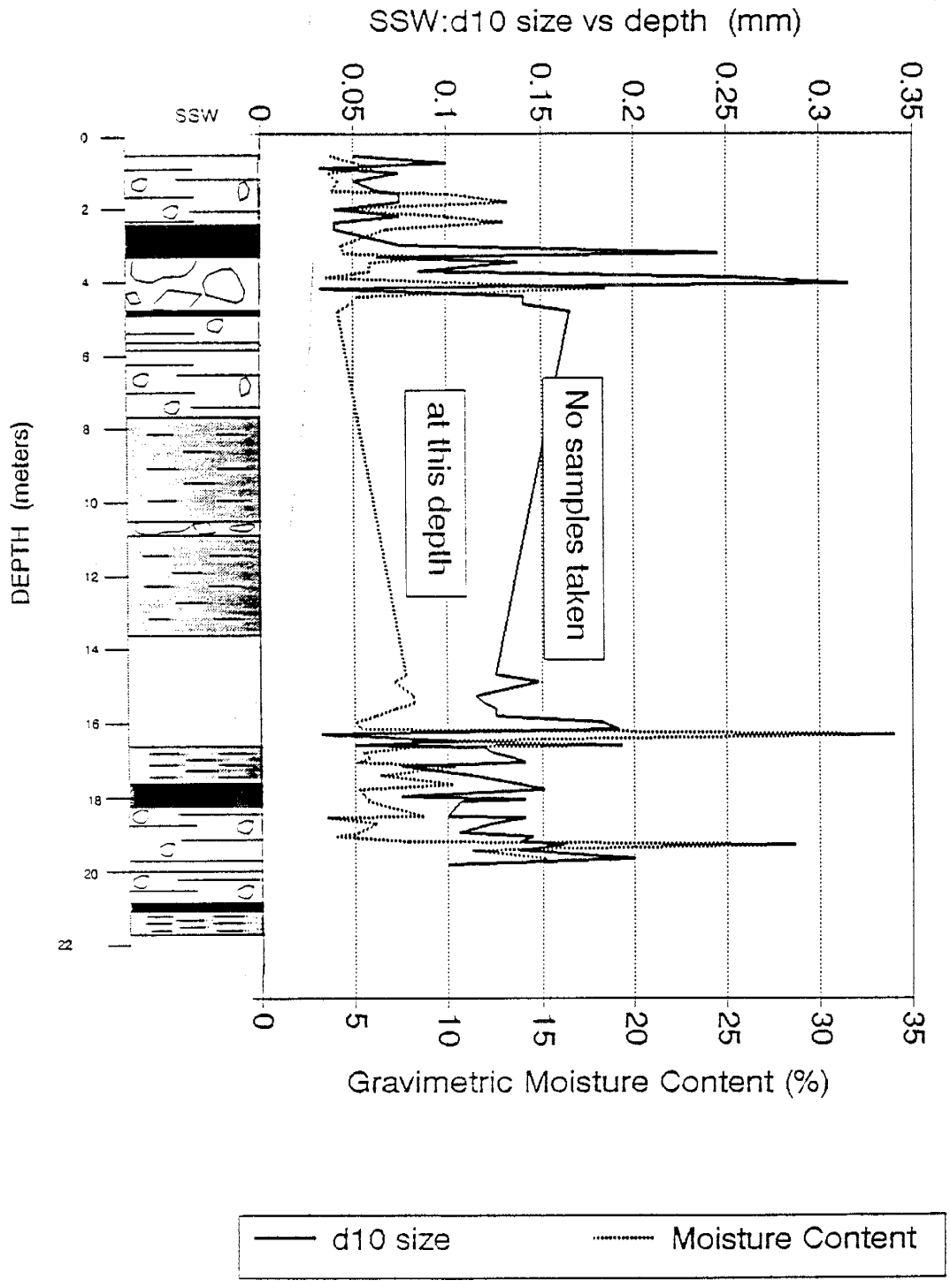

Figure 2-2 SSW: d10 and moisture content.

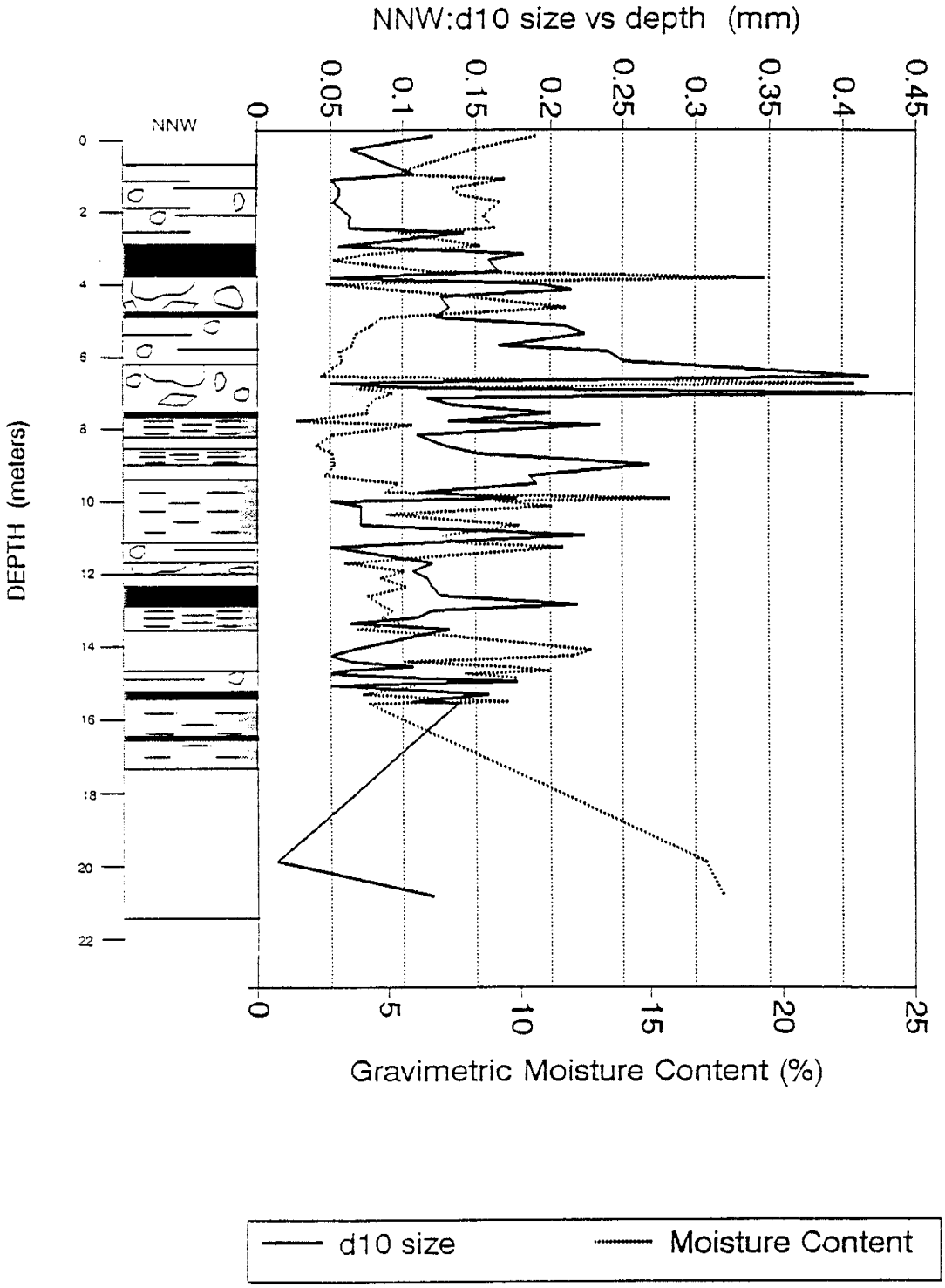

Figure 2-3 NNW: d10 and moisture content

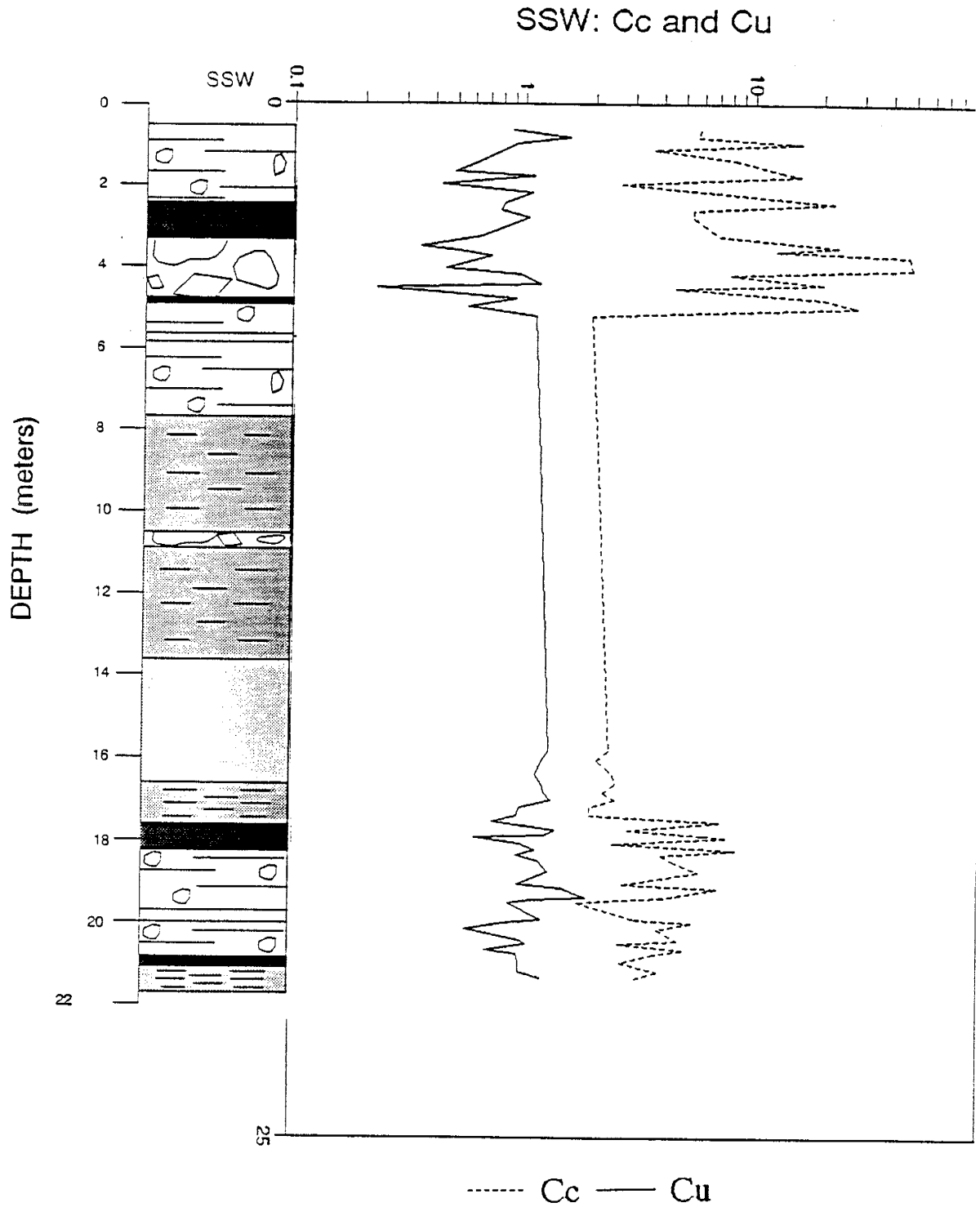

Figure 2-4 SSW: Cc and Cu

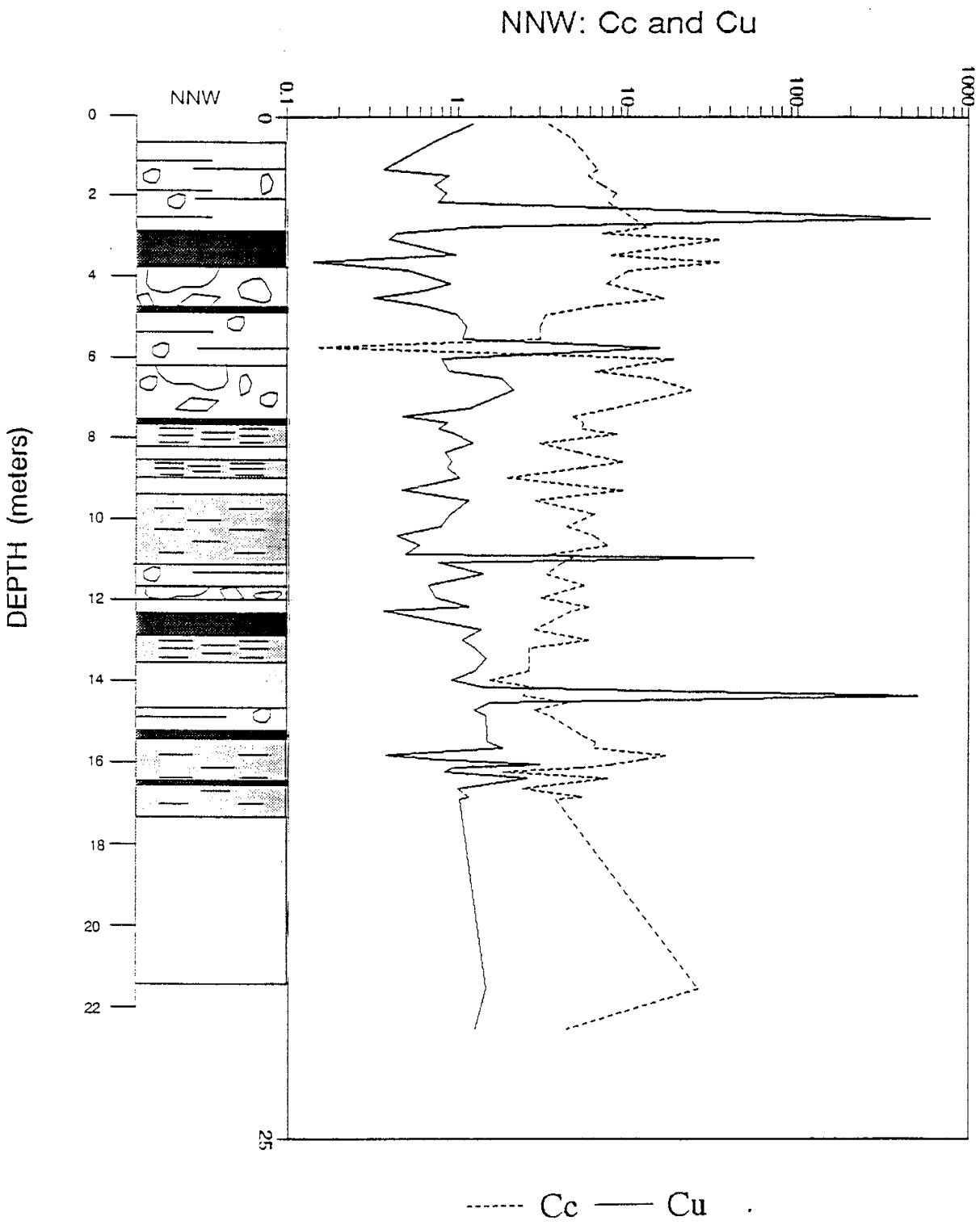

Figure 2-5 NNW: Cc and Cu.

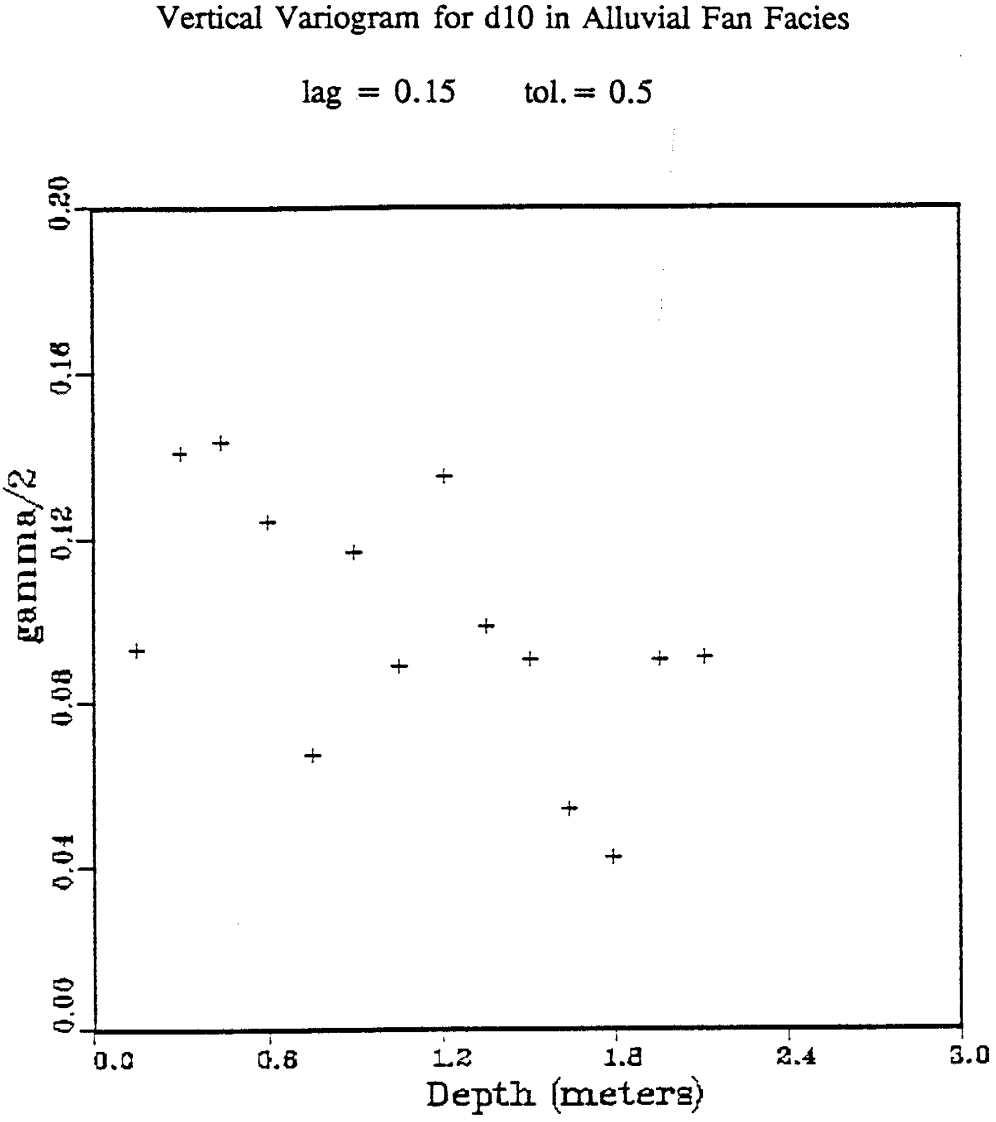

Figure 2-6 Vertical variogram for d10 in alluvial fan facies

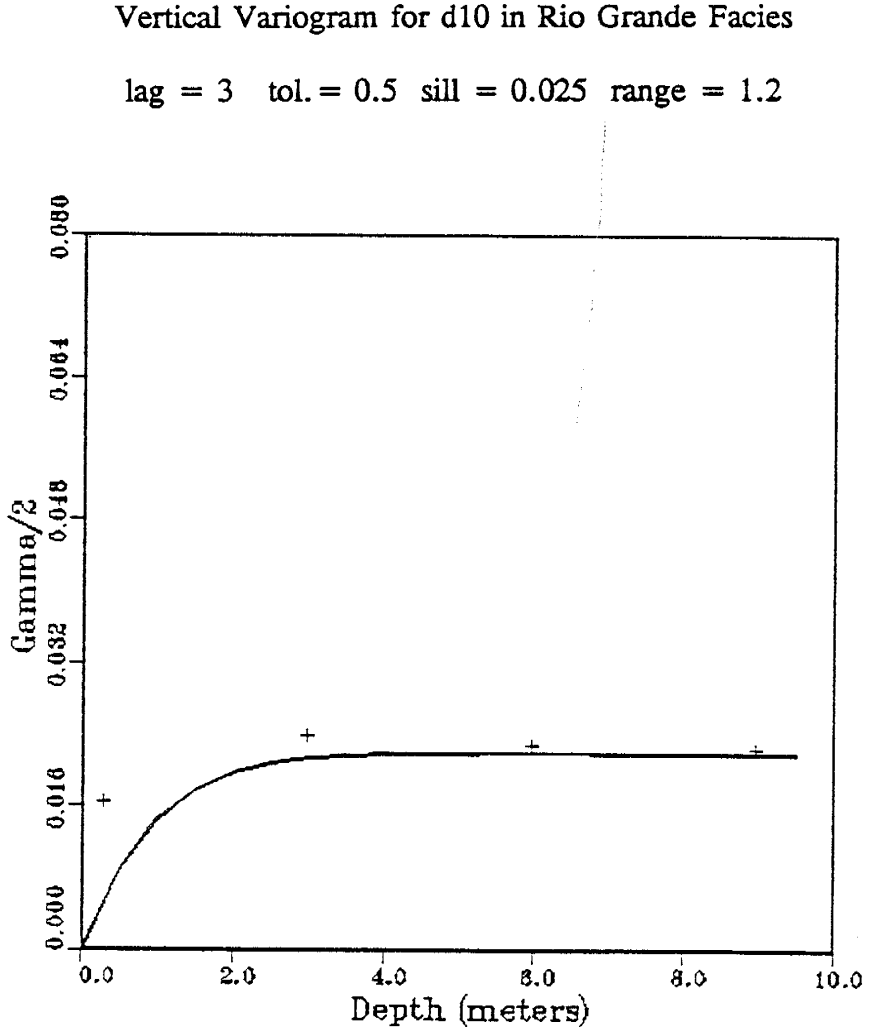

Figure 2-7 Vertical variogram for d10 in Rio Grande facies.

has a very different dominating grain size and a distinct structure within itself. In addition there are not enough samples taken within each alluvial fan unit for a thorough statistical evaluation. On the other hand there appear to be enough samples taken within the underlying Rio Grande facies. As noted above the correlation length shown in the variogram agrees with the general thickness of the beds within the fluvial sand. This correlation may indicate that the fluvial events that deposited the material being examined would last long enough to deposit about one meter thick sequences.

2.2.3 Error and Bias

Due to sampling and drilling difficulty the split spoon samples were taken from depths where there were no cobble layers. As a result there is a certain bias toward a generally smaller than realistic grain size distribution. Therefore gravimetric moisture content results would be impacted since the larger grain size distribution would most likely contain lower in situ moisture contents. There was some error involved in the gravimetric moisture content values due to a loss of moisture in the samples between the field and the laboratory, a loss that was minimized by placing the samples in plastic bags.

2.3 SATURATED HYDRAULIC CONDUCTIVITY WITH THE SHELBY TUBE PERMEAMETER

Now that we have the grain size distribution and gravimetric moisture content of the two

geologic facies, it is necessary to find the hydraulic conductivity profiles for the two facies. One of the three ways that saturated hydraulic conductivity was found for the fluvial sands was to construct permeameters from the continuously sampled shelby tubes.

In addition to continuous split spoon samples, shelby tube core samples were taken during the drilling operation. Fourteen shelby tubes were extracted from borehole ENE, six from SSW, four from NNW, and one from N. These 30-cm long metal tubes were pounded into the ground, yielding a fairly intact core sample from that depth. The 14 cores from ENE represent most of the top 20 meters below datum. These cores were taken into the laboratory and used for creating permeameters. Shelby tube permeameters were constructed to find saturated hydraulic conductivity variation along this vertical section. After the permeameter experiment, samples were extracted from the ENE core and analyzed in the laboratory for additional hydraulic properties. These additional laboratory tests are discussed in Section 2.6. Section 2.3.2 discusses the results and analysis of the permeameter test.

2.3.1 Procedure

The following was the procedure used for constructing the shelby tube permeameter. Figure 2-8 shows a schematic diagram of a shelby tube permeameter. It is advised that before shelby tubes are used during sampling they should be cleaned, dried and an immediate inner coating of a durable rust preventative should be applied before oxidation

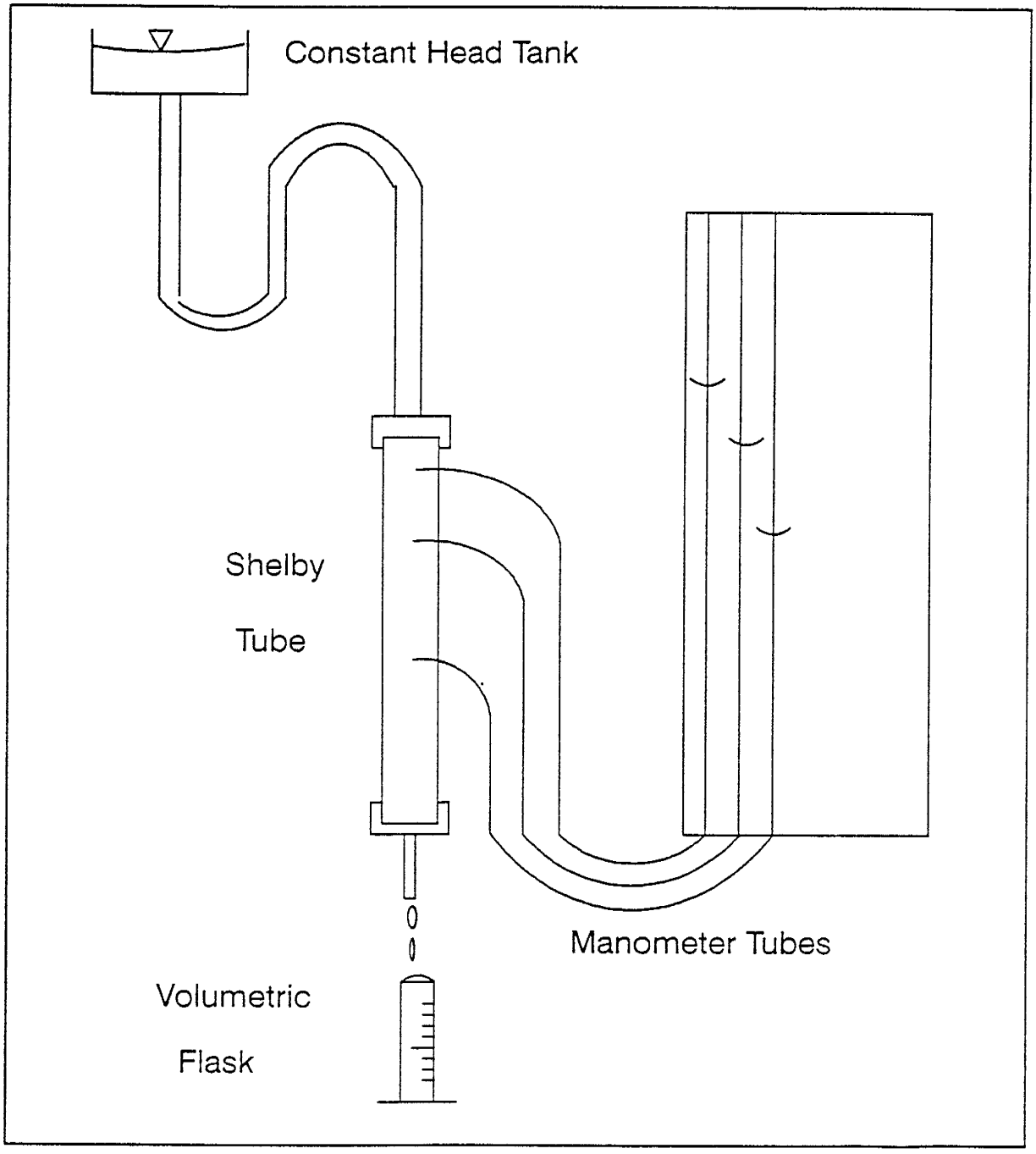

Figure 2-8 Schematic diagram of the shelby tube permeameter

sets in. It was fairly obvious that this coating procedure had not been performed becausethe tubes rusted between the time of sampling and the permeameter operation and because organic matter began growing on the inside of the tubes during the permeameter operation. Assurance of good sample retrieval depends on several factors (Rabold, 1984): a) a good vacuum within the sampling apparatus at retrieval, b) careful shelby tube handling during retrieval, and c) the ability of the sampled zone to lend itself to shelby tube sampling techniques. Sample recovery for these tubes averaged about 50%.

A good vacuum in the sampling device is achieved by a thorough cleaning of the check valve in the shelby tube head prior to sampling. Careful handling necessitates not jarring the shelby tube in the borehole or banging it against the hole walls. After removal from the hole, the shelby tube and head are removed from the drill string and the bottom of the shelby tube is taped to prevent sample loss. The shelby tube is kept in an upright vertical orientation and the sample head is removed.

These shelby tube samples were kept upright for a year before being set up for permeameter operation. In the laboratory, the tube was first removed from the top of the tube (or the end with holes) keeping the tube in the upright position. The length of the sample was determined and the number and position of the proposed manometers and outlet tubes was determined. Manometers were spaced approximately 15 cm apart along the recovered sample. The permeameters at first were constructed with inflow into the top of the tube and then changed to the bottom of the tube. When inflow was from the

top, holes were only put into the tubes for the manometers and any holes near the top had to be scaled off to create a good pressure seal. When inflow was from the bottom, a hole was drilled into the tube approximately 2 cm above the top of the sample to allow for measuring the outflow. When inflow was into the top of the tube the outflow was measured from the bottom of the tube. Either way the bottom of the core had to have a fine mesh screen placed in the bottom to prevent clogging.

The manometer and outflow holes were drilled with a drill press and manometers were placed into the holes. The manometers consisted of 7 to 8 cm long, 0.95-cm (3/8-inch) diameter copper tubing with rubber gasket material placed around the copper tube. Cotton was placed into the copper tube (on the sample end) to prevent soil from clogging up the manometer. The copper tube was inserted into the shelby tube with a compressive fitting around the copper tube up against the rubber gasket material which was pressed against the wall of the shelby tube. After covering up any open drill holes, the cap was removed from the bottom of the sample. If the sample exposed was a dry, non-cohesive sand, a small amount of water was squirted on the sample to provide cohesion. A fitting containing a fine mesh was epoxied into the center of the cap and placed on the bottom end of the shelby tube. This fitting allowed for an outflow or an inflow. The bottom cap had to be epoxied to the shelby tube and then the shelby tube was ready to be clamped into the permeameter rack. The procedure involved 7.6 cm (3-inch) U-bolt clamps for the bottom of the tube and a 7.6-cm sandwich clamp for the top. The copper manometer tubes were clamped onto the shelby tube by placing a flat metal sheet with holes for the

U-bolt ends against the compression fitting and tightening it until there were no leaks. The permeameter rack was positioned near to the manometer board. Once the sample was saturated, the plastic manometer tubes were attached to the copper tubes.

A constant head device and water reservoir were put together near the manometer board. The over-flow tube was positioned into the collector reservoir and the tap was turned on to establish a constant head in the tank. This water was then available to the shelby tubes via the inflow tube. When saturating the sample from the bottom there was no need to flood the sample to deair it. When saturation occurred from the top, the water in the shelby tube had to be all the way to the top of the tube for there to be a vacuum. The copper tubes showed dripping water once the water inside the tube had reached those heights, after which it was appropriate to attach the plastic manometer tubes to the copper tubes. All connections were tightened with plastic ties.

A scale was placed on the manometer board and permeameter board for recording the relative heights of the manometer inlets, water levels in the manometers, the height of the top of the sample and the height of the water level in the constant head tank. Values of dL, dH, and Q were recorded with time until the system had equilibrated. Equilibration occurred in approximately one week. The equations used for calculating the hydraulic conductivity is Darcy's Law:

$$Q = -KA\frac{dH}{dL}$$

Therefore $K_i = \frac{Q}{A*(dL_i/dH_i)}$

Where K_i = interval saturated hydraulic conductivity. (L/t)

Q = discharge from bottom of sample. (L^3/t)

A = cross-sectional sample area. (L^2)

dL_i = sample length between the top of the sample and first manometer, successive manometers, and between the last manometer and sample bottom. (L)

dH_i = difference in elevation between fluid levels measured in applied head and successive manometer water levels. (L)

L = length

t = time

2.3.2 Results and Analysis

Table 2.4 shows the results for this experiment with depth. The saturated hydraulic conductivity from the 20 manometers on the ENE Shelby tube results are plotted against depth and compared to the stratigraphic section of ENE in Figure 2-9.

Table 2-4

SHELBY TUBE PERMEAMETER: HYDRAULIC CONDUCTIVITY RESULTS

ENE SAMPLE #	DEPTH RANGE (m)	AVERAGE DEPTH TESTED (m)	FINAL HYDRAULIC CONDUCTIVITY (cm/s)
ENE1	0 - .762	0.18	0.5*
ENE7	4.57 - 5.33	4.78	0.16*
"		4.96	3.8*
"		5.14	3*
ENE10	6.86 - 7.62	6.93	0.027
ENE11	7.62 - 8.38	7.79	0.61*
"		7.89	0.2*
ENE13	9.14 - 9.91	9.26	0.013
ENE14	9.91 - 10.67	10.06	0.78*
"		10.19	5.65*
ENE15	10.67 - 11.43	10.84	0.016
ENE16	11.43 - 12.19	11.62	0.078
"		11.74	0.0078
ENE17	12.19 - 12.95	12.27	0.0053
ENE18	12.95 - 13.72	13.07	0.014
ENE19	13.72 - 14.48	13.87	0.0049
ENE21	15.24 - 16.00	15.43	0.015
ENE22	16.00 - 16.76	16.13	0.179*
ENE25	18.29 - 19.05	18.34	0.071
ENE26	19.05 - 19.81	19.18	0.042

* Suspect conductivity values

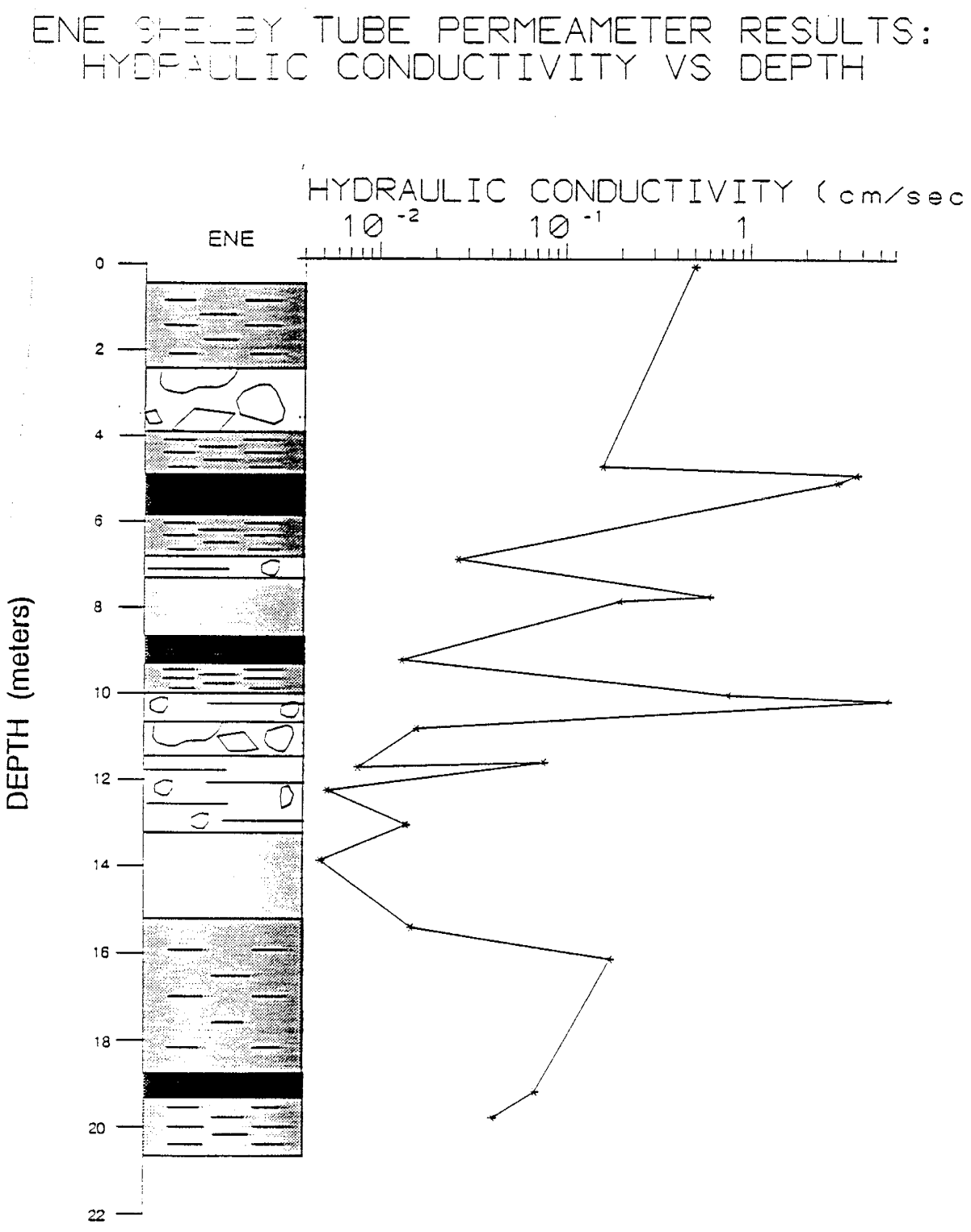

Figure 2-9 ENE shelby tube permeameter results: hydraulic conductivity vs depth.

The shelby tube results showed Ksat values that varied between 5.65 cm/s and $5x10^{-3}$ cm/s along the 20 meter depth interval.

The 10^{-2} and 10^{-3} cm/s values which are from between 6 and 16 meters below datum are quite reasonable for the Rio Grande fluvial sand formation and are not suspect (Stephens, personal communication, 1990). The depths of the higher values correspond to the depths of the gravel layers but the values are too high for such materials as there is a silty matrix associated with these gravel layers. The unusually high results for the cobble layer depths are attributed to the difficulty in sampling these layers without causing disturbance of the sample and therefore causing preferential flow pathways. In general, the Ksat values are high for the types of materials being tested. The values that are being considered as valid are those $2*10^{-2}$ and slower. There are quite a number of possible laboratory errors associated with the shelby tube permeameter, as discussed in Section 2.3.3.

2.3.3 Error and Bias

The errors associated with the shelby tube permeameter experiment may be used to explain the high Ksat results seen in about half of the values. There are four main factors that introduce error into this setup; disturbance of the shelby tubes, preferential flow during the experiment, flow rate regularity, and bacterial growth.

For this experiment it is important that the tubes are not disturbed very much so as to prevent compaction or any other rearrangement of the soil within the tube. These tubes were kept upright in a laboratory for approximately one year before they were used in this procedure. In addition the tubes had to be placed on their side for manometer holes to be drilled. It is expected that some compaction would take place during such handling. Compaction would possibly cause lower than real hydraulic conductivity values.

It is expected that during drilling any gravel zones would have created potential preferential flow paths within the shelby tubes as large size gravel pieces could be dragged along the sides of the shelby tubes. Such preferential flow paths would explain the unusually high conductivity values.

Thirdly it was necessary to keep a constant flow rate through the constant head tank. Fluctuations in the flow rate from the faucet had to be monitored and regulated. There was a small resulting error in the water levels in the manometers.

As with any water permeameter system there was concern over changes in the water quality with time. Factors affecting water quality include bacteria growth, precipitation, or ion exchange reactions. Bacteria growth started affecting the experiment by clogging outflow holes but was disrupted when bleach was introduced into the water.

2.4 SATURATED HYDRAULIC CONDUCTIVITY WITH THE DISC PERMEAMETER

The second way that saturated hydraulic conductivity was found for the two geologic facies was to use a disc permeameter. The disc permeameter was used to infiltrate water onto prepared terraces on each of the individual layers exposed in the deep trench.

Saturated hydraulic conductivity (Ksat) was measured in six places within the deep trench using the disc permeameter as shown in Figure 2-10. Two measurements were taken within the Rio Grande fluvial sands, one in the water-laid sediments, one in the cobble-filled debris flow unit on the southern end of the trench and two samples were taken in silty intermediate deposits. These geologic units are discussed in Section 3. The Ksat of these various media shall increase our understanding of the nature of hydrogeologic heterogeneity within the plot and the behavior of fluid flow when applied toward these media. Disc permeameter data sheets are included in Appendix B.

2.4.1 Procedure

Figure 2-10 shows the location of the six measurement points within the deep trench. A more detailed trench wall figure is shown in Figure 3.4. Samples 1 through 4 were taken on platforms dug into the wall of the trench while samples 5 and 6 were taken on the

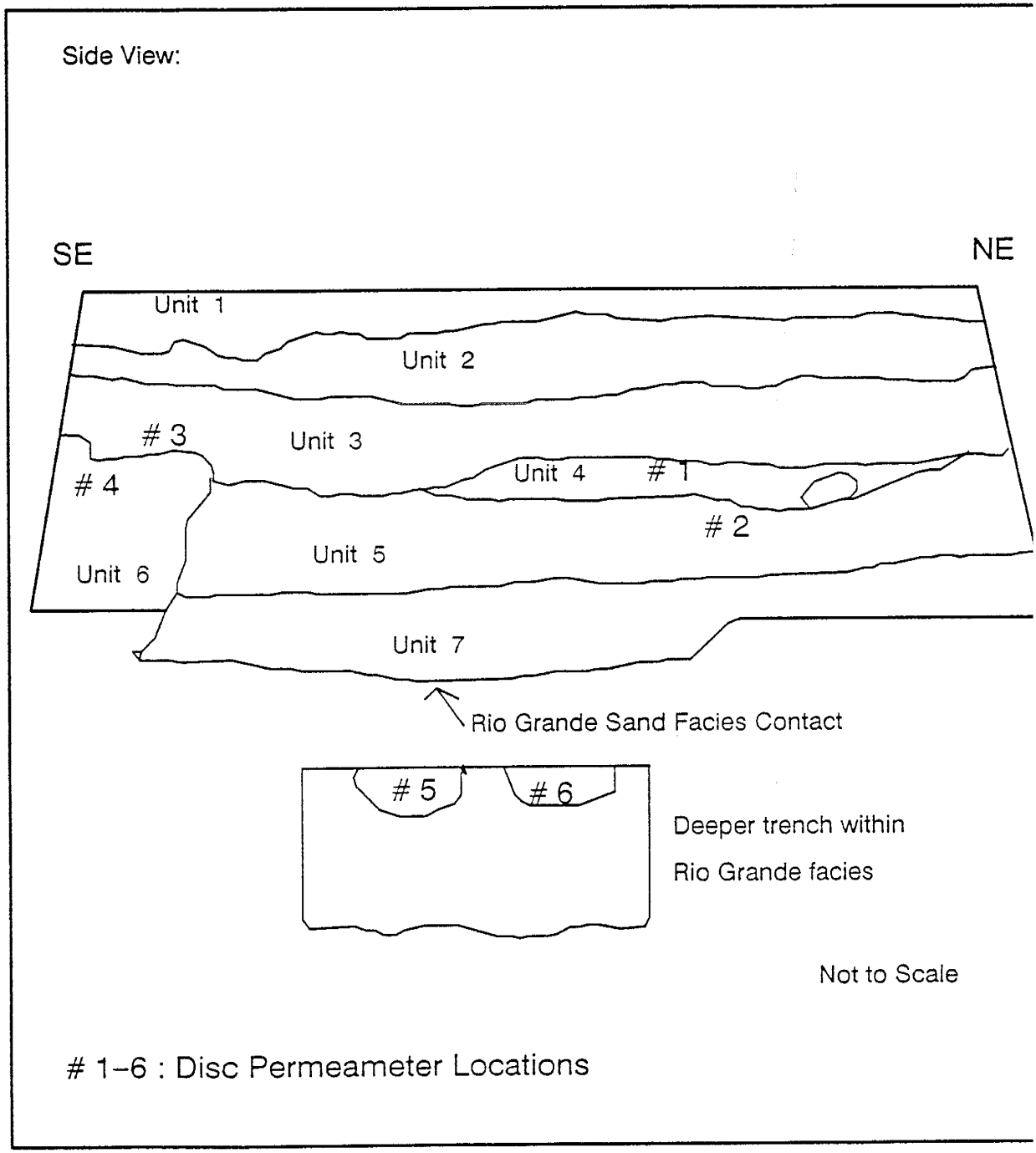

Figure 2-10 Disc permeameter locations on deep wall

floor of the trench within the Rio Grande sands. The geologic units of the alluvial fan or piedmont slope facies are described in Section 3.3. Sample 1 was taken immediately above unit 4, the only fully water-laid unit exposed in the deep trench. Samples 2 and 3 were taken at two different places within the silty intermediate bed, unit 5. Sample 4 was taken immediately above unit 6, a high energy, cobble containing debris flow. Samples 5 and 6 were taken at slightly different depths within the Rio Grande fluvial sands found in the bottom of the trench. Sample 5 had sands beneath it while the sample 6 location had a 2.5 cm thick clay layer running through the sand. Photographs of sample locations 5, 2, and 1, are shown in Figures 2-11 through 2-13.

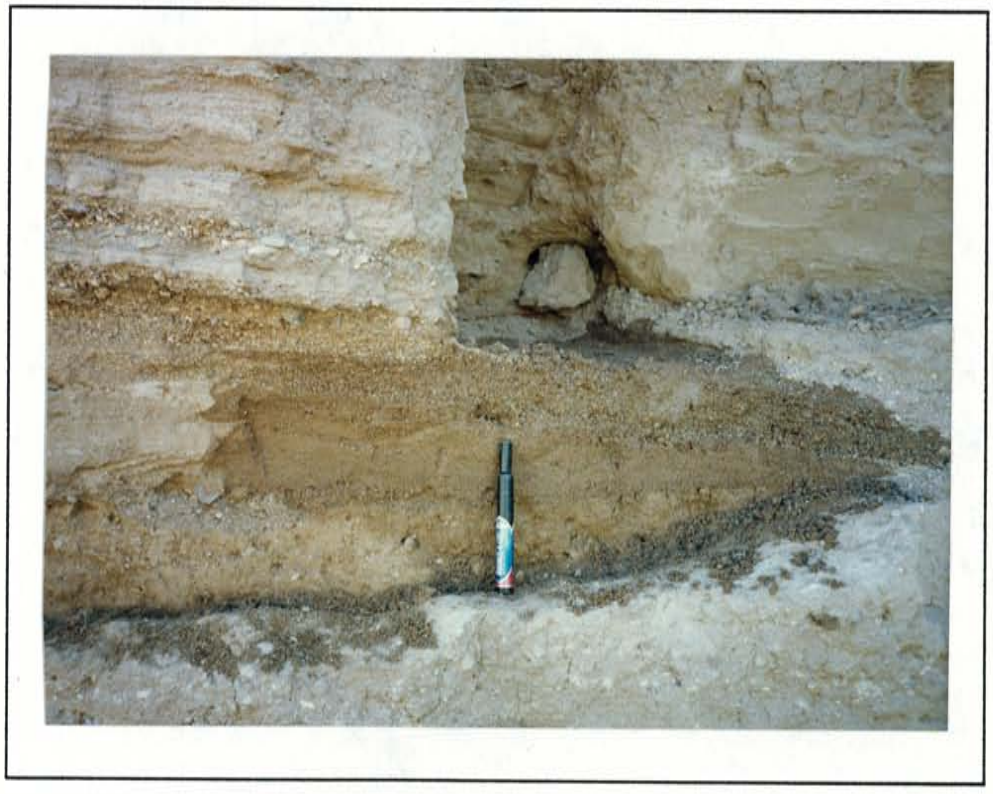

Figure 2-11 Photograph of disc permeameter location #5 after infiltration event.

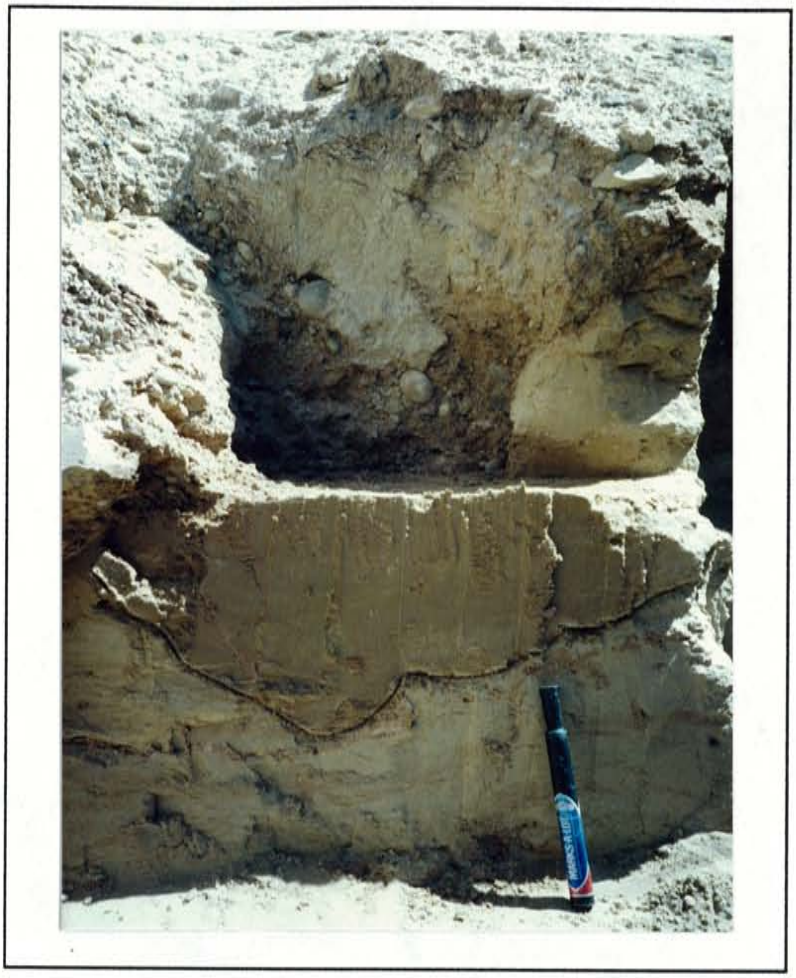

Figure 2-12 Photograph of disc permeameter location #2 after infiltration event.

The wetted regions in Figures 2-11 and 2-12 show the effects of material on the extent of lateral and vertical flow. Prior to the disc permeameter infiltration, a soil sample (approx 100-150 g) was collected from the top few centimeters of soil near the measurement location for initial moisture content determination and grain size analysis.

At the end of infiltration a final moisture content sample was taken from the top few millimeters of soil under the cap material and placed in an air tight container for weighing for moisture content and grain size analyses.

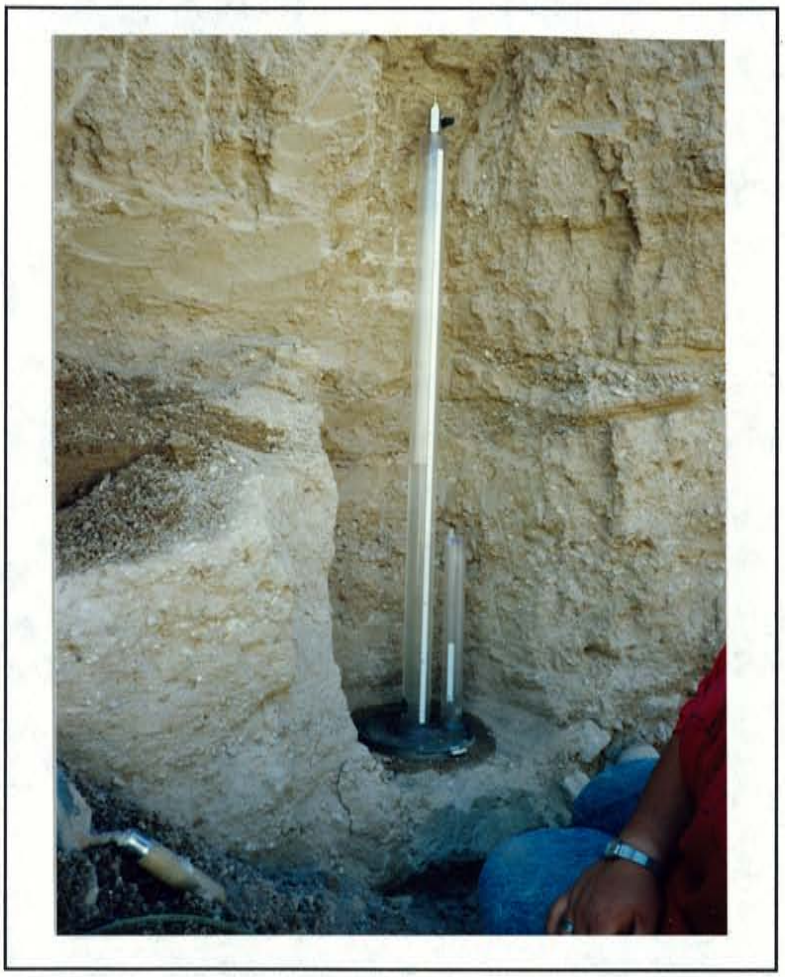

Figure 2-13 Photograph of disc permeameter location #1 during infiltration event.

Figure 2-14 shows a schematic of the disc permeameter. During measurement preparation the disc must be soaked in water for several hours prior to measurements to ensure that it will remain airtight. The desired tension is fixed by raising or lowering water in the bubbling tower. The supply pressure at the membrane is calculated by $Z = z2 - z1$ as seen in Figure 2-14. z2 was fixed at 0.7 mm for this particular disc. Therefore, z1, the height of water in the bubbling tower above the air inlet, was used for the desired supply pressure.

The measurement site was prepared by removing large rocks and vegetation, and by levelling the measurement area. In many cases, a cap of contact material, usually a fine sand was used to ensure a flat measurement surface. The impact of the cap is discussed by Schmidt-Petersen (1991). The thinnest possible cap was used.

The disc permeameter theory, calibration procedures, measurement method and calculations discussed in detail by Perroux and White (1988) and by Schmidt-Petersen(1991). In this study measurements were conducted at negative pressures to find saturated hydraulic conductivity values for the very different alluvial fan units exposed in the deep trench. Operation procedures are described below and in the CSIRO Disc Permeameter Instruction Manual (1988).

The six measurements were conducted at very close to saturated conditions or at approximately one cm of tension to exclude flow from soil cracks formed by evaporation

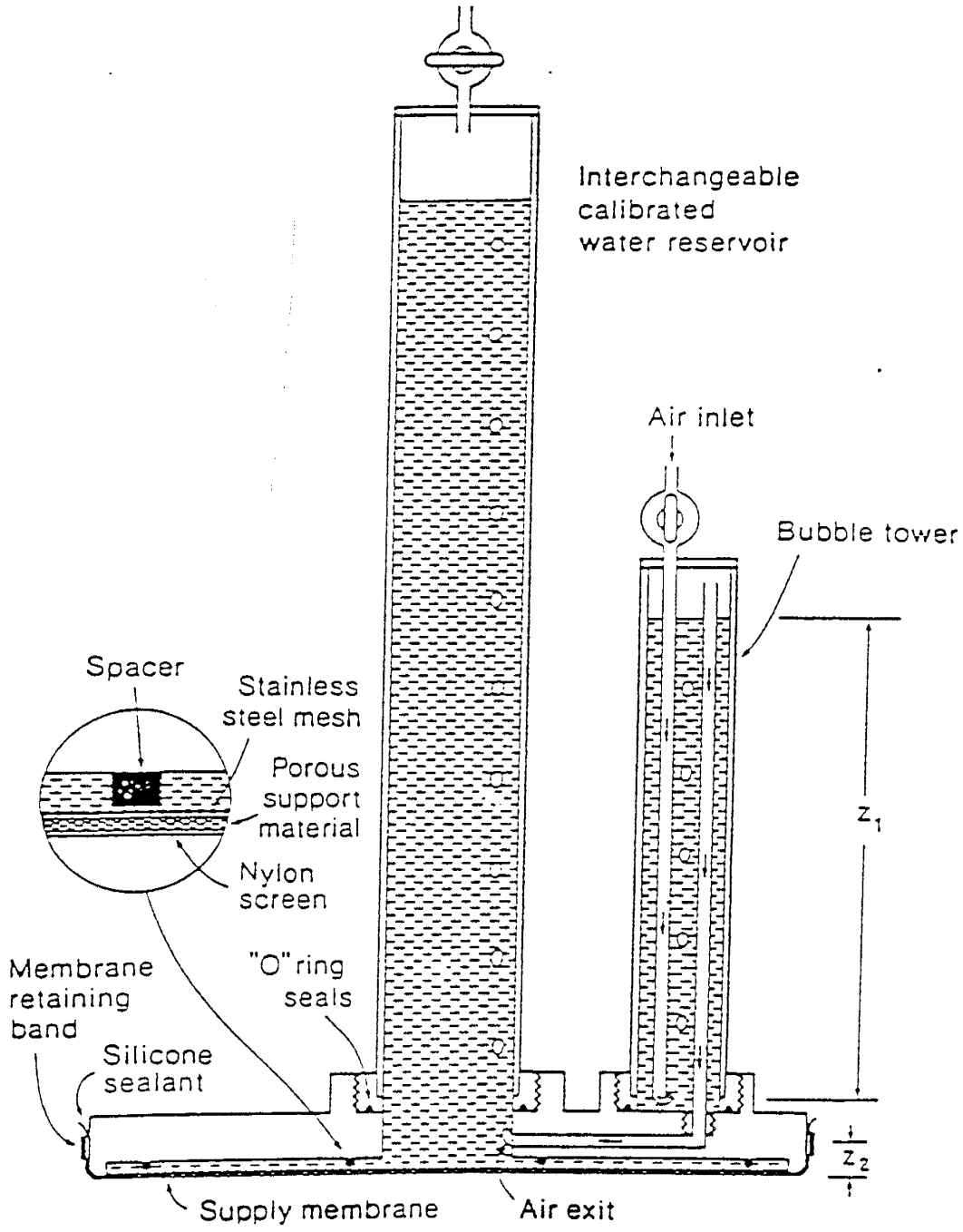

Figure 2-14 Schematic of the disc permeameter (after CSIRO Instruction Manual, 1988).

after trench construction. Firstly, the disc had to be soaked in water for several hours prior to measurements to ensure an airtight fir. The desired tension was fixed by raising or lowering water in the bubbling tower. The supply pressure at the membrane was calculated by Z = z2-z1. Z2 was fixed for each disc and was 0.7 mm for this particular disc. Therefore, z1, the height of water in the bubbling tower above the air inlet, was used to set the desired pressure. The measurement site was prepared by removing the vegetation and large rocks, and by levelling the soil. The impact of the capping material was discussed by Schmidt-Petersen(1991).

The filling of the permeameter reservoir was described in the instruction manual (CSIRO, 1988). Measurements commenced as soon as bubbling begins in the tower after placing the disc firmly on the contact material. Infiltration was recorded with time as quickly as possible during early infiltration. Measurements of consecutive 0.5 cm changes in water level were effective in this study for sorptivity determinations, although not always possible for the highly conductive water-laid deposits.

The steady state flow rate decreased as pressure increased in the fine sand above the cobbles. Using the late time infiltration data as the steady state flow rate resulted in a negative calculated hydraulic conductivity. It is not known if the water was obstructed from flow through the cobbles due to a decreased flow volume or a higher matric pressure in the cobble layer. Such an occurrence was not seen in other locations at this site.As water was infiltrating into the silty to gravelly matrix, it was diverted to different

directions by the embedded cobbles.

2.4.2 Results and Analysis

Tables 2-5 and 2-6 show the results from the disc permeameter infiltration, the particle size distributions, bulk densities used and calculated, and the moisture content results taken from the six deep trench sample locations. The results for the initial and final (or saturated) samples at each location are shown.

The grain size distributions nicely reflect the geologic unit descriptions from Section 3.0. The largest d10 through d60 sizes are found in the water-laid deposit and the debris flow. The fluvial sand with clay has the smallest d10 through d60 of all of the units while sample 5 from the intermediate unit had intermediate grain sizes.

Volumetric moisture content or porosity for these samples ranges between 26% and 57% with bulk densities of 1.5 g/cm^3 and 1.64 g/cm^3 (Parsons, 1988) being used in the calculations.

As seen in Table 2-6 the Ksat varied between 1.05×10^{-2} cm/s and 3.31×10^{-4} cm/s. The fluvial sand had the highest hydraulic conductivity while the clayey fluvial sand sample had the lowest Ksat. The water-laid deposit and debris flow had surprisingly low Ksat; 5.90×10^{-4} cm/s and 3.31×10^{-4} cm/s, respectively. These values confirmed the existence

Table 2-5

Disc Permeameter/ Deep Trench Samples

Sample	Geologic Unit*	d10 (mm)	d30 (mm)	d50 (mm)	d60 (mm)	Bulk Density (g/cc)	Gravimetric Moisture Content%	Volumetric Moisture Content%
TR1i	4	0.155	0.427	1.00	1.738	1.64	2.8	4.59
TR1f	4	0.123	0.245	0.347	0.417	1.64	21.87	35.87
TR2i	5	0.050	0.089	0.158	0.204	1.5	3.24	4.86
TR2f	5	0.050	0.102	0.162	0.200	1.5	22.95	34.43
TR3i	5	0.045	0.079	0.141	0.178	1.5	2.37	3.56
TR3f	5	0.045	0.071	0.100	0.126	1.5	38	57
TR4i	6	0.151	0.407	0.832	1.202	1.5	1.02	1.53
TR4f	6	0.091	0.302	0.759	1.122	1.5	17.52	26.28
TR5i	Rio Gr.	0.069	0.105	0.135	0.151	1.64	1.27	2.08
TR5f	"	0.066	0.112	0.148	0.166	1.64	25.01	41.02
TR6i	"	0.066	0.032	0.126	0.141	1.64	2.25	3.69
TR6f	"	0.065	0.095	0.135	0.158	1.64	25.24	41.39

* Described in Section 3.3

Table 2-6

Disc Permeameter Saturated Hydraulic Conductivity Values

Sample	Geologic Unit*	Geologic Description	Sorptivity ($cm/min^{1/2}$)	Steady State Flow Rate (cm/min)	Ksat (cm/s)
TR1i	4	Water-laid	2.17	0.81	$2.0E^{-04}$
TR1f	4	"			
TR2i	5	Silty Intermediate	1.03	0.36	$1.9E^{-03}$
TR2f	5	"			
TR3i	5	"	0.53	0.20	$2.7E^{-03}$
TR3f	5	"			
TR4i	6	Debris Flow	1.50	0.57	$3.3E^{-04}$
TR4f	6	"			
TR5i	Rio Gr.	Fluvial Sand	1.81	0.91	$1.1E^{-02}$
TR5f	"	"			
TR6i	"	Clay/Fluvial	1.23	0.30	$3.7E^{-04}$
TR6f	"	"			

* Described in Section 3.3

of a fine matrix in both of the deposits which would indicate a strong effect on fluid flow by the matrix of an otherwise fairly coarse grained deposit. The silty intermediate unit exhibited intermediate Ksat values in the $2x10^{-3}$ cm/s range.

2.4.3 Error and Bias

Measurement limitations are discussed in detail by Schmidt-Petersen (1991) and will be summarized briefly here. Firstly, the disc permeameter in its present form is limited to hydraulic conductivity determinations ranging from approximately $1.0x10^{-5}$ cm/s. The accuracy of measurements is greatly reduced for coarse textured, high conductive materials. In fine, textured, low hydraulic conductivity materials outside influences such as any exposure to sunlight have a profound influence on the infiltration results.

The capping material used during the measurements was used to ensure good contact of the disc base with the soil surface. This material should have a high sorptivity and conductivity, but a weak dependence on the supply pressure. Fine sands of the Rio Grande facies were used as cap material and the dependence of the results on the cap material used is discussed further by Schmidt-Petersen.

Finally disc permeameter theory assumes that the porous media being tested are initially devoid of moisture and that the flow from the disc is into a homogeneous isotropic porous medium. The silty mudflows and the clay layer within Sample 6 have some initial

moisture content assumed to be remnant from past irrigation experiments. In addition the sample locations consisted of heterogeneous material. According to Schmidt-Petersen, stratification of moisture content does appear to affect hydraulic conductivities but the impact on the characteristic mean pore size is less certain. Material heterogeneity and anisotropy have little apparent effect on the calculated hydraulic conductivity when compared with laboratory results. It is concluded that the disc permeameter is a reasonable device for estimating effective horizontal hydraulic conductivity in relatively dry soils over at least the above mentioned range of saturated hydraulic conductivities.

2.5 MAPPING AND PHOTOGRAPHY

Field mapping and photography were employed during the geologic characterization. The shallow and deep trenches required mapping and photography for a better understanding of the alluvial fan units found at the site.

2.5.1 Procedure

The trenches were constructed during two different time periods. The locations of the trenches are shown in Figure 1-6. In October, 1989 a backhoe was employed to dig two-thirds of the shallow trench. The interior section of the plot was left intact due to continued drainage monitoring. The dug out section of the trench was covered with plastic each evening to limit evaporation and rainfall impact. In January, 1990 a backhoe

was used to complete the shallow trench. It was dug perpendicular to the interpreted lateral flow direction (which was from southwest to northeast) and at the dripline depth. The final length of the shallow trench was approximately 40 m and the depth was 1.5 m below datum. At this time the backhoe was also used to dig the deep trench in the northeastern corner of the site as seen in Figure 1-6.

The deep trench was located in a region in which monitoring equipment showed lateral water movement (discussed further in Section 4.1) and the depth was to be at least down to the alluvial fan/fluvial sand contact. The western wall of the shallow trench was mapped from the ground surface down to the base of the trench, using the Unified Soil Classification system and the Munsell Color Chart. The contacts between units, structures, and fining and upward and downward fining sequences were drawn with respect to a scale that was extended all along the bottom of the trench. The various units were sampled at regular intervals and inspected with respect to the Unified Soil Classification system and compared to the Munsell Color Chart. The emphasis of this study was to describe and understand the nature of the alluvial deposits near the surface and to relate the textural patterns and structures to the alluvial units discussed in Section 3.

Photography and mapping were used to describe the western wall of the deep trench. After cleaning off the wall to remove slough and to accentuate structures, the deep trench wall was cordoned off with ribbons that hung down vertically along the trench wall

suspended from the datum 1.5 m (5 feet) apart. In addition, ribbon was nailed horizontally onto the outcrop 1.5 m apart to create 1.5 by 1.5 m blocks. These blocks were labeled and photographed from two different distances. These blocks were then mapped by drawing the structures and textural changes within each block. The block drawings were then put together and the composite was taken into the field to compare with the outcrop. Units that had been wetted by the infiltration events were drawn in. Contacts between units and the nature of the matrix in each unit were noted. The photographs and maps were used to produce a figure showing the arroyo units in the northeastern part of the site as shown in Figure 3-4.

2.5.2 Results

The results of the mapping and photographic efforts are represented by the two trench wall maps shown in Section 3.3 and the photographs shown in Sections 2.4 and 3.3.

2.6 HYDRAULIC PROPERTIES OF DEEP CORE

The third way to find saturated hydraulic conductivity was to take cores from the shelby tubes described in Section 2.4. A constant head tank was used to find saturated hydraulic conductivity. The cores were also used to find bulk density, porosity, saturated water content, and d10 size. These parameters were used to characterize the hydraulic properties that controlled unsaturated flow through the Rio Grande fluvial facies.

The two 100 cc sample cores that were extracted from each shelby tube from the ENE borehole were subjected to various laboratory procedures to determine hydraulic properties. These samples come from depths of up 20 meters. Bulk density (g/cm^3), porosity (cc/cc), saturated hydraulic conductivity (cm/sec), hanging column/15 bar pressure plate soil moisture characteristic curve, and particle size distributions were ascertained for the 38 sample cores. The hanging column analyses are not included since many of the results were plagued with errors; the errors stemmed from lack of suction to the porous plate as a results of voids in the samples from cobbles and/or due to air in the lines. The particle size methodology is described in Section 2.2 and the results for the ENE samples are discussed below. All laboratory results for ENE sample cores are tabulated in Appendix C. Four of the 38 samples were from within the piedmont facies and 34 were from the Rio Grande sand facies.

2.6.1 Bulk Density (g/cc)

Dry bulk densities were calculated using (Hillel,1980a):

$$\rho_s = M_s/V_t$$

ρ_s = bulk density (g/cc)

M_s = mass dried soil (g)

V_t = total volume (cc)

The samples were dried in a 105 C oven (Fisher, Econotemp, model #30F) for at least 24 hours and then weighed upon removal to the nearest 0.01 g. Samples with dry volumes less than 100 cc were evaluated to ascertain the actual volume. The sand was loosely pored into the ring and levelled. The sand was transferred to a volumetric cylinder and the deficient volume determined. Parsons (1988) calculated average dry bulk densities for each major soil type at the site with a piedmont slope material average of 1.5 g/cm^3, 1.37 g/cm^3 for the clays and 1.64 g/cm^3 for the fluvial sands. Schmidt-Petersen (1991) showed an average bulk density of 1.5 g/cm^3 for units 2 and 3 of the piedmont facies. Both studies showed a normal distribution for the bulk density at the site.

The bulk densities from the ENE cores also show a normal distribution with a mean of 1.5 g/cm^3 and a standard deviation of 0.151. Since these samples predominantly consist of fine sands, silty sands and clays, this is a very reasonable average value. It is expected that the bulk density distribution is normal. Figure 2-15 shows the geologic profile next to the bulk density profile of ENE in the fluvial section. The distribution does not show any correlation as seen in the variogram in Figure 2-16. The nugget that that is shown with a value of 0.009 is an indication of measurement error, which may possibly account for the lack in vertical correlation. Measurement error may be explained from the voids in the 100 cc rings that resulted from the dragging of cobble pieces during sampling. An explanation for the lack of vertical correlation may be that the matrix material changes consistency throughout the profile; from clay to gravel size particles.

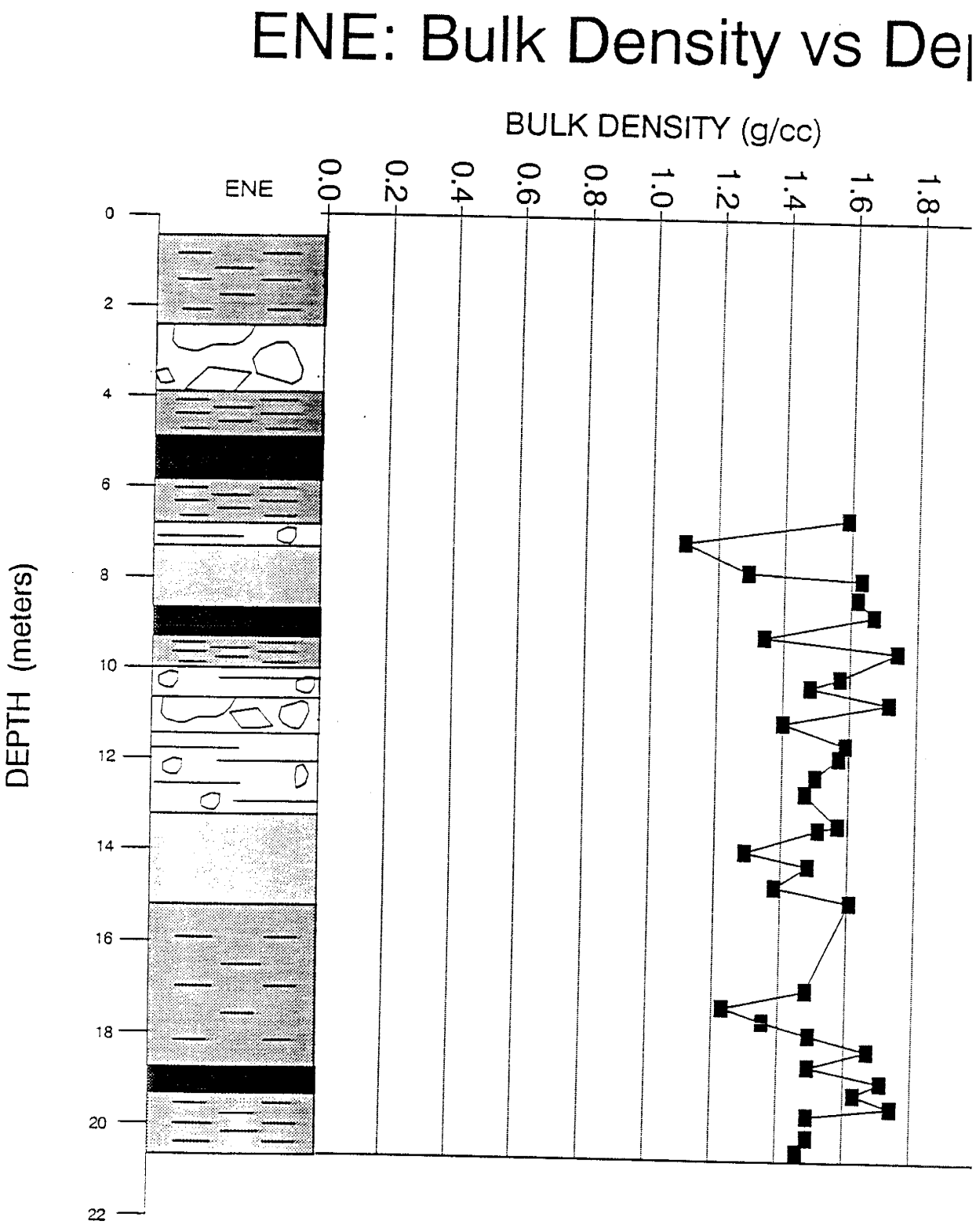

Figure 2-15 ENE: bulk density vs depth.

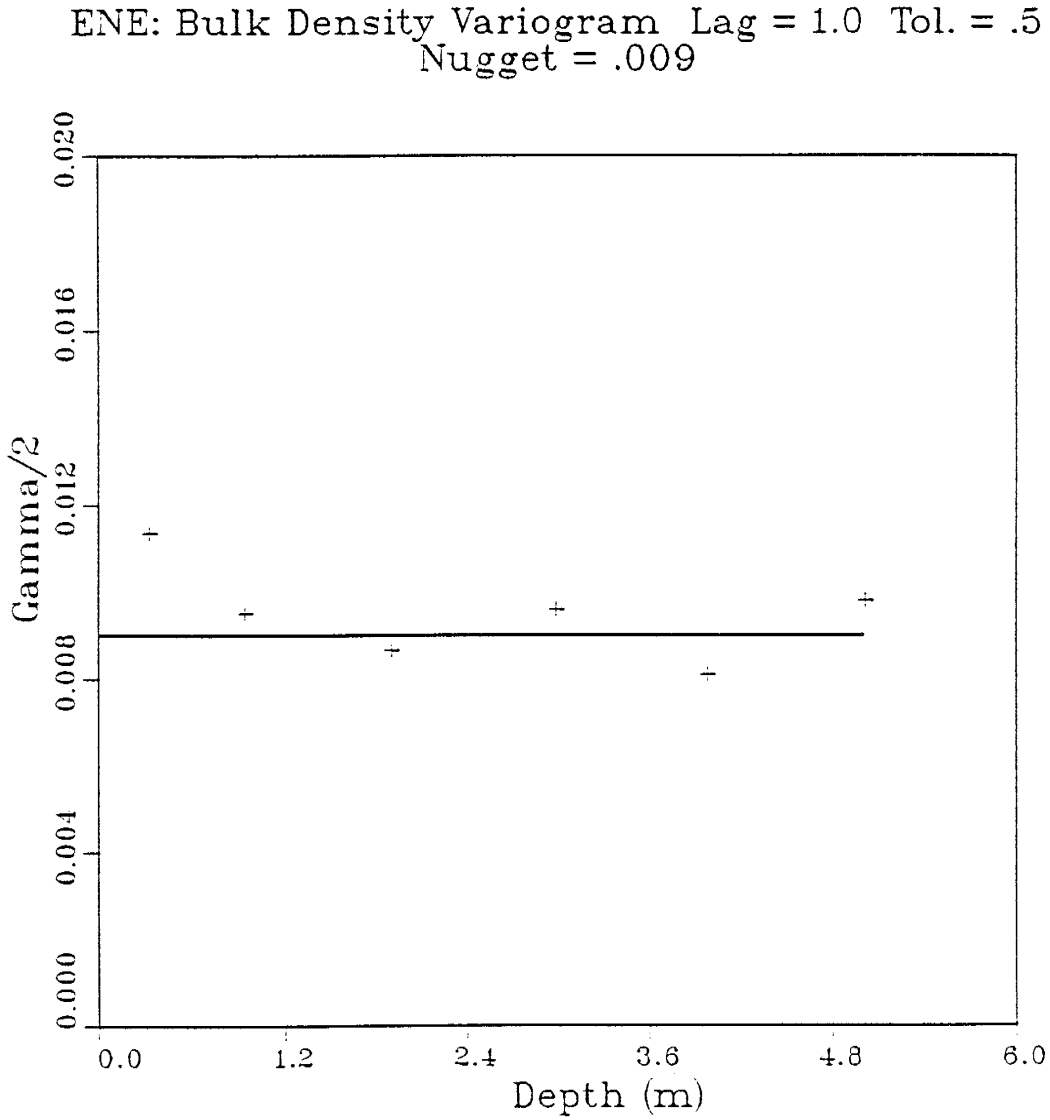

Figure 2-16 ENE: bulk density variogram.

2.6.2 Porosity (cc/cc)

Porosity was determined from the saturated moisture content and the calculated total porosity. Total porosity is calculated using n= 1-ps/pb where n is the calculated porosity, and the particle density (g/cm^3) which is assumed to be 2.65 g/cm^3. Because particle density can vary with soil type, some error is incorporated in the calculated porosity values. The calculated porosities from the ENE cores range from 34% to 58% with an average of 43%. The geologic profile is consistent with the porosity profile as seen in Figure 2-17. These profiles show that the greater the grain size (or the less clay), the larger the porosity value. The distribution can be described as being uncorrelated with a linear trend. It is not unusual to see a vertical porosity profile that is not correlated since porosity may be inhibited by primary or secondary causes. An example of a secondary cause is caliche or pores that have been filled in with a calcite-based fluid after the bed has ben deposited. Such secondary alteration would inhibit vertical correlation from bed to bed in porosity. Figure 2-18 shows the variogram for these samples. The average porosity for the sands in previous work (Parsons, 1988) was 36%.

2.6.3 Saturated Water Content

Saturated moisture contents were estimated by saturating the 100 cc rings in distilled water and weighing prior to pressure plate testing. Error is encountered due to possible

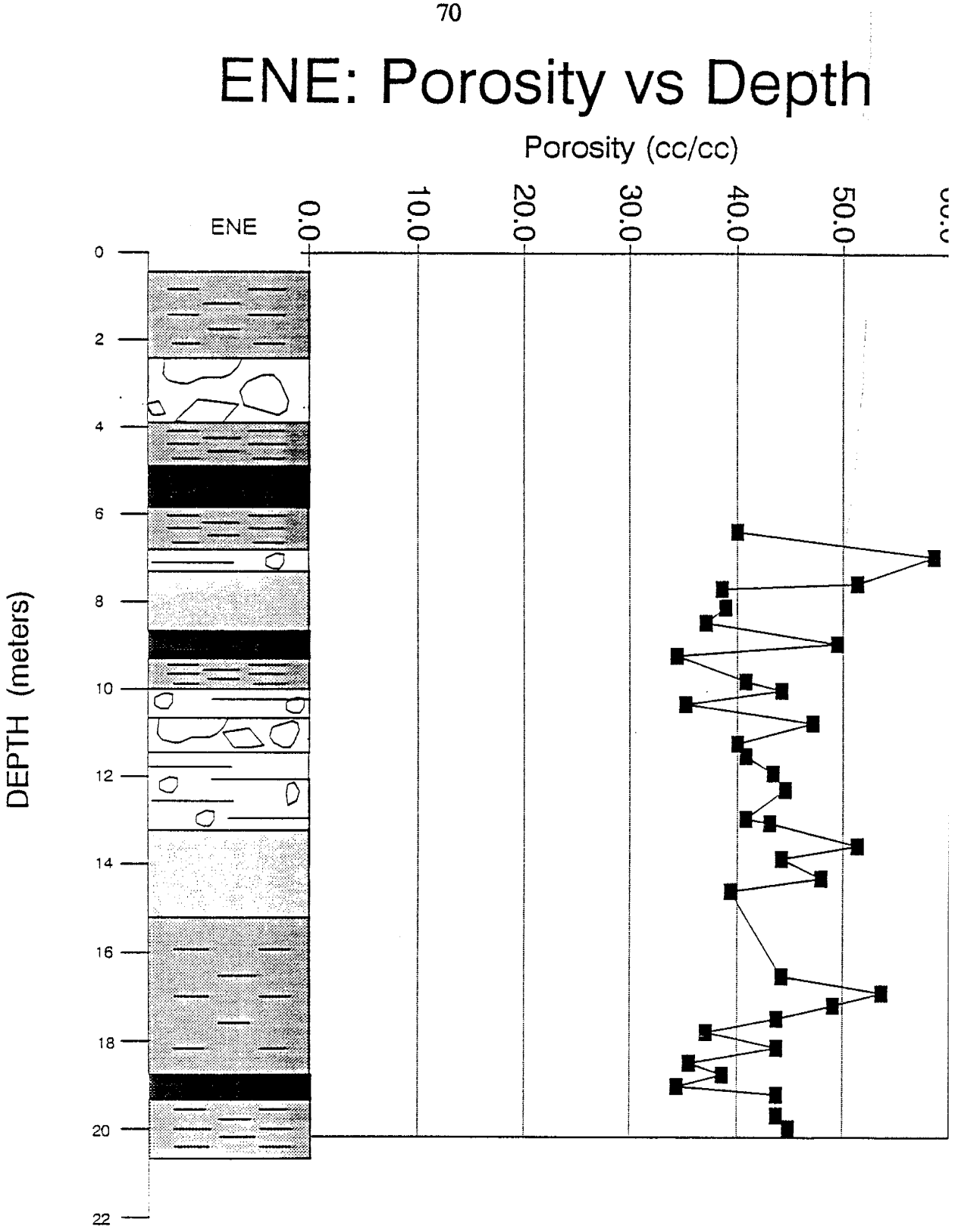

Figure 2-17 ENE: porosity vs depth.

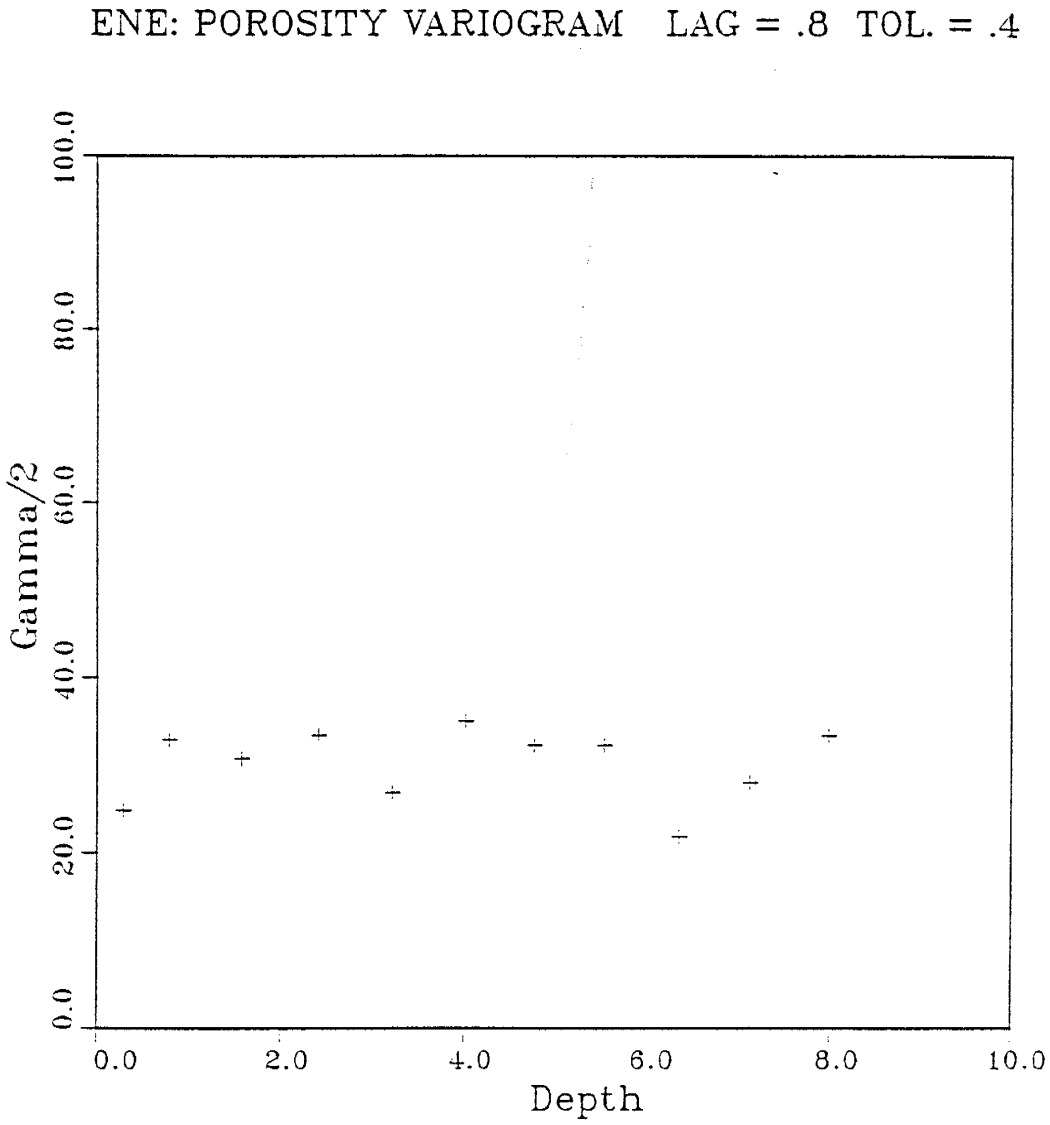

Figure 2-18 ENE: porosity variogram.

entrapped air in the core sample. Saturated moisture content is a direct measure of the water in an individual soil sample. Saturated water content for the fluvial cores showed an average of 42.8%. Figure 2-19 shows the geologic profile for ENE next to the profile for saturated water content. The lowest saturated water content is seen at around the depths of the clay layers. The variogram in Figure 2-20 shows a vertical correlation in saturated water content within the fluvial sands with a correlation length of one meter and a nugget of 1.75. This result agrees very much with the correlation found for d10 size within the fluvial sands (Section 2.2). Previous average values of saturated water content were 43% and 36% (Schmidt-Petersen (1991) and Parsons (1988)).

2.6.4 Saturated Hydraulic Conductivity

Saturated hydraulic conductivity of the 100 cm^3 ring samples was estimated using a constant head apparatus (Eijelkamp, 6988 BG Latham, The Netherlands). Sample dimensions were known and steady state flow occurs within several days for most samples. At equilibrium, the samples were assumed to be saturated, with all entrapped air eliminated. Measurements were taken for several days to ensure equilibrium conditions. Volumetric saturated hydraulic conductivity is then calculated using Darcy's law.

Errors included possible channeling around rings that were not tightly connected to the ring holders during the operation of the constant head apparatus.

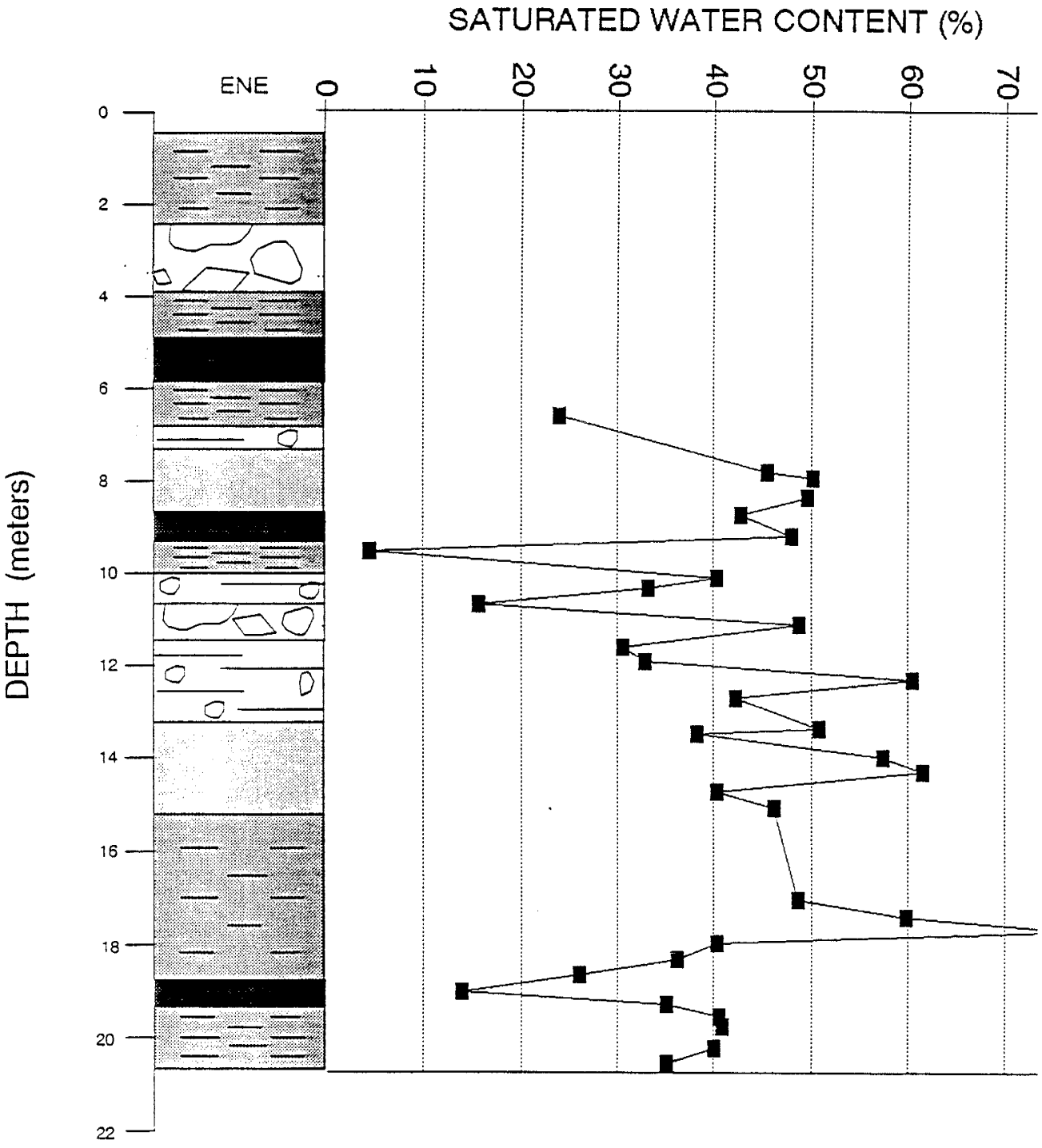

Figure 2-19 ENE: saturated water content vs depth.

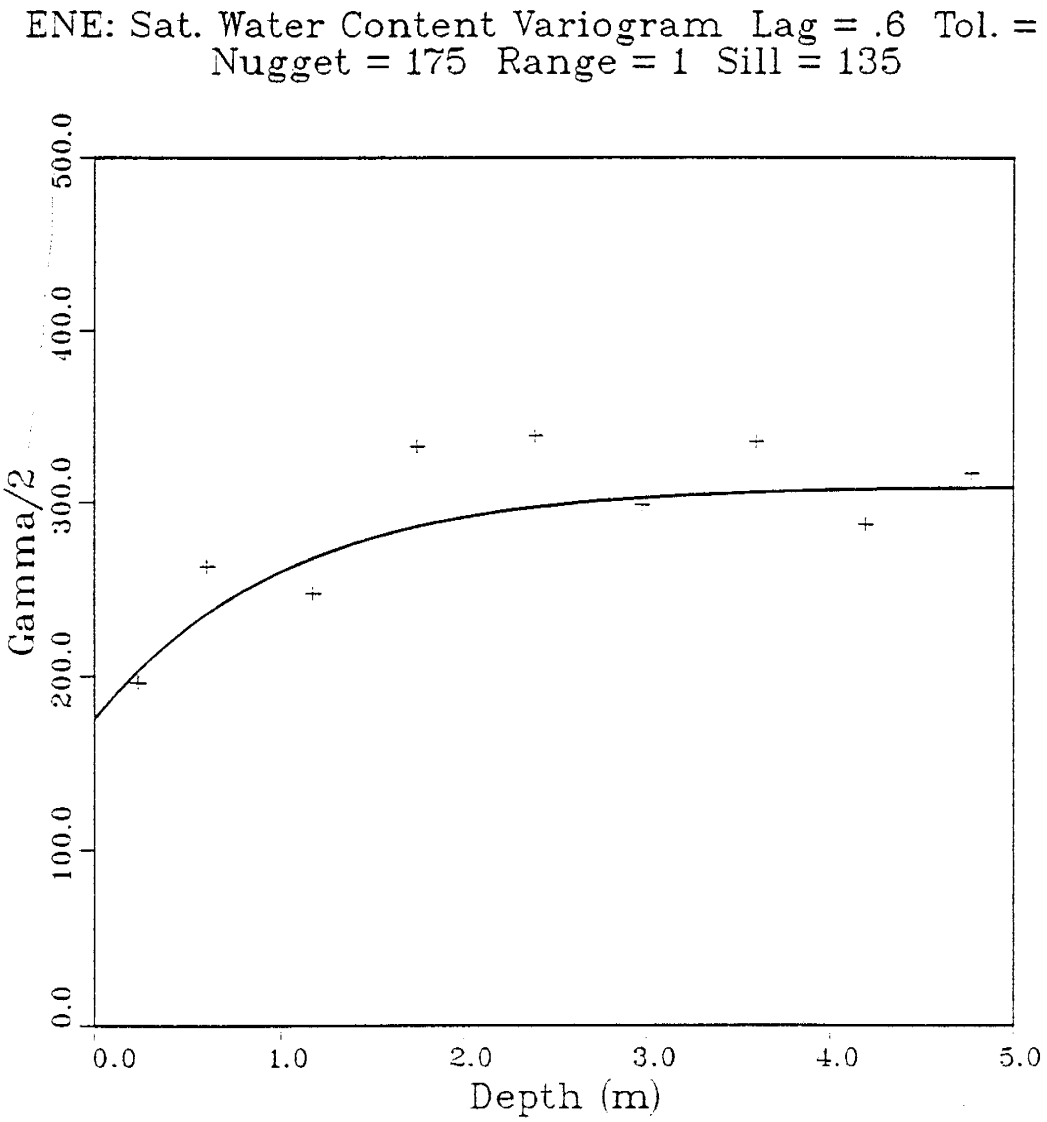

Figure 2-20 ENE: saturated water content variogram.

The hydraulic conductivity was log normally distributed as observed by Byers and Stephens (1983) and other researchers. The hydraulic conductivity is lowest for the finest material which is seen in Figure 2-21, a superposition of the ENE geologic log and the log Ksat profile. The ENE cores showed an uncorrelated log-normal distribution with mean log Ksat of -3.852 cm/sec (the arithmetic mean was $4.4x10^{-1}$ cm/sec for the fluvial sands in this study). The variogram for this distribution is presented in Figure 2-22. Previous (Parsons, 1988) Ksat values ranged from $2x10^{-1}$ cm/sec in coarse sand to $8.0x10^{-6}$ cm/sec in clays. The arithmetic mean for the piedmont slope had been $2.7*10^{-2}$ cm/sec and $3.0x10^{-2}$ cm/sec (or $2.0x10^{-4}$ to $3.7x10^{-4}$ cm/sec when log-Ksat) for the underlying fluvial sands. Schmidt-Petersen (1991) saw Ksat values of $2.13x10^{-1}$ cm/sec in the coarse sands near the southeastern end of the shallow trench and $4.24x10^{-7}$ cm/sec in silts and clays approx. 20 m along the bottom of the trench. The log-normal distribution in hydraulic conductivity conforms to the two previous investigations. As discussed previously (Schmidt-Petersen, 1991), it is not useful to present the arithmetic mean when the distribution is log-normal.

The lack in vertical correlation may be attributed to the sparsity of samples in the vertical direction for the ENE profile. It is also important to note that the fluvial sand facies is not homogeneous as there are occasional clay layers and cobble layers that are "randomly" interspersed within the sand.

ENE: Log Ksat vs Depth

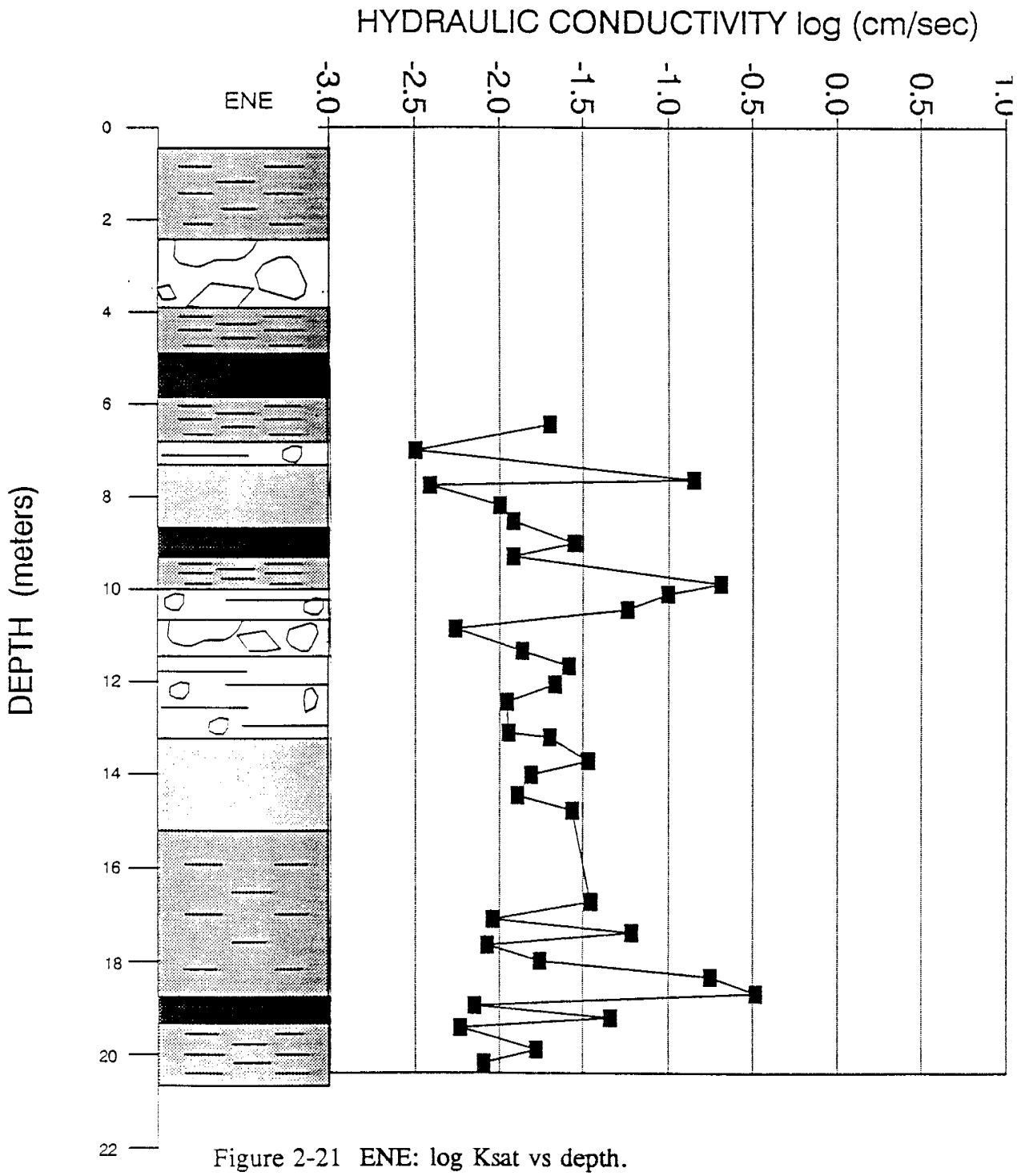

Figure 2-21 ENE: log Ksat vs depth.

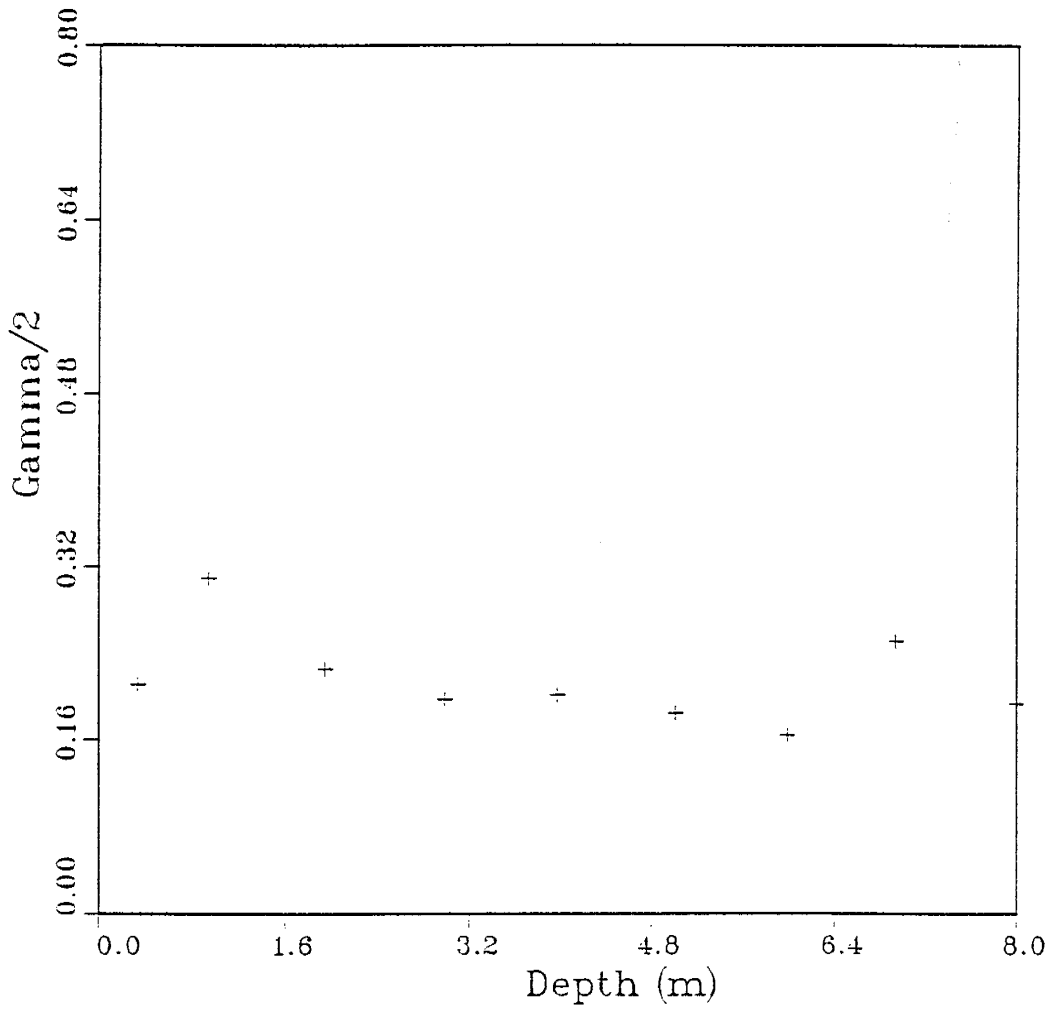

Figure 2-22 ENE: log Ksat variogram.

2.6.5 d10 size

The mean d10 size for the fluvial sands was 3.528 mm which included some unusually high values taken from the two cobble layers found in the shelby tubes. These unusually high values were eliminated from the data set for the variogram estimation shown in Figure 2-23. The ENE profile of d10 next to the stratigraphic column shown in Figure 2-24 shows a similar trend in grain size distribution. The d10 profile does not show the cobble layers or some of the gravel portions because the samples those particular samples contained the matrix between the cobbles, without the cobbles themselves.The spherical variogram model that has been fit to the d10 distribution shows a correlation of under one meter long and a nugget of 0.002.

It is expected that saturated hydraulic conductivity and d10 size may be correlated but in this case they are not. d10 size and saturated water content are nicely correlated with similar vertical correlation lengths. As mentioned earlier this may be due to the amount of samples required for full characterization of hydraulic conductivity or due to experimental error. Hydraulic conductivity was found to be correlated in the horizontal direction by Schmidt-Petersen (1991) within the alluvial fan facies at this site but these samples were collected at a much finer spacing than the ENE samples. This would lead us to believe that the vertical spacing was not fine enough for the hydraulic conductivity measurements. For further information, the structure, thickness, and matrix of the individual layers are discussed in detail in Chapter 3.

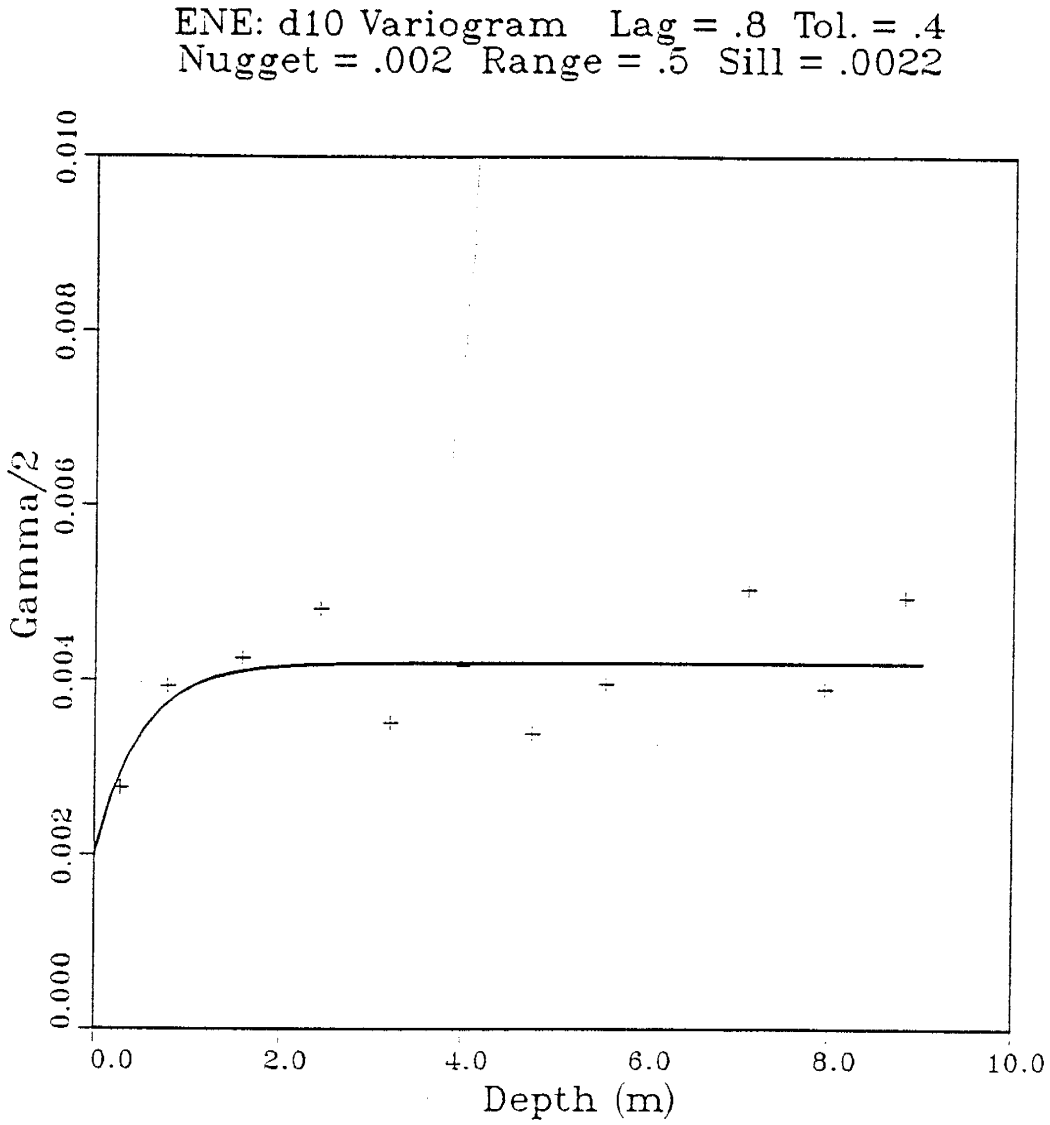

Figure 2-23 ENE: d10 variogram.

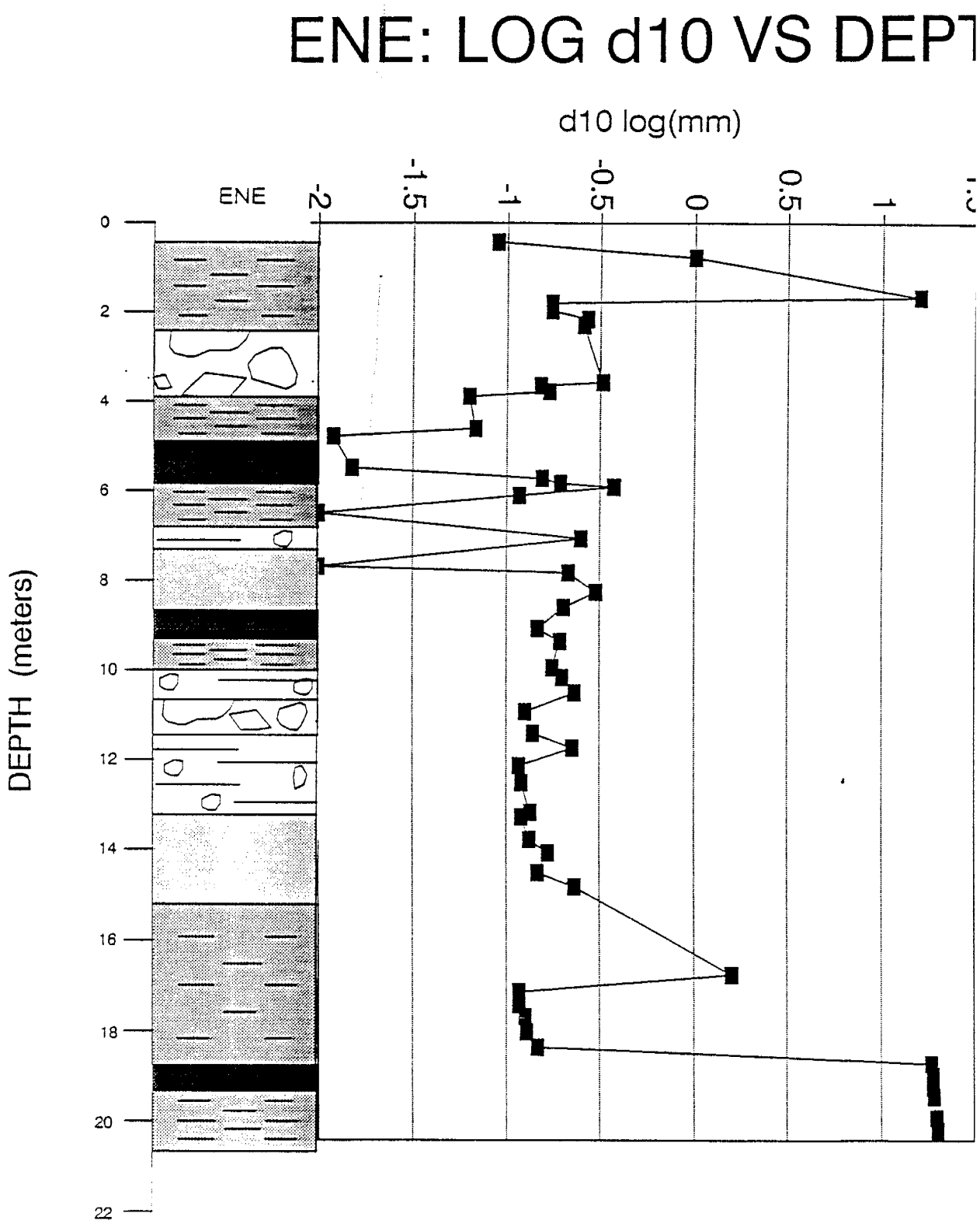

Figure 2-24 ENE: log d10 vs depth.

The results from the 34 fluvial samples were analyzed using the USEPA geostatistical software, GEOEAS (Englund and Sparks, 1988), and a geostatistical package called gamv3 (Deutsch and Journel, 1991) with results discussed below.

Table 2-7 shows the batch statistics for these fluvial samples using GEOEAS as compared with the statistical results for other soil samples analyzed at the site. The previous studies listed in this table include Schmidt-Petersen's (1991) alluvial samples collected from the floor of the shallow trench and Parsons' (1988) alluvial and fluvial samples collected during the original drilling phase.

Table 2-7

Hydrologic Properties of ENE core samples: Batch Statistics

Variable	Bulk Density (g/cc)	Nc[1] (%)	S.W.C[2] (%)	Ksat (cm/sec)	d10 (mm)
CURRENT STUDY: ENE fluvial sands					
Mean	1.51	43.0	42.8	0.0213	3.53
Variance	0.023	32.4	305.7	1.3	53.10
Coeff. of Variation	9.988	13.2	40.9	29.6	206.55
Skewness	-0.613	0.613	0.75	0.65	1.70
Kurtosis	3.156	3.156	5.27	2.87	3.89
Number of Samples	34	34	34	34	34
SOIL CORE SAMPLES: Alluvial Fan Material					
(Schmidt-Petersen,1991)					
Mean	1.496	43.5	40.76	0.018	
Variance	0.011	0.1	39.57	0.527	
Coeff. of Variation	7.01	9.08	15.43	18.9	
Skewness	-0.296	-0.296	16.92	3.83	
Kurtosis	0.25	-0.251	-3.315	-.271	
Number of Samples	102	102	102	100	
ALLUVIAL FAN MATERIAL (Piedmont Slope Facies)					
(Parsons, 1988)					
Arithmetic Mean	1.5	43.4	42.3	0.027	
Variance	0.03	38.9	62.8	0.005	
Coeff. of Variation	11.3	14.4	18.7	270.0	
Number of Samples	68	68	67	66	
FLUVIAL SAND FACIES					
(Parsons, 1988)					
Arithmetic Mean	1.7	36.0	37.1	0.030	
Variance	0.01	20.6	54.4	0.003	
Coeff. of Variation	7.1	12.6	19.9	190.0	
Number of Samples	21	21	20	15	

[1]Nc = Calculated porosity
[2]S.W.C. = Saturated water content
Ksat = Saturated hydraulic conductivity

3.0 INTERPRETATION OF THE GEOLOGIC FRAMEWORK

Now that we have quantitatively described the material that the water has drained through, it is necessary to describe those forces that have geologically shaped this material and it is necessary to describe in detail the layers encountered during the drainage. If those forces described in the sections below can be tied to a certain type of geologic product that controls the drainage of water through it in a particular way, then we have achieved some measure of predictability.

The geologic characterization of the study area has been investigated on 3 major scales. The pertinent depositional history of the middle Rio Grande valley is reviewed in Section 3.1 to establish the origin of the alluvial and fluvial environments encountered in the intermediate and small scale geologic investigations. The hydraulic vertical characterization study discussed in Section 2.0 focuses on the heterogeneous alluvial piedmont slope facies, therefore the intermediate scale geologic investigation of Section 3.2 is centered on describing and classifying this alluvial fan environment. The small scale investigation discussed in Section 3.3 describes the geology beneath the site as applied toward textural control of fluid transport through the unsaturated zone. A geologic time scale is included in Appendix D. The site was mapped as described in Section 2.4.

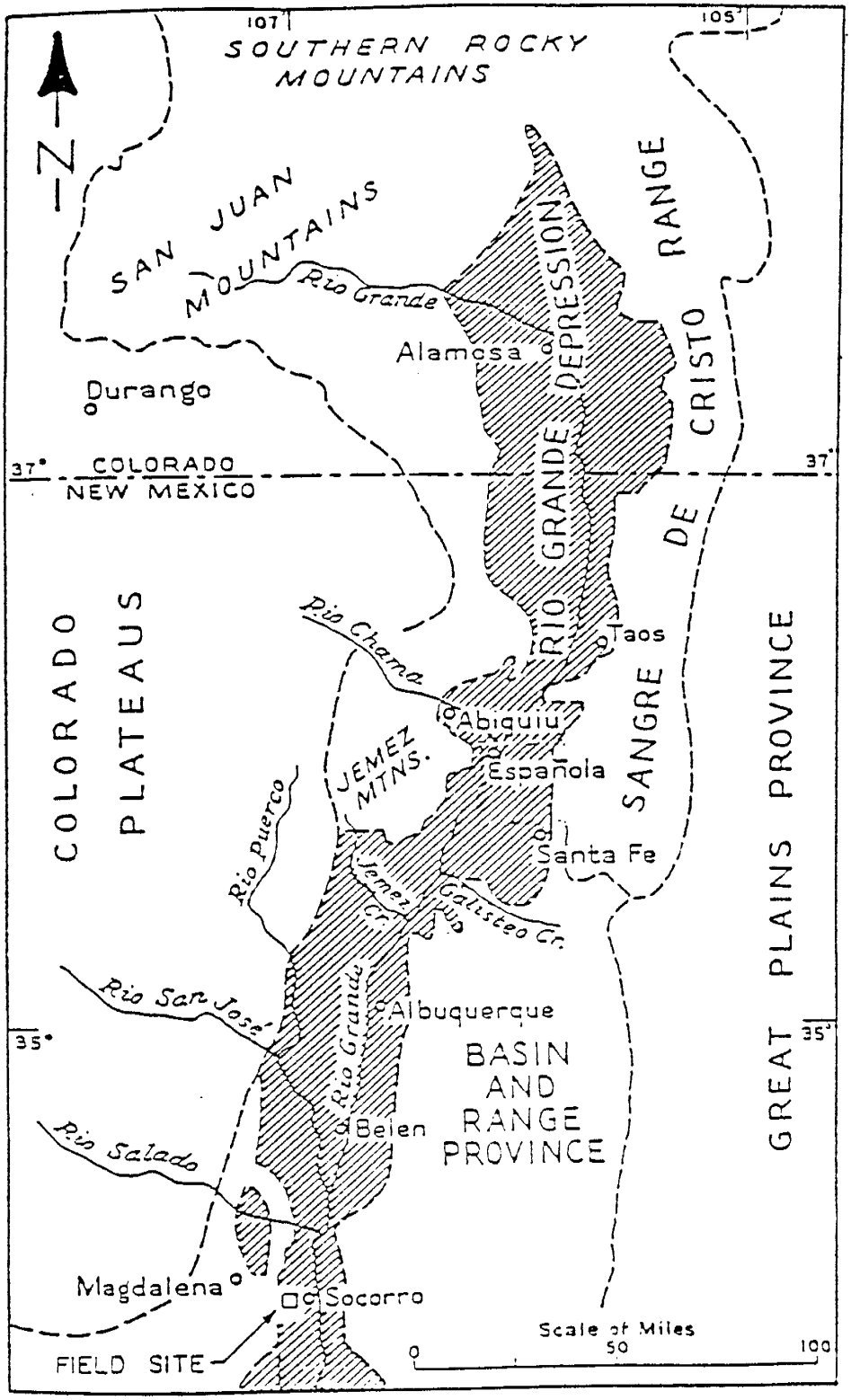

Figure 3-1 Rio Grande depression (after Denny, 1940).

3.1 LARGE SCALE: DEPOSITIONAL HISTORY

The experimental field site is located in the eastern most part of the Basin and Range Province within the Rio Grande Depression as shown in Figure 3-1. The field site is underlain by alluvial and fluvial sediments of the Sierra Ladrones Formation (Fm), the upper subdivision within the Santa Fe Group in central New Mexico. The following is an account of the regional depositional history, and a summary of the history of geologic classification in the middle Rio Grande valley with a view of where the field site fits into these classifications.

3.3.1 Geologic history and local evidence

The Rio Grande Depression extends from central Colorado south to El Paso, Texas. In central New Mexico, the Rio Grande flows through a series of north-south trending structural basins which are underlain by Tertiary rocks and bordered in most places by highlands of older rocks. The valley is semiarid, precipitation ranging from tens on the piedmont to twenties in the highlands. The alluvial fan surfaces rise steplike above the river and have been described as primarily stream-eroded surfaces graded to a successfully lowered base level, the Rio Grande.

The lithologic composition of upper Santa Fe Group basin fills and post-Santa Fe valley fills reflect major structural and topographic elements of the Rio Grande rift that had

formed by early Pliocene time (Chamberlain, 1980). The erosional valley of the Rio Grande, formed since mid-Pleistocene time, was the only major geomorphic feature not yet present. Previous deposits of volcanic basins, the bolson-fill facies and intrarift basins of the upper Oligocene-Miocene Popotosa Fm, are deeply buried in this area: they reflect Laramide-formed terrains largely obliterated by erosion, sedimentation, and structural deformation in the past 10 million years (m.y).

Sometime after 7 m.y. and before 4 m.y. ago, the Popotosa basin had been disrupted by extensional forces breaking it into fault block uplifts and grabens (Chapin and Seager, 1975). A combination of rifting and contemporaneous epirogenic uplifting of the southern Rocky Mountains and adjacent areas may explain the development of modern mountain ranges in the Socorro area at this time (Chamberlain, 1980). Extensive pediment surfaces were carved across uplifted and tilted beds and older rocks. Alluvial fan material was deposited into the Socorro basin on the east, forming part of the lower Sierra Ladrones Fm. Concurrently, the regional drainage system integrated the Rio Grande River into the Socorro basin. The river flowed along the eastern edge of the basin from San Acacia to San Antonio (Debrine, 1963). Broad, gently sloping pediment plains graded into the tan well-sorted, arkosic sands and muddy overbank facies of the ancestral river. As regional uplifting occurred, an eastward prograding wedge of alluvial fans shed by the developing western mountain front caused the ancestral Rio Grande to retreat to the east, burying the older fluvial sands in the Socorro basin.

Early Sierra Ladrones facies do not indicate the presence of significant relief where the modern Lemitar, Socorro, and Chupadera mountains now exist; however ,the coarsening sequence of mud, silt, sands, and gravels of this formation indicate an increase in topographical relief since late Miocene or early Pliocene time (approx. 4 to 7 m.y.a.). Younger Sierra Ladrones piedmont slope gravels can be directly related to modern topography (Chamberlain, 1980).

The diagrammatic cross-section in Figure 3-2 from the Magdalena Mountains (southwest of Socorro) to the vicinity of Loma de las Cañas, east of the Rio Grande illustrates the complex history of late stages of basin filling and the episodic nature of middle to late Pleistocene valley cutting. The earliest axial-river deposits during the early Pliocene (or between 3 and 5 m.y. ago) were apparently emplaced along the western margin of the basin and are now partly incorporated in the uplifted Socorro Mountain block (Chamberlain, 1980). The site is located approximately 2 miles west of the Rio Grande therefore lying above a unit of tributary arroyo facies with axial-river facies below.

Between 1.5 and 0.5 m.y., the ancestral Rio Grande had again shifted westward to a position just west of the present valley in the Socorro-Escondida area. Volcanic ash from caldera-forming eruptions in the Jemez Mountains between 1.1 and 1.4 m.y.a. is present in axial-river deposits of the Sierra Ladrones Formation exposed in the Lopezville Road gravel pit about 1 mile north of the New Mexico Tech campus. Tephra from these eruptions is also present in Sierra Ladrones fluvial facies about 3 miles NE of San

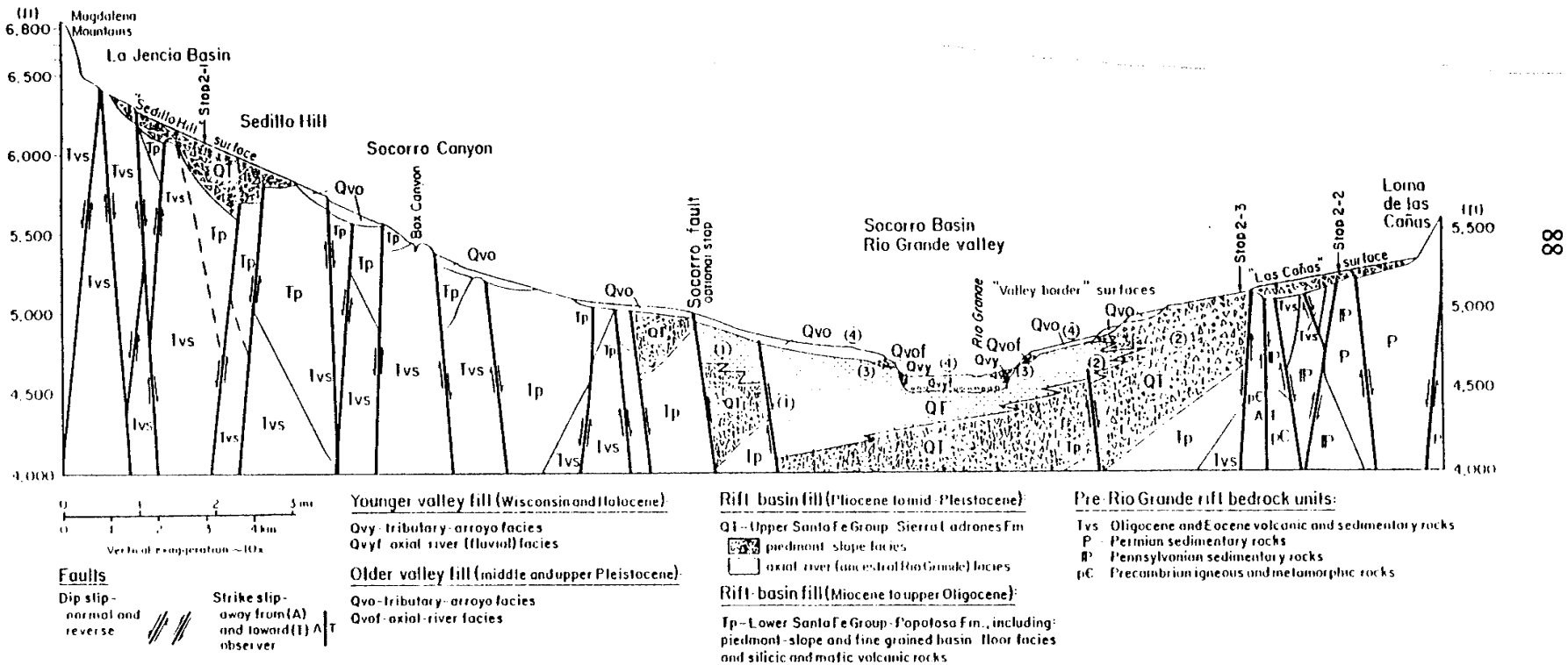

Figure 3-2 Diagrammatic cross-section near Socorro (after McLemore and Bowie, 1987).

Antonio. Culmination of basin filling and the end of Santa Fe Group deposition occurred about 0.5 m.y.a. throughout the Albuquerque to El Paso region (Hawley et al., 1976).

The Rio Grande system was internally drained until the capture of the ancestral Rio Grande at El Paso in middle Pleistocene time or 300,000 - 500,000 y.a. (Kottlowski, 1958). This event lowered the river's baselevel throughout its course, creating deep entrenchment into earlier deposits. The highest outcrops of the ancestral Rio Grande surfaces in the Socorro area are about 180 meters above the present floodplain, due to entrenchment and localized effects of rifting (Chapin and Seager, 1975). Quaternary cycles of erosion and deposition correspond with the stage of recent glaciations (Chamberlain, 1980). These events are evident in the stepped landscape of broad piedmont surfaces, terraces, (Qvy), and entrenched arroyos (Qvo) in the Socorro area. Much of the eastern slopes of Socorro Peak are covered by a thin mantle of surficial deposits of Quaternary age consisting of alluvial fan and piedmont slope deposits resting unconformably on broad pediment surfaces, landslide deposits, colluvium, and young alluvium in arroyo flows, valley bottoms, and low drainages.

Valley landforms represent at least four major events of river entrenchments separated by periods of partial valley backfilling or relatively steady-state conditions in terms of local flood plain base levels. Along most of the river's course through the area, the boundary between the valley floor and sideslope is marked by a low bluff or scarp, here designated the inner-valley scarp (Chamberlain, 1980). This erosional landform is the

product of river trimming of the valley sides whenever the laterally shifting channel or flood flow impinges upon them. The site exists on the outer limits, or rims, of the valley which vary considerably in terms of distinctiveness and regularity. The extensive remnants of graded surfaces flanking the inner Rio Grande valley in this region represent not only early valley degradational stages, but also long periods of valley-floor aggredation or relative gradational stability. The latter intervals probably reflect interglacial environments of the type exhibited in the Holocene (past 10,000 years) when tributary (or arroyo) drainage systems delivered more sediment to valley floors than master streams could remove from the middle Rio Grande basin.

In this discussion, the piedmont refers to the plain with locally complex topography that slopes from highland to playa or floodplain. The piedmont is an important part of the arid landscape of the Basin and Range province. Part of a piedmont may be more or less a bare rock surface, a pediment. Part is alluvium, and if its surface has the form of a section of a very low cone it is a fan. This fan-forming alluvium produces washes or arroyos.

The term arroyo is used throughout the project region (and many parts of the Southwest) to designate the channels of ephemeral streams, particularly those with broad, flat floors and vertical walls several feet or more in height. Valleys of these tributary streams comprise the dominant landforms of dissected terrains adjacent to the river floodplain, and they are termed arroyo valleys. This material was studied and sampled as discussed

in Sectons 2.2, 2.4, and 2.5.

In the tributary-arroyo valleys of the project area, hillslope components include erosional slopes on older alluvial fill or bedrock, valley-floor depositional forms and valley-mouth alluvial fans graded to the Rio Grande. The most gentle longitudinal gradients of arroyo valley floors and valley-mouth fans are 1-2% and contrast markedly with the less than 0.1% slope of the river floodplain.

3.3.2 History of classification and local evidence

Today, most geologists agree that the Santa Fe deposits are a group and should include essentially all basin filling materials related to the Rio Grande rift ranging in age from Miocene to middle Pleistocene (Baldwin, 1963; Hawley et al., 1976; Machette, 1978; Chamberlain, 1980). Its broad usage is an advantage in areas where the basin fill is not or cannot be subdivided (Baldwin, 1963). Machette (1978) mapped the San Acacia Quadrangle about 20 km north of the field site, and subsequently redefined the Santa Fe deposits into an upper and lower unit; the Sierra Ladrones Fm and Popotosa Fm respectively. Machette reported the upper Santa Fe unit as "...of early Pliocene to middle Pleistocene age is here named for the Sierra Ladrones (low foothills of the Ladron Mountains) and consists of alluvial fan, piedmont slope, alluvial flat, flood plain, and axial stream deposits, and locally derived basalt flows" (Machette, 1978). These units had previously been called the Santa Fe Fm in San Acacia (Denny, 1940). The Popotosa

Fm had not been included in the Santa Fe Group before this time and represents the lower Santa Fe deposit in central New Mexico. The Popotosa Fm consists of several fanglomerates, gypsiferous playa beds, and piedmont slope deposits (Machette, 1978).

The axial stream deposits (discussed in Sections 2.2, 2.3, 2.5, and 2.6), also known as ancestral deposits of the Rio Grande, are the main characteristic to distinguish the valley-fill sequence of the Sierra Ladrones Fm from the underlying Popotosa closed basin deposits. Geologists mapped ancestral sand deposits across the Rio Grande River, east of Socorro. They found a grey, well-sorted sand and gravel unit composed of materials derived from sources to the north. Ancestral Rio Grande sands form a continuous stratum in the subsurface of the Rio Grande Valley between the type locality in San Acacia and Socorro (Chamberlain, 1980). The sands crop out fairly continuously along the course of the present Rio Grande from as far north as Santa Fe to south of El Paso, Texas.

Chamberlain (1980) divides the Sierra Ladrones Fm into three sedimentary facies in the Socorro Peak area just west of Socorro. They are a mud and silt facies (Tslo), a fluvial facies (Tslf) of the ancestral Rio Grande River, and a piedmont slope facies (Tslp) derived from adjacent mountain ranges. In the Socorro Peak area, the Sierra Ladrones Formation lies in angular unconformity over the upper Popotosa Fm. The Sierra Ladrones Fm grades upward from alluvial flat mud and silts into lower axial stream sand deposits. The sands interfinger with the upper overlapping piedmont slope reddish brown sandstones and fanglomerates (Machette, 1978). The top of the formation is placed at the

base of thin veneers of gravelly alluvium which rest on piedmont surfaces cut across strata of Popotosa and Sierra Ladrones Fm. Thickness and extent of the Sierra Ladrones deposits are predominantly controlled by varying amounts of erosion across tilted faulted blocks. The thickest Sierra Ladrones exposure crops out in Nogal Canyon where 350 meters of strata can be observed. The exact thickness of the Sierra Ladrones Fm in the Socorro Basin east of Socorro Peak is unknown but it may be significantly greater than 350 meters (Chamberlain, 1980).

There is alluvial fan (or arroyo) material overlying ancestral Rio Grande deposits at the site. Chamberlain's divisions of the Sierra Ladrones Fm will be used as a basis for characterizing the intermediate and small scale geologic features of the study area. The fluvial facies (Tslt) exists below 5 meters at the site and the piedmont slope facies (Tslp) exists between the surface and 5 meters. These units and the contact between them is discussed in Section 3.3.

3.2 INTERMEDIATE SCALE: ALLUVIAL FAN ENVIRONMENT

Since the alluvial fan environment is that which presents the complicated layered profile being it studied between 0 and 5 meters, it is prudent to discuss those forces which form the different deposits that make up the arid alluvial fan. Sections 2.2 through 2.6 have indicated that there is a layering of hydraulic properties as well as a complicated arrangement of material within each layer.

Alluvial fans are found in several arid and semi-arid parts of the world, including the southwestern United States, parts of India, South Africa and around the Mediterranean. Many potentially hazardous operations are located on these alluvial fans. The alluvial fan or tributary-arroyo facies is quite heterogeneous (as opposed to the fairly uniform sands of the ancestral Rio Grande), and therefore represents a complicated but common medium for contaminant or fluid transport. Therefore it is prudent to examine in detail the formation of alluvial fans and to identify the most useful and hydraulically applicable classification system for the various types of fan deposits. The classification system chosen is based on textural and therefore hydraulic differences between the units and is discussed with respect to the units mapped at the site in Section 3.3.

3.2.1 Formation of alluvial fans

The following are the general alluvial fan characteristics that should be reviewed for this study. Fans always occur in areas of decreased confinement (Bull, 1977). Fans are usually wedge-shaped and up to tens of kms in area. From top (or source area) to valley bottom, they are divided into the apex, fanhead, midfan and distal fan as shown in Figure 3-3. The upper most portion of the fans or fanhead usually consists of debris flows and channel-forming processes, while the midfan is dominated by sheetflood and braided stream deposits. The distal fan has similar deposits as the midfan though finer in grain size and with the tendency to exhibit or interfinger with valley playa or eolian deposits. The tectonic setting for these fans is active, including fault blocks, mountain fronts, and

Depositional model for arid and semiarid alluvial fans

ZONE	PROCESS	DESCRIPTION
FANHEAD	Debris Flow	matrix–supported boulder conglomerate
	Streamflood	channel–form, grain–supported congl.
MIDFAN	Streamflood near intersection point	laterally continuous gravel composed of single crossbed set
	Braided Stream	trough crossbedded sandstone and conglomerate
	Sheetflood	laterally continuous silt and shallow gravel channels
DISTAL FAN	Braided Stream	trough crossbedded sandstone and congl.
	Sheetflood	laterally continuous silt and shallow gravel channels
	Playa	laminated, gypsiferous silty mud and clay
	Eolian	crossbedded, well–sorted, f. to m. sand

DRY ALLUVIAL FAN MODEL:

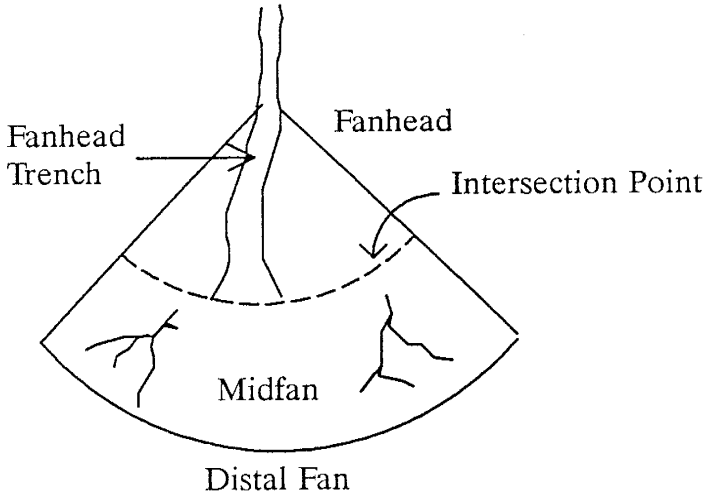

Figure 3–3 Depositional model for arid and semiarid alluvial fans (from Mack and Rasmus sen, 1984)

volcanic highlands (McPherson et al., 1987). The characteristic facies associated with fans are conglomerates, sandstones, and mudstones with clasts up to boulder size. The gradients of fan surfaces are as steep as 25 degrees on small fans and less than 1 degree on large fans (Allen, 1970). Sorting is usually poor with grading increasing downfan. Clast shape in fan deposits is angular to subrounded. Chemical characteristics for these deposits include a large degree of oxidation and a common association with pedogenic carbonates and evaporite containing playa-lake deposits (Bull, 1972).

Other diagnostic features of fans include, vertical and lateral variability of lithofacies, a high bedload to total load ratio, a short distance from source to fan toe, and a low relative stability of distributaries found on the fan surface (McPherson et al., 1987). Each bed of a fan represents a single depositional event that has resulted from one of a spectrum of precipitation and erosion events within the source area. In radial sections of a fan, individual beds may be traced for long distances, while cross-fan sections reveal overlapping beds of limited extent that are interrupted by cut-and-fill structures (Bull, 1972).

It should be noted that fan morphology and surface processes are controlled by allocyclic variables, such as climate and tectonism, and by autocyclic variables, such as channel diversion and bar migration that are inherent to fan depositional systems (Mack and Rasmussen, 1984). Together these factors dictate the morphology of the fans with respect to their source areas.

To be able to understand the alluvial fan products at the site and their hydrologic roles it is important to understand the allocyclic processes that contribute to their formation. The processes that most actively shaped these fans are climatic and tectonic in nature. These processes largely work independently of one another, but their affects can cause similar products, therefore creating a difficult task of recreating the climatic and/or tectonic past.

The climatic factors that produce deposits or affect the depositional slope of the semi-arid fans center around the abundance or lack thereof of precipitation events and the regularity or lack thereof of precipitation events.

Semi-arid regions are known for precipitation events that are intermittent but strong and mostly short in duration. (Blissenbach, 1954). In particular, these are the contributing factors behind debris flows. The more steady the rainfall, the larger the tendency for waterlaid deposits to form. The mountain ranges in these fan environments contribute to a larger amount of rainfall over the mountains than the surrounding area would receive, thereby adding to the transporting and depositing capabilities of flows.

In general, the more humid the climate (or the more precipitation), the more aggradation will take place further downfan, while fanhead entrenchment and stream incision will occur in response to more arid situations. For example, periods of accumulation of thin temporary alluvial fans may coincide with climatically controlled times of increased

sediment yield of the source area, or decreased competence of transportational processes (Bull, 1977). It is therefore seen that climatic changes may contribute to changes in the depositional slope of a fan.

Tectonic factors are the second process responsible for fan deposits being discussed. Semi-arid fans are known to have existed in tectonically active areas, namely in rift valleys and along mountain front fault scarps as found in the Basin and Range province. Tectonic control on alluvial fan deposition can be summarized in the following manner: large scale coarsening-upward cycles in a fan sequence would represent uplift and fan progradation while large scale fining upward cycles would be a result of reduced relief between fan and source area or source area retreat (Mack and Rasmussen, 1984).

In particular, the rate of uplift of the mountains relative to the adjacent basins, either by pulsatory or continuous uplift, largely determines the thickness or loci of fan deposition (Bull, 1977). Uplift counteracts the tendency for the fanhead to entrench and it allows both channel downcutting in the mountains and fan deposition next to the mountains. The latter processes occur only when the rate of uplift equals or exceeds the sums of the two base-level trenching processes. On the other hand, recession of a mountain front results in the formation of a rock pediment normally covered by the fanhead portion of the fans. A rock pediment may be an important indicator of the extent of an alluvial fan at its maturity.

3.2.2 Classification system

Bedding of deposits is one of the best methods of identifying the alluvial-fan environment of deposition. Within a single outcrop a variety of strata generally can be observed, each bed representing a particular set of hydraulic conditions that determined the thickness, particle size and distribution, particle orientation, and type of contact with the underlying bed. Fans composed entirely of water-laid deposits, differences in flow result in marked differences in the sedimentological characteristics of the beds. Bedding differences are even more striking in the many fans composed of both water-laid and debris flow deposits. The poorly sorted, massive beds of debris flow deposits stand out in marked contrast to the beds water-laid sediments.

The sheetflood-streamflood stream classification of alluvial fan deposits described by Davis and Reading or Miall's lithofacies classification will not be used because it is difficult to infer the shape of a deposit and the place of deposition from subsurface samples. This system of characterization focuses more on structural characteristics rather than textural characteristics that may be discerned in core samples. A useable classification (for the deposits found on alluvial fans) must include deposits of mudflows, and all the intermediate gradations. It should be applicable to both surface and subsurface deposits and should be adaptable to alluvial-fan deposits in any part of the world.

Bull's classification of alluvial fan deposits which is based on textural and sediment/water ratio during deposition is of most use in this study. This method of classification distinguishes between mudflow deposits and water-laid sediments which are distinct depositional types and are separated by deposits whose properties are intermediate between the two. The scheme can be used to classify subsurface samples because parameters from grain-size analyses can be used to help describe each type. The following are relevant characteristics of mudflow (or debris flow) deposits, water-laid deposits, and intermediate or between the two classes deposits. These products are directly related to the processes discussed in 3.2.1.

Debris flows are dense, viscous flows capable of transporting very large boulders in "suspension". As a result they are poorly sorted, with a very high sediment to water ratio. Debris flows are commonly formed near the apex of a fan but if the flow is persistent enough it will form lobate tongues extending from sheetlike deposits further downfan. Debris flows and mudflows have abrupt, well-defined margins along the sides and downslope edges of the deposit (Bull, 1963). Farther downstream the mudflow overtops both banks and spreads out as a sheetlike deposit on the fan. Factors that promote debris flow formation (Bull, 1963) are 1. abundant precipitation over short periods of time, 2. steep slopes with insufficient vegetative cover to prevent erosion, and 3. a source material that provides a matrix of silt and clay.

The relative viscosities of debris flows can be obtained by study of the position and

orientation of the larger clasts. A low-viscosity debris flow will have grade bedding and a horizontal or imbricated orientation of the tabular gravel fragments. The more viscous flows have the larger clasts distributed uniformly throughout the flow. The most viscous flows not only have uniform distribution of the larger clasts, but the tabular particles commonly have a vertical preferred orientation normal to the direction of flow.

Mudflows are types of debris flows consisting mainly of sand-size and finer sediments with silt or clay matrix. Many debris flow deposits are so coarse grained that it is difficult to obtain a representative sample for determining the particle-size distribution of the material. As a result, few particle size analyses have been made of debris flows. Logarithmic plots of the coarsest one-percentile vs median particle size may make patterns distinctive of depositional environments on fans. For example sinuous patterns indicate shallow ephemeral-stream environments, while rectilinear patterns indicate debris flows (Bull, 1962). Bull (1963) analyzed the grain size distribution of fan samples from Fresno County, CA and published an average clay content of 31% for debris flows.

Because the bulk of the fan deposits are deposited as sheets and lobes, uniform thickness for a given bed is common in most outcrops, particularly for debris-flow deposits. When individual beds can be identified at more than one outcrop, another diagnostic stratigraphic indicator becomes readily apparent: the extensive sheet-like aspect of the individual beds. The sheetlike character of the bedding commonly is not apparent in those fans consisting mainly of gravel. The braided-stream mode of deposition that is

characteristic of these gravel deposits results in small-scale, cut and fill structures being common in those exposures parallel to the fan contour. As will be seen in Section 3.3, the coarse grained debris flows at the site are irregularly shaped while the fine grained debris or mud flows have consistent thicknesses. The thick, sheetlike bed of water-laid gravel may be attributed to large volumes of previously deposited material.

Mudflows pick up air in two ways. Air may be incorporated into mudflows as they move down both tributary ravines and main stream channels and this entrained air actually may decrease the viscosity of the mudflow. The other source of air is the deposits beneath the mudflow, as it spreads out on the alluvial fan. Part of the air in the soil moves upward and becomes trapped by the mudflow to form bubble cavities. Air may be trapped by water-laid sediments if they are deposited on soils that contain air which can move up into the saturated sediments.

Very few grain-size analyses and even fewer comparisons have been made of the sorting of debris flows and water-laid sediments. Bull (1964) performed 50 particle size analyses of mudflows. The cumulative curves (grain diameter vs cum% on semilog scale) have gentle slopes which range from clay to predominantly gravel. The clay content of the 50 mudflow samples analyzed ranged from 12 to 76 % and averaged 31%.

The proportions of water-laid and debris-flow deposits vary greatly from fan to fan and may change during the history of accumulation of the deposits of a single fan. Most fans

whose source areas produce debris flows also have flood events that result in the deposition of water-laid deposits. Thus, the deposits of many fans consist of interbedded deposits of debris and water flows in varying proportions.

Water-laid flows consist of sheets of sand, silt, and gravel deposited by a network of braided distributary channels. More steady rainfall is needed for the formation of these flows. They are clast supported (with very little clay), well sorted, cross-bedded, and laminated. The laminations represent fluctuations or repeated periods of deposition (Bull, 1963). These tend to fill in stream channels that were temporarily entrenched into the fan and they tend to occur on the lower parts of the fan. Sieve deposits are part of the water-laid category as they are formed when earlier surficial fan material is so coarse and permeable that even large discharges infiltrate into the fan completely before reaching the fan toe.

The nature of water-laid deposits shows progressive change downfan. There is an increase in the abundance of cross-bedding with transitions such as coarse gravel through clast-supported fine-grained gravel, sand matrix-supported gravel to sand. These changes reflect gradual decrease in the particle size to water depth ratio as stream competence decreases downfan.

Bull's study showed a 6% clay content for the water-laid samples from the Fresno County fans and they were marked by S-shaped grain size distributions indicating a

coarse and fine portion as opposed to the flat (straight-line) plots of the mudflow deposits.

Intermediate deposits, as the name suggests, are deposits intermediate between debris flows and water-laid deposits. They are better sorted than debris flow sediments with bedding defined partly due to horizontally oriented gravels in the lower parts of the beds and only partly defined margins. Intermediate flows have some clay grain coating but are not able to carry very large clasts. These deposits include sheetflood sediments and streamchannel sediments, possibly the most abundant lithofacies of alluvial fan sequences (McPherson et al., 1987). Deposition of these sediments is caused by the widening of the flow into sheets as a result of more steady rainfall in the source area than for debris flows. These deposits are most likely found in the midfan area. Bull's (1963) fan study showed an average clay content of 17% for these beds with a grain size distribution slope intermediate between debris flows and water-laid sediments.

3.3 SMALL SCALE: GEOLOGY OF THE SITE

Now that the pertinent history and forces that shape alluvial fan formation have been described, it is necessary to describe in detail the geologic structure and stratigraphy beneath the site. This section shall add qualitative information to the quantitative information developed in Sections 2.2 through 2.6.

The detailed subsurface geology of the study area came from the initial study conducted by Parsons (1988), subsequent mapping of the shallow and deep trenches (as discussed in sections 2.4 and 3.3), and a 2-D reconstruction of the plot down to 20 meters below datum using stratigraphic sections of the boreholes drilled at the site as discussed in Section 3.3. As discussed in Sections 3.1 and 3.2 the site consists of a piedmont slope facies underlain by the Rio Grande fluvial sand facies. The geologic heterogeneities of the piedmont slope facies need to be defined to be able to reconstruct and support the infiltration and drainage results discussed and interpreted in Section 4.0. The nature of the Piedmont slope facies/fluvial sand facies contact and the nature of the Rio Grande sand facies are also discussed.

3.3.1 Piedmont slope facies

As discussed by Parsons (1988) the profile beneath the 30 m x 30 m field site consists of two distinct facies of the Sierra Ladrones Fm...The soil profile is stratified, consisting of an upper zone of red brown silty sands and pebbles interbedded with cobbles, and a lower zone of clean, tan fine sand and fine to coarse sands and pebbles. Clay lenses of undetermined extent are present throughout both zones. The underlying tan sands represent Chamberlain's (1980) ancient Rio Grande fluvial sand facies (Tslf), while the red brown silty sands and pebbles are piedmont slope facies (Tslp) derived from the Socorro Range to the west. This was confirmed during the continuation of the study. A 4 m wide by 15 m long by 4 m deep trench was dug by backhoe in the piedmont slope

facies roughly oriented perpendicular to the strike of the alluvial fan material coming off of the Socorro Peak area. The present relief between the top of Socorro Peak and the trench units is about 2500 feet. The trench spans the northeastern corner of the plot and the section studied was the western wall of this NW-SE trending trench. Figure 3-4 shows a map of the western wall of this trench.

The western wall was cleaned off using shovels, picks, brooms and brushes to take off the slough from the trench digging and to accentuate the structural features and contacts between the units. Approximately 2.5 meters of arroyo facies were exposed (or the entire arroyo section in this spot) and approximately 1 meter of Rio Grande facies were exposed. An additional meter of Rio Grande facies was seen via hand auger samples through the bottom of the trench.

The deep trench exposed a perpendicular or head on view of an arroyo section that contained source material from the Socorro Peak area. The section exposed at the site is approximately 4 m deep. At 4 m there is a very undulating contact between the arroyo and the Rio Grande sand that the arroyo deposits moved over.

The following is a geologic description of the arroyo facies and the nature of its contact with the undulating Rio Grande sands. The arroyo facies has been divided into 7 separate stratigraphic beds, based on source differences, grain size distributions, and structural differences. The 7 beds are described from the surface downward.

Arroyo Sequence as Exposed
in SE-NW Trending Trench

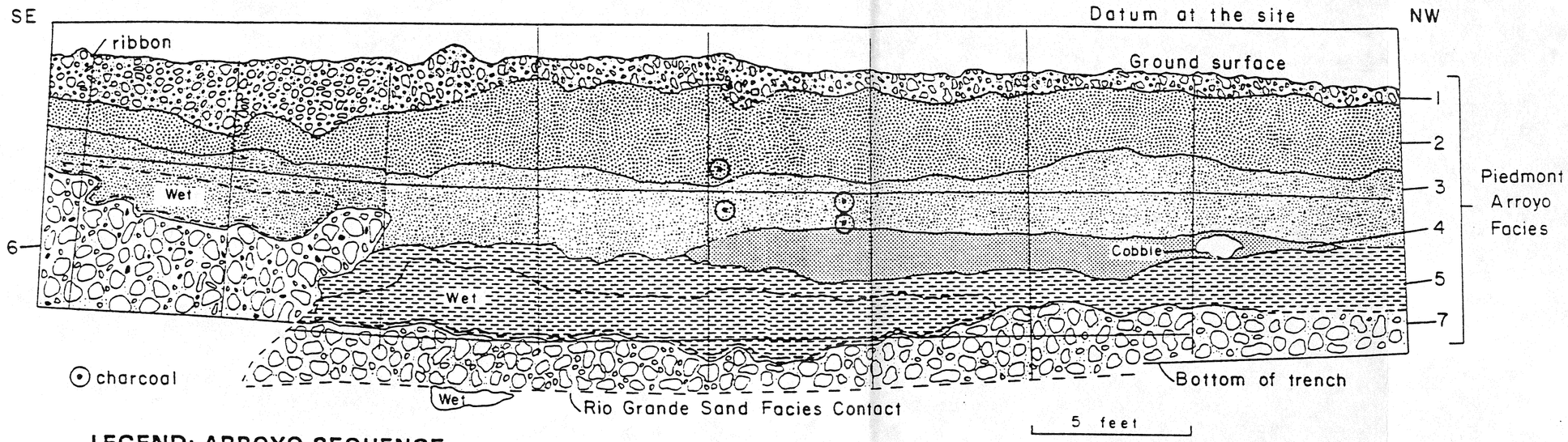

LEGEND: ARROYO SEQUENCE

UNIT 1: A 1 to 2 foot thick continuous silty sand bed with either bedded or suspended sands and gravels. The bedded gravels represent high energy flow. This unit was deposited in the last 200 years.

UNIT 2: A massive and continuous 1 to 3 foot thick silty sand with interbedded subrounded to subangular sands and gravels in bottom half. Bounded by a discontinuity on the top and a scoured surface at the base. This unit contains small fining upward bedded channel deposits.

UNIT 3: A 2 to 3 foot thick silty to sandy clay with little sand and gravel lenses. This unit is characterized by up to 30% clay, scattered pieces of charcoal, entrapped air and a blocky texture. The southern end of this unit became wet due to irrigation experiment.

UNIT 4: A 1½ foot thick distinctly bedded sand and gravel subunit of Unit 3 found on northern side of well. Deposited with substantial amounts of water in a high energy environment. The beds in the lower half of the unit bend down toward the depositional surface. Black hematite and manganese stains are found within this unit.

UNIT 5: A 2 foot thick silty sand with some clay and little lenses of sand and gravel that was interrupted in the southern end of the trench by Unit 6. This unit is characterized by a blocky texture due to its high clay content and low energy depositional environment. Parts of this unit became wet due to the irrigation experiment.

UNIT 6: A high energy debris flow that is seen in southern end of the trench. The debris flow carried cobbles up to 1 foot in diameter suspended in a viscous, fine to coarse sand and gravel matrix.

UNIT 7: An extensive 1 to 3 foot thick high energy debris flow that lies conformably on top of the Rio Grande sands. This unit may represent the last discharge event of the Pleistocene. The unit consists of bedded sand and gravel layers on top of a layer of cobbles suspended in a sand matrix.

Figure 3-4 Deep trench cross-secti

The first bed, continuous across the face and less than 2 es thick consists of very recent silty sand with either bedded or suspended sands and gravels. This bed acts as the root zone at the site and its age is not more than 200 years old as pieces of metal were found with in the bedded gravels on the southern end of face. According to J. Hawley (personal communication, 1990) this bed is quite a bit younger than the underlying bed as is seen in the pronounced discontinuity on the southern side. The bedded gravels represent a high energy flow regime. In places there was some evidence of soil development with the characteristic desert climate carbonate layers forming within this layer.

It should be noted at this point that according to the Soil Conservation Service (Johnson, 1988), the soils found in the study area are characteristic of the local soils that form on bajadas and fan terraces, in alluvium derived dominantly from rhyolite and river deposits. These soils are to have a light brown gravelly sandy loam surface layer with a 12 thick light brown and pink gravelly sandy clay loam subsoil. The substratum usually consists of gravelly loam and gravelly loamy sand.

The second bed is also continuous but quite a bit more massive. Bed #2 is 1 to 3 feet thick and consists of a massive silty sand with interbedded sands and gravels in its bottom half. It appears that the higher the silt content is in this layer the more massive it appears. The bedded fine to coarse sands and fine to coarse gravels found in the lower half of this unit are subangular to subrounded. These larger grains are more bedded on the southern end of the trench and they mark a high energy event which left a scour

surface at the base of this bed. In places there are small fining upward bedded channel type deposits.

The third unit consists of a 2 to 3 foot thick, massive silty to sandy clay. This bed has up to 30% clay in it with little amounts of gravel and sand lenses. Other characteristics of this unit are that it has charcoal scattered throughout, large amounts of bubbles or entrapped air and on the whole it has a bubbly texture.

At this point it should be mentioned that the infiltration experiment performed at the site, left a pronounced, effect on the area cut by the trench. The moisture that left the irrigation plot in the Northeastern direction was seen in the trench wall. Most of it appears to have travelled deeper than 16 feet below the surface by the time of the trench construction but a substantial amount of moisture was retained in the mostly clay rich parts of the trench.

Unit 2 was wet on the southern side of the wall (as shown in Figure 3.4) and unit 5 was almost completely wet. The clays and some of the sand in the top 1.5 meters of the Rio Grande sand that were investigated in this trench were quite moist. The flow direction and results of the irrigation experiment will be discussed by A. Stark (personal communication, 1991).

The fourth unit could be considered as a subunit of the third unit as it is quite distinct in

structure but does not appear to have any distinct contacts with the units above.It does however have a very pronounced scoured surface at the base. This unit is up to 0.5 meters thick and consists of beautifully bedded sands and gravels that had been deposited with quite a bit of water in a high energy environment. These interbedded fine sands and medium to coarse sands have created very distinct layers with scoured lenses of gravels. The beds within this structure are horizontal at the top but bend down toward the bottom half of the unit, towards the depositional surface. One is able to see that where these beds meet at the depositional surface,is a locus of deposition. In addition, there are black hematite and manganese stains within this structure.

The fifth bed is the second most clayey bed after unit 2, and is extensive across the wall except for the southernmost two meters of the trench where it was interrupted by the 6th unit. This unit was almost all wet from the irrigation experiment (except for the northernmost two meters) when the trench was first dug. This bed consists of silty sand, some clay and little lenses of sand and gravel. Due to its relatively high clay content and uniform grain size, the texture of this bed appears blocky and smeared. The bed would have been deposited in a low energy environment. This bed has fairly distinct contacts with the units above and below.

Unit 6, located on the southern end of the trench, was deposited in a very high energy environment. From its contact with units 5 and 3, it appears to have flowed down the mountain side as a debris flow displacing unit 5 in that area. Unit 3 was deposited on top

of this debris flow. All contacts with this unit are distinct. The debris flow carried cobbles up to 12 es in diameter suspended in a fine to coarse viscous sand and gravel matrix. A very interesting feature of this unit is that it was surrounded by units that were wet from the irrigation experiment but the pore pressure of the unit never reached a point where it would take in some of the surrounding moisture.

Unit 7 is the deepest unit in the arroyo facies and lies conformably on top of the Rio Grande unit. According to J. Hawley (personal communication, 1990) this was the last discharge event of the Pleistocene (early Holocene at about 7000 years). This is also the first cobble layer described by Parsons (1988) in previous studies. It consists of bedded sand and gravel layers on top of 8 cobbles which are suspended in a moist sand matrix. In the northern section this unit dips upward and consists of bedded sands and gravels below a thick cobble layer. This cobble layer is also suspended in a sand matrix. This unit is approximately 1 meter thick in the trench but it has the most inconsistent thickness of all of the units. Its bottom surface has quite an undulating shape where it meets the Rio Grande sand.

The deep trench wall was mapped as shown in Figure 3-4, according to textural and therefore previous energy flow regime conditions. After characterizing the units it was easy to see that they fit into Bull's three product categories very well. There were 7 discernable beds above the axial Rio Grande sands (which are found below unit 7). Below the alluvium at the top (or unit 1) are two mudflow units (units 2 and 3) separated

by a discontinuity. Samples from these units had 28% and 33% clay (as found by grain size analyses). Below unit 3 is the only waterlaid deposit (unit 4) exposed in the trench. Unit 4 is about 0.5 meters thick and consists of distinctly bedded sands and gravels that exhibit fining upward and fining downward sequences. Samples taken from unit 4 exhibit 8% and 4% clay. Figure 3-5 shows a photograph (top) of unit 3(a mudflow) above unit 6 (debris flow) and the bottom photograph which is a part of the water-laid deposit (unit 4). Beneath unit 4 is an intermediate deposit which is seen in the bottom photograph in Figure 3-5. Samples from this unit contained 20 and 23% clay fractions. Units 6 and 7 are debris flows with gravel to cobble-sized clasts held in suspension within a silt to gravel matrix. Darker colored units were wet from a previous infiltration experiment.

Figure 3-5

a.)

Figure 3-5

b.)

Figure 3-5 Photographs of deep trench wall.

a.) Mudflow overlying a debris flow.

b.) Unit 3 overlying Unit 4(water-laid) and Unit 5.

Unit 7 exhibits some bedding as seen in the bottom photograph of Figure 3-6, a view of units 1, 2, 3, 4, 5, and 7. The top photograph shows units 1 and 2 near the surface. Samples of the matrix in unit 6 have a clay content of 4% and 8%. The clay content of the mudflows, water-laid and intermediate deposits agreed very well with Bull's clay content of Fresno County fan deposits. The bottom photograph shows unit 4, the only real waterlaid deposit exposed in the trench.

In addition to noting textural variations and changes, structures such as blocky structure

in the clayey units, laminations, fining upward and downward, and crossbedding were described. Finally the contact beneath disturbed and undisturbed material, and the areas that were stained with blue dye, were noted. Figure 3-6 shows a map of the western wall of the shallow trench. Another study at the site (Stark, personal communication, 1991) conducted a detailed study of dye movement at the depth of the shallow trench. Some of this dye is shown in Figure 3-6. In areas where the drip emitter irrigation system had been installed, the top 1/2 meter of section consisted of disturbed material. In other parts of the trench there was up to 1/10 meter of disturbed material at the surface. The one meter deep section contained varying combinations of clay, silt, sand, and gravel with occasional cobbles. The various textural combinations are described on Figure 3-6.

In terms of the larger scale arroyo unit descriptions used to describe the deep trench facies, we see units 1, 2, and the top of unit 3 (from the surface downward) exposed in the shallow trench. In the shallow trench unit 1 is between 1/3 and 2/3 meter thick and consists of horizontally laminated, water-laid, sands and gravels or cobbles entrained in a silty sand matrix. Parts of this unit had been interrupted during the installation of the irrigation system. In addition the unit contains pieces of metal and wood contributing to the young age of this unit as described earlier. Its lower surface is quite undulating. In this trench as an in the deep trench unit 1 is found at the surface, underlain by unit 2, which is underlain by unit 3. The floor of the trench was the location of a detailed disc permeameter study conducted by Schmidt-Petersen (1991). As a result it was prudent to

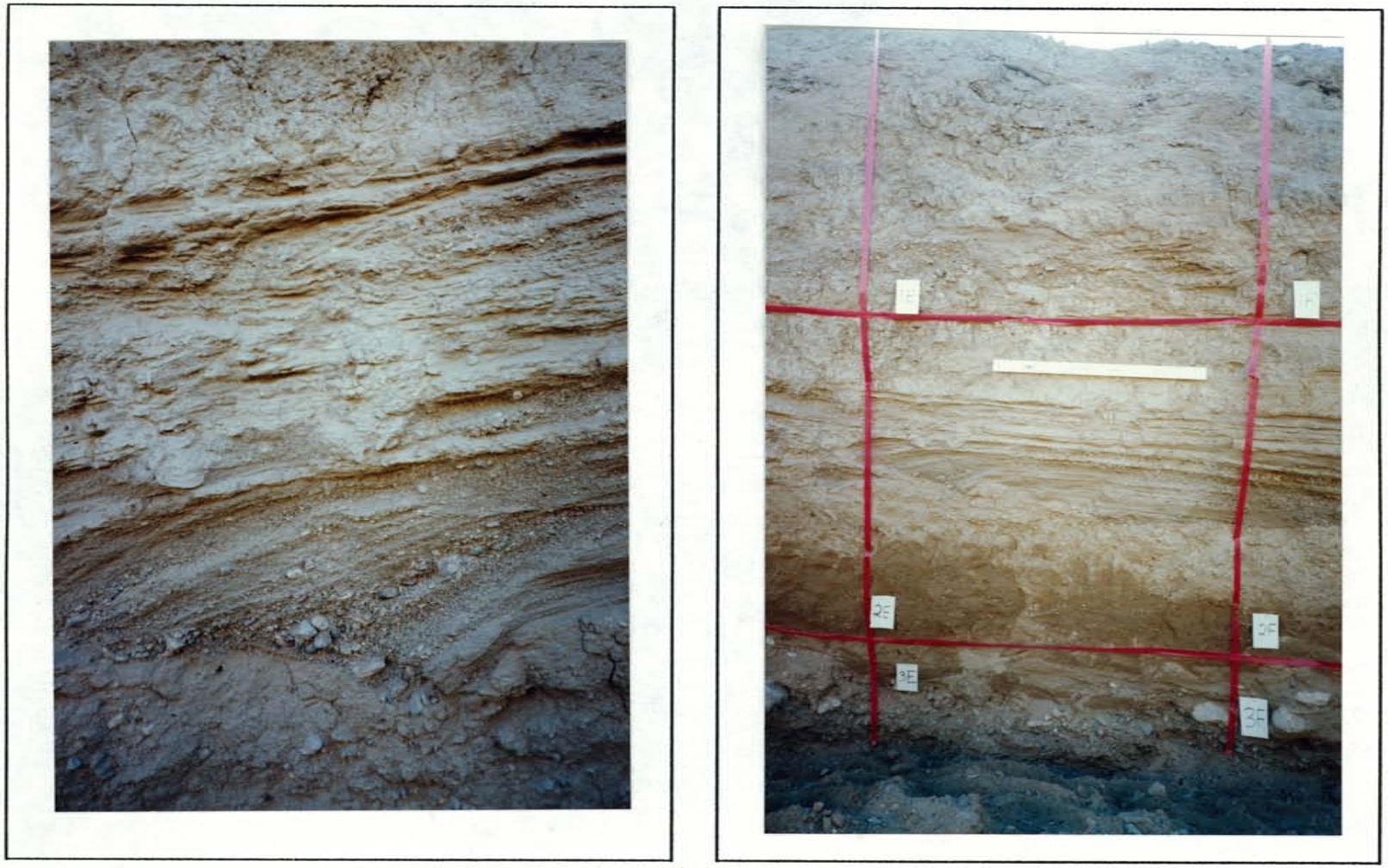

Figure 3-7 Photographs of deep trench wall.

c.) Close-up view of Unit 4.

d.) View f[illegible]

identify the units that intersect the floor of the trench. Starting from the SE and moving toward NW along the floor of trench, unit 1 is seen from 0 to 3.5 meters, unit 2 seen from 3.5 to 19 meters, unit 3 is seen from 19 to 27 meters and unit 2 extends from 27 meters to the NW end of the trench.

As in the deep trench, unit 2 is bounded by a discontinuity on the top and a scoured surface on the bottom. It is approximately 1/3 of a meter thick and consists of a silty sand with interbedded and gravels. There are quite a few structures in this unit with the northern end of the trench containing quite a bit of silt/clay blocky structure and cross-bedding and the southern end of the trench containing a lot of cross bedding and interbedded sands and gravels. Units 2 and 3 show the blue dye stains in the center of the plot (or trench).

Part of unit 3, identified as SM with the USCS is the lowermost unit seen in the shallow trench. This unit consists of a blocky silty sand with gravel imbedded in it. Unit 3 is not seen in the southern end of the trench. In the center of the plot this unit is up to 1/3 of a meter thick.

3.3.2 Piedmont slope/fluvial sand facies contact

At the deep trench location, the contact between the Rio Grande sands and the arroyo facies is about 12 ft. and 7.5 meters below the surface (or approximately 4.5 meters

below datum). J. Hawley (personal communication, 1990) says that the gradient of the arroyo (longitudinally) is about 100 feet/mile. The slope of the surface between the two facies can be determined from 3 different contact locations and elevation, the average attitude of the conformable contact between the piedmont slope facies and fluvial sand facies in the area near the field site is strike N32E, dip 4.5 SE. The bottom of the arroyo sequence is characterized by a high energy cobble suspended in sand and gravel sequence.

The sand and arroyo contact is highly irregular due to the high energy environment that the arroyo was deposited in. J. Hawley (personal communication, 1991) calls the arroyo an alluvial deposit, not under sustained flow. The gradient vs discharge equation would be exponential for such a flow. Locally , the contact between the piedmont slope facies and fluvial sands is irregular (Parsons, 1988). Prior to the piedmont slope facies deposition, arroyos were created in the ancestral fluvial sands during epierogenic uplift (Chamberlain 1980). Within the site the contact appears to dip slightly to the NE. A direct correlation of the piedmont slope facies and fluvial sand facies from one location to another is not easy because the two facies are known to interfinger.

As pointed out by Chamberlain (1980), the alluvial fan piedmont slope gravels in the Socorro Basin are thought to have graded eastward as Socorro Peak grew, thus burying the ancestral Rio Grande sands and forcing the channel eastward. Accordingly, there may be a transition zone between the two facies, between two cobble horizons as originally

discussed by Parsons (1988). This explanation is supported by the poorly sorted, red brown sand, silt and pebbles which interfinger with well sorted, tan fine sands and silty clays to the east. This depositional sequence suggests that cobbles were washed from western highlands. Subsequently the ancestral Rio Grande encroached onto the field site one last time, leaving fine sand and silty clay deposits before the piedmont slope deposits forced the river to the east. Several outcrops to the west and to the south of the field site exhibit similar characteristics, reinforcing such a hypothesis (Parsons, 1988). The two cobble horizons can be seen in the deep well logs (Appendix E) and in the cross-sections that include these logs.

For the purpose of simplification for the discussion in Section 4.0, we'll assume that the contact between the alluvial fan facies and the Rio Grande sands to be at that depth where the uppermost fluvial sand is seen. This depth is approximately four to five meters below datum and corresponds in most cases to the top most cobble layer. Figure 3-8 shows a key to the boring logs and cross-sections. The log for Porous Cup Sampler 10 was not constructed. Figure 3-9 shows the cross-section locations presented in Figures 3-10 through 3-15. These cross-sections were constructed by classifying all of the split spoon samples and shelby tube samples collected from the porous cup sampler boreholes and well borings. For comparison, Parsons (1988) had constructed two cross-sections from the original instrumentation borings labeled according to their X,Y locations on the 30 by 30 meter plot as seen in Figures 3-16 and 3-17.

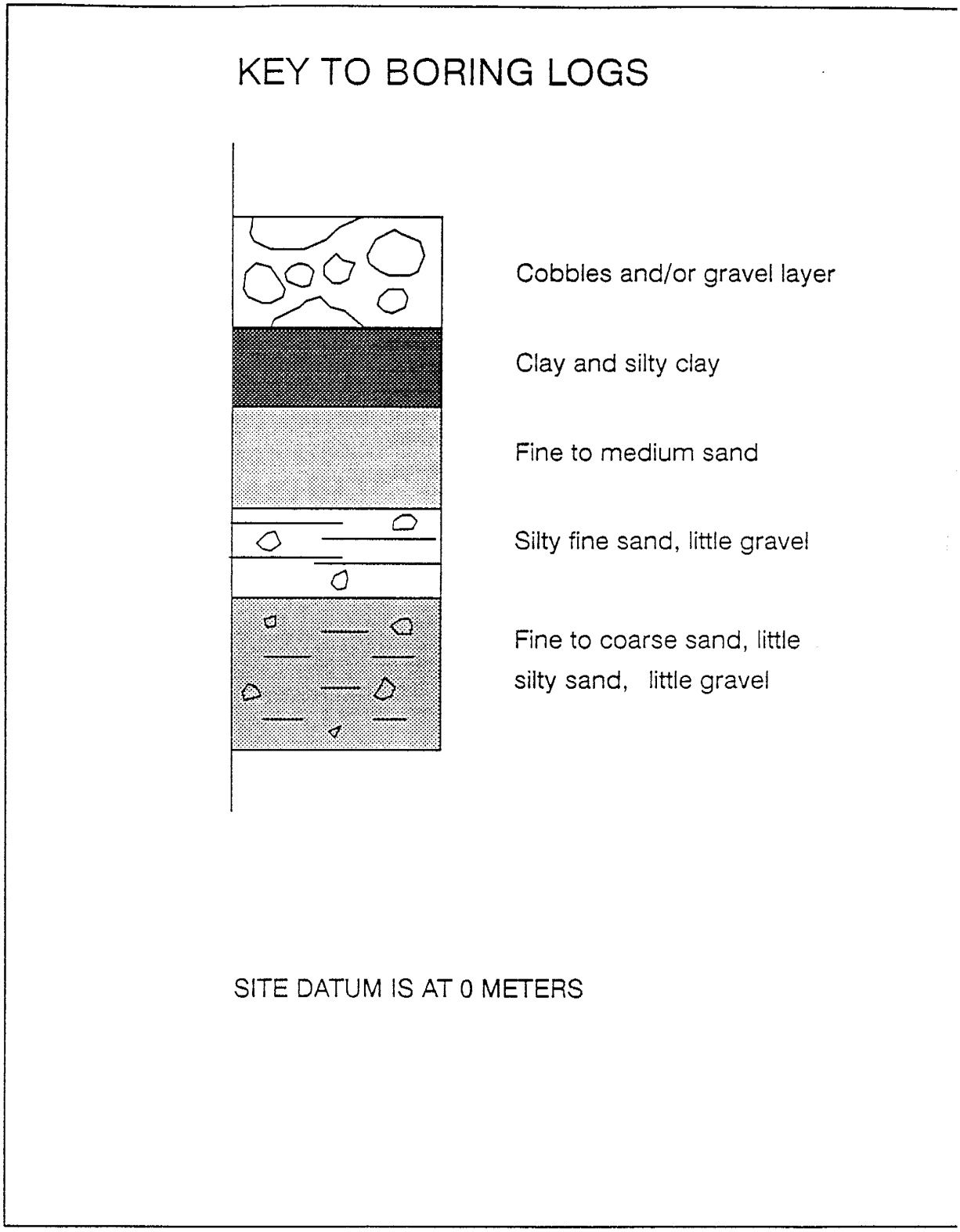

Figure 3-8 Key to the boring logs

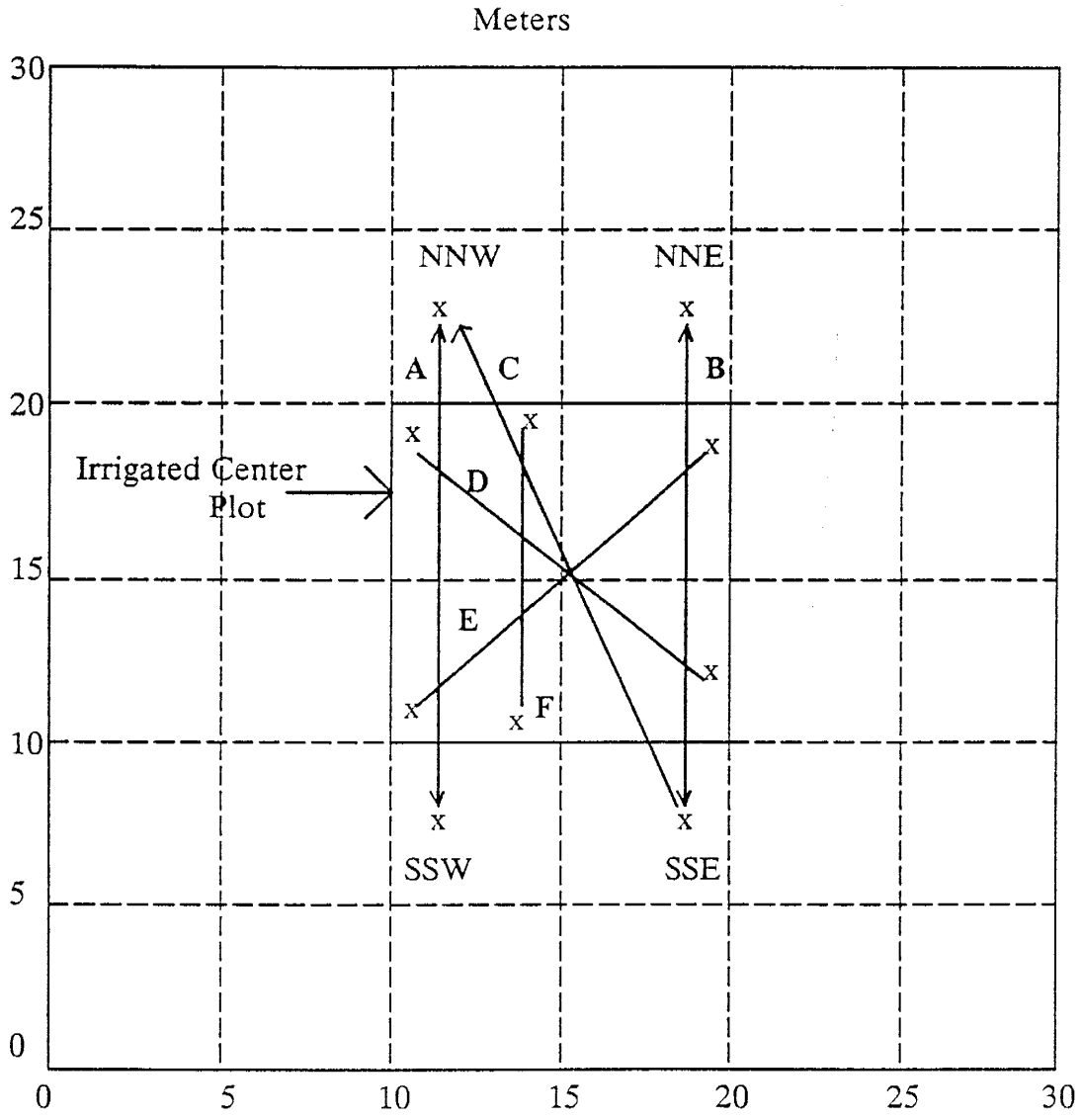

x = A station such as a well or porous cup sampler

Distance measured in meters

Figure 3-9 Cross-section locations

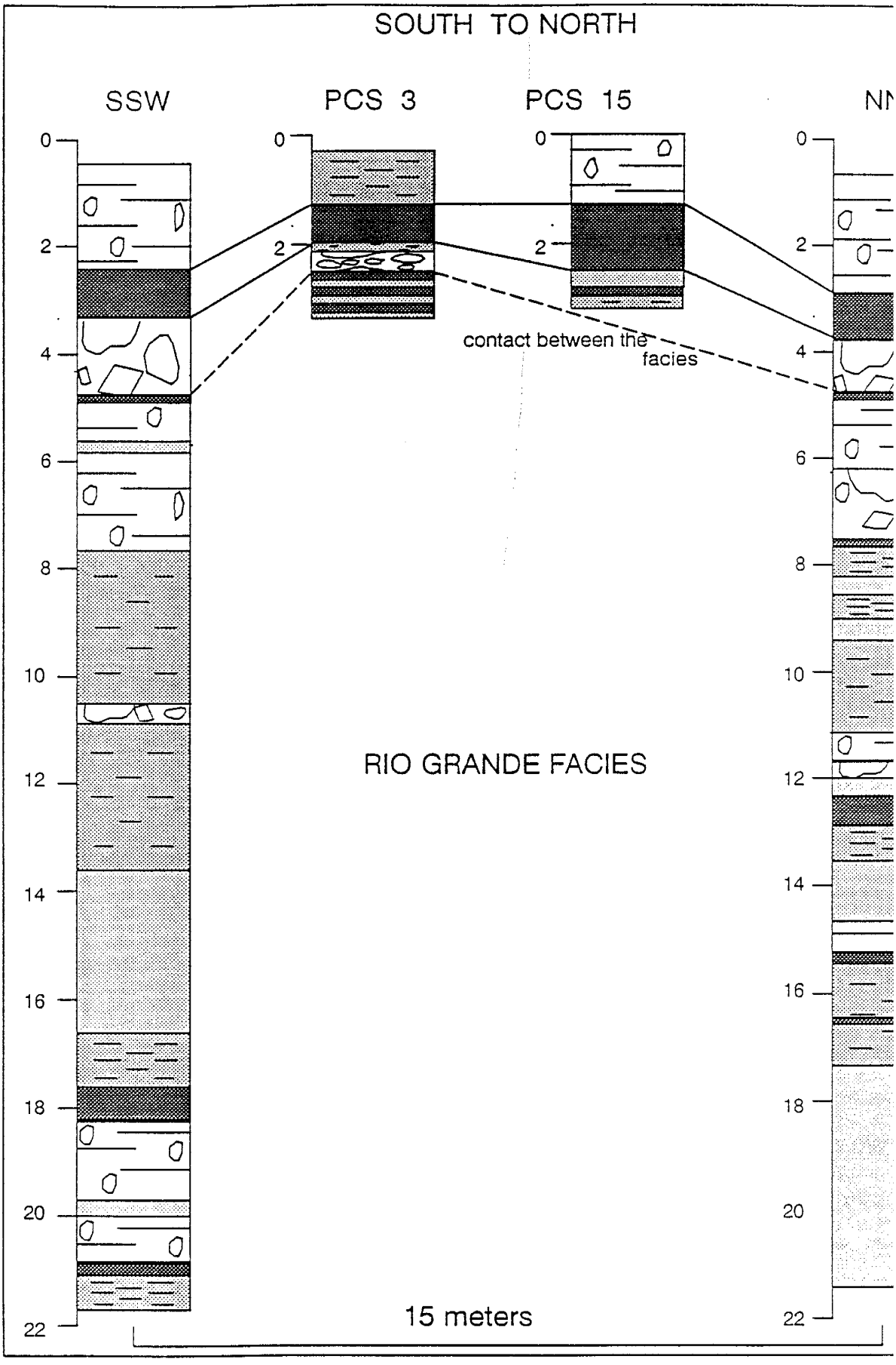

Figure 3–10 Cross-section A.

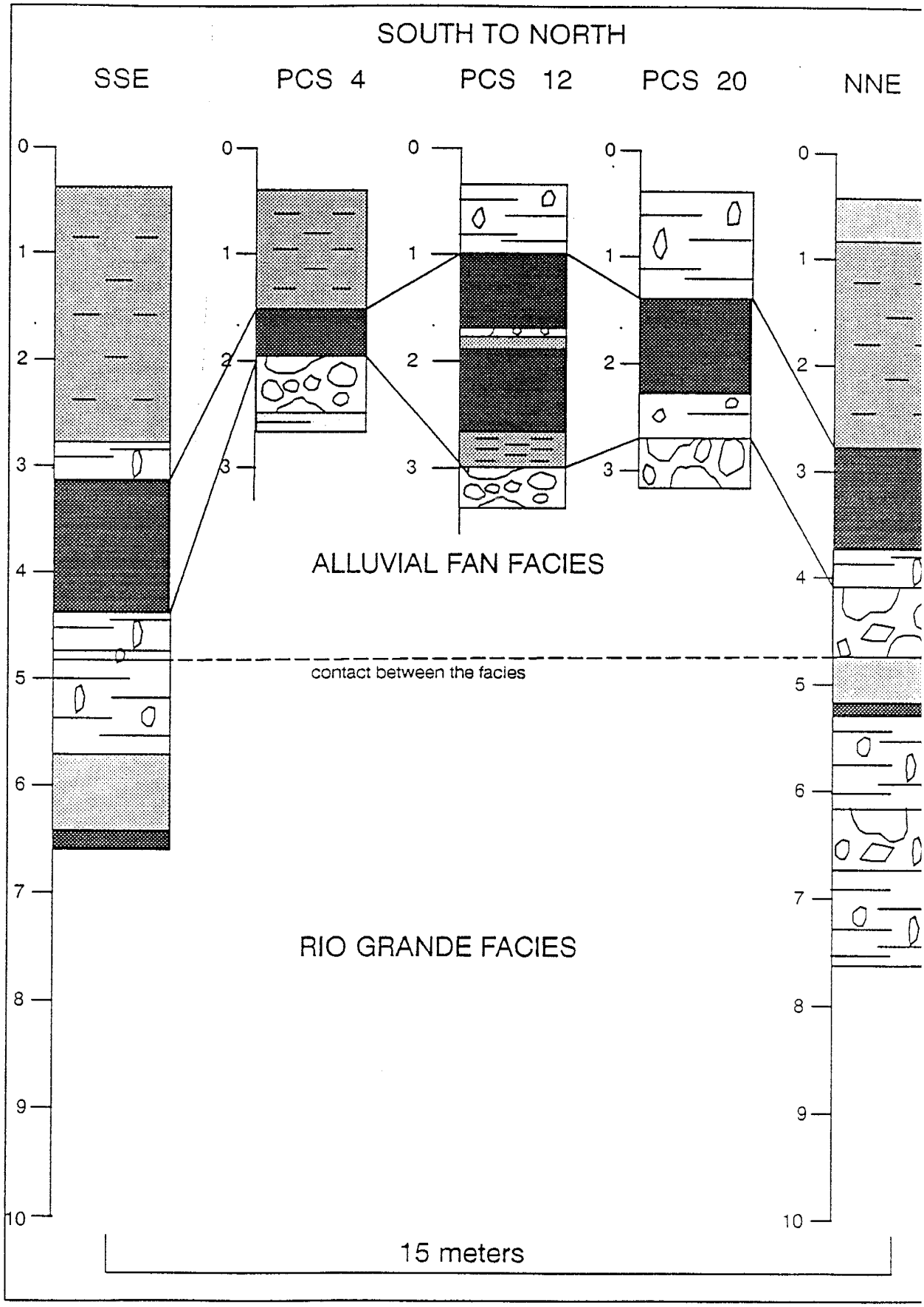

Figure 3-11 Cross-section B.

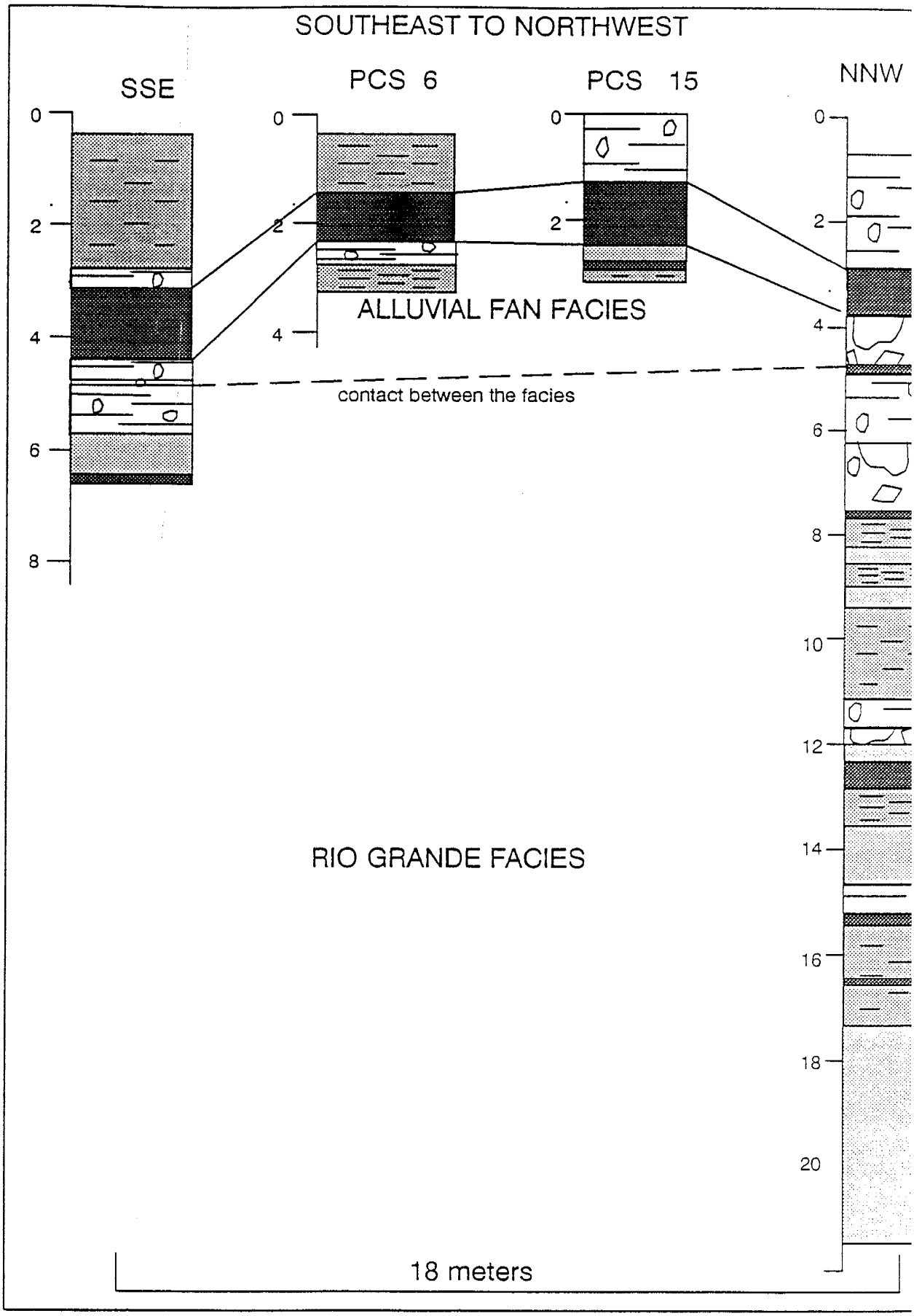

Figure 3–12 Cross-section C.

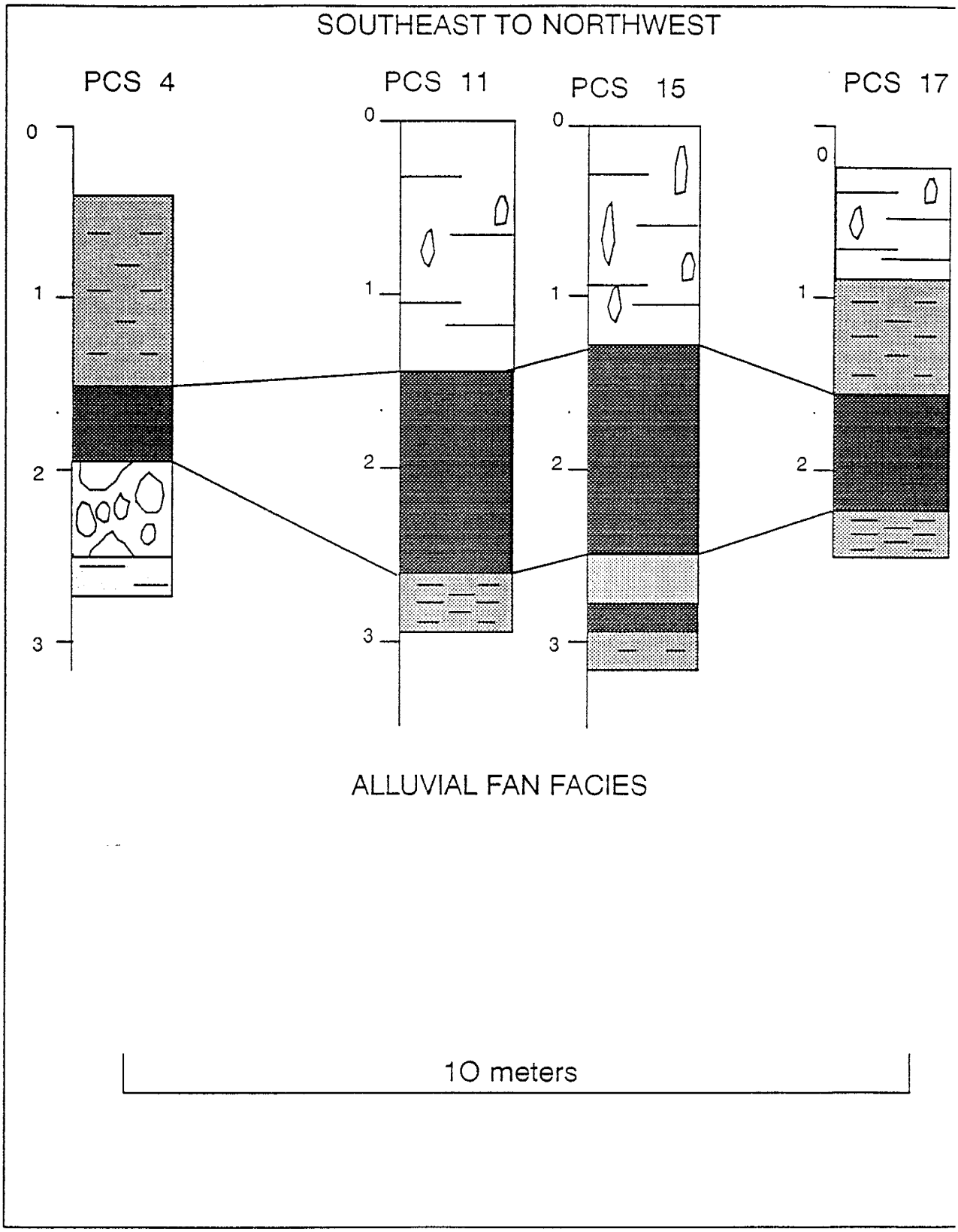

Figure 3–13 Cross-section D.

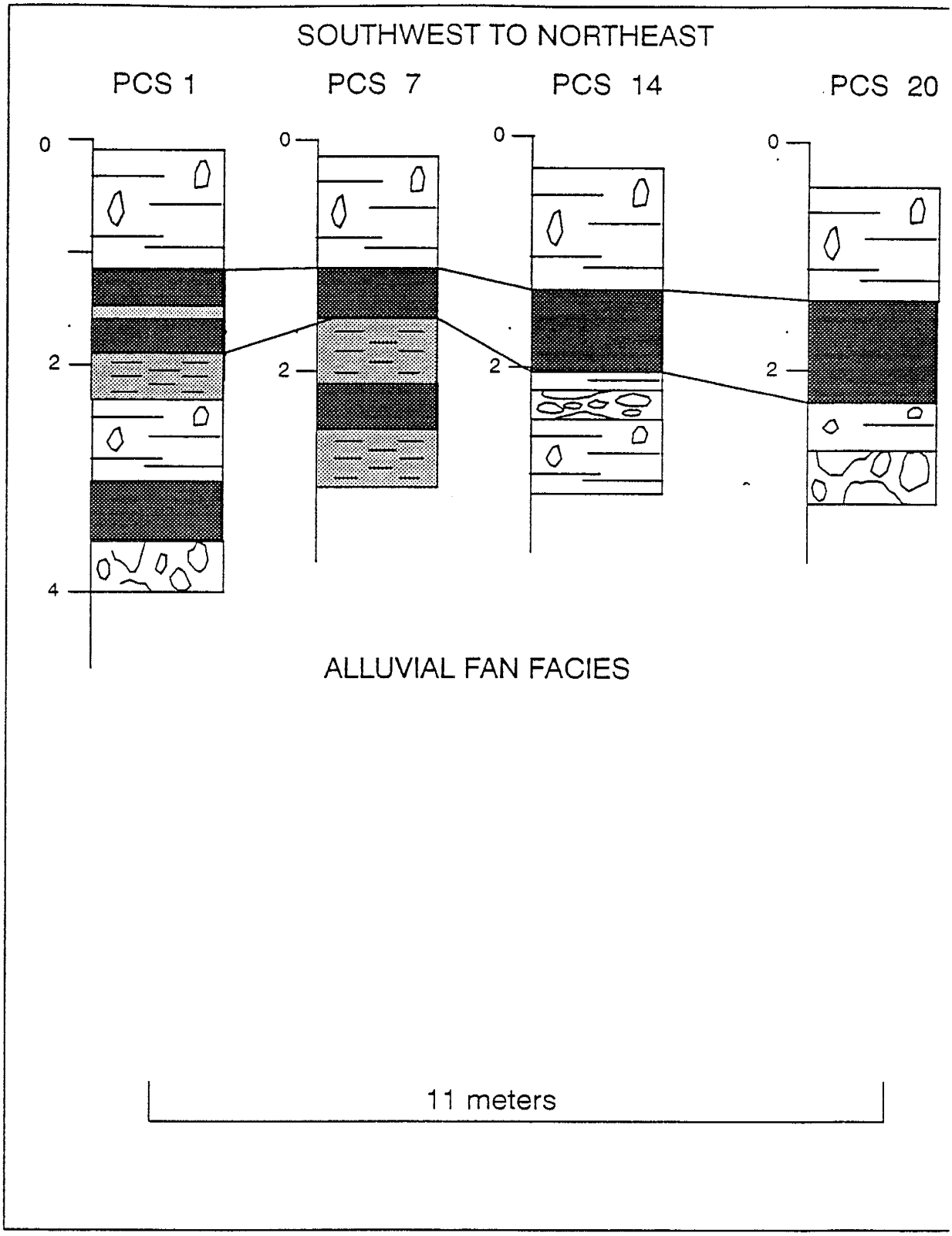

Figure 3–14 Cross–section E.

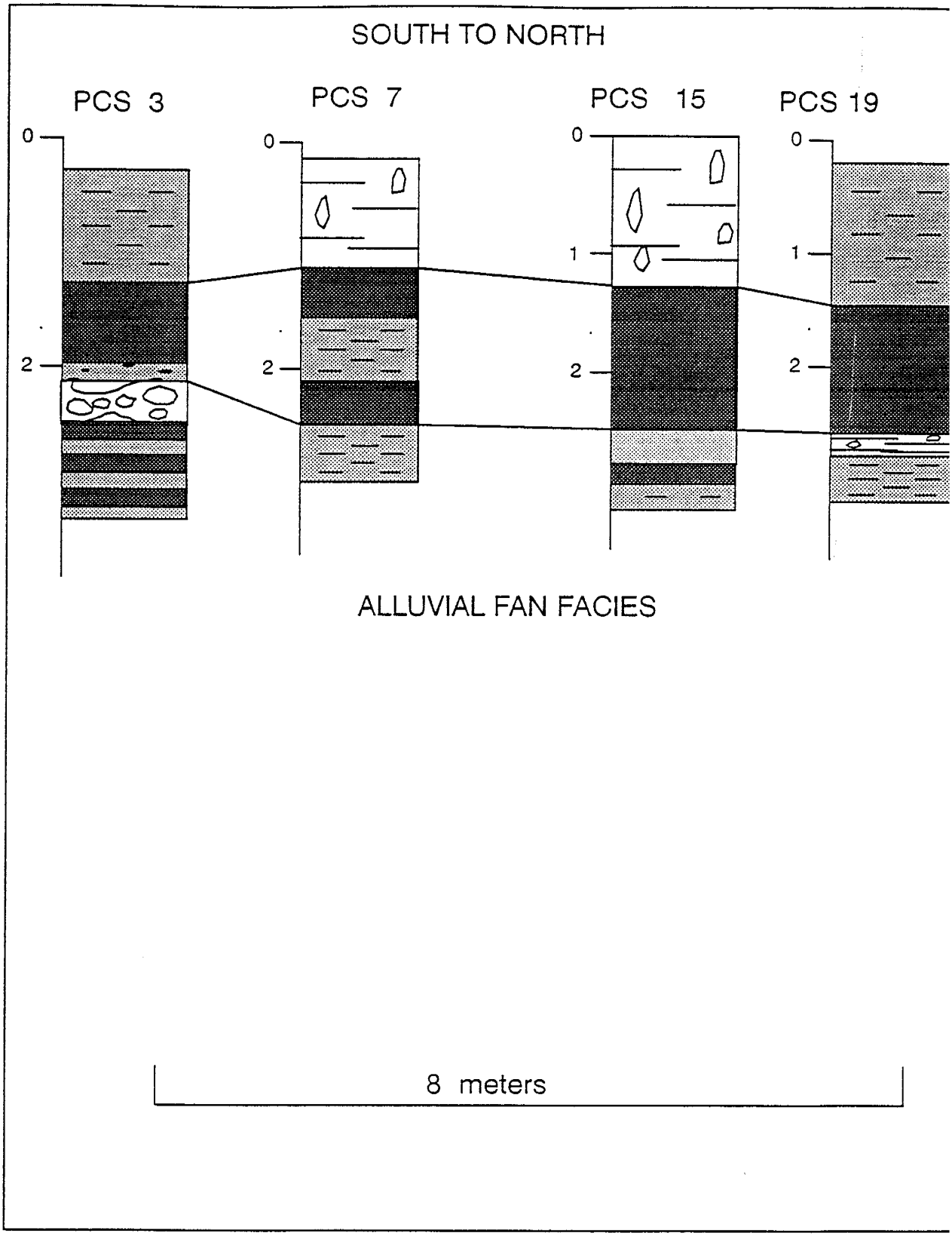

Figure 3–15 Cross–section F.

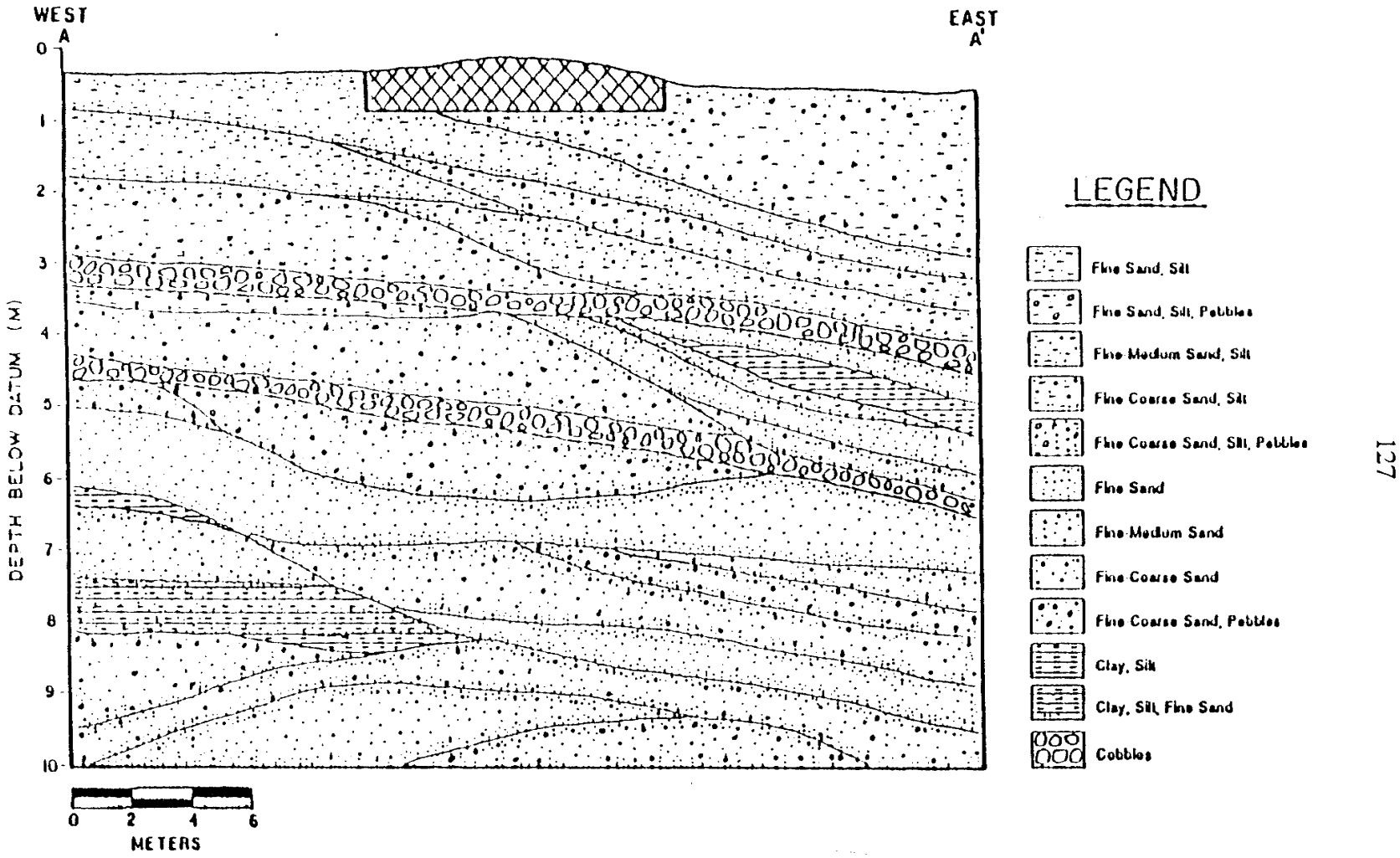

Figure 3-16 E-W transect from Parsons (1988)

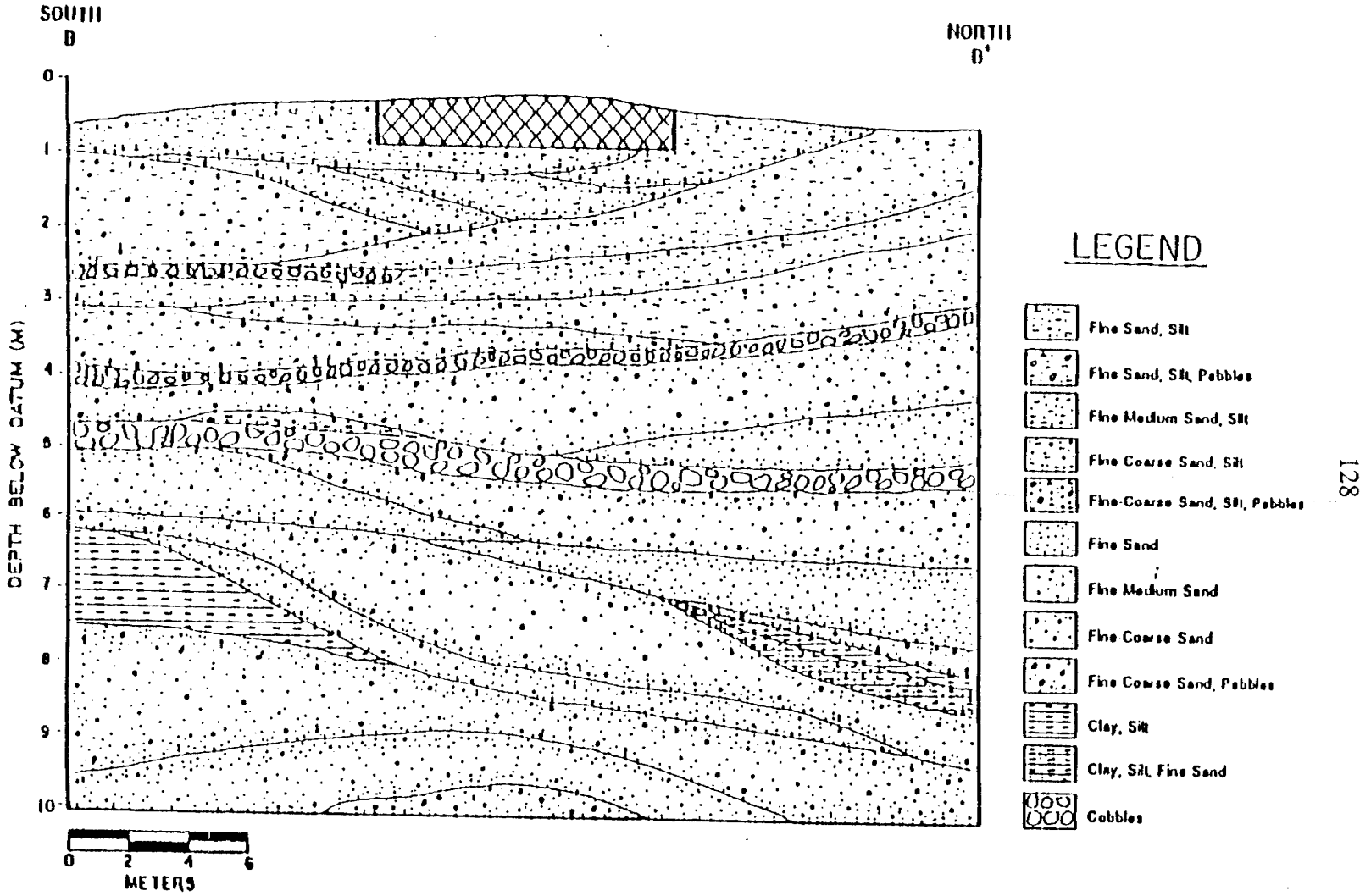

Figure 3-17 N-S transect from Parsons (1988)

All of the cross-sections show the following trends. At the surface is a one to three meter thick section of silty sands overlying a one meter thick clay section. The upper layer corresponds to units 1 and 2 and the underlying layer corresponds to units 3 and 5 of the deep trench alluvial fan classification. As in the deep trench, under the clay section is an extensive cobble layer which marks the bottom of the alluvial facies. Beneath this upper cobble layer is a two meter thick section of silty sands and clay layers which overlies the lower cobble layer. This lower cobble layer and the Rio Grande sand facies are only seen in the outside deep boreholes. The Rio Grande sands as shown in these stratigraphic sections consist of clean sands and silty sands with thin layers of clay and gravel, as would be expected from a fluvial section. Both cobble layers are shown but the individual alluvial fan units are not shown in the cross-sections constructed by Parsons.

Cross-sections A though C extend across the irrigated plot and a little outside of the plot, while cross-sections D through F extend only across the irrigated plot. Cross-section A as shown in Figure 3-10 extends from the south to the north inside the western edge of the plot. It shows the contact between the facies as dipping to the north with a little mounding in the center of the plot. Cross-section B in Figure 3-11 extends south to north along the eastern edge of the plot and shows a very similar trend to cross-section A with an even steeper dipping toward the north. Cross-section in C in Figure 3-12 traverses the plot diagonally from southeast to northwest perpendicular to the units' orientation and it shows a dip toward the northeast of the alluvial fan facies. Cross-sections D through F in Figures 3-13 through 3-15 show the above trends in greater detail within the irrigated

plot. These sections will be used for interpretation of the drainage results in Section 4. The general trend of the cobble layers in agrees with that shown in Parsons' cross-sections.

Figures 3-16 and 3-17 show the cross-sections constructed by Parsons (1988). In general they correspond to the sections prepared in the current study. It is not clear from the deep borings whether the lower cobble layer is as extensive as depicted in Figures 3-16 and 3-17.

3.3.3 Fluvial sand facies

Approximately 1 m of the Rio Grande fan was exposed within the deep trench (by augering deeper within the center of the trench). The formation consisted of very uniform fine to medium sand with very thin layers of clay. Within the deeper pit (in the middle of the trench) was a large boulder that marked the bottom of the arroyo sequence. The boulder appears to have come down off of the mountain in a very high energy regime (flow) and fallen into the underlying arroyo sand producing a scoured gravel from water that was turbulent on the downside of the rock (boulder) and a flame structure within the sand as the sand was being pushed outward from the boulders impact. This is seen in the photograph in Figure 3-18.

The Rio Grande sand is rounded, fine and uniform. Within the sand are wet and

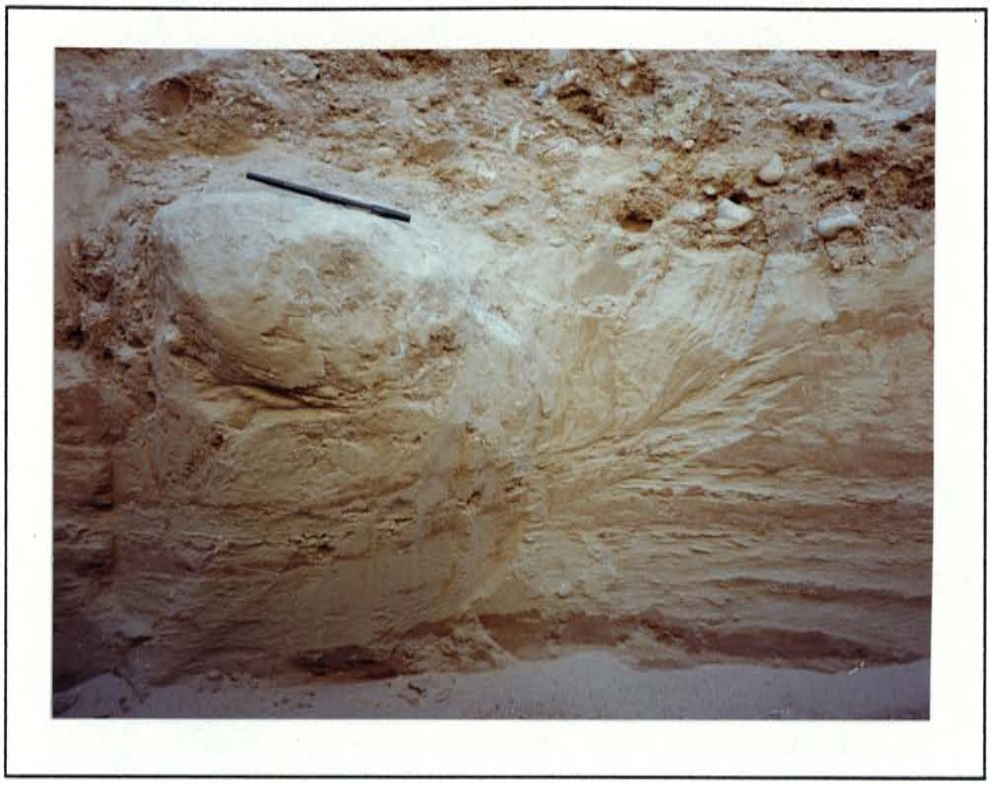

Figure 3-18 Photograph of cobble at alluvial fan/Rio Grande facies interface.

drylayers and layers of "Hershey" type clays (J. Hawley, personal communication, 1990). The sand contains yellow limonite staining and some black charcoal streaking. There are also ripples within the sand. Approximately 1 meter below the top of the sand is a very impressive 0.5 meter thick clay. Below that are 0.5 meters of clean sand and less than 0.5 meters of interbedded sand and clay below that. These interbedded sands and clays contain orange, brown, iron stained sand with flat pebbles in it. At this point there is a cobble layer that was not penetrated by hand auger. This is the lower cobble layer as discussed earlier. The cross-sections presented in Figures 3-10 through 3-15 show the above sequence near the northeast part of the field plot.

4. DISCUSSION

The drainage study performed by A. Stark (personal communication, 1991) relies heavily on the geologic interpretations of the borehole logs for the instrumentation stations (performed by Parsons, 1988). The moisture content profiles for 12 stations are analyzed using other borehole data and recently acquired geologic knowledge (Section 3.). Finally, a review of the amount of data that is needed for such a study is presented.

The type of geologic information that is valuable in such a study includes knowing what the matrix in the cobble layers consists of and understanding how many layers make up the alluvial fan facies. The new hydraulic information includes the vertical spatial variability of such parameters as d10 size, hydraulic conductivity, porosity, bulk density, and saturated water content.

4.1 DRAINAGE ANALYSIS

The factors that control soil infiltrability are discussed by Hillel (1980). These factors include the time from the onset of rain or irrigation, the initial moisture content of the soil, the hydraulic conductivity of the soil, soil surface conditions, and (most appropriately to this study) the presence of impeding layers inside the profile. Generally, the wetter the soil is initially, the faster it attains the final constant rate of infiltration. The higher its saturated hydraulic conductivity, the higher its steady-state infiltration rate.

Layered profiles cause complex flow behavior in unsaturated material. For example a clay may impede flow due to its lower saturated conductivity, while a sand layer retards the wetting front (under unsaturated conditions) due to its lower unsaturated hydraulic conductivity. Flow occurs into such a sand once the pressure head builds up sufficiently for the water fill the large sand pores. The initial infiltration rate from one layer down to another (ie coarse-over-fine or fine-over-coarse scenarios) is controlled by the upper layer. If the lower layer is a finer textured, less conductive layer the infiltration is expected to drop and tend to that of the finer soil (Hillel, 1980). Since there may be too much water for the finer soil to take in, there may be some ponding or perched saturated conditions above the coarse-fine interface. If the underlying layer is a coarse-textured soil such as the cobble layers beneath the field site, the infiltration rate decreases as it reaches the fine-coarse interface. Under unsaturated conditions this scenario may present ceased infiltration for a period of time (Miller and Gardner, 1962). These textural and physical interactions as well as the dependence on initial soil moisture contents are discussed with respect to the specific drainage results for the instrumentation stations.

The locations of the twelve moisture content profiles presented in this section are shown in Figure 4-1. These moisture content profiles with time were put together by A. Stark (personal communication, 1991) using the neutron probe data collected by A. Stark during the drainage period and using the geologic log put together by Parsons (1988) for each respective station. A detailed review of the field work and analysis is described by A. Stark (personal communication, 1991). These profiles will be described by A. Stark

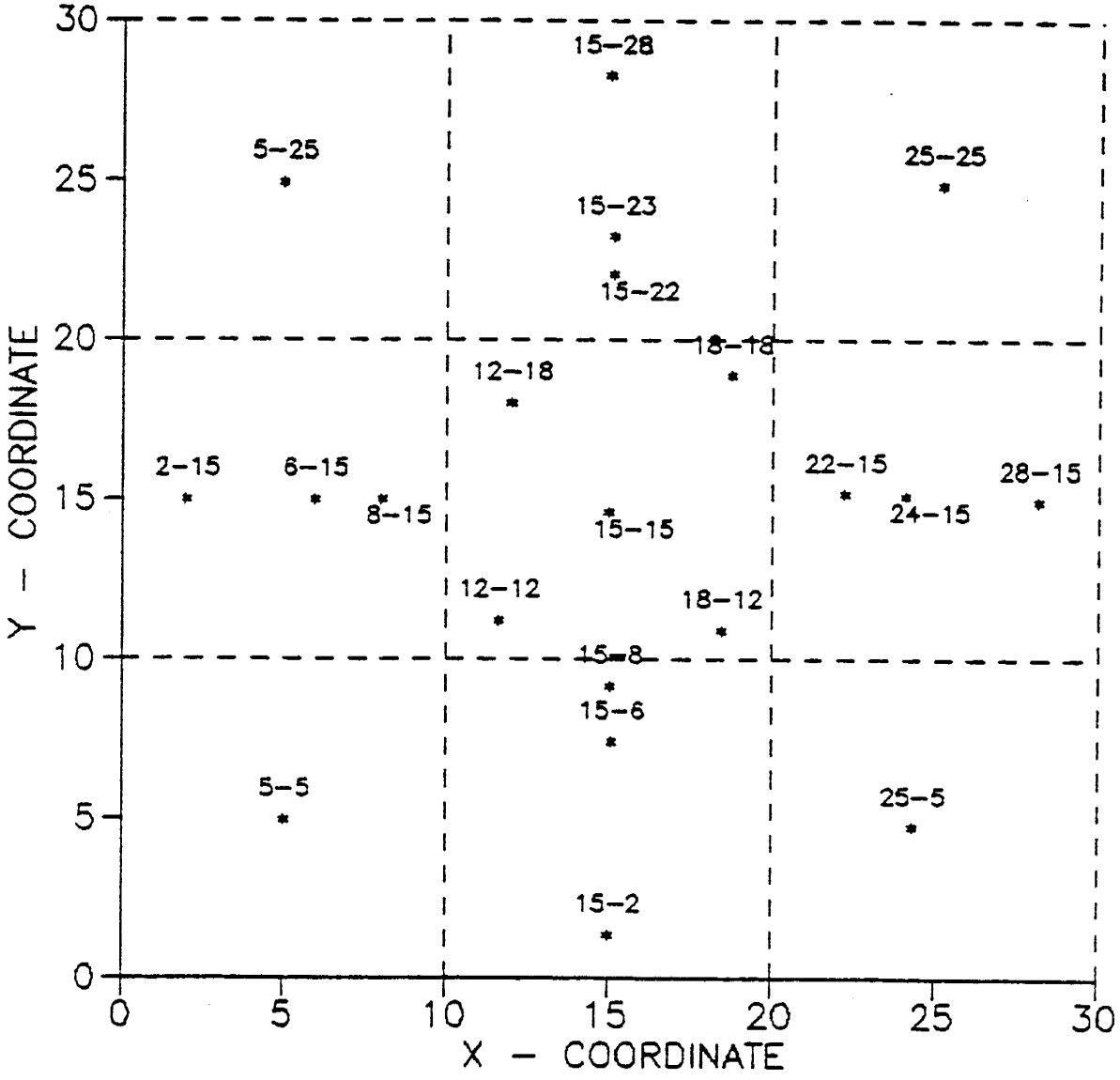

Each asterisk (*) represents a monitoring station: one or two tensiometer nests and one access tube.

Figure 4-1 Monitoring station locations.

as part of the drainage analysis with emphasis on unsaturated flow behavior and how it is manifested in these profiles. An example of the instrumentation stations is shown in Figure 1-5. A. Stark concentrated most of the analysis on Station 15-15 as it was in the center of the profile and as it displayed the least lateral flow of all of the stations. The least amount of lateral flow was seen in this profile as explained by three main reasons. Firstly, at this station there was a unit gradient in hydraulic conductivity indicating mostly gravity caused drainage. Secondly, being at the center of the irrigated plot, this station experienced the least amount of boundary effects from the unirrigated outside soil. Thirdly, the cobble layers were not as thick in the center of the plot as they were at some of the outside stations which would contribute to less ponding and therefore less lateral flow.

Before the first infiltration phase, the initial moisture content profiles across the site indicated moisture contours dipping to the east and to the north with some mounding beneath the irrigated plot at about seven meters (Mattson,1989). During initial stages of infiltration, the above trend continued in addition to a fairly uniform wetted zone directly beneath the irrigated plot. During the spring and summer months of 1986 moisture was detected to be moving beneath the two cobble zones and toward the north at about eight meters. The head fields constructed by A. A. Stark (personal communication, 1991) show vertical downward contours directly beneath the site with deviations out to the sides on the outer edges of the plot. Beneath four meters most of the contours showed a north easterly direction of flow.

In the following discussion these profiles are analyzed with a greater emphasis on the role that the geologic structure plays in controlling and guiding the drainage of water. This study included the comparison of each porous cup sampler or well boring to each moisture content profile location and comparing the geology in the nearby boring and the geology shown in the superposed profile. Table 4-1 reviews boreholes that were compared to the instrumentation locations.

Table 4-1 GEOLOGIC INFORMATION USED IN DRAINAGE ANALYSIS

Parsons' Log/Station Location	Closest Porous Cup Sampler* or well boring log
6-15	WSW
8-15	WSW, WNW
12-12	PCS 9, PCS 13, WSW
12-18	PCS 15, PCS 17, NNW
15-6	PCS 11
15-8	PCS 18, PCS 15
15-15	PCS 11
15-22	NNW, NNE
18-12	PCS 4
18-18	PCS 20, PCS 18
22-15	ENE

* The PCS or porous cup sampler boreholes are usually about 3 m deep as opposed to the deeper instrumentation locations.

Station 6-15:

Moisture content is highest above the two cobble layers seen by Parsons at 3.2 and 4.5 m due to ponding. The geologic profile does not show the variability and sorting present between 1 and 3 m while the geology at WSW and the moisture profile do. Moisture content drops a lot from 9% to 4% below 5.5 meters where there is a sand in WSW. The bulge in moisture content at 2.5 m is due to the clay seen at 2 m. Figure 4-2 shows the moisture content profile superposed with the geologic profile.

Station 8-15:

The lowest moisture contents are between 3.5 and 7 m which doesn't match the sandy profile between 4 and 7 m shown in WSW. There is a bulge at 3 m above the cobble. WSW doesn't show the second cobble layer and the moisture profile does not indicate its existence. Figure 4-3 shows the moisture content profile superposed with the geologic profile.

Station 12-12:

The highest moisture content is a ponding event above the large cobble layer between 5 and 6.5 m. The lower moisture contents are right below this cobble layer where the sandy layer is. This is an example of a fine-over-coarse-interface where the fluid pressures must reach the water-entry pressure of the lower layer, before allowing the wetting front to rapidly move through the coarse layer. The initial moisture content was

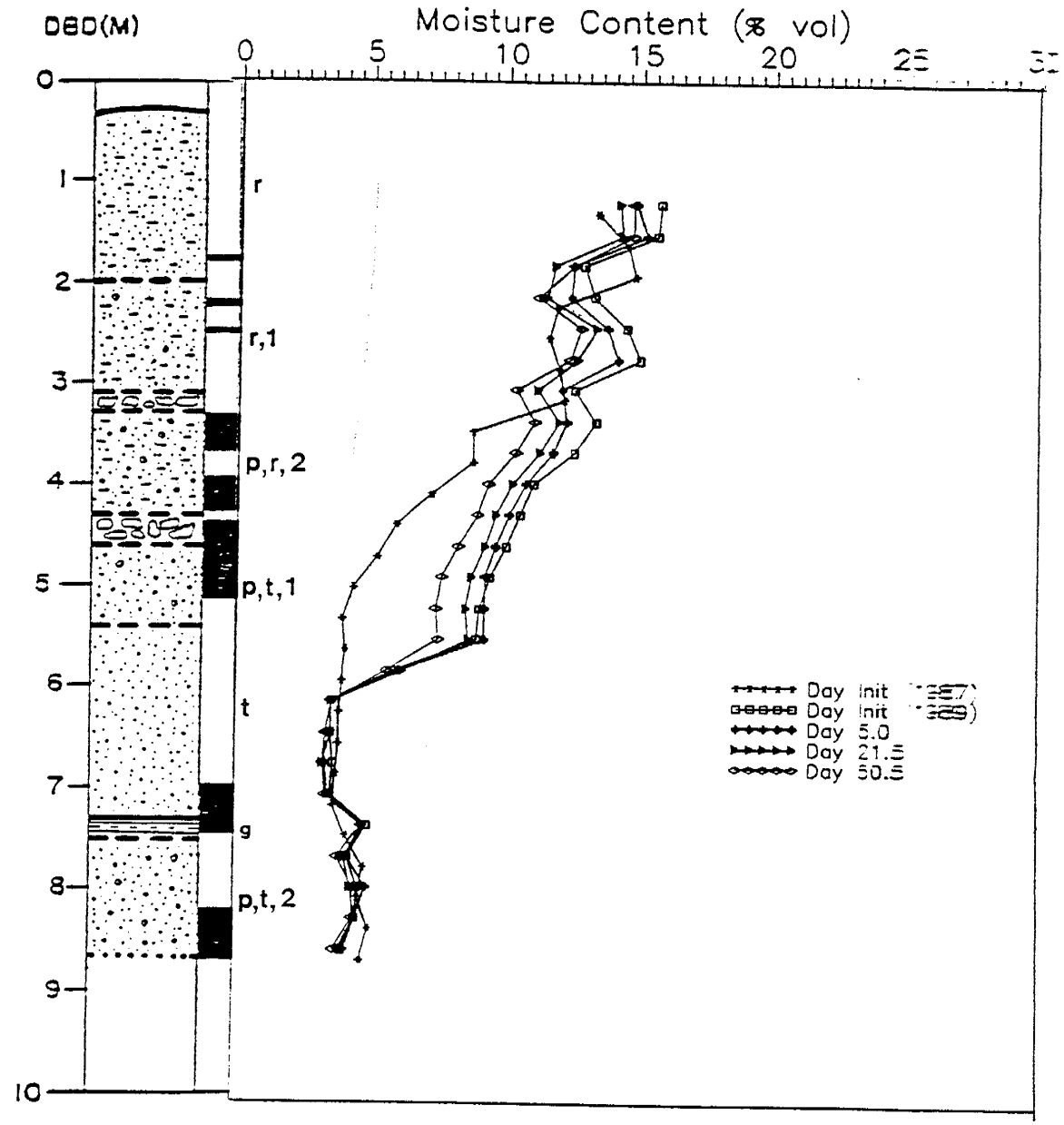

Figure 4-2 Station 6-15: moisture content profile and geology (after A. Stark 1991).

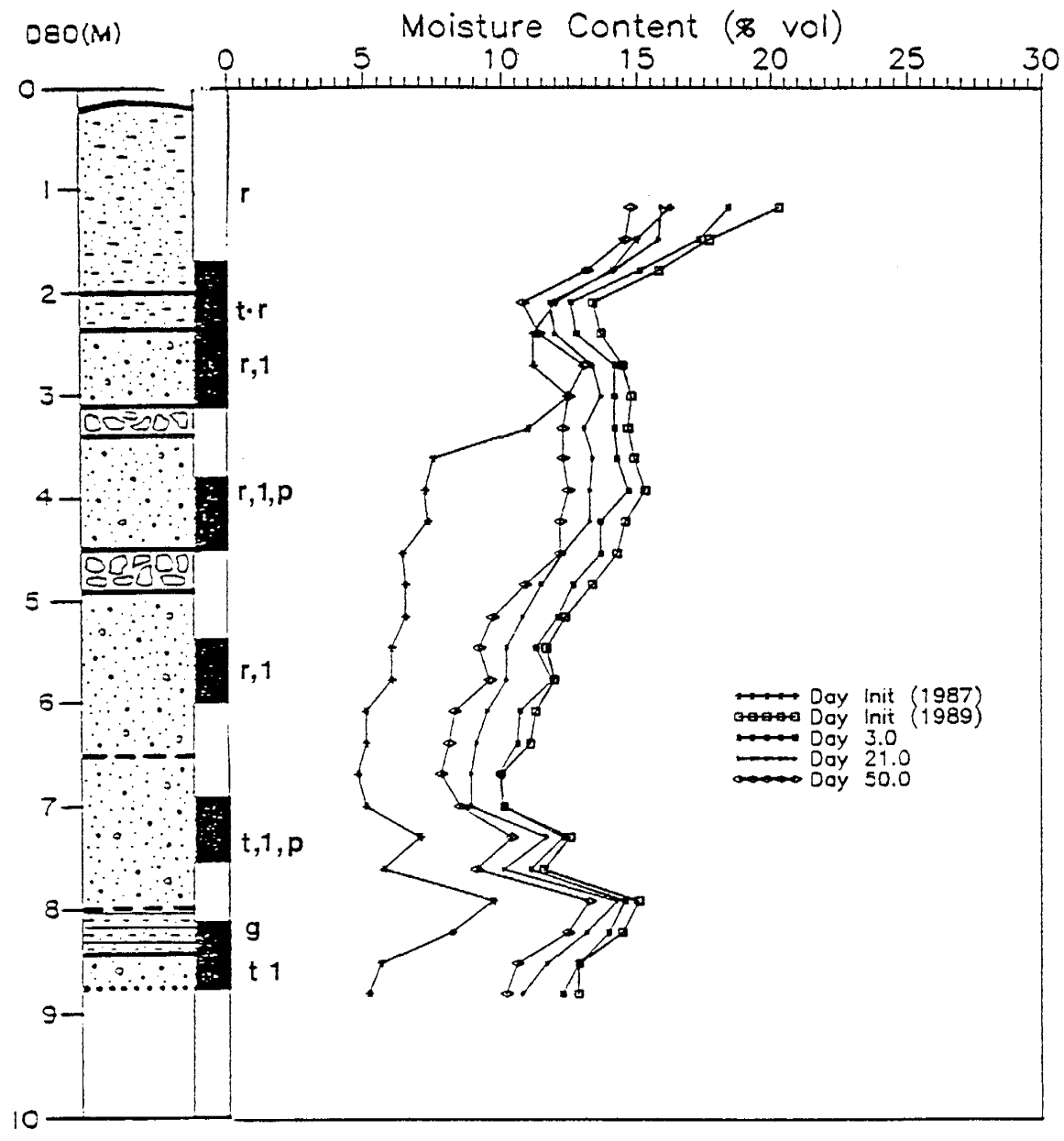

Figure 4-3 Station 8-15: moisture content profile and geology (after A. Stark, 1991).

lowest at this station and the change in moisture content from initial to stabilized conditions are the greatest at this location, lending support to the moisture dependent heterogeneity in hydraulic conductivity. Figure 4-4 shows the moisture content profile superposed with the geologic profile.

Station 12-18:

A similar phenomenon is happening at 3 m as at station 12-12. Ponding takes place right above the top most cobble layer which is between 3 and 4 m. There is a slight increase in moisture content at the lower cobble layer at 5 m and a third moisture content bulge above a third cobble between 6.3 and 7 m. There is also an increase in moisture at 8 m which is where there is a silty clay. Figure 4-5 shows the moisture content profile superposed with the geologic profile.

Station 15-6:

Initially there was a high moisture content at 2 m, the location of a 1 m thick clay (as seen in nearby PCS 11) but upon infiltration the largest moisture content was above the cobble layer at 4 m. Figure 4-6 shows the moisture content profile superposed with the geologic profile.

Station 15-8:

The initial profile showed a little low spot at the top most cobble layer at 2.4 m. Once infiltration started, the cobble at 5 m created a bulge in theta above it. PCS 18 shows the

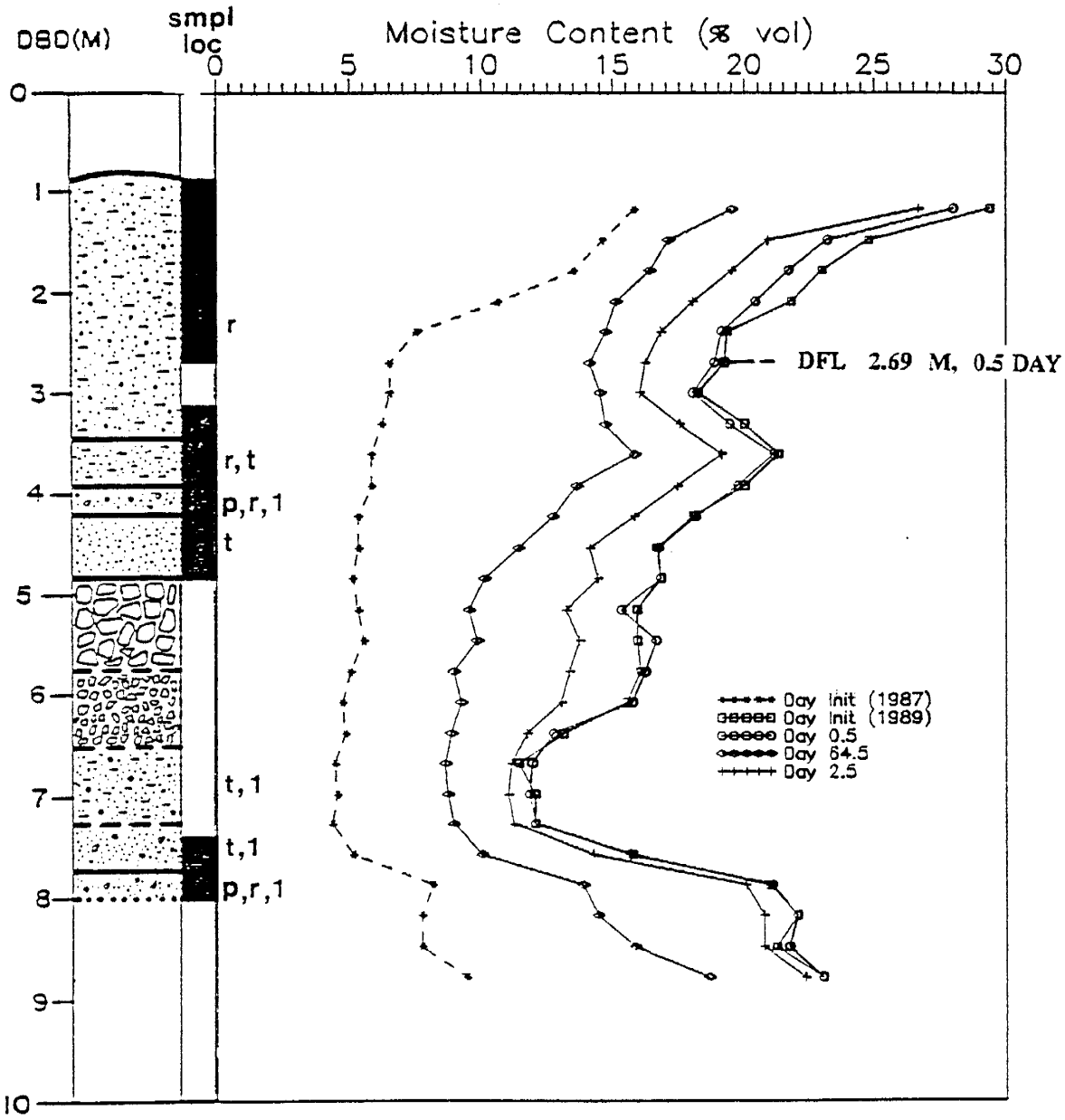

Figure 4-4 Station 12-12: moisture content profile and geology (after A. Stark, 1991).

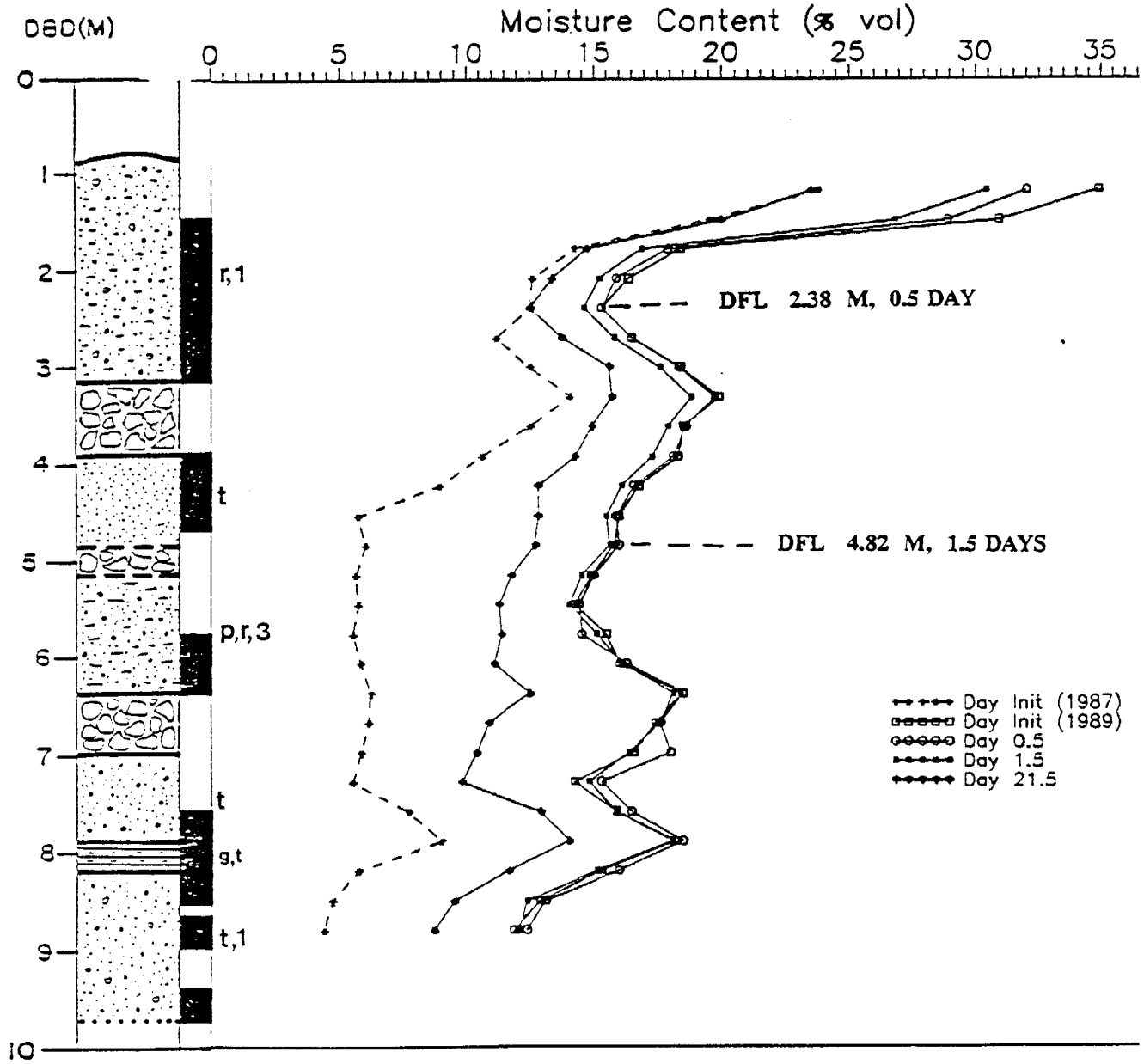

Figure 4-5 Station 12-18: moisture content profile and geology (after A. Stark, 1991).

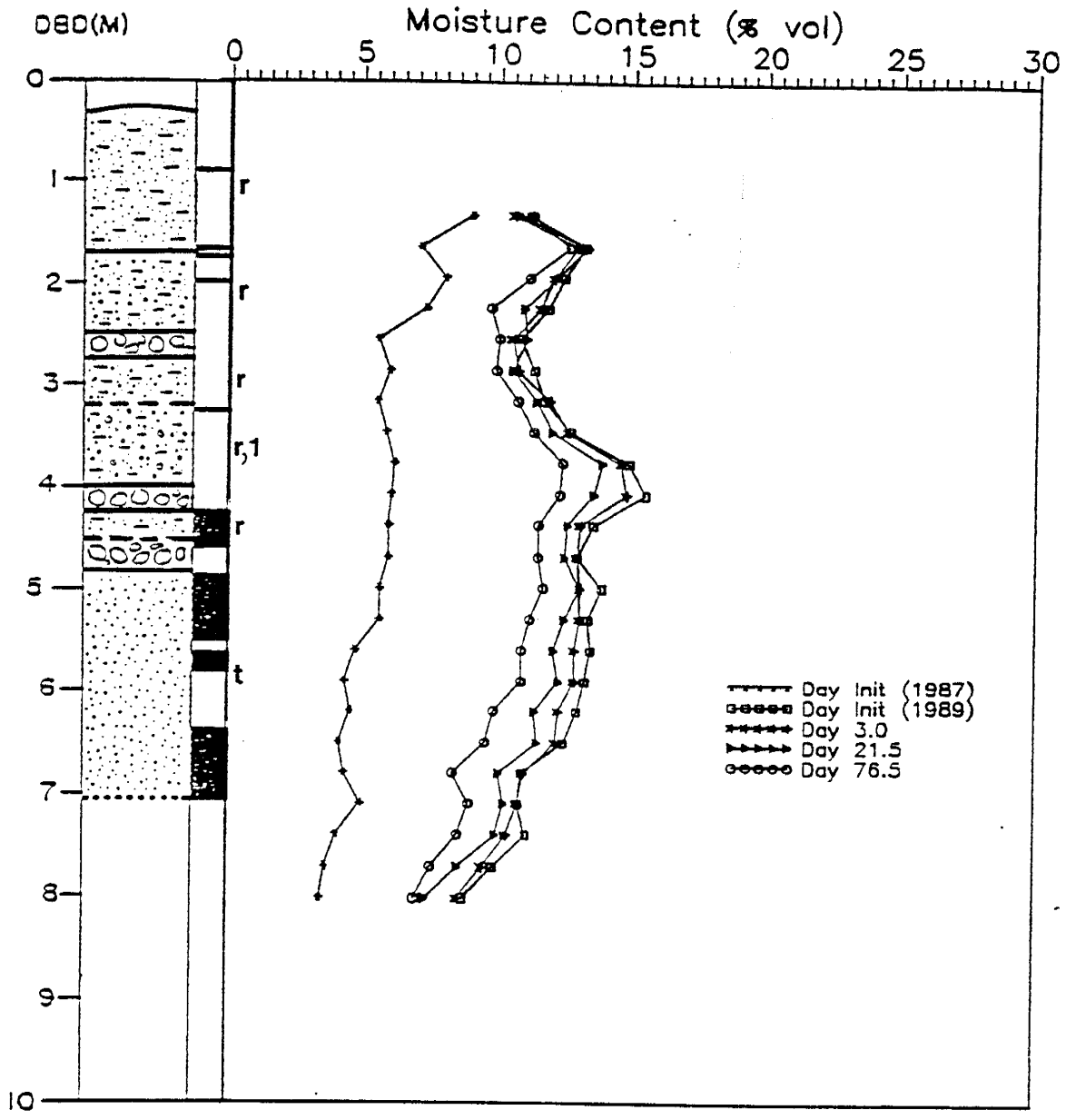

Figure 4-6 Station 15-6: moisture content profile and geology (after A. Stark, 1991).

top cobble also. Figure 4-7 shows the moisture content profile superposed with the geologic profile.

Station 15-15:

This station was located in the exact center of the irrigated plot and as a result was used by A. Stark (1991a) to analyze in detail the moisture content profile and to calculate unsaturated hydraulic conductivity. Initially and throughout the infiltration there was a bulge at the clay and silty/clay sand between 1.5 m and 2.5 m. Then there was a bulge at 3 m indicating ponding above the cobble layer at 3.5 m. The cobble layer at 5 m is not seen in the moisture content. There is a gravel layer at 7 m where the moisture content is the lowest, which would indicate that the moisture has traveled below this layer. In addition, below this depth, the moisture has not decreased to the initial theta yet so it has been wetted down to at least 9 m (the bottom of the profile). Figure 4-8 shows the moisture content profile superposed with the geologic profile.

Station 15-22:

Initially and throughout infiltration, the highest moisture content in this profile is at 2 m which is where a clay layer is, an expected event in unsaturated flow. Going downward, the moisture content is high above the cobble layer at 35 m. Figure 4-9 shows the moisture content profile superposed with the geologic profile.

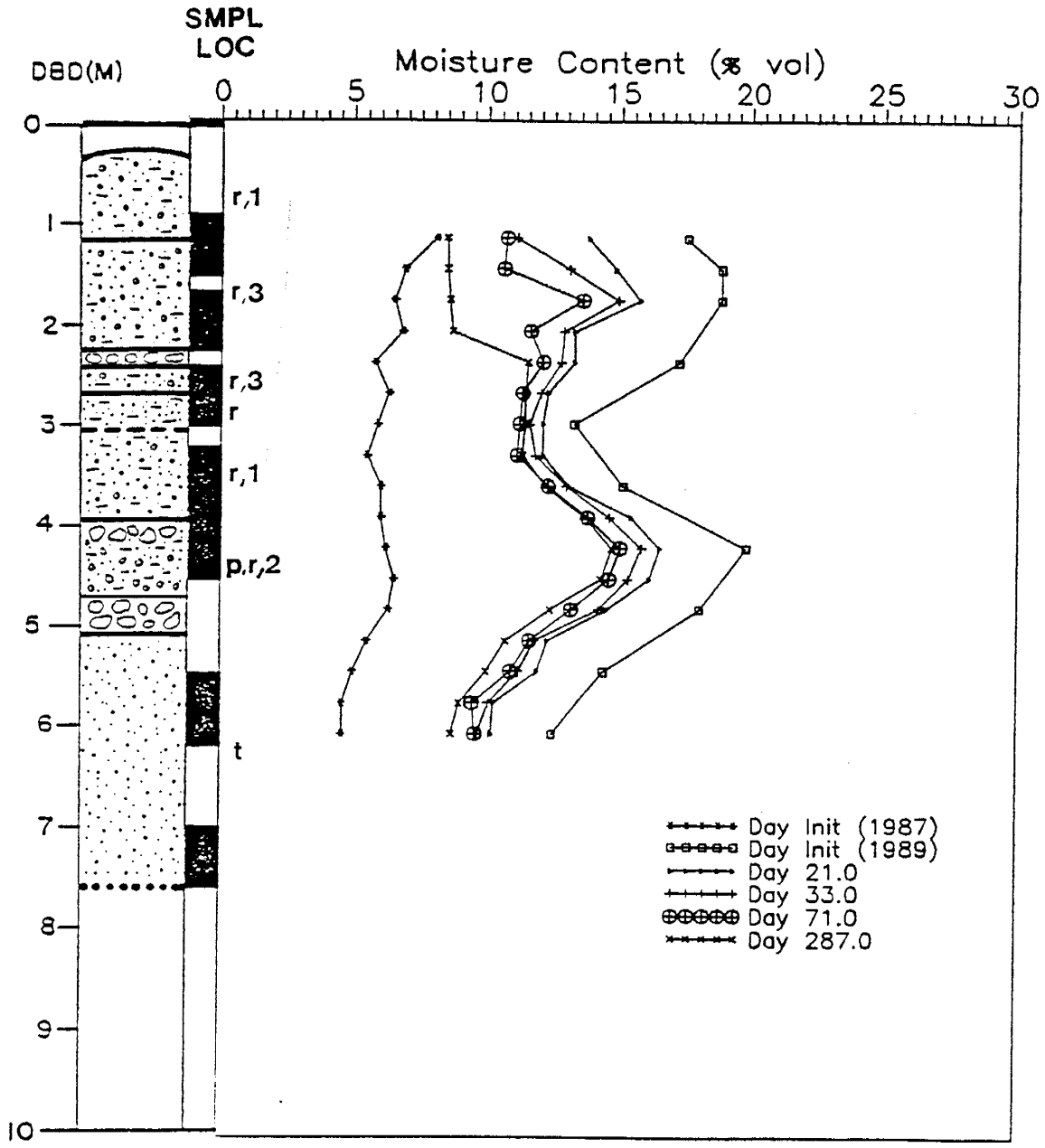

Figure 4-7 Station 15-8: moisture content profile and geology (after A. Stark, 1991).

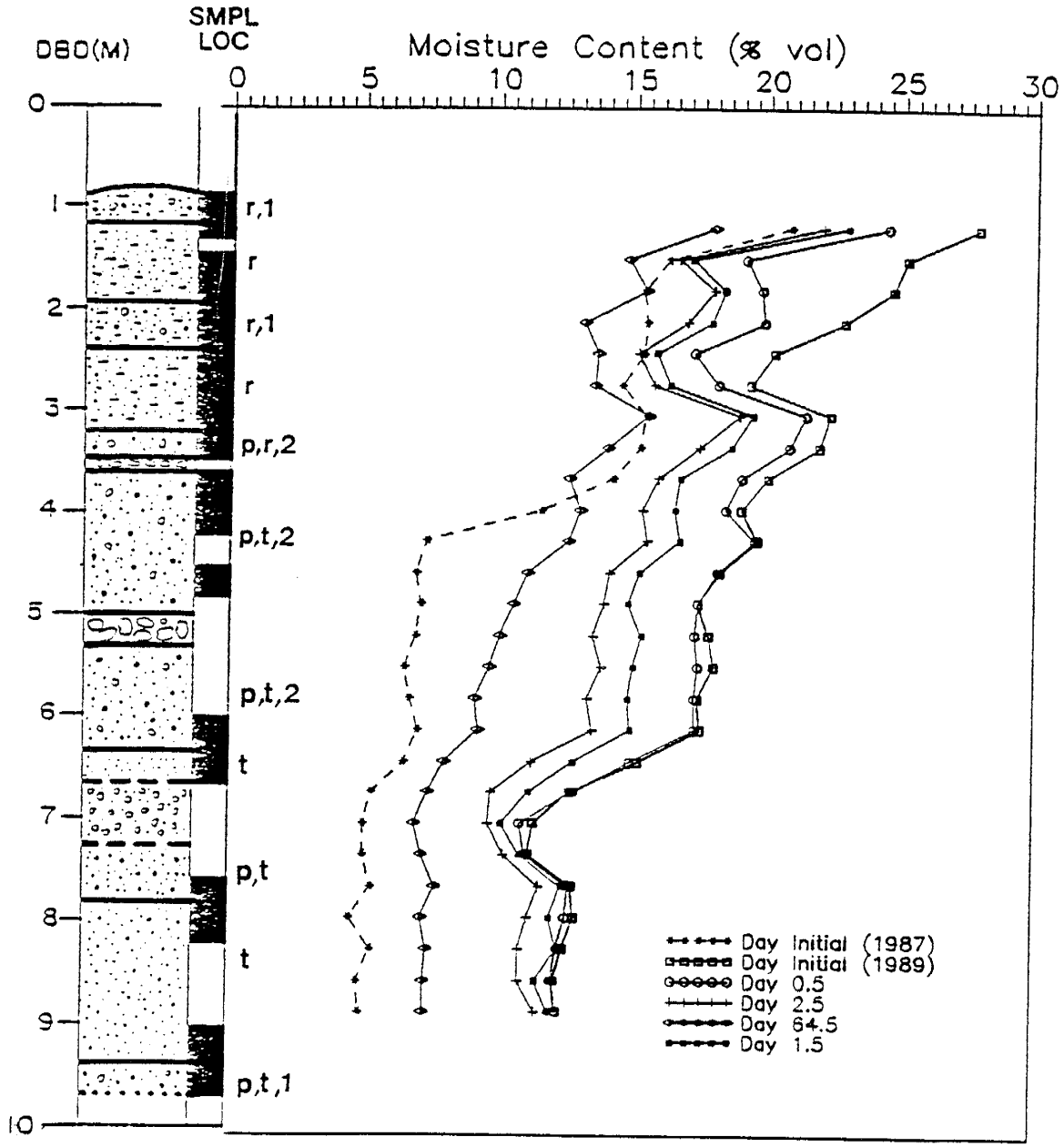

Figure 4-8 Station 15-15: moisture content profile and geology (after A. Stark, 1991).

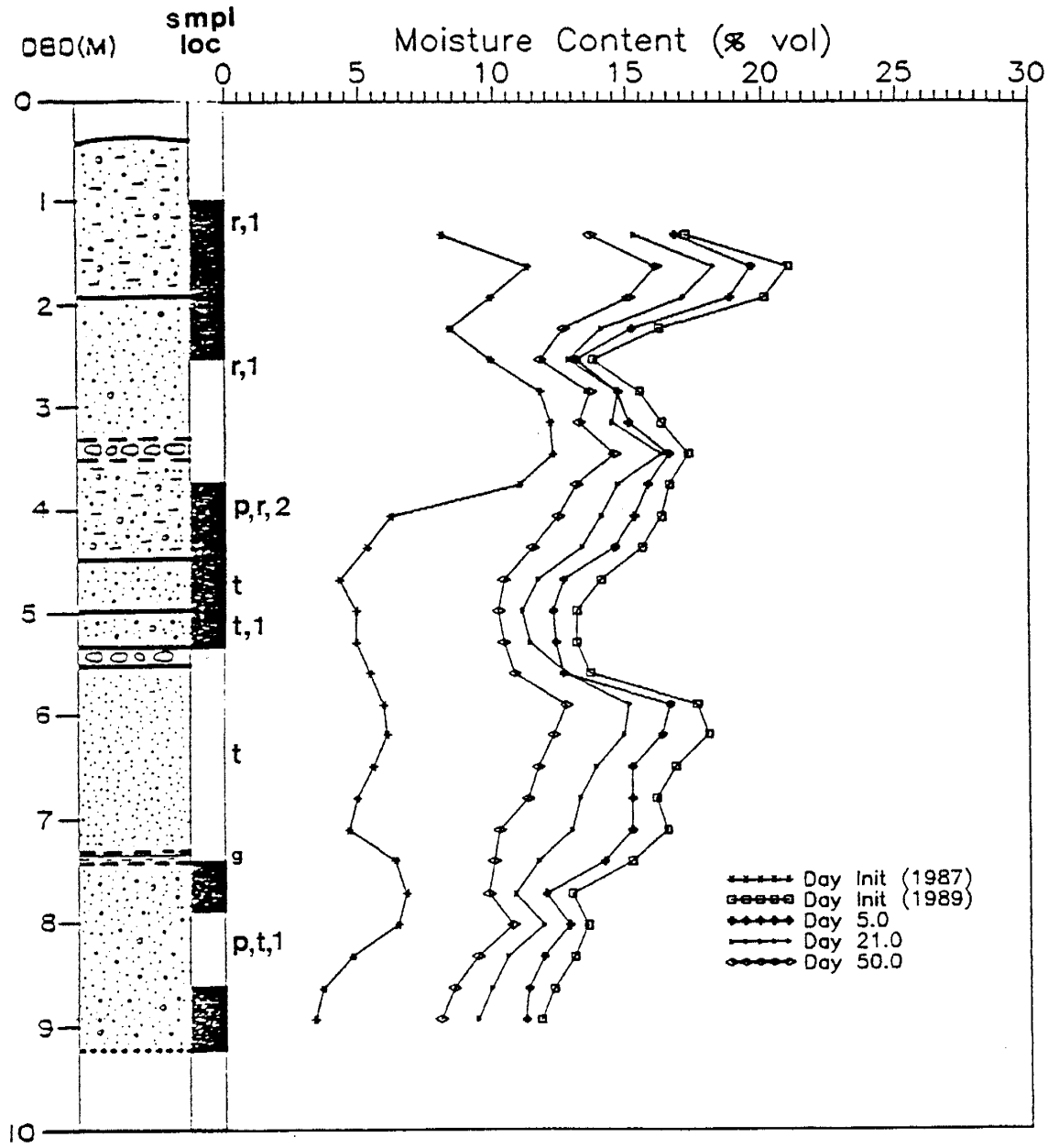

Figure 4-9 Station 15-22: moisture content profile and geology (after A. Stark, 1991).

Station 18-12:

The moisture content highs are at 2, 3.5, and 7 m, the depths that are shown to be high in clay and silt in this profile and in the NNE profile. The low moisture contents are found at 3 m and 6 m, the depths where the two cobble layers are. The drainage occurred quickly through this profile such that moisture levels quickly moved toward initial moisture contents. Figure 4-10 shows the moisture content profile superposed with the geologic profile.

Station 18-18:

The thick silty clay between 1 and 2 m creates a very high initial and infiltrating moisture contents at shallow depths. As expected the high moisture levels are at clay levels and the lowest levels are at cobble layer depths. Figure 4-11 shows the moisture content profile superposed with the geologic profile.

Station 22-15:

This station is located closest to the deep trench. Here the high moisture contents are at 2, 4.5, and 7 m. At 2 m there is a silty sand just as there is in the deep trench cross-section so the high moisture content may be attributed to grading or a high percentage of clay in the matrix. The low moisture contents are at 3 and 6 m, the depths of the cobble layers shown in the profile and discussed in Section 3.3. Figure 4-12 shows the moisture content profile superposed with the geologic profile.

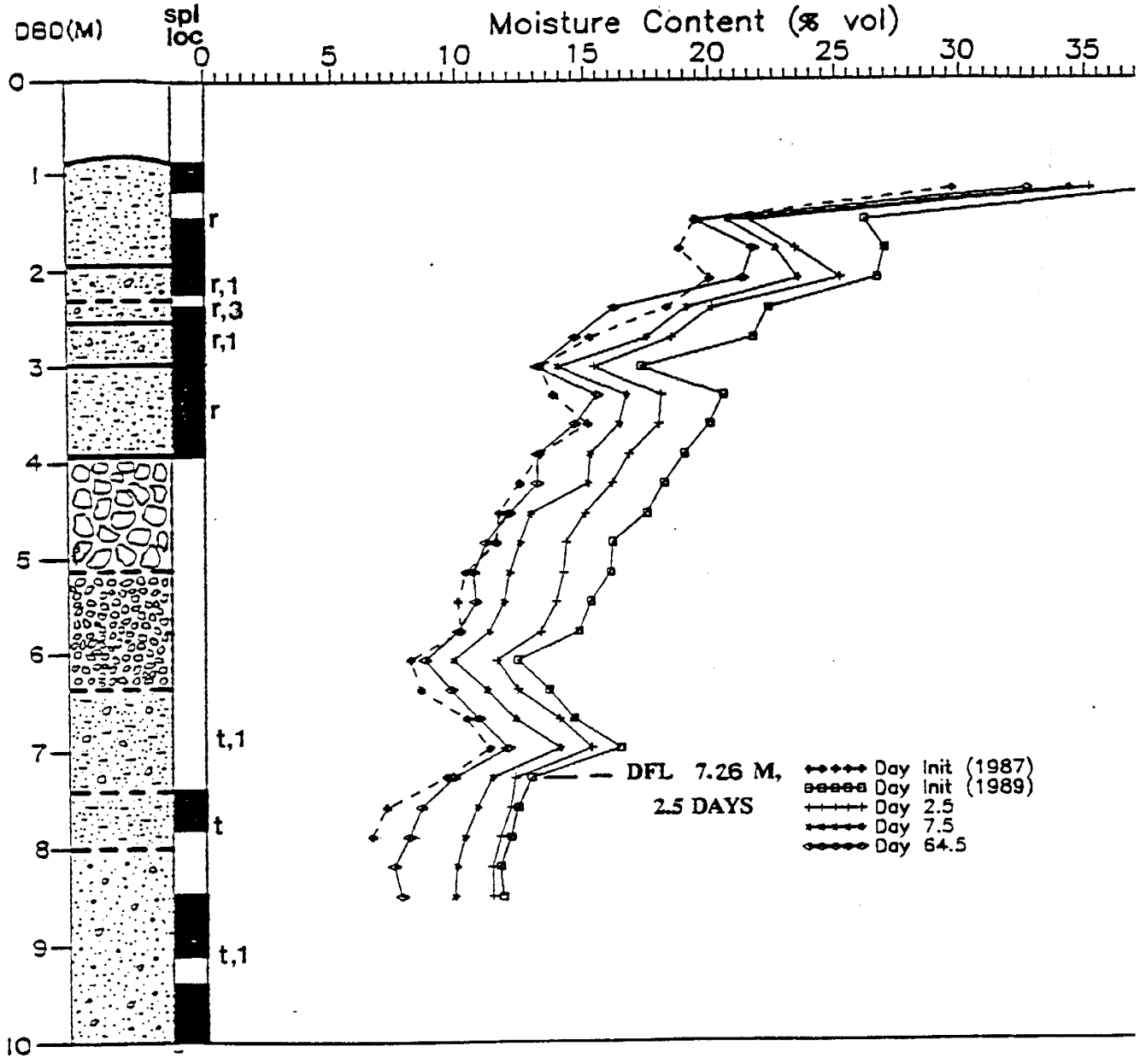

Figure 4-10 Station 18-12: moisture content profile and geology (after A. Stark, 1991).

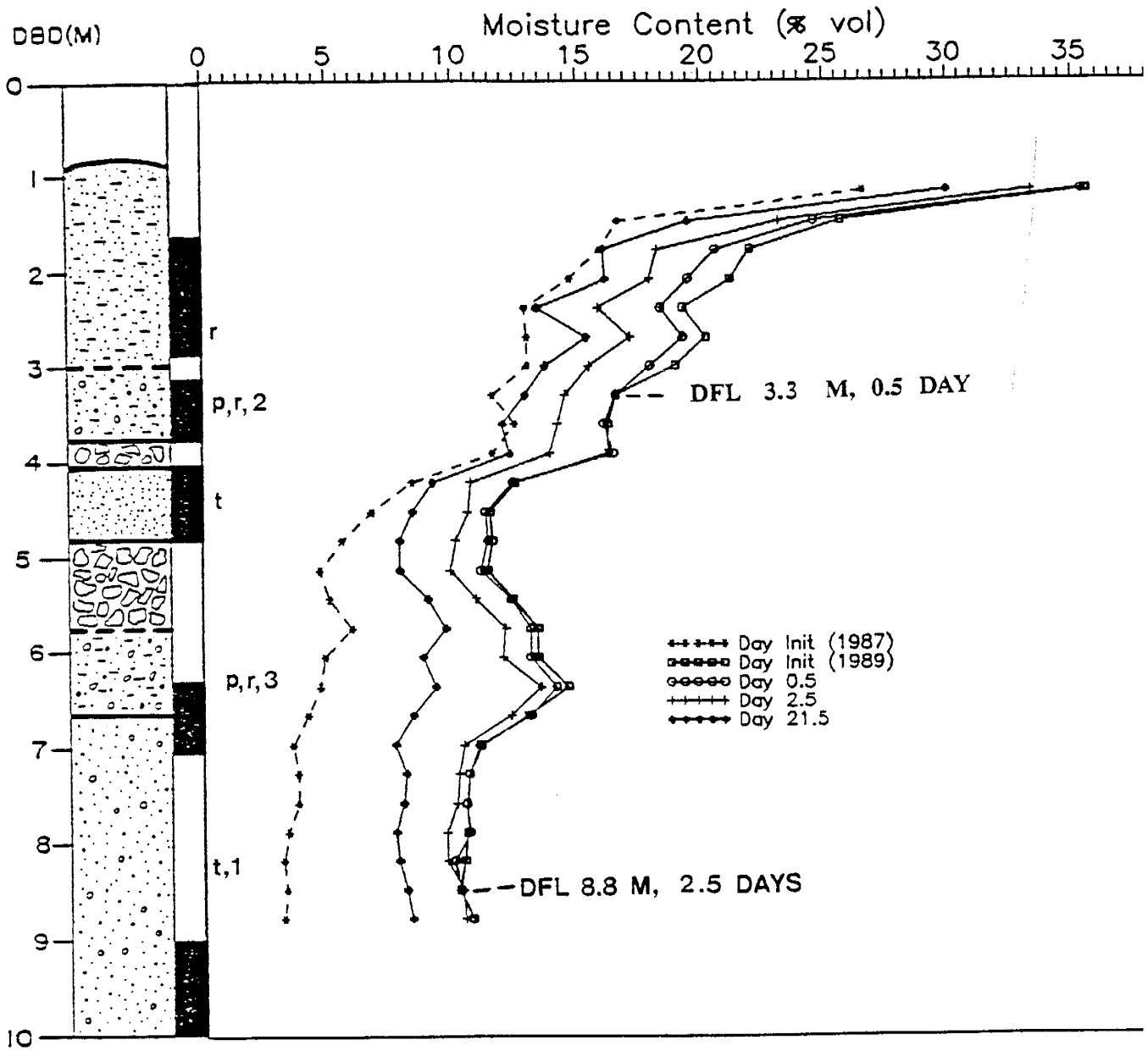

Figure 4-11 Station 18-18: moisture content profile and geology (after A. Stark, 1991).

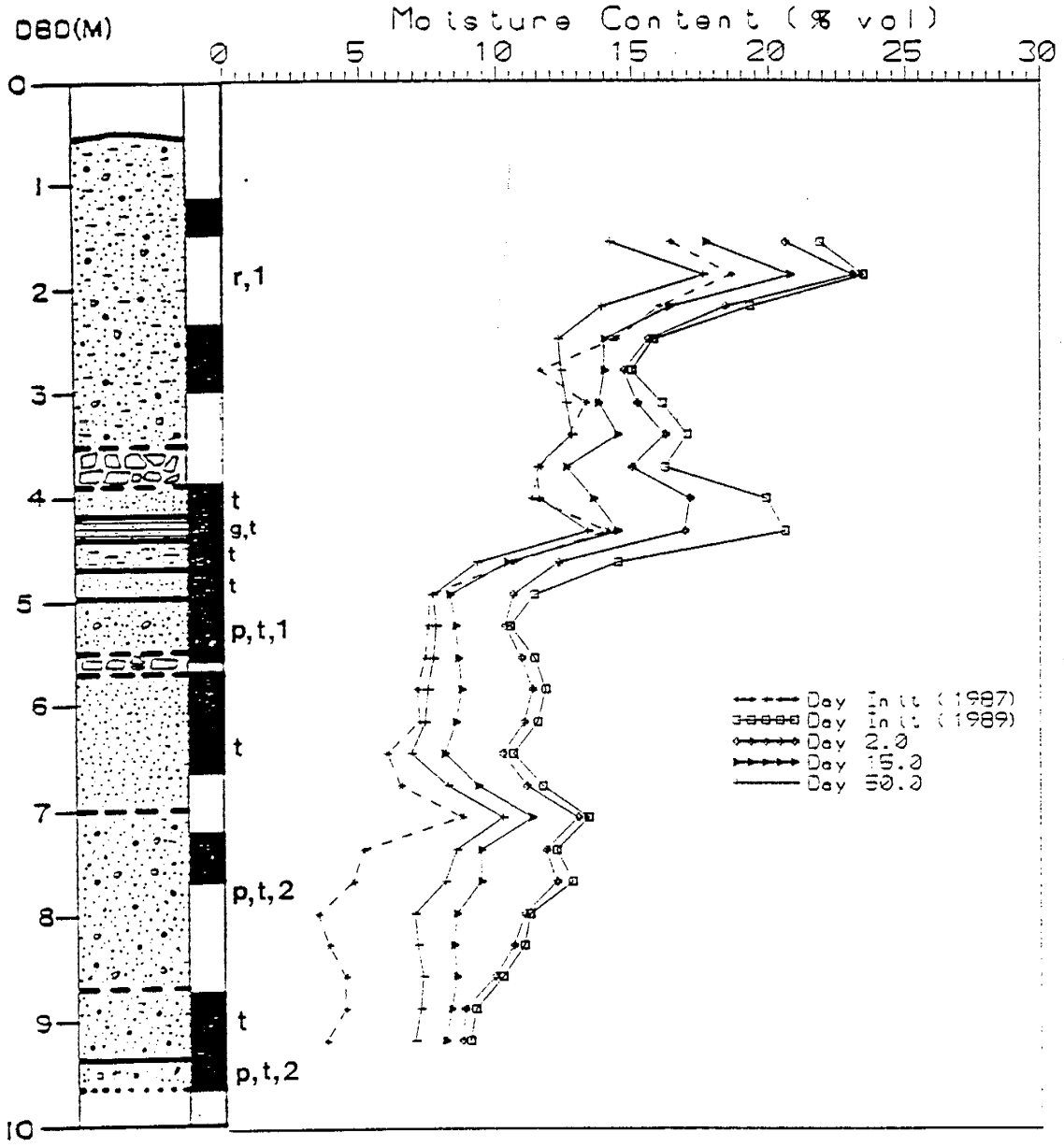

Figure 4-12 Station 22-15: moisture content profile and geology (after A. Stark, 1991).

In summary, the factors affecting the nature of drainage through this complex, stratified, system, are drastic changes in mean grain size (e.g. from silt to cobble), resulting differences in background or initial moisture content profiles, and the individual textural and structural patterns within each layer, the most difficult factor to characterize.

4.2 DATA REQUIREMENTS

When performing a remedial investigation, for example, a feasibility study of a clay or synthetic liner for a mill tailings pile, or when studying the geologic controls on drainage in the unsaturated zone as in this study, it is necessary to begin with a site assessment or site characterization. A site characterization, if performed successfully, includes the formulation of a conceptual model, and a study of the physical factors that shape the site and that shape the processes that the particular study is focused on. Since cost and time are of critical value in most cases, it is necessary to decide the quantity of data necessary to characterize and appropriately interpret a site. It is important to decide how accurate the characterization should be for the given purpose and scope of the project.

For the entire project, the main goals (as related to this particular study) were to:

1) study the infiltration and drainage of water beneath the plot
2) study the stratigraphy beneath the plot
3) characterize the hydraulic and geologic properties of the plot and their spatial distribution

4) study the geologic controls on the drainage phase

5) revise the conceptual model

Goals that are not related to this particular study and are not being discussed are related to model validation and to tracer studies that were performed at the site.

The conceptual model that was the original driving force for the entire project was based on infiltration theory and on similar previously performed unsaturated zone experiments. The model dictated the placement of instrumentation, the infiltration rate, sampling frequency, etc. The conceptual model had included a sequence of distinct layers (Mattson, personal communication, 1991) but now that the project is in its final stages, it is clear that the original plans had not called for the type of complexity and heterogeneity found in the geology and hydraulic properties beneath the plot. It is now seen that each layer has coarsening and fining sequences with complex variability in matrix grain size distributions. This is a system that is unusually difficult to characterize as well as to simulate.

Sources of error in soil moisture field investigations have been investigated by Bruce and Luxmore(1986) and Russo and Bresler(1982) among others. The three main sources of error encountered in the field during estimation of hydraulic parameters for a given error tolerance are:

1) errors arising from poor reproducibility of measurements

2) errors resulting from spatial variability inherent in the field

3) errors resulting from the finiteness of an area over which the measurements are made These three sources of error must be considered before proceeding with a field program. Other site related considerations that should be thought about before beginning a field study such as this are variation in erosion, drainage, slope or other readily determined features that are related to water or matrix properties and the nature of spatial heterogeneity. Such variability may take the form of geologic characteristics or sequences that restrict or encourage drainage, or temperature, evaporation and transpiration differences or patterns. Instrument considerations should include sampling volumes, cost, insulation, practicality, data manipulation, calibration procedures, operator performance and instrument performance among others.

The data that were collected to satisfy the above goals and to test the conceptual model have been discussed in the present study, and by Mattson (1989), Parsons (1988), Schmidt-Petersen (1991), and A. Stark (personal communication, 1991). The following is a summary of the data that were appropriately collected and data that was insufficient or overabundant for satisfying the goals.

The data that were successfully collected to satisfy the goals of the project involved:

1) the soil moisture contents collected from the neutron access tubes. The tubes were spatially arranged to cover the entire plot and were installed deep enough to see the effects of drainage throughout the alluvial fan facies.
2) the split spoon samples taken from each borehole. There were enough samples taken

to characterize the geologic framework both vertically and aerially.

3) the two trenches. The trenches afforded a revealing view of the geology of the alluvial fan beds with a small glimpse of the Rio Grande facies.

4) the tensiometer locations. The tensiometers were spatially arranged to cover the field plot sufficiently for hydraulic head measurements.

5) disc permeameter measurements. The horizontal characterization of the variability of hydraulic conductivity along a transect within the alluvial fan facies was performed on such a fine scale that the characterization was quite adequately performed (Schmidt-Petersen, 1991).

6) the laboratory experiments. Most of the hydraulic property assessment through experimentation was successful. The grain size distribution samples showed the extensive variability in grain size within the alluvial fan material. The only other way to see this was through the trenches but in most other studies only borehole samples would be available. Therefore the grain size analyses were quite useful.

The data and/or methodology that involved unforseen and/or unexpected problems involved:

1) the cobble layers. There was no reliable way to drill through or sample the cobble layers and/or the cobble layer matrix at the site. This is an area within vadose zone hydrology which still needs much research. Gardner (1986) presents a way to calculate hydraulic conductivity in a stony soil but this would not be appropriate for a hazardous waste site or for a study where many measurements are needed, such as in this study.

In this case the cobble layer(s) controlled and guided much of the drainage and hydraulic properties at the site. The only in situ view of some of the cobble layers was in the deep trench. There it was seen that the matrix consists of everything from a clay to a gravel. The thickness of the gravel layers was not as accurately portrayed in the stratigraphic column presented in this study and by Parsons (1988) due to sampling and drilling difficulties within the cobble layers. The sorptivity of the gravel/cobble layers was not accurately measured with the disc permeameter.

2) the tensiometer depths. The tensiometers did not access enough depths to capture the vertical heterogeneity in the two geologic facies. They were not installed to sufficient depths to match the neutron probe moisture data. The moisture contents were available to about 10 m while the tensiometer head data was only available to five meters.
3) the thermistors that were installed to measure soil temperature. The instruments did not work reliably.
4) The bulk density, shelby tube permeameter, and hanging column experiments all suffered from sample disturbance among other problems.
5) It would have been helpful to have had more boreholes to the 10 m depth so see what the character of the deep cobble layer better and to be able to better correlate the drainage at that depth.
6) Piping of water and tracers occurred along some of the less well constructed monitoring stations. This problem would not have been detected without the trench construction.

6) Now that the geology is known it is known that the most useful information would be to have the hydraulic characteristics of each layer. Unfortunately the grain size distribution data can not be divided by layer.

5. Summary and Conclusions

Summary

A three scale geologic characterization was performed of the middle Rio Grande valley, alluvial fan formation, and the specific sequence found in the 20 m section investigated below the vadose zone research plot just west of Socorro, New Mexico. This characterization set the stage for vertical hydraulic characterization of the five meter thick heterogeneous alluvial fan sequence and the underlying mostly homogeneous ancestral Rio Grande facies. Laboratory studies were performed on samples from a deep core and a study of the drainage results from a two year long infiltration experiment was conducted. The variable initial moisture contents, particle size distributions, and hydraulic conductivities (determined with the disc permeameter) within the alluvial fan units would suggest that any water infiltrating through this profile would travel laterally as well as vertically downward. The profound layering of coarse-over-fine and fine-over-coarse sequences also influenced the drainage paths. In general, the water followed the natural dip in the alluvial material. The results from this study indicate that a highly stratified profile would inhibit and slow down the movement of leachate from a waste site located at the surface. The drainage analysis through such a profile would be quite helpful in predicting future fluid movement through a similar geologic environment.

Conclusions

The following were the interpretations that would be drawn from this study:

1) The initial moisture content and grain size distribution of the alluvial fan beds were quite a bit more variable than those of the Rio Grande facies. This quantitative analysis agreed with the ponding events and possible lateral flow during drainage through the alluvial fan units.

2) The vertical spatial variability of grain size, and saturated water content within the Rio Grande facies, ranged from about 0.5 to 2.0 meters. Up to two meter thick deposits were not unusual for a meandering river such as the Rio Grande to leave behind. The average thickness of beds within the Rio Grande material were about one meter. Therefore these correlation lengths may be attributed to the various deposits left by an ancestral meandering river.

3) Hydraulic conductivity within the Rio Grande sands was found to be about 10^{-2} to 10^{-3} cm/sec, confirming previous studies.

4) The disc permeameter study presented hydraulic conductivity values within the individual alluvial fan units that ranged from 1.05×10^{-2} cm/sec to 3.31×10^{-4} cm/sec. The

waterlaid and debris flow deposits had unusually low hydraulic conductivities due to their fine matrix.

5) The laboratory results for the ENE fluvial sand samples presented vertical correlation for saturated water content and d10 size and uncorrelated results for bulk density, porosity, and log Ksat. The uncorrelated results between d10 and log Ksat may be explained by insufficient sampling frequency (in the vertical direction) for the Ksat analyses. The d10 analysis was performed on hundreds of samples while the saturated hydraulic conductivity analysis was performed on approximately 50 samples.

6) The detailed geologic investigation revealed a very complex set of clayey, sandy, and cobble-filled beds interrelated in such a way as to create conduits and barriers to drainage. All three types of alluvial fan deposits were found within the deep trench; debris flows, intermediate deposits, and waterlaid deposits. These deposits were overlying the finer grained ancestral Rio Grande sands.

6. Recommendations for Future Work

Several analyses that are beyond the scope of the present project include a modeling project, analyzing the tracer experiments performed previously, and performing further geostatistical analyses on the laboratory data. The modeling project should simulate unsaturated drainage through a set of beds where the thickness, grain size distribution, and hydraulic properties of each of the beds are defined. The tracer experiment results from previous studies at this field site should be analyzed with respect to the specific geologic information presented in Section 3.3. Thirdly, more geostatistical analyses such as kriging may be employed in analyzing the nature of the alluvial fan/fluvial sand contact and the trends in grain size, hydraulic conductivity, and saturated water content. Inverse or experimental vertical variograms could be found from simulations of real profiles where the bed thicknesses, and average hydraulic properties had been assigned to beds. If the resulting variograms matched those calculated from field data, there could be more confidence in the field results.

Finally, if a similar project is to be performed elsewhere it is important to know as much as possible about the geologic variability involved. Geologic variability and its nature, money permitting, is best found with test borings though the trench method has been most helpful in this study. More often than not it is not practical to dig trenches across field sites.

REFERENCES

Allen, J.R. 1970. Physical Processes of Sedimentation, American Elsevier Publishing Company, Inc. New York.

Andrews, E. 1982. Geologic Predictors of Saturated Hydraulic Conductivity in the fluvial sand of the Sevilleta Wildlife Refuge, Unpublished Independent Study, New Mexico Institute of Mining and Technology, Socorro, NM.

Arya, L.M. and J.F. Paris. 1981. A physioempirical model to predict the soil moisture characteristic from particle size and bulk density data, Soil Science Soc. of America J., 45:1023-1030.

Baldwin, B.1963. Geology and water resources of the Santa Fe area, New Mexico, USGS Water Supply Paper, 1528: 21-89.

Bakr, A.A., L.W. Gelhar, A.L. Gutjahr, and J.R. MacMillan. 1978. Stochastic analysis of spatial variability in subsurface flows 1. Comparison of one and three-dimensional flows, Water Resour. Res., 14: 263-271.

Blissenbach, E. 1954. Geology of Alluvial Fans in Semiarid Regions, GSA Bulletin, **65**: 175-190.

Bruce, R.R. and R.J. Luxmore. 1986.Methods of Soil Analysis, Part 1, American Society of Agronomy-Agronomy Monograph no.9.

Bull, W.B. 1962. Relation of textural (CM) patterns to depositional environment of alluvial-fan deposits, J. Sed. Petrology, 32: 211-216.

_____. 1963. Alluvial-fan deposits in western Fresno County, CA, Jour. Geology, 71: 243-251.

_____. 1964. Alluvial fans and near surface subsidence in western Fresno County, CA, USGS Professional Paper, 437-A.

_____. 1972. Recognition of ancient sedimentary environments, Soc. Econ. Paleontologists and Mineralogists, Special Publ. 16: 68-83, Tulsa.

_____. 1977. The alluvial fan environment, Progr. Phys. Geogr., 1: 222-270.

Byers, E. and D. B. Stephens. 1983. Statistical and Stochastic Analysis of Hydraulic Conductivity and Particle-Analysis in a Fluvial Sand, Soil Sci. Am. J., 47-56: 1072-1081.

Chamberlain, R.M. 1980. Cenezoic stratigraphy and structure of the Socorro Peak volcanic center, Central New Mexico, New Mexico Bureau of Mines and Mineral Resources, Open File Report 118, 2 vol. 495 p.

Chapin, C.E., and Seager, W.R. 1975. Evolution of the Rio Grande rift in the Socorro and Las Cruces areas, New Mexico Geol. Soc., Guidebook to the 26th field conference, p.297-321.

CSIRO Disc Permeameter Instrumentation Manual. 1988. Cnberra, Australia.

Delhomme, J.R. 1978. Kriging in the hydrosciences, Advances in Water Resources, 1(5): 251-266.

_____. 1979. Spatial variability and uncertainty in groundwater flow parameters: A geostatistical approach. Water Resources Res., 15(1): 269-280.

Denny, C.S. 1940. Tertiary geology of the San Acacia area, New Mexico, J. of Geol., 48: 73-106.

Deutsch, C.V. and Journel, A.G. 1991. "GSLIB: Geostatistical Software Library User's Guide", Submitted to Oxford University Press, New York.

Englund, E. and Sparks, A. 1988. "GEOEAS: Geostatistical Environmental Assessment Software", USEPA, Las Vegas, Nevada.

Flannigan, K.G. 1989. Field simulation of waste impoundment seepage in the vadose zone: Non-reactive solute transport through a stratified, unsaturated field soil, Unpubished MS Independent Study Paper, New Mexico Instititute of Mining and Technology, Socorro, New Mexico.

Gardner, W.H. 1986. Water content In Klute, A. (ed.) Methods of Soil Analysis, Part I. Physical and Mineralogical Methods, 2nd edition, American Society of Agron., Madsion, WI 493-544.

Grabka, D.P. 1991. Field simulation of waste impoundment seepage in the vadose zone: multiple-tracer transport experiment in a stratified, heterogeneous, unsaturated field soil, Unpublished Independent Study, New Mexico Institute of Mining and Technology, Socorro, New Mexico.

Greenholtz, D.E., T-CJim-Yeh, M.S.B. Nash, and P.J. Wierenga. 1988. Geostatistical

analysis of soil hydrologic properties in a field plot, Jour. Cont. Hydr., 3:227-250.

Gutjahr, A.L., L.W. Gelhar, A.A. Bakr, and J.R. MacMillan. 1978. Stochastic analysis of spatial variability in subsurface flows 2. Evaluation and application, Water Resour. Res., 14(5): 953-959.

Hawley, J. et al. 1976. Quaternary stratigraphy in the Basin and Range and Great Plains provinces, New Mexico and Western Texas, In Quaternary stratigraphy of North America, Dowden, Hutchinson, and Ross, Inc. 235-279.

Hillel, D. 1980. Infiltration and Surface Runoff, Internal Drainage and Redistribution Following Infiltration **In** Applications of soil physics. Edited by D. Hillel, 5-75. New York: Academic Press.

_____. 1980a. Fundamentals of Soil Physics, Academic Press,Inc., New York,413p.

_____. 1980b. Applications of Soil Physics, Academic Press,Inc., New York, 385p.

Hillel, D., V.D. Krentos and Y. Stylianou. 1972. Procedure and Test of an Internal drainage method for measuring soil hydraulic characteristics *In situ*, Soil Science, 114(5).

Johnson, N.M. and S.J. Dreiss. 1989. Hydrostratigraphic interprtation using indicator geostatistics, Water Resour. Res., 25(12): 2501-2510.

Johnson, T.M., K. Cartwright and R.M. Schuller. 1981. Monitoring of leachate migration in the unsaturated zone in the vicinity of sanitary landfills, Ground Water Monitoring Review, Fall: 55-63.

Johnson, W.R. 1988. Soil Survey of Socorro County Area, New Mexico, Soil Conservation Service, USDA.

Journel, A.G., and Ch. J. Huijbregts. 1978. Mining Geostatistics, Academic Press, Inc., New York.

Kottlowski, F.E. 1958. Geologic history of the Rio Grande near El Paso, West Texas Geological Society, Guidebook 1958 field trip 46-54.

Lambe, T. William. 1951. Soil Testing for Engineers, John Wiley and Sons, New York.

Larson, M.B. and D.B. Stephens. 1985. A comparison of methods to characterize unsaturated hydraulic properties of mill tailings, Proc. Seventh Symposium on Management of uranium Mill Tailings, Low Level Waste and Hazardous Waste,

Fort Collins, CO.

Machette,M.N. 1978. Geologic map of the San Acacia quadrangel, Socorro County, New Mexico, USGS Map GQ-1415 1:24,000.

Mack, G.H. and K.A. Rasmussen. 1984. Alluvial-fan sedimentation of the Cutler Formation near Gateway, Colorado, Geological Society of America Bulletin, 95:109-116.

Masch,F.D. and K.T. Denny. 1966. Grain size distribution and its effect on the permeability of unconsolidated sands, Water Resources Research, 2: 665-677.

Mattson, E. 1989. Field simulation of waste impoundment seepage in the vadose zone: Experiment design and 2-D modeling, Unpublished Independent Study, New Mexico Institute of Mining and Technology, Socorro, New Mexico.

McCord, J.T. and D.B. Stephens. 1987. Lateral moisture flow beneath a sandy hillslope without an apparent impeding layer, Hydro. Proc., 1:225-238.

McLemore, V.T. and M.R. Bowie. 1987. Guidebook to the Socorro area, New Mexico, 24th annual meeting of the Clay Minerals Society and 36th annual Clay Minerals Conference, New Mexico Bureau of Mines and Mineral Res., 75 p.

McPherson et al. 1987. Fan-deltas and braid deltas: varieties of coarse-grained deltas, Geol. Soc. of America Bulletin, 99:331-340.

McWhorter, D.B. and J.D. Nelson. 1979. Unsaturated flow beneath tailings impoundments, In Journal of the Geotechnical Division, Proceedings of the American Society of Civil Engineers, Vol. 105.

Miall, . 1973. Markov chain analysis applied to an ancient alluvial plain succession, Sedimentology, 20: 347-364.

Miller, D.E., and W.H. Gardner. 1962. Water infiltration into stratified soil, Soil Sci. Soc. Am. Proc., 26: 115-118.

Mualem,Y. 1984. Anisotropy of unsaturated soils, Soil Sci. Soc. Am. J., 48:505-509.

Nielsen, D.R., J.W. Biggar, and K.T. Erh. 1973. Spatial variability of field measured soil water properties. Hilgardia, 42(7): 215-260.

Palmquist, W.N. and A.I. Johnson. 1962. Vadose flow in layered and nonlayered materials, USGS Professional Paper, 450-C: C142-C143.

Parsons, A.M. 1988. Field Simulation of Waste Impoundment Seepage in the Vadose Zone: Site Charaterization and one-dimensional analytical modeling, Unpublished Independent Study, New Mexico Institute of Technology, Socorro, New Mexico.

Perroux, K.M. and I. White. 1988. Designs for disc permeameters, Soil Sci. Am. J. 52(5).

Rabold, R.R. 1984. The results of a borhole infiltration test with a shallow water table, Unpublished Independent Study, New Mexico Institute of Mining and Technology, Socorro, New Mexico.

Russo, D. and E. Bresler. 1982. Soil hydraulic properties as stochastic processes:II. Errors of estimates in a heterogeneous field, Soil Soc. Am. J. 46:20-26.

Schmidt-Petersen, R.I. 1991. Field simulation of waste impoundment seepage in the vadose zone: Horizontal spatial variability of the geologic and hydraulic properties of an alluvial fan facies, Unpublished Independent Study, New Mexico Institute of Mining and Technology, Socorro, New Mexico.

Soil Test Inc. 1975. Munsell Color Chart. MacBeth; Division of Koll Morgen Instruments Corp, Baltimore, MD.

Stark, A.M. 1991. Late stage infilration and drainage in a heterogeneous, partially saturated soil profile, Unpublished Independent Study, New Mexico Institute of Mining and Technology, Socorro, New Mexico.

Stephens, D.B. and S. Heerman. 1988. Dependence of anisotropy on saturation in a stratified sand, Water Resources Research, 24(5):770-778.

Traitwein, S.J. and D.B. Daniel. 1983. Case history of water flow through unsaturated soil, In The role of the unsaturated zone in hazardous waste disposal, Ed. by Mercer et al.

U.S. Geological Survey. 1979. Socorro Quadrangle, New Mexico-Socorro County, 7.5 Minute Series, Scale 1:24,000

Warrick, A.W. and D.R. Nielsen. 1980. Spatial variability of soil physical properties. **In** Applications of soil physics. Edited by D. Hillel, 319-44. New York: Academic Press.

Yeh, T.C. and L.W. Gelhar. 1983.Unsaturated flow in heterogeneous soils, In The role of the unsaturated zone in hazardous waste disposal, Ed. by Mercer et al.

APPENDICES

A. Particle size distribution and moisture content results

B. Disc permeameter data sheets

C. ENE laboratory results

D. Geologic time scale

E. Boring logs

APPENDIX A

SUMMARY OF PARTICLE SIZE DISTRIBUTION
DEEP BOREHOLES

SAMPLE	AVERAGE DEPTH BELOW DATUM (m)	d10 (mm)	d30 (mm)	d50 (mm)	d60 (mm)	Cu	Cc	GRAVIMETR MOISTURE CONTENT %
ENE1T	0.43	0.089	0.295	1.148	1.995	22.387	0.490	*
ENE1B	0.76	1.000	0.079	0.105	5.623	5.623	0.001	*
ENE3a	1.62	15.849	0.158	0.316	0.427	0.027	0.004	10.82
ENE3b	1.75	0.174	1.148	6.310	NA	NA	NA	4.1
ENE3C	1.9	0.178	2.512	NA	NA	NA	NA	3.84
ENE3d	2.08	0.269	3.981	NA	NA	NA	NA	4.21
ENE3e	2.22	0.257	1.950	NA	NA	NA	NA	2.05
ENE5a	3.46	0.324	4.677	NA	NA	NA	NA	0.5
ENE5b	3.55	0.151	1.023	6.166	NA	NA	NA	0.98
ENE5c	3.67	0.170	0.398	1.445	2.754	16.218	0.339	2.25
ENE5d	3.78	0.063	0.095	0.132	0.166	2.630	0.871	10.15
ENE6	4.48	0.068	0.214	0.479	0.661	9.772	1.023	5.62
ENE7T	4.65	0.012	0.126	0.363	0.562	46.862	2.349	*
ENE7B	5.33	0.015	0.085	0.112	0.135	8.993	3.580	*
ENE8a	5.57	0.155	0.407	3.020	6.310	40.738	0.170	1.98
ENE8b	5.67	0.195	0.955	3.802	6.310	32.359	0.741	0.73
ENE8c	5.75	0.372	5.888	1.000	1.000	NA	NA	0.069
ENE8d	5.94	0.117	0.214	0.269	3.236	27.542	0.120	1.41
ENE9T	6.33	0.010	0.107	0.178	0.240	23.988	4.786	*
ENE9B	6.86	0.251	0.372	0.501	0.646	2.570	0.851	*
ENE10T	7.49	0.010	1.000	0.251	0.324	32.359	309.030	*
ENE10B	7.62	0.214	0.447	1.122	1.622	7.586	0.575	*
ENE11T	8.03	0.302	0.479	0.794	1.259	4.169	0.603	*
ENE11B	8.38	0.204	0.389	0.871	1.514	7.413	0.490	*
ENE12T	8.85	0.148	0.282	0.447	0.603	4.074	0.891	*
ENE12B	9.14	0.195	0.380	0.708	1.047	5.370	0.708	*
ENE13T	9.71	0.178	0.331	0.603	0.891	5.012	0.692	*
ENE13B	9.91	0.200	0.398	0.813	1.202	6.026	0.661	*
ENE14T	10.24	0.234	0.417	1.047	1.995	8.511	0.372	*
ENE14B	10.67	0.126	0.200	0.282	0.316	2.512	1.000	*
ENE15T	11.13	0.138	0.251	0.347	0.912	6.607	0.501	*
ENE15B	11.43	0.224	0.324	0.490	0.589	2.630	0.794	*
ENE16T	11.82	0.117	0.282	0.457	0.589	5.012	1.148	*
ENE16B	12.19	0.120	0.178	0.251	0.269	2.239	0.977	*
ENE17T	12.84	0.135	0.269	0.417	0.589	4.365	0.912	*
ENE17B	12.95	0.120	0.251	0.676	0.589	4.898	0.891	*
ENE18T	13.43	0.132	0.234	0.316	0.355	2.692	1.175	*
ENE18B	13.72	0.166	0.240	0.282	0.316	1.905	1.096	*
ENE19T	14.17	0.148	0.240	0.282	0.316	2.138	1.230	*
ENE19B	14.48	0.234	0.355	0.575	0.912	3.890	0.589	*
ENE21T	16.39	1.585	1.995	2.089	2.239	1.413	1.122	*
ENE21B	16.76	0.117	0.251	0.437	0.603	5.129	0.891	*
ENE22T	17.04	0.117	0.245	0.380	0.501	4.266	1.023	*
ENE22B	17.32	0.126	0.263	0.437	0.589	4.677	0.933	*
ENE23T	17.65	0.158	0.257	0.324	0.380	2.399	1.096	*
ENE23B	17.98	0.148	0.398	0.776	1.023	6.918	1.047	*

ENE24T	18.33	0.078	0.191	0.324	0.417	5.370	1.122	*
ENE24B	18.59	0.079	0.257	0.661	1.122	14.125	0.741	*
ENE25T	18.85	0.093	0.209	0.372	0.501	5.370	0.933	*
ENE25B	19.05	0.013	0.079	0.398	0.603	46.351	0.805	*
ENE26T	19.51	0.115	0.204	0.269	0.316	2.754	1.148	*
ENE26B	19.81	0.151	0.257	0.347	0.407	2.692	1.072	*
NNW1a	0.19	0.120	0.240	0.355	0.398	3.311	1.202	10.55
NNW1b	0.57	0.063	0.120	0.214	0.295	4.677	0.776	8.21
NNW2b	1.32	0.107	0.166	0.257	0.708	6.607	0.363	5.17
NNW2c	1.46	0.050	0.112	0.195	0.288	5.754	0.871	9.42
NNW3a	1.68	0.056	0.126	0.263	0.389	6.918	0.724	7.42
NNW3b	1.89	0.056	0.151	0.324	0.479	8.511	0.851	7.74
NNW3c	2.11	0.052	0.126	0.269	0.398	7.586	0.759	9.2
NNW4a	2.51	0.063	5.012	0.447	0.676	10.715	588.844	8.61
NNW4b	2.71	0.062	0.245	0.501	0.776	12.589	1.259	8.78
NNW4c	2.87	0.062	0.107	0.288	0.427	6.918	0.437	9.03
NNW4d	3	0.141	0.513	2.188	4.786	33.884	0.389	5.36
NNW5a	3.4	0.056	0.155	0.316	0.447	7.943	0.955	8.51
NNW5b	3.6	0.182	0.398	1.259	6.166	33.884	0.141	4.07
NNW5c	3.76	0.158	1.259	NA	NA	NA	NA	2.91
NNW6a	4.11	0.166	0.427	0.832	1.230	7.413	0.891	6.65
NNW6b	4.29	0.050	0.132	0.407	0.562	11.220	0.617	19.27
NNW6c	4.46	0.191	0.427	1.175	3.020	15.849	0.316	2.62
NNW7a	4.64	0.214	0.427	0.891	1.413	6.607	0.603	5.16
NNW7b	4.86	0.126	0.224	0.324	0.407	3.236	0.977	7.94
NNW7c	5.17	0.132	0.240	0.363	0.398	3.020	1.096	11.69
NNW8a	5.46	0.123	0.219	0.316	0.372	3.020	1.047	4.72
NNW8b	5.69	0.209	0.316	1.950	0.032	0.151	15.136	4.33
NNW8c	5.94	0.224	0.851	2.512	4.074	18.197	0.794	3.75
NNW9a	6.26	0.166	0.389	0.776	1.047	6.310	0.871	3.6
NNW9b	6.44	0.240	1.202	2.570	3.388	14.125	1.778	3.13
NNW9c	6.72	0.251	1.738	3.802	5.754	22.909	2.089	3.2
NNW10a	7.18	0.417	1.259	2.344	3.311	7.943	1.148	2.45
NNW10b	7.38	0.050	0.074	0.158	0.234	4.677	0.468	22.67
NNW10c	7.53	0.117	0.251	0.398	0.631	5.370	0.851	3.77
NNW11a	7.68	0.447	0.891	1.622	2.344	5.248	0.759	5.18
NNW11b	7.81	0.117	0.331	0.676	1.000	8.511	0.933	4.55
NNW11c	8.02	0.135	0.251	0.331	0.398	2.951	1.175	4.2
NNW11d	8.27	0.200	0.407	0.708	1.000	5.012	0.832	4.19
NNW12a	8.48	0.132	0.380	0.794	1.202	9.120	0.912	1.51
NNW12b	8.62	0.234	0.490	0.912	1.202	5.129	0.851	5.9
NNW12c	8.9	0.110	0.151	0.195	0.209	1.905	1.000	2.81
NNW13a	9.21	0.129	0.263	0.525	1.175	9.120	0.457	2.26
NNW13b	9.45	0.151	0.269	0.363	0.427	2.818	1.122	2.84
NNW13c	9.77	0.269	0.631	0.891	1.660	6.166	0.891	2.97
NNW14a	10.08	0.186	0.339	0.603	0.794	4.266	0.776	2.57
NNW14b	10.3	0.191	0.309	0.589	1.175	6.166	0.427	5.35
NNW14c	10.54	0.112	0.234	0.589	0.832	7.413	0.589	4.9
NNW15a	10.73	0.178	0.224	0.427	0.589	3.311	0.479	15.73
NNW15b	10.84	0.050	0.794	0.170	0.234	4.677	53.703	9.05
NNW15c	10.96	0.071	0.380	6.310	NA	NA	NA	11.15
NNW15d	11.22	0.071	0.148	0.200	0.229	3.236	1.349	4.91
NNW16a	11.51	0.071	0.132	0.234	0.380	5.370	0.646	9.91

NNW16b	11.79	0.224	0.331	0.525	0.676	3.020	0.724	7.12
NNW16c	12.05	0.107	0.269	0.417	0.603	5.623	1.122	7.73
NNW16d	12.15	0.050	0.063	0.112	0.224	4.467	0.355	11.59
NNW17a	12.6	0.120	0.229	0.295	0.331	2.754	1.318	3.34
NNW17b	12.84	0.107	0.257	0.417	0.603	5.623	1.023	5.57
NNW18a	13.05	0.117	0.209	0.257	0.302	2.570	1.230	4.68
NNW18b	13.29	0.120	0.229	0.282	0.309	2.570	1.413	5.67
NNW18c	13.58	0.126	0.224	0.302	0.324	2.570	1.230	4.18
NNW19a	13.82	0.219	0.251	0.302	0.324	1.479	0.891	4.67
NNW19b	14.01	0.120	0.229	0.295	0.324	2.692	1.349	5.17
NNW19c	14.2	0.110	3.715	0.316	0.257	2.344	489.779	4.76
NNW19d	14.39	0.063	0.158	0.240	0.269	4.266	1.479	5.46
NNW20a	14.56	0.132	0.240	0.316	0.363	2.754	1.202	3.81
NNW20b	14.71	0.112	0.245	0.324	0.380	3.388	1.413	7.09
NNW20d	15.19	0.063	0.174	0.269	0.331	5.248	1.445	12.68
NNW21a	15.35	0.050	0.151	0.263	0.316	6.310	1.445	11.97
NNW21b	15.51	0.063	0.209	0.316	0.389	6.166	1.778	5.57
NNW21c	15.67	0.107	0.263	1.175	1.738	16.218	0.372	9.44
NNW21d	15.78	0.056	0.162	0.447	0.661	11.749	0.708	11.07
NNW21e	15.88	0.050	0.240	0.324	0.389	7.762	2.951	7.89
NNW21f	15.97	NA	0.162	0.347	0.525	NA	NA	9.82
NNW22a	16.08	0.178	0.214	0.275	0.316	1.778	0.813	5
NNW22b	16.22	0.050	0.214	0.316	0.372	7.413	2.455	6.01
NNW22c	16.46	0.158	0.240	0.309	0.372	2.344	0.977	3.99
NNW22d	16.67	0.107	0.257	0.427	0.550	5.129	1.122	9.49
NNW22e	16.73	0.138	0.263	0.398	0.501	3.631	1.000	4.24
NNW27a	21.34	0.013	0.076	0.257	0.324	25.704	1.413	17.12
NNW27b	22.34	0.120	0.275	0.407	0.513	4.266	1.230	17.78
SSW1	0.64	0.050	0.112	0.200	0.288	5.754	0.871	3.78
SSW2a	0.84	0.100	0.295	0.891	0.562	5.623	1.549	5.06
SSW2b	0.99	0.032	0.120	0.269	0.501	15.849	0.912	6.02
SSW2c	1.14	0.074	0.126	0.209	0.269	3.631	0.794	3.61
SSW2d	1.37	0.050	0.115	0.245	0.407	8.128	0.646	4.14
SSW3a	1.65	0.063	0.158	0.427	0.813	12.882	0.490	3.93
SSW3b	1.78	0.075	0.309	0.776	1.175	15.668	1.084	10.15
SSW3c	1.96	0.075	0.079	0.141	0.195	2.600	0.432	13.28
SSW3d	2.18	0.040	0.107	0.200	0.269	6.761	1.072	4.01
SSW4a	2.4	0.075	0.316	0.955	1.660	22.131	0.804	9.66
SSW4b	2.58	0.040	0.081	0.151	0.214	5.370	0.776	13
SSW4c	2.77	0.040	0.093	0.162	0.214	5.370	1.023	6.73
SSW5a	3.22	0.075	0.158	0.324	0.525	6.998	0.638	4.32
SSW5b	3.48	0.245	0.692	3.890	5.623	22.909	0.347	4.5
SSW5c	3.59	0.063	0.158	0.427	0.794	12.589	0.501	9.88
SSW5d	3.71	0.138	0.794	4.398	6.457	46.774	0.708	5.95
SSW6a	4	0.085	0.398	1.585	4.169	48.978	0.447	5.87
SSW6b	4.18	0.251	0.692	1.514	1.995	7.943	0.955	3.57
SSW6c	4.37	0.316	1.514	4.365	6.310	19.953	1.148	11.27
SSW6d	4.51	0.032	0.032	0.105	0.141	4.467	0.224	18.49
SSW7a	4.73	0.141	0.603	1.660	2.818	19.953	0.912	5.25
SSW7b	4.94	0.141	0.562	1.995	3.981	28.184	0.562	4.69
SSW7c	5.17	0.166	0.245	0.302	0.324	1.950	1.122	4.16
SSW14a	15.69	0.126	0.224	0.269	0.302	2.399	1.318	7.77
SSW14b	15.9	0.148	0.240	0.295	0.316	2.138	1.230	7.15

SSW15a	16.27	0.115	0.195	0.251	0.288	2.512	1.148	8.15
SSW15b	16.48	0.120	0.214	0.263	0.309	2.570	1.230	8.23
SSW15c	16.67	0.126	0.214	0.257	0.288	2.291	1.259	7.14
SSW16a	16.86	0.126	0.234	0.302	0.324	2.570	1.349	6.06
SSW16b	17.06	0.182	0.257	0.316	0.363	1.995	1.000	5.08
SSW16c	17.24	0.191	0.263	0.331	0.380	1.995	0.955	5.32
SSW16d	17.39	0.032	0.075	0.162	0.234	7.413	0.759	33.93
SSW17a	17.6	0.105	0.214	0.263	0.309	2.951	1.413	8.03
SSW17b	17.71	0.050	0.141	0.269	0.316	6.310	1.259	19.32
SSW17c	17.78	0.120	0.269	0.550	0.955	7.943	0.631	8.19
SSW17d	17.92	0.123	0.195	0.257	0.309	2.512	1.000	5.47
SSW17e	18.08	0.135	0.427	0.851	1.175	8.710	1.148	5.79
SSW17f	18.2	0.141	0.282	0.427	0.589	4.169	0.955	5.12
SSW18a	18.34	0.075	0.178	0.295	0.347	4.624	1.216	10.44
SSW18b	18.58	0.112	0.316	0.525	0.676	6.026	1.318	6.36
SSW18c	18.88	0.138	0.229	0.316	0.389	2.818	0.977	10.27
SSW18d	19	0.151	0.501	0.813	1.096	7.244	1.514	5.27
SSW19a	19.22	0.075	0.214	0.269	0.316	4.217	1.928	7
SSW19b	19.28	0.141	0.245	0.447	0.380	2.692	1.122	5.73
SSW19c	19.36	0.107	0.135	0.170	0.191	1.778	0.891	5.67
SSW20a	19.78	0.100	0.200	0.282	0.324	3.236	1.230	8.62
SSW20b	19.82	0.141	0.309	0.575	0.794	5.623	0.851	3.47
SSW20c	19.99	0.123	0.186	0.407	0.490	3.981	0.575	6.14
SSW21a	20.27	0.106	0.234	0.389	0.513	4.842	1.012	5.21
SSW21b	20.36	0.145	0.245	0.324	0.389	2.692	1.072	3.96
SSW21c	20.51	0.138	0.263	0.457	0.708	5.129	0.708	7.94
SSW22a	20.6	0.162	0.316	0.501	0.631	3.890	0.977	28.65
SSW22b	20.8	0.138	0.229	0.316	0.380	2.754	1.000	11.31
SSW22c	21	0.200	0.398	0.631	0.794	3.981	1.000	15.13
SSW22d	21.18	0.100	0.200	0.282	0.324	3.236	1.230	15.2

* SEE SECTION 2.5 FOR HYDRAULIC PROPERTIES OF THESE SAMPLES

SUMMARY OF PARTICLE SIZE DISTRIBUTION
SHALLOW BOREHOLES

SAMPLE	AVERAGE DEPTH BELOW DATUM (m)	d10 (mm)	d30 (mm)	d50 (mm)	d60 (mm)	Cu	Cc	GRAVIMETR MOISTURE CONTENT %
NNE1a	0.18	1.000	1.000	0.098	0.123	0.123	8.128	8
NNE1b	0.28	1.000	0.427	1.413	1.738	1.738	0.105	1.5
NNE1c	0.43	0.023	1.000	0.079	0.200	8.675	217.907	9.96
NNE1d	0.58	0.010	0.141	0.339	0.372	35.725	5.164	4.27
NNE1e	0.68	0.012	0.081	0.148	0.200	16.627	2.759	12.88
NNE2b	1.34	0.075	0.240	0.562	0.813	10.839	0.944	6.04
NNE2c	1.47	0.050	0.120	0.263	0.398	7.962	0.726	7.62
NNE4a	2.38	0.075	0.245	0.708	1.180	15.740	0.681	9.83
NNE4b	2.68	1.000	7.943	0.269	0.398	0.398	158.489	11.57
NNE5a	3.00	0.093	0.166	0.269	0.324	3.467	0.912	9.81
NNE5b	3.21	0.219	0.871	3.311	1.000	4.571	3.467	9.56
NNE5c	3.44	1.000	0.178	0.398	0.676	0.676	0.047	7.17
NNE6a	3.72	0.251	0.631	1.288	2.188	8.710	0.724	3.75
NNE6b	3.92	0.049	0.195	0.407	0.692	14.119	1.122	7.68
NNE6c	4.10	0.001	0.079	0.105	0.126	125.893	50.119	1.1
NNE6d	4.24	1.000	1.000	1.000	1.000	1.000	1.000	7.72
NNE6e	4.34	0.106	0.141	0.186	0.219	2.065	0.861	11.8
NNE7a	4.46	0.063	0.251	0.501	0.776	12.303	1.288	4.17
NNE7b	4.27	0.025	0.162	0.240	0.282	11.274	3.733	5.2
NNE7c	5.02	0.123	0.251	0.407	0.724	5.888	0.708	7.12
NNE8a	5.26	0.117	0.151	0.200	0.234	1.995	0.832	7.73
NNE8b	5.45	0.178	0.324	0.617	0.891	5.012	0.661	4.96
NNE8c	5.64	0.045	0.062	0.075	0.129	2.884	0.661	4.24
NNE8d	5.71	0.257	1.072	3.802	6.295	24.491	0.710	9.88
NNE8e	5.82	0.214	1.023	2.512	1.000	4.677	4.898	2.97
NNE9a	6.01	0.309	1.585	3.311	1.000	3.236	8.128	2.82
NNE9b	6.24	0.245	0.794	1.660	2.239	9.120	1.148	2.15
NNE9c	6.43	0.102	0.245	0.363	0.427	4.169	1.380	2.62
NNE9d	6.69	0.245	1.096	3.802	1.000	4.074	4.898	3.11
SSE1	2.59	0.078	0.214	0.562	0.955	12.303	0.617	7.27
SSE2	4.12	1.000	0.309	1.023	1.514	1.514	0.063	7.73
SSE3	4.37	0.138	0.490	1.122	3.162	22.909	0.550	6.78
SSE3a	4.54	0.275	2.239	1.000	1.000	3.631	18.197	2.26
SSE4	4.74	0.151	0.257	0.331	0.389	2.570	1.122	2.25
SSE5	4.97	0.178	0.251	0.316	0.347	1.950	1.023	5.61
SSE6	5.13	0.126	0.427	1.180	2.630	20.893	0.550	2.87
SSE7	5.28	0.195	0.257	0.331	0.372	1.905	0.912	3.01
SSE8	5.93	0.191	0.251	0.309	0.331	1.738	1.000	3.15
SSE10	5.56	0.068	0.229	0.363	0.501	7.413	1.549	3.2
SSE11	5.72	0.162	0.200	0.309	0.339	2.089	0.724	3.27
SSE12	5.86	0.186	0.251	0.316	0.339	1.820	1.000	3.07
SSE13a	5.97	0.214	0.269	0.347	0.398	1.862	0.851	3.2
SSE13b	6.03	0.178	0.302	0.417	0.550	3.090	0.933	3.39

SSE14	6.06	1.000	0.138	0.302	0.427	0.427	0.045	31.69
WSW1	0.45	0.100	0.480	1.580	2.880	28.840	0.800	5.33
WSW2a	0.83	0.065	0.160	0.400	0.790	12.300	0.499	3.78
WSW2b	1.11	0.191	0.790	2.570	3.980	20.890	0.821	5.17
WSW2c	1.41	0.063	0.140	0.360	0.550	8.710	0.566	11.78
WSW3a	1.79	1.000	3.631	1.000	1.000	1.000	13.183	8.32
WSW3b	1.95	0.126	0.580	2.400	4.270	33.880	0.625	5.49
WSW3c	2.16	0.068	0.130	0.250	0.390	5.750	0.637	10.83
WSW4	2.48	1.000	1.000	1.000	1.000	1.000	1.000	12.82
WSW5	3.01	1.000	1.000	1.000	1.000	1.000	1.000	15.71
WSW5a	3.51	0.066	0.170	0.390	0.590	8.910	0.742	10.39
WSW5b	3.64	0.214	1.070	6.030	7.940	37.150	0.674	3.58
WSW6a	3.75	0.240	0.910	4.070	7.080	29.510	0.487	2.20
WSW6b	4.27	0.040	0.060	0.210	0.320	7.940	0.281	3.02
WSW7	4.56	0.155	0.630	2.090	3.980	25.700	0.643	12.90
WSW8	5.24	0.155	1.350	1.000	1.000	6.452	11.758	2.42
WSW9	6.25	0.148	0.290	0.460	0.630	4.270	0.902	9.03
WSW9a	6.71	0.148	0.250	0.320	0.360	2.450	1.173	0.80
WNW1b	0.67	0.003	0.130	0.260	0.420	138.960	13.413	5.81
WNW2a	0.84	0.063	0.120	0.250	0.400	6.310	0.571	7.58
WNW2b	1.21	0.068	0.100	0.160	0.220	3.310	0.668	11.9
WNW3	2.21	0.059	0.090	0.170	0.260	4.370	0.528	9.69
WNW4a	2.43	0.062	0.100	0.210	0.480	7.760	0.336	8.88
WNW4b	2.72	0.191	0.320	0.620	0.790	4.170	0.679	11.18
WNW4c	2.96	0.074	0.190	0.350	0.460	6.170	1.061	9.45
WNW5b	3.25	0.071	0.180	0.410	0.630	8.910	0.724	7.7
WNW5c	3.33	0.191	1.120	6.610	8.910	46.770	0.737	4.05
CUTTINGS	3.51	0.138	0.480	1.170	2.000	14.450	0.835	9.33
WNW6a	4.04	0.138	0.250	0.360	0.440	3.160	1.029	6.94
WNW6b	4.29	0.078	0.210	0.350	0.450	5.750	1.256	14.85
WNW6c	4.37	0.132	0.250	0.360	0.430	3.240	1.101	4.45
WNW6d	4.50	0.129	0.300	0.600	0.830	6.460	0.841	6.01
WNW7a	4.88	0.155	0.410	1.050	2.450	15.850	0.443	7
WNW7b	5.08	0.087	0.220	0.450	0.710	8.130	0.784	13.84
WNW7c	5.22	0.182	1.410	4.680	7.080	38.900	1.543	2.3
WNW8a	5.46	0.093	0.420	0.590	0.890	9.550	2.131	4.64
E1a	0.40	0.112	0.251	0.589	1.000	8.913	0.562	3.85
E1b	0.54	0.071	0.145	0.302	0.550	7.762	0.537	5.38
E1c	0.69	0.158	0.603	1.995	3.311	20.893	0.692	4.95
E2a	0.92	0.138	0.501	1.479	2.399	17.378	0.759	4.39
E2b	1.21	0.141	0.550	1.738	3.236	22.909	0.661	4.7
E2c	1.45	0.331	1.096	3.890	1.000	3.020	3.631	3.18
E3a	1.96	0.158	0.661	1.995	2.754	17.378	1.000	5.51
E3b	2.18	0.316	1.995	7.079	8.511	26.915	1.480	3.05
E4a	2.51	0.251	1.318	4.677	1.000	3.981	6.920	4.21
E4b	2.74	0.063	0.100	0.120	0.282	4.467	0.560	10.34
E4c	2.92	1.000	0.123	0.316	0.490	0.490	0.031	7.41
E4d	3.03	0.105	0.331	0.912	1.660	15.349	0.631	4.24
E5a	3.54	0.011	0.112	0.219	0.302	27.454	3.790	9.45
E5b	3.69	0.158	0.631	1.660	2.455	15.488	1.023	5.08
E5c	3.79	0.209	3.981	1.000	1.000	4.786	75.360	0.94

E6a	4.53	0.158	0.603	1.995	3.388	21.380	0.676	4.62
N3a	1.72	0.007	1.000	0.126	0.195	27.855	732.659	6.43
N3b	2.10	0.023	0.120	0.245	0.363	15.786	1.731	3.76
N4a	2.36	1.000	0.085	0.209	0.339	0.339	0.021	3.94
N4b	2.51	0.079	0.251	0.589	0.955	12.023	0.832	2.13
N5	3.66	1.000	0.151	0.417	0.794	0.794	0.029	2.51
N6	4.04	0.063	0.166	0.389	0.457	7.244	0.955	3.39
S1a	0.13	0.091	0.263	0.603	0.851	9.333	0.891	2.88
S1b	0.29	0.033	0.209	0.388	0.575	17.438	2.299	7.31
S1c	0.48	0.066	0.148	0.309	0.468	7.079	0.708	5.39
S1d	0.67	0.079	0.200	0.363	0.513	6.457	0.980	4.55
S2	1.24	0.030	0.155	0.324	0.513	17.095	1.559	5.85
S3a	1.59	0.091	0.263	0.603	0.851	9.333	0.891	4.83
S3b	1.71	0.068	0.158	0.316	0.437	6.457	0.850	4.08
S3c	1.88	0.062	0.178	0.355	0.501	8.128	1.023	2.01
S3d	2.09	0.219	0.537	1.148	1.660	7.586	0.794	5.34
S3e	2.24	0.214	0.631	1.413	1.995	9.333	0.933	5.66
S4	2.96	0.110	0.339	0.891	1.413	12.882	0.741	3.26
W1a	0.40	0.072	0.162	0.427	1.096	15.136	0.331	3.65
W1b	0.63	0.229	1.202	4.266	1.000	4.365	6.310	4.01
W2a	1.04	0.100	0.562	2.399	4.467	44.668	0.708	3.23
W2b	1.20	1.000	0.089	0.158	0.209	0.209	0.038	15.47
W2c	1.30	0.417	0.562	0.794	0.891	2.138	0.851	19.6
W3a	1.65	0.079	0.209	0.912	0.955	12.023	0.575	7.35
W3b	1.88	0.089	0.240	0.603	0.891	10.000	0.724	8.02
W4a	2.43	1.000	0.158	0.447	0.661	0.661	0.038	13.01
W4b	2.66	0.214	0.537	1.175	1.995	9.333	0.676	14.83
W4c	2.91	0.282	1.259	4.169	6.761	23.988	0.832	4.03
W5a	3.09	0.063	0.158	0.380	0.575	9.120	0.692	4.65
W5b	3.18	1.000	0.135	0.295	0.437	0.437	0.042	7.69
W5c	3.31	0.251	0.955	4.365	7.943	31.623	0.457	9.82
W5	3.51	0.182	0.631	0.871	7.943	43.652	0.275	3.01
W5	3.72	0.229	0.501	1.023	1.698	7.413	0.646	3.69
W6	3.88	0.071	0.195	0.417	0.589	8.318	0.912	3.37
W6	3.99	0.158	0.490	1.413	2.344	14.791	0.646	4.52
W6	4.13	0.151	0.562	1.995	3.981	26.303	0.525	2.17
1-1	0.58	0.074	0.427	1.318	2.188	29.512	1.122	12.26
1-2	0.97	1.000	0.120	0.269	0.437	0.437	0.033	18.18
1-3	1.12	1.000	0.851	1.000	1.148	1.148	0.631	17.65
1-4	1.22	0.083	0.282	0.631	0.832	10.000	1.148	14.45
1-5	1.40	0.059	0.095	0.166	0.240	4.074	0.646	19.89
1-6	1.73	0.071	0.186	0.398	0.589	8.318	0.832	15.65
1-7	1.98	1.000	0.158	0.398	0.603	0.603	0.042	14.82
1-8	2.16	1.000	0.126	0.347	0.575	0.575	0.028	16.12
1-9	2.39	0.117	0.490	1.318	1.820	15.488	1.122	12.23
1-10	2.51	0.100	0.537	2.042	3.388	33.884	0.851	9.8
1-11	2.62	1.000	0.151	0.389	0.550	0.550	0.042	15.18
1-12	3.26	0.214	0.631	1.622	2.570	12.023	0.724	6.41
1-13	3.48	0.324	1.413	7.943	8.318	25.704	0.741	7.34

2-1	0.71	0.081	0.251	0.589	0.832	10.233	0.933	24.48
2-2	0.81	0.074	0.209	0.603	0.933	12.589	0.631	18.44
2-3	1.07	0.145	0.389	0.741	1.072	7.413	0.977	11.35
2-4	1.24	1.000	0.093	0.174	0.251	0.251	0.035	19.1
2-5	1.45	0.063	0.105	0.191	0.269	4.266	0.646	17.79
2-6	1.85	0.087	0.219	0.479	0.832	9.550	0.661	18.27
2-7	2.18	0.071	0.214	0.575	0.955	13.490	0.676	15.53
2-8	2.44	0.087	0.302	0.794	1.230	14.125	0.851	12.55
2-9	2.84	1.000	0.158	0.389	0.575	0.575	0.044	11.04
3-2	1.04	0.072	0.240	0.562	0.794	10.965	1.000	18.75
3-3	1.32	1.000	0.132	0.339	0.933	0.933	0.019	16
3-4	1.47	1.000	0.117	0.263	0.437	0.437	0.032	17.2
3-5	1.63	1.000	0.166	0.417	0.661	0.661	0.042	22.4
3-6	1.73	0.316	1.738	5.248	8.710	27.542	1.096	14.31
3-7	1.96	0.063	0.120	0.269	0.501	7.943	0.457	7.9
3-8	2.36	0.063	0.135	0.263	0.398	6.310	0.724	17.1
3-9	2.79	0.062	0.229	0.631	0.955	15.488	0.891	15.37
4-1	0.64	0.079	0.251	0.537	0.741	9.333	1.072	18.94
4-2	0.94	0.063	0.145	0.316	0.479	7.586	0.692	19.94
4-3	1.09	0.050	0.126	0.501	0.759	15.136	0.417	18.49
4-4	1.19	1.000	0.162	0.347	0.550	0.550	0.048	17.22
4-5	1.73	0.068	0.162	0.389	0.603	8.913	0.646	9.79
4-6	1.78	0.251	0.468	0.692	0.832	3.311	1.047	9.49
4-7	1.96	0.295	0.525	0.813	1.000	3.388	0.933	7.52
5-1	0.58	0.219	1.047	3.162	5.248	23.988	0.955	10.44
5-3	1.02	1.000	0.100	0.204	0.316	0.316	0.032	21.62
5-4	1.27	1.000	0.148	0.380	0.575	0.575	0.038	18.47
5-5	1.60	1.000	0.138	0.316	0.490	0.490	0.039	12.24
5-2-1	1.98	1.000	0.141	0.363	0.575	0.575	0.035	7.95
5-2-2	2.21	0.158	0.457	0.871	1.259	7.943	1.047	22.36
5-2-3	2.64	1.000	0.117	0.234	0.331	0.331	0.042	21.99
6-1	0.71	0.107	0.372	1.000	1.585	14.791	0.813	16.3
6-2	0.94	0.083	0.126	0.398	0.631	7.586	0.302	24.48
6-3	1.12	1.000	0.145	0.302	0.457	0.457	0.046	21.64
6-4	1.32	0.100	0.417	0.955	1.380	13.804	1.259	19.79
6-5	1.57	1.000	0.135	0.372	0.631	0.631	0.029	19.44
6-6	1.85	1.000	0.132	0.229	0.347	0.347	0.050	17.01
6-7	2.31	0.081	0.251	0.603	0.832	10.233	0.933	12.48
6-8	2.67	1.000	0.126	0.324	0.501	0.501	0.032	17.2
7-1	0.79	0.331	1.175	4.266	7.762	23.442	0.537	8.37
7-2	0.89	0.166	0.676	2.042	3.631	21.878	0.759	8.37
7-3	1.04	0.060	0.158	0.417	0.661	10.965	0.631	18.93
7-4	1.17	1.000	0.126	0.309	0.479	0.479	0.033	25.18
7-5	1.42	1.000	0.129	0.363	0.617	0.617	0.027	23.08
7-6	1.65	1.000	0.100	0.209	0.347	0.347	0.029	12.83
7-7	1.96	1.000	0.148	0.269	0.398	0.398	0.055	23.59
7-8	1.98	0.079	0.339	0.794	1.202	15.136	1.202	11.77
7-9	2.21	0.234	0.457	0.025	0.398	1.698	2.239	14.05
7-10	2.64	0.063	0.204	0.550	0.871	13.804	0.759	14.8

8-1	0.64	1.000	0.209	0.550	0.794	0.794	0.055	19.76
8-2	0.86	0.078	0.240	0.490	0.631	8.128	1.175	23.02
8-3	1.07	0.158	0.355	0.646	0.912	5.754	0.871	12.73
9-1	0.84	0.316	0.933	2.188	3.311	10.471	0.832	7.53
9-2	1.19	1.000	0.112	0.309	0.501	0.501	0.025	22.2
9-3	1.55	1.000	0.087	0.158	0.251	0.251	0.030	23.5
9-4	1.80	0.079	0.166	0.295	0.398	5.012	0.871	20.6
9-5	2.21	0.074	0.200	0.389	0.550	7.413	0.977	11.9
9-6	2.64	0.074	0.120	0.562	0.933	12.589	0.209	13.9
10-1	0.94	1.000	0.138	0.339	0.631	0.631	0.030	NA
11-1	0.94	0.251	0.589	1.023	1.445	5.754	0.955	9.94
11-2	1.22	1.000	0.095	0.309	0.525	0.525	0.017	27.9
11-3	1.55	0.068	0.129	0.229	0.302	4.467	0.813	21.9
12-1	0.66	0.141	0.490	1.905	2.042	14.454	0.832	10.9
12-2	1.02	0.081	0.251	0.891	2.399	29.512	0.324	14.8
12-3	1.73	0.120	0.234	0.309	0.347	2.884	1.318	14.3
12-5	2.10	0.062	0.083	0.126	0.174	2.818	0.646	17
12-6	2.44	0.091	0.200	0.372	0.513	5.623	0.851	21.8
13-1	0.91	0.068	0.209	0.501	0.776	11.482	0.832	13.7
13-2	1.17	0.245	0.891	3.090	5.888	23.988	0.550	8.68
13-3	1.42	0.063	0.089	0.129	5.248	83.176	0.024	23.9
13-5	1.68	0.209	0.302	0.417	0.501	2.399	0.871	6.78
13-7	2.51	0.091	0.234	0.398	0.617	6.761	0.977	12.8
14-1	0.86	0.069	0.093	0.148	0.195	2.818	0.646	7.99
14-4	1.98	1.000	0.282	0.501	0.676	0.676	0.117	23.4
14-5	2.51	0.063	0.158	0.389	0.417	6.607	0.955	13.6
15-1	0.91	0.062	0.105	0.166	0.209	3.388	0.851	9.39
15-2	1.24	0.062	0.123	0.200	0.251	4.074	0.977	18
15-6	2.51	0.062	0.132	0.240	0.309	5.012	0.912	17.2
15-7	2.77	1.000	0.126	0.269	0.380	0.380	0.042	17.1
15-8	3.02	0.219	0.427	0.891	1.318	6.026	0.631	8.32
16-1	0.76	0.158	0.537	1.585	3.236	20.417	0.562	8.94
16-2	0.91	1.000	0.251	0.457	0.708	0.708	0.089	19.87
16-3	1.40	0.105	0.288	0.813	1.549	14.791	0.513	15.81
17-1	0.86	0.074	0.195	0.324	0.417	5.623	1.230	15.63
17-2	1.19	1.000	0.129	0.224	0.269	0.269	0.062	16.55
17-3	1.52	1.000	0.182	0.372	0.617	0.617	0.054	18.43
17-7	2.59	0.076	0.174	0.269	0.316	4.169	1.259	13.86
17-8	2.79	1.000	0.316	0.933	1.318	1.318	0.076	14.69
18-1	0.61	0.363	1.549	2.291	1.000	2.754	6.607	12
18-2	1.02	1.000	0.195	0.331	0.417	0.417	0.091	19.35
18-8	2.62	0.479	2.042	5.370	8.913	18.621	0.977	5.43

19-1	0.86	0.076	0.158	0.263	0.331	4.365	1.000	17.35
19-2	1.22	1.000	0.083	0.151	0.204	0.204	0.034	20.65
19-5	2.24	0.078	0.151	0.275	0.380	4.898	0.776	18.91
19-6	2.51	0.063	0.147	0.309	0.417	6.607	0.820	14.39
20-2	0.76	0.240	1.698	3.090	3.802	15.849	3.162	11.01
20-3	1.07	0.069	0.112	0.224	0.347	5.012	0.525	21.53
20-4	1.32	1.000	0.095	0.200	0.269	0.269	0.034	23.74
20-5	1.63	0.050	0.123	0.214	0.269	5.370	1.122	17.15
20-6	1.93	1.000	0.095	0.178	0.251	0.251	0.036	25.38
20-7	2.21	0.158	0.457	0.891	1.318	8.318	1.000	8.05

APPENDIX B
Disc Permeameter Data Sheets

Disk Permeameter Data Sheet
Number: TR1
Location (x,y,z):
Sample #:
Initial: TR1-Oi
Final: TR1-Of
Ring:

Z =

Moisture Content:
Initial:
Final:
Reservior Calibration (RC): 17.500

HEIGHT (cm)	TIME (min)	:	VOLUM INFIL.	CUM.IN (cm)	SQUARE TIME	ROOT
674.300	0.000	:	0.000	0.00	0.0000	
667.800	0.083	:	6.500	0.35	0.2887	
665.800	0.117	:	8.500	0.46	0.3416	
663.800	0.133	:	10.500	0.57	0.3651	
661.800	0.200	:	12.500	0.68	0.4472	
659.800	0.233	:	14.500	0.79	0.4830	
657.800	0.300		16.500	0.90	0.5477	
655.800	0.333		18.500	1.01	0.5774	
653.800	0.367		20.500	1.12	0.6055	
651.800	0.433		22.500	1.23	0.6583	
649.800	0.467		24.500	1.34	0.6831	
647.800	0.500		26.500	1.45	0.7071	
645.800	0.533		28.500	1.56	0.7303	
643.800	0.600		30.500	1.67	0.7746	
641.800	0.650		32.500	1.77	0.8062	
639.800	0.700		34.500	1.88	0.8367	
637.800	0.750		36.500	1.99	0.8660	
635.800	0.817		38.500	2.10	0.9037	
633.800	0.867		40.500	2.21	0.9309	
631.800	0.917		42.500	2.32	0.9574	
629.800	0.967		44.500	2.43	0.9832	
627.800	1.017		46.500	2.54	1.0083	
625.800	1.100		48.500	2.65	1.0488	
623.800	1.150		50.500	2.76	1.0724	
621.800	1.200		52.500	2.87	1.0954	
619.800	1.267		54.500	2.98	1.1255	
617.800	1.333		56.500	3.09	1.1547	
615.800	1.400		58.500	3.19	1.1832	

613.800	1.450	60.500	3.30	1.2042
611.800	1.533	62.500	3.41	1.2383
609.800	1.600	64.500	3.52	1.2649
607.800	1.667	66.500	3.63	1.2910
605.800	1.733	68.500	3.74	1.3166
603.800	1.783	70.500	3.85	1.3354
601.800	1.867	72.500	3.96	1.3663
599.800	1.933	74.500	4.07	1.3904
597.800	2.000	76.500	4.18	1.4142
595.800	2.067	78.500	4.29	1.4376
593.800	2.150	80.500	4.40	1.4663
591.800	2.233	82.500	4.51	1.4944
589.800	2.300	84.500	4.61	1.5166
587.800	2.367	86.500	4.72	1.5384
582.800	2.567	91.500	5.00	1.6021
563.800	3.617	110.500	6.03	1.9018
558.800	3.850	115.500	6.31	1.9621
553.800	4.083	120.500	6.58	2.0207
548.800	4.317	125.500	6.85	2.0777
543.800	4.567	130.500	7.13	2.1370
538.800	4.783	135.500	7.40	2.1871
533.800	5.050	140.500	7.67	2.2472
528.800	5.317	145.500	7.95	2.3058
515.800	5.967	158.500	8.66	2.4427
508.800	6.300	165.500	9.04	2.5100
498.800	6.817	175.500	9.58	2.6109
488.800	7.317	185.500	10.13	2.7049
483.800	7.583	190.500	10.40	2.7538
463.800	8.883	210.500	11.49	2.9805
453.800	9.400	220.500	12.04	3.0659
443.800	9.967	230.500	12.59	3.1570
433.800	10.533	240.500	13.13	3.2455
423.800	11.100	250.500	13.68	3.3317
413.800	11.667	260.500	14.23	3.4157
403.800	12.250	270.500	14.77	3.5000
393.800	12.817	280.500	15.32	3.5800
388.800	13.117	285.500	15.59	3.6217
370.500	14.400	303.800	16.59	3.7947
365.500	14.683	308.800	16.86	3.8319

355.500	15.300	318.800	17.41	3.9115
340.500	16.183	333.800	18.23	4.0229
330.500	16.783	343.800	18.77	4.0967
320.500	17.383	353.800	19.32	4.1693
310.500	17.983	363.800	19.87	4.2407
300.500	18.583	373.800	20.41	4.3108
290.500	19.183	383.800	20.96	4.3799
273.500	20.433	400.800	21.89	4.5203
263.500	21.133	410.800	22.43	4.5971
258.500	21.483	415.800	22.71	4.6350
253.500	21.800	420.800	22.98	4.6690
243.500	22.500	430.800	23.52	4.7434
232.500	23.233	441.800	24.13	4.8201
223.500	23.850	450.800	24.62	4.8836
213.500	24.517	460.800	25.16	4.9514
203.500	25.217	470.800	25.71	5.0216
193.500	25.867	480.800	26.25	5.0859
180.400	27.250	493.900	26.97	5.2202
175.400	27.600	498.900	27.24	5.2536
170.400	27.967	503.900	27.52	5.2884
155.400	29.033	518.900	28.34	5.3883
145.400	29.733	528.900	28.88	5.4528
135.400	30.450	538.900	29.43	5.5182
122.400	31.400	551.900	30.14	5.6036
115.400	31.933	558.900	30.52	5.6510
105.400	32.633	568.900	31.07	5.7126
100.400	33.000	573.900	31.34	5.7446
80.000	34.550	594.300	32.45	5.8779
70.000	35.483	604.300	33.00	5.9568
60.000	36.083	614.300	33.54	6.0069
50.000	36.850	624.300	34.09	6.0704
40.000	37.617	634.300	34.64	6.1332
29.000	38.433	645.300	35.24	6.1995
20.000	39.133	654.300	35.73	6.2557
10.000	39.867	664.300	36.28	6.3140
5.000	40.233	669.300	36.55	6.3430

SORPTIVITY

Regression Output:

Constant		-0.261
Std Err of Y Est		0.028
R Squared		0.988
No. of Observations		7.000
Degrees of Freedom		5.000
X Coefficient(s)	2.165	
Std Err of Coef.	0.105	

Regression Output:

Constant		-1.062
Std Err of Y Est		0.026
R Squared		0.997
No. of Observations		14.000
Degrees of Freedom		12.000
X Coefficient(s)	3.535	
Std Err of Coef.	0.055	

STEADY STATE FLOWRATE

Regression Output:

Constant		2.109
Std Err of Y Est		0.017
R Squared		1.000
No. of Observations		8.000
Degrees of Freedom		6.000
X Coefficient(s)	1.099	
Std Err of Coef.	0.008	

Disk Permeameter Data Sheet
Number: TR2 Z =0.5
Location (x,y,z):
Sample # TR2 Moisture Content:
Initial: TR2-Oi Initial:
Final: TR2-Of Final:
Ring: Reservior Calibration (RC): 17.500

HEIGHT (cm)	TIME (min)	:	VOLUM INFIL.	CUM.IN (cm)	SQUARE ROOT TIME
97.200	0.000	:	0.000	0.00	0.0000
96.000	0.100	:	1.200	0.07	0.3162
95.000	0.150	:	2.200	0.12	0.3873
94.000	0.233	:	3.700	0.20	0.4830
93.500	0.283	:	4.700	0.26	0.5323
93.000	0.350	:	5.700	0.31	0.5916
92.500	0.417	:	6.700	0.37	0.6455
92.000	0.483	:	7.700	0.42	0.6952
91.500	0.533	:	8.700	0.48	0.7303
91.000	0.617	:	9.700	0.53	0.7853
90.500	0.700	:	10.700	0.58	0.8367
90.000	0.783	:	11.700	0.64	0.8851
89.500	0.867	:	12.700	0.69	0.9309
89.000	0.950	:	13.700	0.75	0.9747
88.500	1.067	:	14.700	0.80	1.0328
88.000	1.150	:	15.700	0.86	1.0724
87.500	1.233	:	16.700	0.91	1.1106
87.000	1.333	:	17.700	0.97	1.1547
86.500	1.450	:	18.700	1.02	1.2042
86.000	1.533	:	19.700	1.08	1.2383
85.500	1.650	:	20.700	1.13	1.2845
85.000	1.767	:	21.700	1.18	1.3292
84.500	1.867	:	22.700	1.24	1.3663
84.000	1.967	:	24.200	1.32	1.4024
83.000	2.183	:	26.200	1.43	1.4776
82.000	2.417	:	28.200	1.54	1.5546
81.000	2.650	:	30.200	1.65	1.6279
80.000	2.900	:	32.200	1.76	1.7029

79.000	3.150	:	34.200	1.87	1.7748
78.000	3.400	:	37.700	2.06	1.8439
75.500	4.067	:	43.700	2.39	2.0166
72.000	5.033	:	49.200	2.69	2.2435
70.000	5.550	:	53.200	2.91	2.3558
68.000	6.183	:	57.200	3.12	2.4866
66.000	6.733	:	61.200	3.34	2.5949
64.000	7.317	:	65.200	3.56	2.7049
62.000	7.933	:	69.200	3.78	2.8166
60.000	8.567	:	73.200	4.00	2.9269
58.000	9.167	:	77.200	4.22	3.0277
56.000	9.800	:	81.200	4.43	3.1305
54.000	10.433	:	85.200	4.65	3.2301
52.000	11.067	:	89.200	4.87	3.3267
50.000	11.550	:	93.200	5.09	3.3985
48.000	12.350	:	97.200	5.31	3.5143
46.000	12.983	:	101.200	5.53	3.6032
44.000	13.583	:	105.200	5.74	3.6856
42.000	14.200	:	109.200	5.96	3.7683
40.000	14.850	:	113.200	6.18	3.8536
38.000	15.467	:	117.200	6.40	3.9328
36.000	16.133	:	121.200	6.62	4.0166
34.000	16.733	:	125.200	6.84	4.0906
32.000	17.367	:	129.200	7.06	4.1673
30.000	17.950	:	133.200	7.27	4.2367
28.000	18.600	:	137.200	7.49	4.3128
26.000	19.217	:	141.200	7.71	4.3837
24.000	19.850	:	145.200	7.93	4.4553
22.000	20.450	:	149.200	8.15	4.5222
20.000	21.117	:	153.200	8.37	4.5953
18.000	21.783	:	157.200	8.58	4.6673
16.000	22.467	:	161.200	8.80	4.7399
14.000	22.983	:	165.200	9.02	4.7941
12.000	23.633	:	169.200	9.24	4.8614
10.000	24.267	:	173.200	9.46	4.9261
8.000	24.883	:	176.200	9.62	4.9883
7.000	25.167	:	178.200	9.73	5.0166
6.000	25.500	:	180.200	9.84	5.0498
5.000	25.750	:	182.200	9.95	5.0744

4.000	26.067	:	184.200	10.06	5.1056
3.000	26.417	:	186.200	10.17	5.1397
2.000	26.700	:	188.200	10.28	5.1672
1.000	26.983	:	190.200	10.39	5.1945

SORPTIVITY Regression Output:

Constant		-0.28
Std Err of Y Est		0.01
R Squared		1.00
No. of Observations		11.00
Degrees of Freedom		9.00
X Coefficient(s)	1.027	
Std Err of Coef.	0.023	

STEADY STATE FLOWRATE Regression Output:

Constant		0.66
Std Err of Y Est		0.01
R Squared		1.00
No. of Observations		8.00
Degrees of Freedom		6.00
X Coefficient(s)	0.360	
Std Err of Coef.	0.004	

Disk Permeameter Data Sheet

Number: TR3 Z =0.5

Location (x,y,z):

Sample # Moisture Content:

Initial: TR3-0i Initial:

Final: TR3-0n Final:

Ring: Reservior Calibration (RC): 17.500

HEIGHT (cm)	TIME (min)	:	VOLUM INFIL.	CUM.IN (cm)	SQUARE TIME	ROOT
164.300	0.000	:	0.000	0.00	0.0000	
163.300	0.150	:	1.000	0.05	0.3873	
162.800	0.167	:	1.500	0.08	0.4082	
162.300	0.217	:	2.000	0.11	0.4655	
161.800	0.283	:	2.500	0.14	0.5323	
161.300	0.350	:	3.000	0.16	0.5916	
160.800	0.433	:	3.500	0.19	0.6583	
160.300	0.533	:	4.000	0.22	0.7303	
159.800	0.583	:	4.500	0.25	0.7638	
158.800	0.750	:	5.500	0.30	0.8660	
158.300	0.850	:	6.000	0.33	0.9220	
157.800	0.917	:	6.500	0.35	0.9574	
157.300	1.017	:	7.000	0.38	1.0083	
156.800	1.100	:	7.500	0.41	1.0488	
156.300	1.200	:	8.000	0.44	1.0954	
155.800	1.283	:	8.500	0.46	1.1328	
155.300	1.383	:	9.000	0.49	1.1762	
154.800	1.483	:	9.500	0.52	1.2179	
154.300	1.583	:	10.000	0.55	1.2583	
153.800	1.700	:	10.500	0.57	1.3038	
153.300	1.800	:	11.000	0.60	1.3416	
152.800	1.933	:	11.500	0.63	1.3904	
152.300	2.017	:	12.000	0.66	1.4201	
151.800	2.133	:	12.500	0.68	1.4606	
150.800	2.350	:	13.500	0.74	1.5330	
149.800	2.617	:	14.500	0.79	1.6176	
148.800	2.850	:	15.500	0.85	1.6882	
147.800	3.117	:	16.500	0.90	1.7654	

145.300	4.167	:	19.000	1.04	2.0412
143.800	4.717	:	20.500	1.12	2.1718
141.800	5.250	:	22.500	1.23	2.2913
139.800	5.833	:	24.500	1.34	2.4152
137.800	6.400	:	26.500	1.45	2.5298
135.800	6.983	:	28.500	1.56	2.6426
133.800	8.150	:	30.500	1.67	2.8548
126.700	9.367	:	37.600	2.05	3.0605
122.700	10.567	:	41.600	2.27	3.2506
118.700	11.767	:	45.600	2.49	3.4303
112.700	13.550	:	51.600	2.82	3.6810
105.700	15.617	:	58.600	3.20	3.9518
96.700	18.217	:	67.600	3.69	4.2681
92.700	19.300	:	71.600	3.91	4.3932
88.700	20.417	:	75.600	4.13	4.5185
84.700	21.567	:	79.600	4.35	4.6440
80.700	22.700	:	83.600	4.57	4.7645
76.700	23.800	:	87.600	4.78	4.8785
72.700	24.867	:	91.600	5.00	4.9866
68.700	25.550	:	95.600	5.22	5.0547
60.000	27.933	:	104.300	5.70	5.2852
56.000	29.033	:	108.300	5.91	5.3883
52.000	30.433	:	112.300	6.13	5.5166
48.000	31.233	:	116.300	6.35	5.5887
42.000	32.933	:	122.300	6.68	5.7388

Regression Output:

Constant		-0.129
Std Err of Y Est		0.008
R Squared		0.995
No. of Observations		11.000
Degrees of Freedom		9.000
X Coefficient(s)	0.495	
Std Err of Coef.	0.012	

Regression Output:

Constant		0.202
Std Err of Y Est		0.029
R Squared		0.996
No. of Observations		5.000
Degrees of Freedom		3.000
X Coefficient(s)	0.196	
Std Err of Coef.	0.008	

Disk Permeameter Data Sheet
Number: TR4 Z =0.5
Location (x,y,z):
Sample #: Moisture Content:
Initial: TR4-Oi Initial:
Final: TR4-Of Final:
Ring: Reservior Calibration (RC): 17.500

HEIGHT (cm)	TIME (min)	:	VOLUM INFIL.	CUM.IN (cm)	SQUARE ROOT TIME	
179.800	0.000	:	0.000	0.00	0.0000	
176.800	0.117	:	3.000	0.16	0.3416	
175.800	0.133	:	4.000	0.22	0.3651	
174.800	0.167	:	5.000	0.27	0.4082	
173.800	0.200	:	6.000	0.33	0.4472	
172.800	0.233	:	7.000	0.38	0.4830	
171.800	0.267	:	8.000	0.44	0.5164	
170.800	0.300	:	9.000	0.49	0.5477	
169.800	0.333	:	10.000	0.55	0.5774	
168.800	0.400	:	11.000	0.60	0.6325	
167.800	0.450	:	12.000	0.66	0.6708	
166.800	0.483	:	13.000	0.71	0.6952	
165.800	0.533	:	14.000	0.76	0.7303	
164.800	0.583	:	15.000	0.82	0.7638	
163.800	0.633	:	16.000	0.87	0.7958	
162.800	0.717	:	17.000	0.93	0.8466	
161.800	0.767	:	18.000	0.98	0.8756	
160.800	0.817	:	19.000	1.04	0.9037	
159.800	0.883	:	20.000	1.09	0.9399	
158.800	0.950	:	21.000	1.15	0.9747	
157.800	1.000	:	22.000	1.20	1.0000	
156.800	1.083	:	23.000	1.26	1.0408	
155.800	1.150	:	24.000	1.31	1.0724	
154.800	1.217	:	25.000	1.37	1.1030	
153.800	1.283	:	26.000	1.42	1.1328	
152.800	1.350	:	27.000	1.47	1.1619	
151.800	1.417	:	28.000	1.53	1.1902	
150.800	1.500	:	29.000	1.58	1.2247	

148.800	1.650	:	31.000	1.69	1.2845
146.800	1.800	:	33.000	1.80	1.3416
144.800	1.967	:	35.000	1.91	1.4024
142.800	2.150	:	37.000	2.02	1.4663
140.800	2.317	:	39.000	2.13	1.5221
138.800	2.500	:	41.000	2.24	1.5811
136.800	2.683	:	43.000	2.35	1.6381
134.800	2.850	:	45.000	2.46	1.6882
132.800	3.033	:	47.000	2.57	1.7416
130.800	3.233	:	49.000	2.68	1.7981
128.800	3.433	:	51.000	2.78	1.8529
124.800	3.800	:	55.000	3.00	1.9494
120.800	4.200	:	59.000	3.22	2.0494
116.800	4.617	:	63.000	3.44	2.1486
108.800	5.450	:	71.000	3.88	2.3345
102.800	6.100	:	77.000	4.20	2.4698
98.800	6.533	:	81.000	4.42	2.5560
92.800	7.200	:	87.000	4.75	2.6833
80.000	9.217	:	99.800	5.45	3.0359
73.000	10.083	:	106.800	5.83	3.1754
65.000	11.083	:	114.800	6.27	3.3292
56.000	12.200	:	123.800	6.76	3.4928
50.000	12.967	:	129.800	7.09	3.6009
42.000	13.967	:	137.800	7.52	3.7372
31.000	15.350	:	148.800	8.13	3.9179
28.000	15.767	:	151.800	8.29	3.9707
26.000	16.033	:	153.800	8.40	4.0042
24.000	16.300	:	155.800	8.51	4.0373
22.000	16.550	:	157.800	8.62	4.0682
20.000	16.833	:	159.800	8.73	4.1028
18.000	17.117	:	161.800	8.84	4.1372
14.000	17.650	:	165.800	9.05	4.2012
10.000	18.200	:	169.800	9.27	4.2661
5.000	18.867	:	174.800	9.55	4.3436
2.000	19.250	:	177.800	9.71	4.3875

SORPTIVITY

Regression Output:

Constant		-0.359
Std Err of Y Est		0.010
R Squared		0.999
No. of Observations		20.000
Degrees of Freedom		18.000
X Coefficient(s)	1.542	
Std Err of Coef.	0.011	

STEADY STATE FLOWRATE

Regression Output:

Constant		1.901
Std Err of Y Est		0.004
R Squared		1.000
No. of Observations		10.000
Degrees of Freedom		8.000
X Coefficient(s)	0.405	
Std Err of Coef.	0.001	

Disc Permeameter Data Sheet
Number: TR5 z = .5 cm
Location (x,y,z):
Sample #: Moisture Content:
Initial: TR5-Oi Initial:
Final: TR5-Of Final:
Ring: Reservior Calibration (RC): 17.500

HEIGHT (cm)	TIME (min)	:	VOLUM INFIL.	CUM.IN (cm)	SQUARE ROOT TIME	
398.130	0.000	:	0.000	0.00	0.0000	
394.530	0.083	:	3.600	0.20	0.2887	
392.530	0.117	:	5.600	0.31	0.3416	
390.530	0.150	:	7.600	0.42	0.3873	
388.530	0.200	:	9.600	0.52	0.4472	
386.530	0.267	:	11.600	0.63	0.5164	
384.530	0.350	:	13.600	0.74	0.5916	
382.530	0.400	:	15.600	0.85	0.6325	
380.530	0.483	:	17.600	0.96	0.6952	
378.530	0.550	:	19.600	1.07	0.7416	
376.530	0.633	:	21.600	1.18	0.7958	
374.530	0.733	:	23.600	1.29	0.8563	
372.530	0.817	:	25.600	1.40	0.9037	
370.530	0.900	:	27.600	1.51	0.9487	
368.530	0.983	:	29.600	1.62	0.9916	
367.530	1.067	:	30.600	1.67	1.0328	
366.530	1.100	:	31.600	1.73	1.0488	
365.530	1.150	:	32.600	1.78	1.0724	
364.530	1.183	:	33.600	1.83	1.0878	
362.530	1.267	:	35.600	1.94	1.1255	
360.530	1.367	:	37.600	2.05	1.1690	
358.530	1.467	:	39.600	2.16	1.2111	
356.530	1.567	:	41.600	2.27	1.2517	
352.530	1.750	:	45.600	2.49	1.3229	
348.530	1.950	:	49.600	2.71	1.3964	
344.530	2.150	:	53.600	2.93	1.4663	
340.530	2.367	:	57.600	3.15	1.5384	
336.530	2.550	:	61.600	3.36	1.5969	

332.530	2.750	:	65.600	3.58	1.6583
328.530	2.950	:	69.600	3.80	1.7176
322.530	3.250	:	75.600	4.13	1.8028
314.530	3.667	:	83.600	4.57	1.9149
310.530	3.883	:	87.600	4.78	1.9706
291.530	4.883	:	106.600	5.82	2.2098
286.530	5.067	:	111.600	6.09	2.2509
283.530	5.233	:	114.600	6.26	2.2876
273.530	5.700	:	124.600	6.80	2.3875
263.530	6.167	:	134.600	7.35	2.4833
253.530	6.633	:	144.600	7.90	2.5755
243.530	7.100	:	154.600	8.44	2.6646
233.530	7.583	:	164.600	8.99	2.7538
223.530	8.050	:	174.600	9.53	2.8373
213.530	8.533	:	184.600	10.08	2.9212
185.430	10.000	:	212.700	11.61	3.1623
175.430	10.517	:	222.700	12.16	3.2429
165.430	11.067	:	232.700	12.71	3.3267
155.430	11.600	:	242.700	13.25	3.4059
145.430	12.133	:	252.700	13.80	3.4833
135.430	12.667	:	262.700	14.35	3.5590
125.430	13.200	:	272.700	14.89	3.6332
105.430	13.733	:	292.700	15.98	3.7059
80.000	15.183	:	318.130	17.37	3.8966
70.000	15.817	:	328.130	17.92	3.9770
60.000	16.417	:	338.130	18.46	4.0517
40.000	17.650	:	358.130	19.56	4.2012
30.000	18.233	:	368.130	20.10	4.2701
20.000	18.783	:	378.130	20.65	4.3340
10.000	19.417	:	388.130	21.19	4.4064

SORPTIVITY: (cm/min 1/2)

Regression Output:	Constant		-0.305
	Std Err of Y Est		0.021
	R Squared		0.991
	No. of Observations		6.000
	Degrees of Freedom		4.000
	X Coefficient(s)	1.805	
	Std Err of Coef.	0.084	

STEADY STATE FLOWRATE

Regression Output:	Constant		3.577
	Std Err of Y Est		0.024
	R Squared		1.000
	No. of Observations		7.000
	Degrees of Freedom		5.000
	X Coefficient(s)	0.907	
	Std Err of Coef.	0.006	

Disk Permeameter Data Sheet
Number: TR6
Location (x,y,z):
Sample #:
Initial: TR6-Oi
Final: TR6-Of
Ring:

Z =0.5

Moisture Content:
Initial:
Final:
Reservior Calibration (RC): 17.500

HEIGHT (cm)	TIME (min)	VOLUM INFIL.	CUM.IN (cm)	SQUARE ROOT TIME
290.900	0.000	0.000	0.00	0.0000
289.700	0.083	1.200	0.07	0.2887
288.700	0.117	2.200	0.12	0.3416
287.700	0.150	3.200	0.17	0.3873
286.700	0.183	4.200	0.23	0.4282
285.700	0.217	5.200	0.28	0.4655
284.700	0.250	6.200	0.34	0.5000
283.700	0.317	7.200	0.39	0.5627
282.700	0.350	8.200	0.45	0.5916
281.700	0.417	9.200	0.50	0.6455
280.700	0.483	10.200	0.56	0.6952
279.700	0.533	11.200	0.61	0.7303
278.700	0.600	12.200	0.67	0.7746
277.700	0.667	13.200	0.72	0.8165
276.700	0.783	14.200	0.78	0.8851
275.700	0.833	15.200	0.83	0.9129
274.200	0.950	16.700	0.91	0.9747
273.200	1.050	17.700	0.97	1.0247
272.200	1.133	18.700	1.02	1.0646
271.200	1.200	19.700	1.08	1.0954
270.200	1.317	20.700	1.13	1.1475
269.200	1.417	21.700	1.18	1.1902
268.200	1.517	22.700	1.24	1.2315
267.200	1.617	23.700	1.29	1.2715
266.200	1.717	24.700	1.35	1.3102
265.200	1.817	25.700	1.40	1.3478
263.200	2.050	27.700	1.51	1.4318
261.200	2.250	29.700	1.62	1.5000

259.200	2.500	:	31.700	1.73	1.5811
257.200	2.717	:	33.700	1.84	1.6482
255.200	2.983	:	35.700	1.95	1.7272
253.200	3.217	:	37.700	2.06	1.7935
250.200	3.583	:	40.700	2.22	1.8930
246.200	4.083	:	44.700	2.44	2.0207
242.200	4.600	:	48.700	2.66	2.1448
238.200	5.133	:	52.700	2.88	2.2657
234.200	5.667	:	56.700	3.10	2.3805
230.200	6.183	:	60.700	3.31	2.4866
225.200	6.883	:	65.700	3.59	2.6236
221.200	7.417	:	69.700	3.81	2.7234
215.200	8.250	:	75.700	4.13	2.8723
205.200	9.633	:	85.700	4.68	3.1038
187.000	11.500	:	103.900	5.67	3.3912
181.000	12.417	:	109.900	6.00	3.5237
176.000	13.233	:	114.900	6.27	3.6378
171.000	14.067	:	119.900	6.55	3.7506
166.000	14.900	:	124.900	6.82	3.8601
161.000	15.717	:	129.900	7.09	3.9644
156.000	16.533	:	134.900	7.37	4.0661
151.000	17.383	:	139.900	7.64	4.1693
146.000	18.233	:	144.900	7.91	4.2701
141.000	19.067	:	149.900	8.19	4.3665
136.000	19.917	:	154.900	8.46	4.4628
131.000	20.783	:	159.900	8.73	4.5589
129.000	21.117	:	161.900	8.84	4.5953
127.000	21.433	:	163.900	8.95	4.6296
125.000	21.767	:	165.900	9.06	4.6655
123.000	22.100	:	167.900	9.17	4.7011
121.000	22.450	:	169.900	9.28	4.7381
119.000	22.800	:	171.900	9.39	4.7749
117.000	23.133	:	173.900	9.50	4.8097
115.000	23.467	:	175.900	9.61	4.8442
113.000	23.833	:	177.900	9.71	4.8819
111.000	24.167	:	179.900	9.82	4.9160
101.000	24.967	:	189.900	10.37	4.9967
85.000	27.517	:	205.900	11.24	5.2456
80.000	28.450	:	210.900	11.52	5.3339

75.000	29.383	:	215.900	11.79	5.4206
70.000	30.317	:	220.900	12.06	5.5061
65.000	31.283	:	225.900	12.34	5.5932
60.000	32.183	:	230.900	12.61	5.6730
55.000	33.117	:	235.900	12.88	5.7547
50.000	34.050	:	240.900	13.15	5.8352
40.000	35.900	:	250.900	13.70	5.9917
35.000	36.767	:	255.900	13.97	6.0636
30.000	37.683	:	260.900	14.25	6.1387
28.000	38.083	:	262.900	14.36	6.1712
26.000	38.433	:	264.900	14.47	6.1995
24.000	38.800	:	266.900	14.57	6.2290
22.000	39.167	:	268.900	14.68	6.2583
20.000	39.517	:	270.900	14.79	6.2862
19.000	39.700	:	271.900	14.85	6.3008
18.000	39.883	:	272.900	14.90	6.3153
17.000	40.067	:	273.900	14.96	6.3298
15.000	40.450	:	275.900	15.07	6.3600
14.000	40.633	:	276.900	15.12	6.3744
13.000	40.800	:	277.900	15.18	6.3875
12.000	41.000	:	278.900	15.23	6.4031
11.000	41.183	:	279.900	15.28	6.4174
10.000	41.367	:	280.900	15.34	6.4317
9.000	41.517	:	281.900	15.39	6.4433
8.000	41.700	:	282.900	15.45	6.4576
7.000	41.883	:	283.900	15.50	6.4717
6.000	42.067	:	284.900	15.56	6.4859
5.000	42.250	:	285.900	15.61	6.5000

Regression Output:

Constant		-0.293
Std Err of Y Est		0.010
R Squared		0.999
No. of Observations		16.000
Degrees of Freedom		14.000
X Coefficient(s)	1.231	
Std Err of Coef.	0.012	

Regression Output:

Constant		2.910
Std Err of Y Est		0.004
R Squared		1.000
No. of Observations		14.000
Degrees of Freedom		12.000
X Coefficient(s)	0.301	
Std Err of Coef.	0.001	

APPENDIX C

ENE LAB CORE RESULTS

DEPTH (m)	d10 (mm)	SATURATED HYDRAULIC CONDUCTIVITY (cm/s)	SATURATED WATER CONTENT %	POROSITY %	DRY BULK DENSITY (g/cm3)	GRAVIMETRIC MOISTURE CONTENT %
0.43	0.089	0.031	0	28.30	1.9	*
0.76	1.000	0.003	38.29	35.85	1.7	*
1.62	15.849	*	*	*	*	10.82
1.75	0.174	*	*	*	*	4.1
1.9	0.178	*	*	*	*	3.84
2.08	0.269	*	*	*	*	4.21
2.22	0.257	*	*	*	*	2.05
3.46	0.324	*	*	*	*	0.5
3.55	0.151	*	*	*	*	0.98
3.67	0.170	*	*	*	*	2.25
3.78	0.063	*	*	*	*	10.15
4.48	0.068	*	*	*	*	5.62
4.65	0.012	3.700	60.87	43.77	1.49	*
5.33	0.015	1.400	61.1	43.40	1.5	*
5.57	0.155	*	*	*	*	1.98
5.67	0.195	*	*	*	*	0.73
5.75	0.372	*	*	*	*	0.069
5.94	0.117	*	*	*	*	1.41
6.33	0.010	0.020	23.9	40.00	1.59	*
6.86	0.251	0.003	99.55	58.49	1.1	*
7.49	0.010	0.139	45.48	51.32	1.29	*
7.62	0.214	0.004	50.21	38.49	1.63	*
8.03	0.302	0.010	49.65	38.87	1.62	*
8.38	0.204	0.012	42.71	36.98	1.67	*
8.85	0.148	0.028	47.98	49.43	1.34	*
9.14	0.195	0.012	4.54	34.34	1.74	*
9.71	0.178	0.201	40.15	40.75	1.57	*
9.91	0.200	0.099	33.06	44.15	1.48	*
10.24	0.234	0.057	15.72	35.09	1.72	*
10.67	0.126	0.005	48.68	47.17	1.4	*
11.13	0.138	0.014	30.51	40.00	1.59	*
11.43	0.224	0.026	32.86	40.75	1.57	*
11.82	0.117	0.022	60.36	43.40	1.5	*
12.19	0.120	0.011	42.12	44.53	1.47	*
12.34	0.135	0.011	50.76	40.75	1.57	*
12.95	0.120	0.020	38.09	43.02	1.51	*
13.43	0.132	0.034	57.38	51.32	1.29	*
13.72	0.166	0.015	61.5	44.15	1.48	*
14.17	0.148	0.013	40.25	47.92	1.38	*
14.48	0.234	0.028	46.04	39.25	1.61	*
16.39	1.585	0.035	48.6	44.15	1.48	*
16.76	0.117	0.009	59.3	53.58	1.23	*
17.04	0.117	0.060	77.28	49.06	1.35	*
17.32	0.126	0.008	40.14	43.77	1.49	*

17.65	0.128	0.018	36.17	36.98	1.67	*
17.98	0.148	0.174	25.99	43.77	1.49	*
18.33	18.330	0.325	13.98	35.47	1.71	*
18.59	18.590	0.007	34.93	38.49	1.63	*
18.85	18.850	0.046	40.4	34.34	1.74	*
19.05	19.050	0.006	40.7	43.77	1.49	*
19.51	19.510	0.017	39.9	43.77	1.49	*
19.81	19.810	0.008	34.91	44.91	1.46	*

* Sample not analyzed with particular test

APPENDIX D
GEOLOGIC TIME SCALE

EON	ERA	PERIOD	EPOCH	TIME (million years)
			Holocene	0
		Neogene	Pleistocene	
			Pliocene	
	CENEZOIC		Miocene	25
			Oligocene	
		Paleogene	Eocene	
			Paleocene	65
		Cretaceous		135
	MESOZOIC	Jurassic		192
		Triassic		230
		Permian		290
PHANEROZOIC		Pennsylvanian		320
		Mississippian		350
	PALEOZ.	Devonian		410
		Silurian		435
		Ordivician		485
		Cambrian		560
		Eocambrain		700+
	PROTEROZ.			2500
CRYPTOZOIC	ARCHEOZ.			3800+

APPENDIX E

Boring logs

KEY TO BORING LOGS

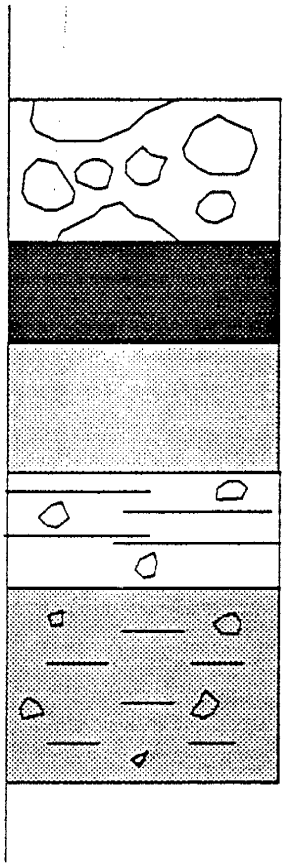

Cobbles and/or gravel layer

Clay and silty clay

Fine to medium sand

Silty fine sand, little gravel

Fine to coarse sand, little silty sand, little gravel

Site datum is at 0 meters

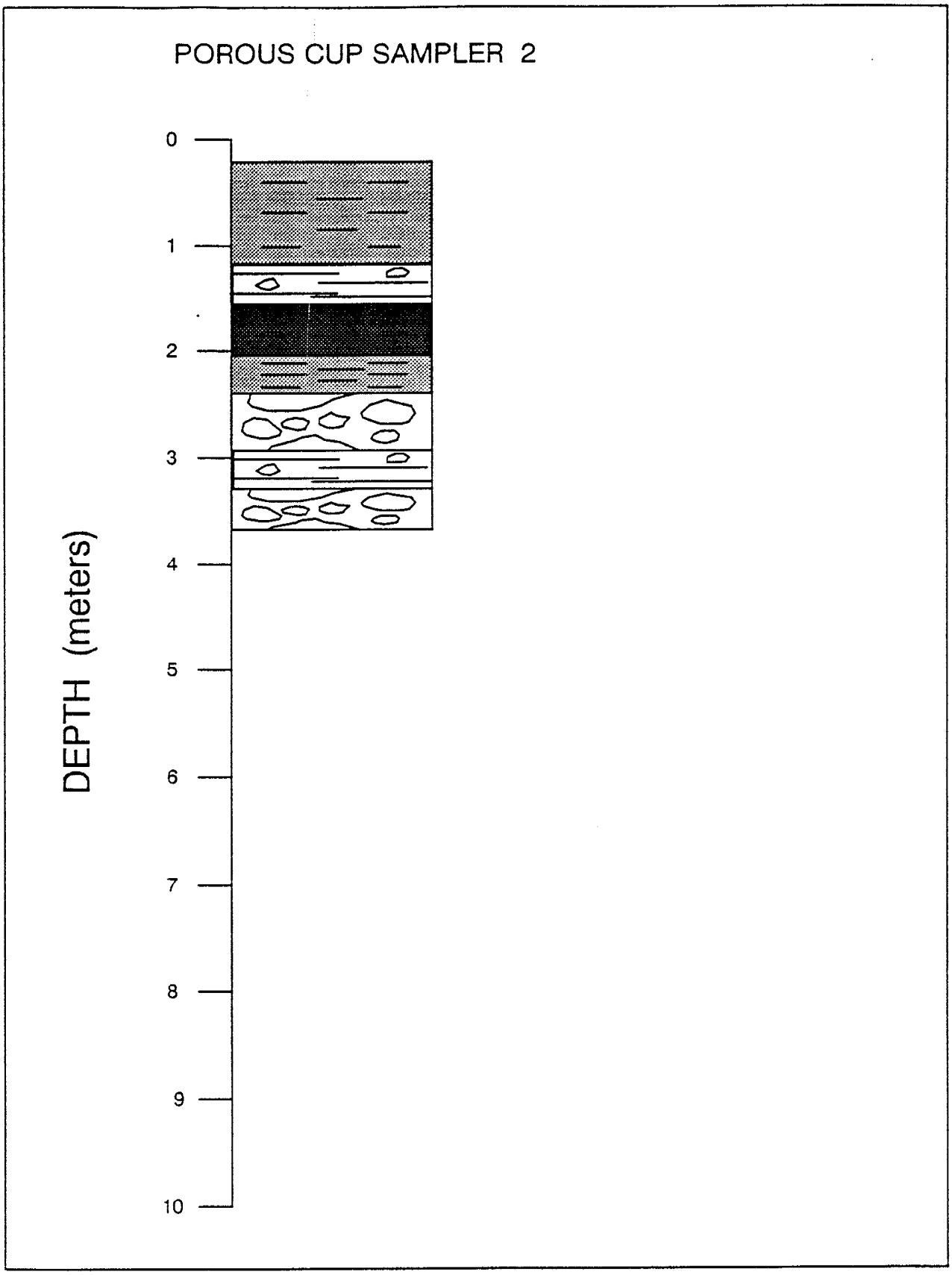
POROUS CUP SAMPLER 2
DEPTH (meters)
0
1
2
3
4
5
6
7
8
9
10

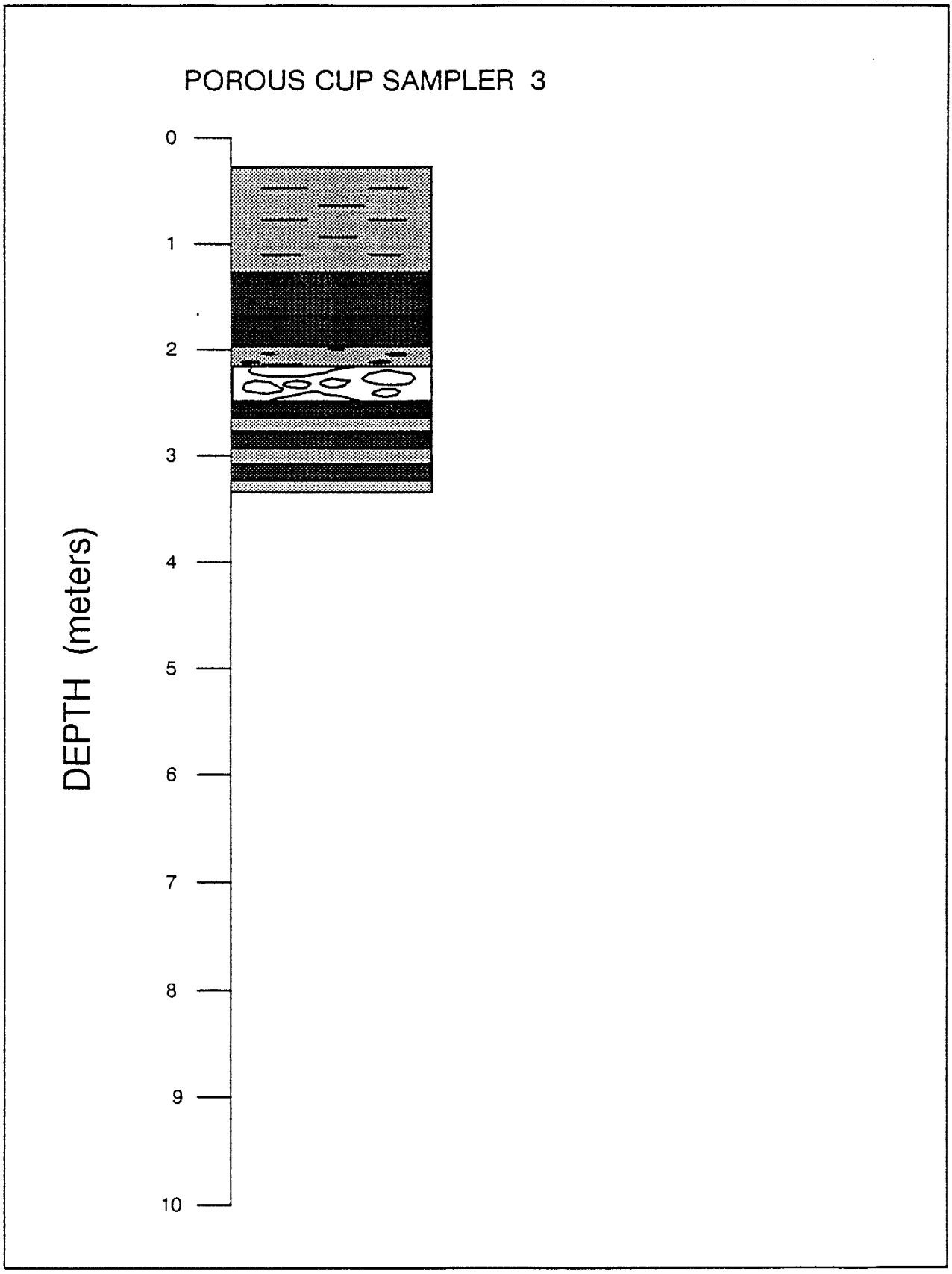
POROUS CUP SAMPLER 3
DEPTH (meters)
0
1
2
3
4
5
6
7
8
9
10

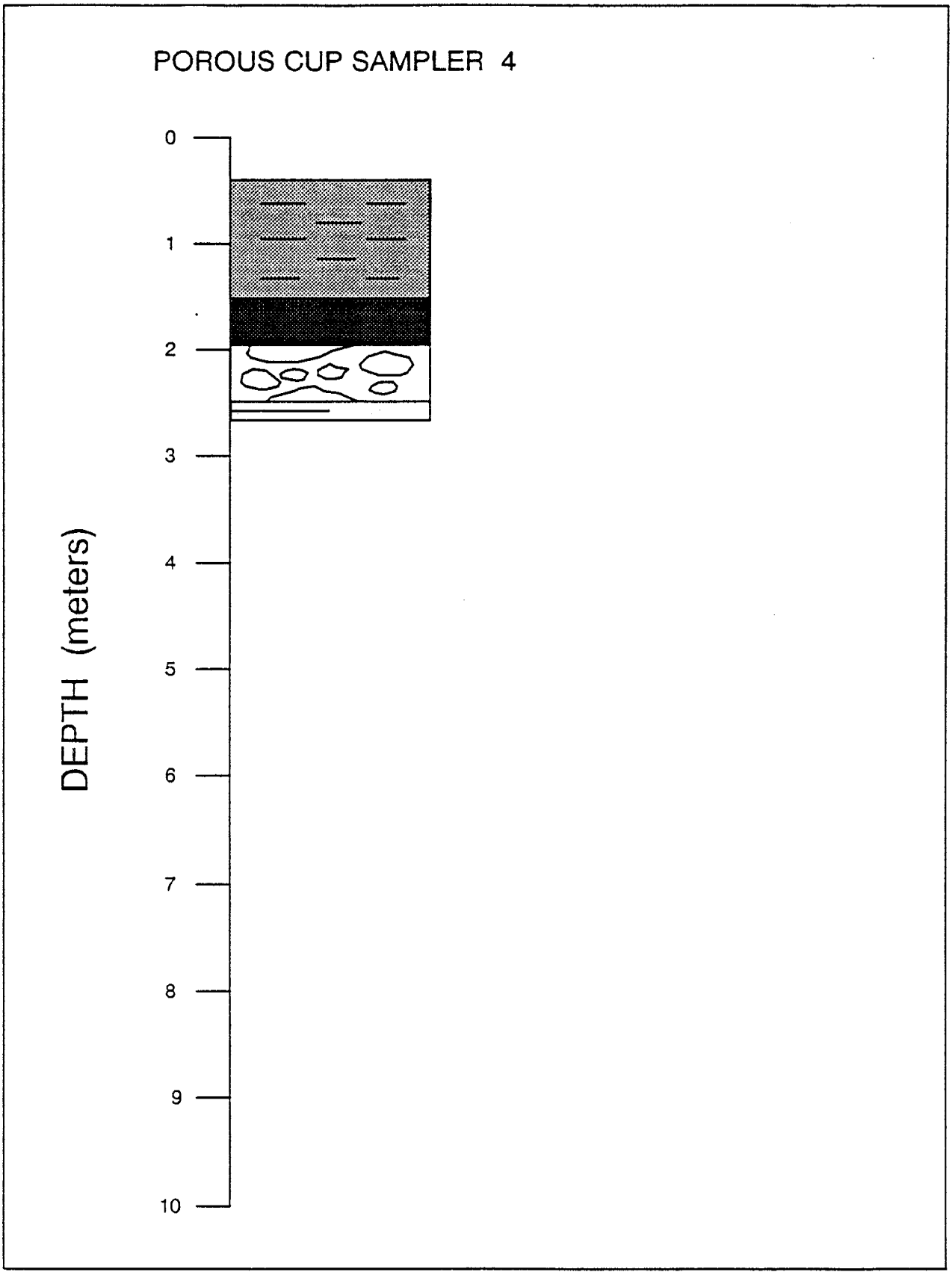
POROUS CUP SAMPLER 4
DEPTH (meters)
0
1
2
3
4
5
6
7
8
9
10

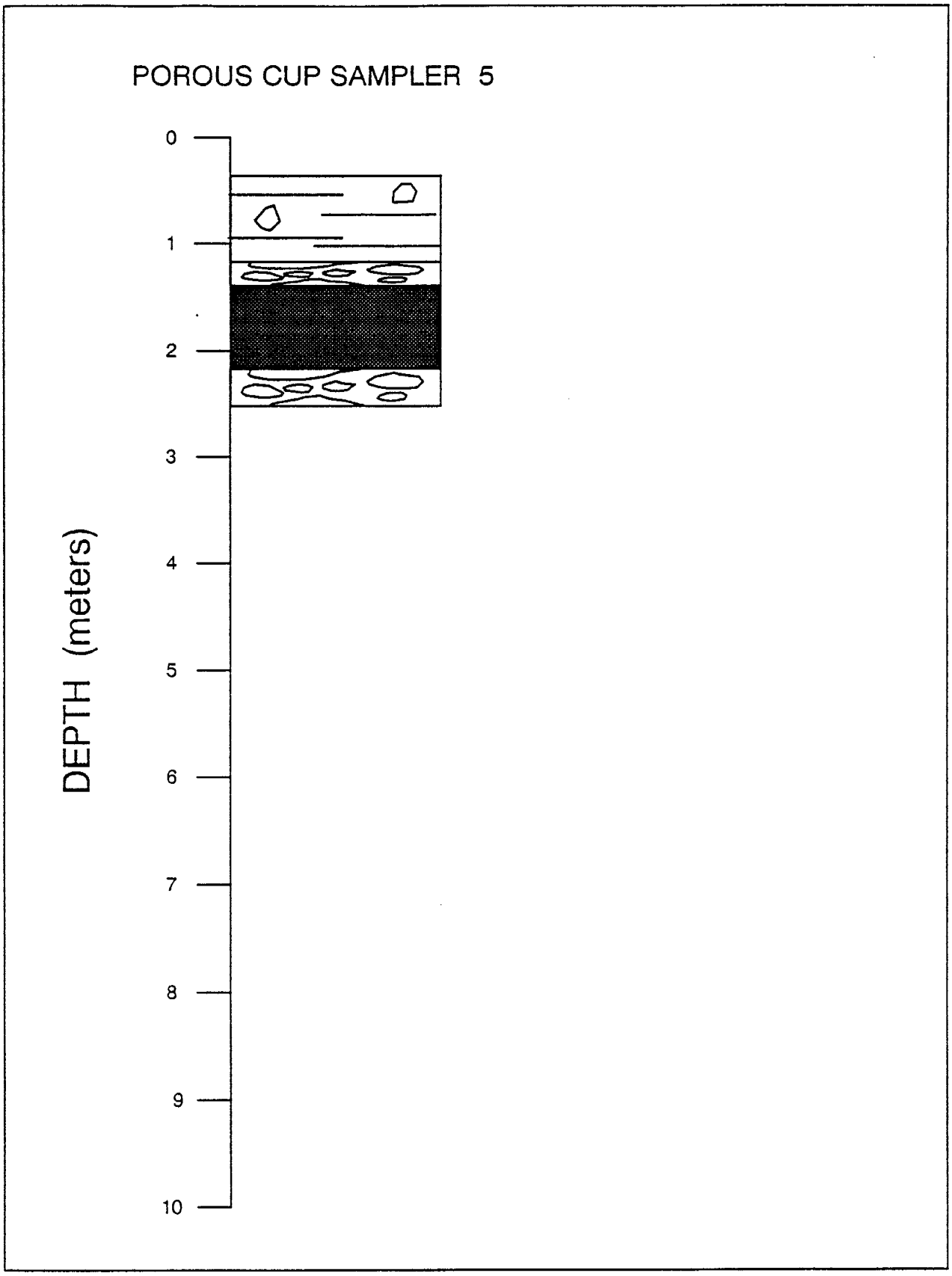
POROUS CUP SAMPLER 5
DEPTH (meters)
0
1
2
3
4
5
6
7
8
9
10

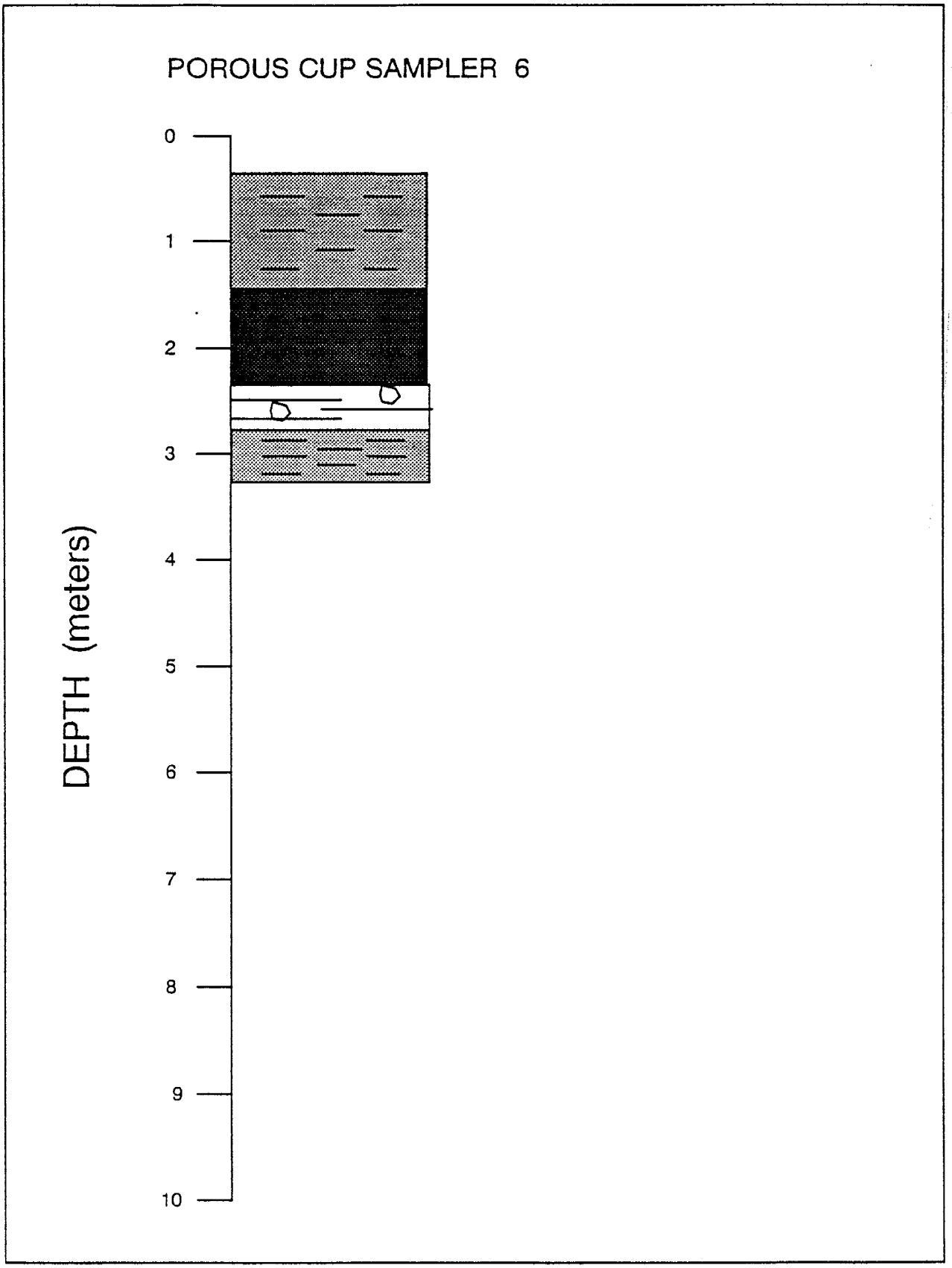
POROUS CUP SAMPLER 6
DEPTH (meters)
0
1
2
3
4
5
6
7
8
9
10

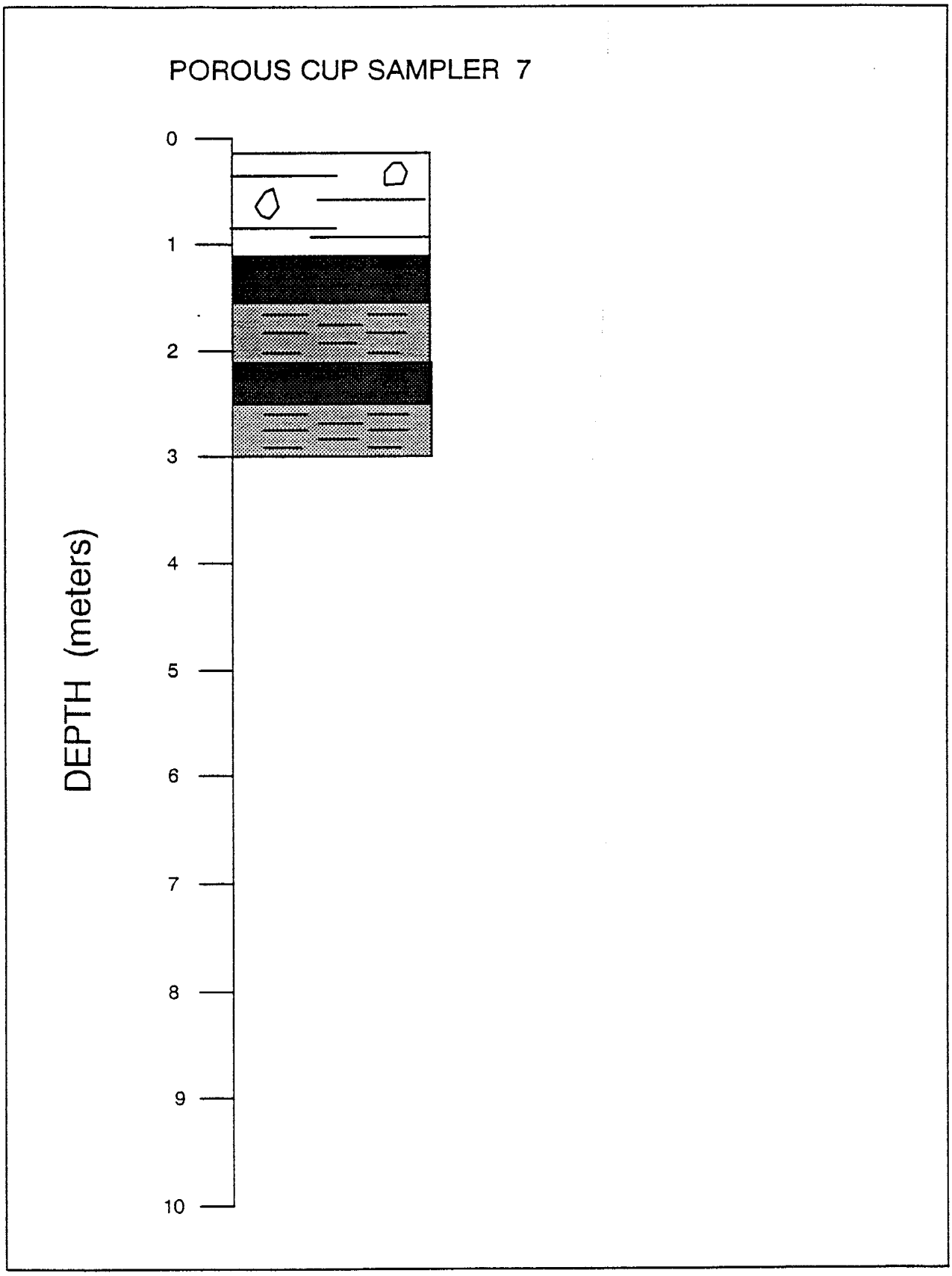
POROUS CUP SAMPLER 7
DEPTH (meters)
0
1
2
3
4
5
6
7
8
9
10

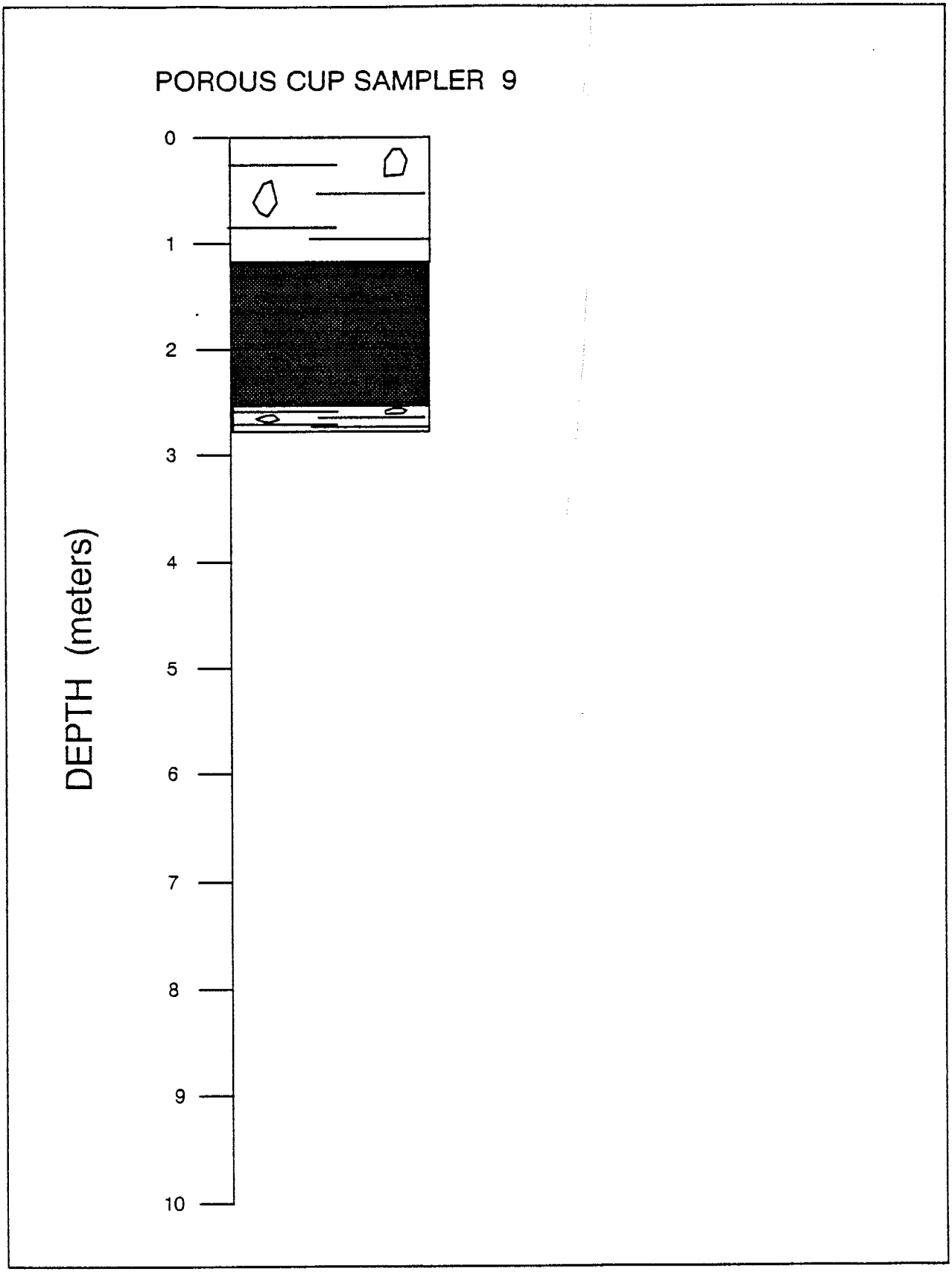
POROUS CUP SAMPLER 9
DEPTH (meters)
0
1
2
3
4
5
6
7
8
9
10

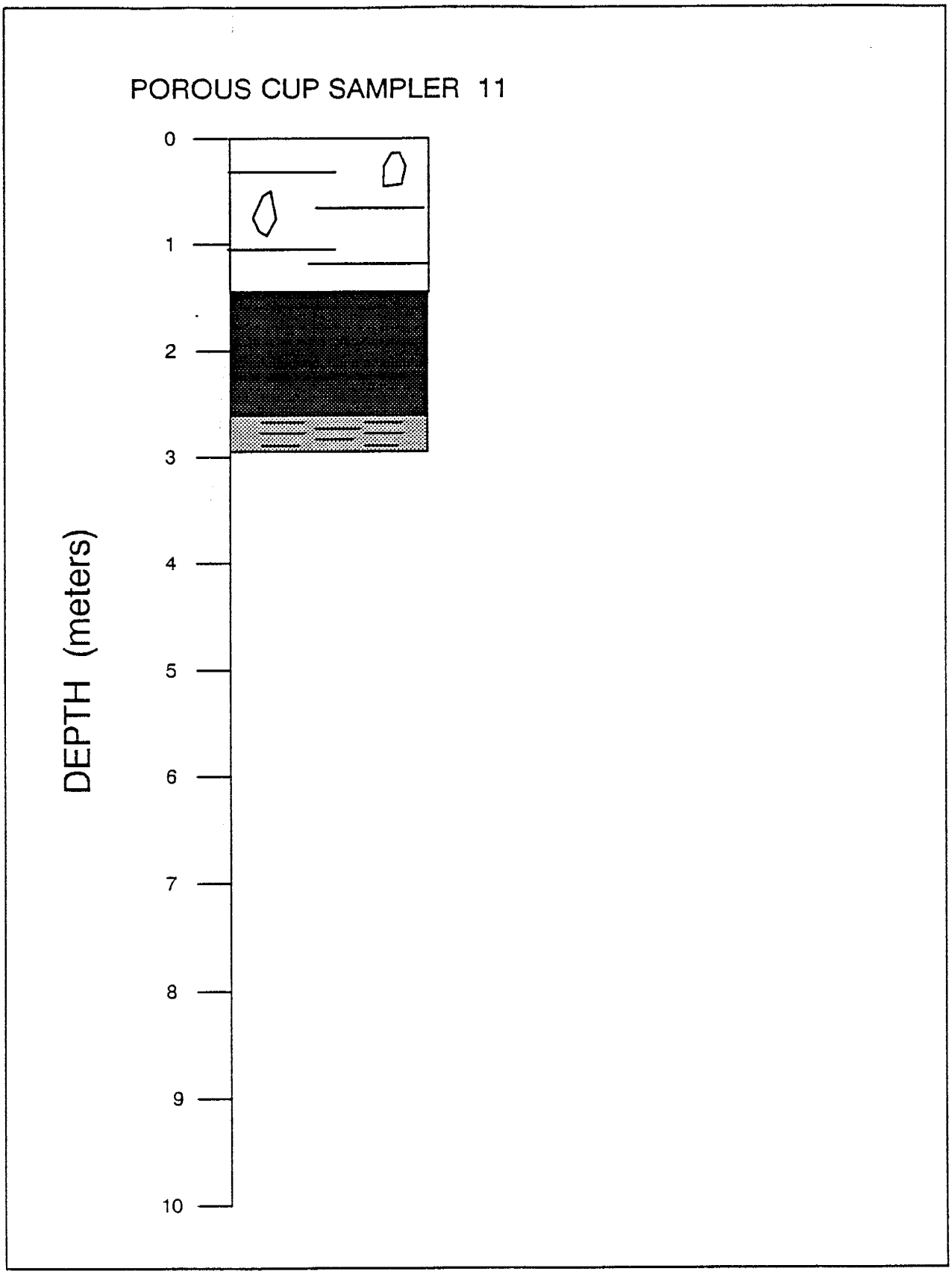
POROUS CUP SAMPLER 11
DEPTH (meters)
0
1
2
3
4
5
6
7
8
9
10

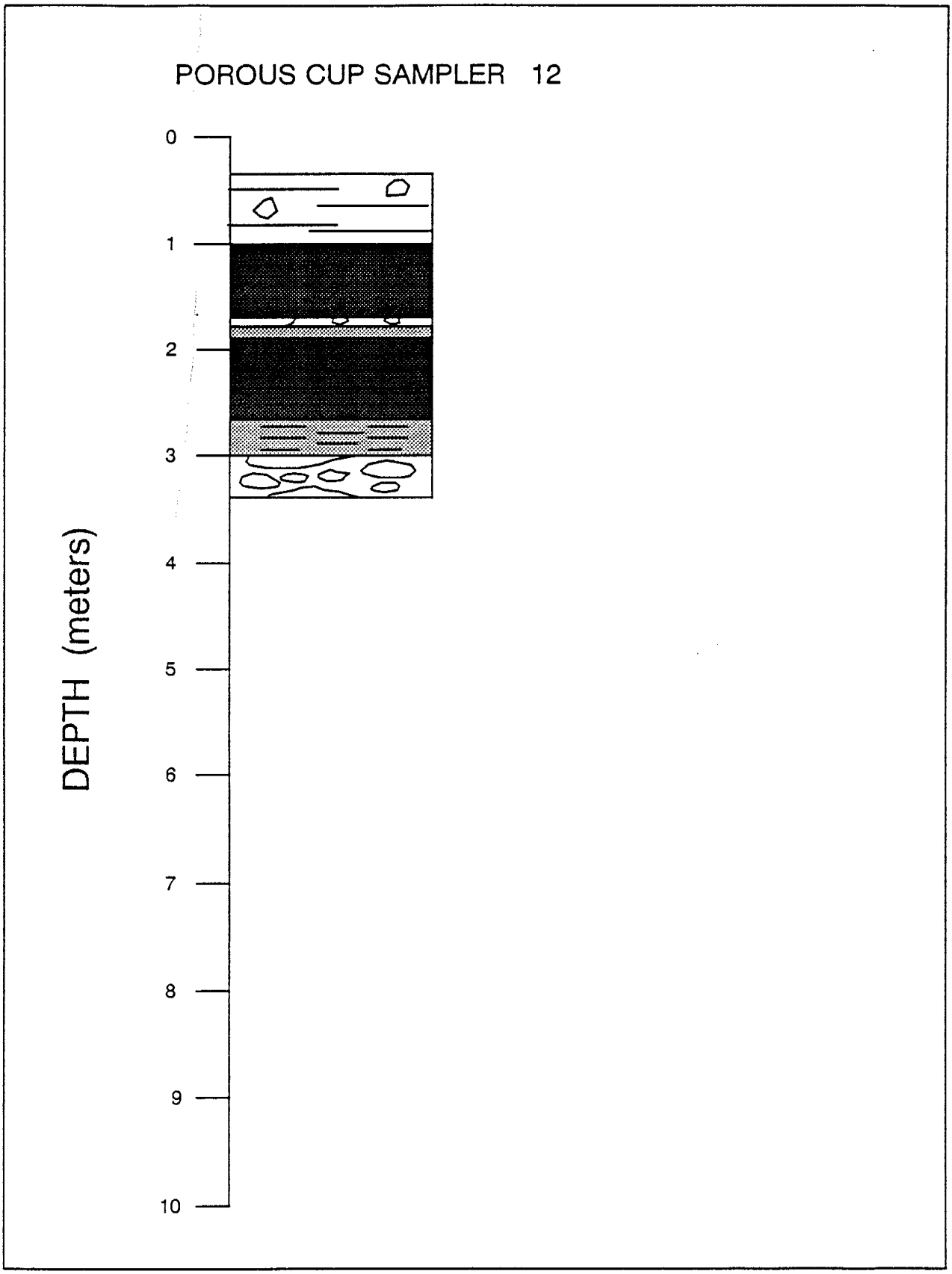
POROUS CUP SAMPLER 12
DEPTH (meters)
0
1
2
3
4
5
6
7
8
9
10

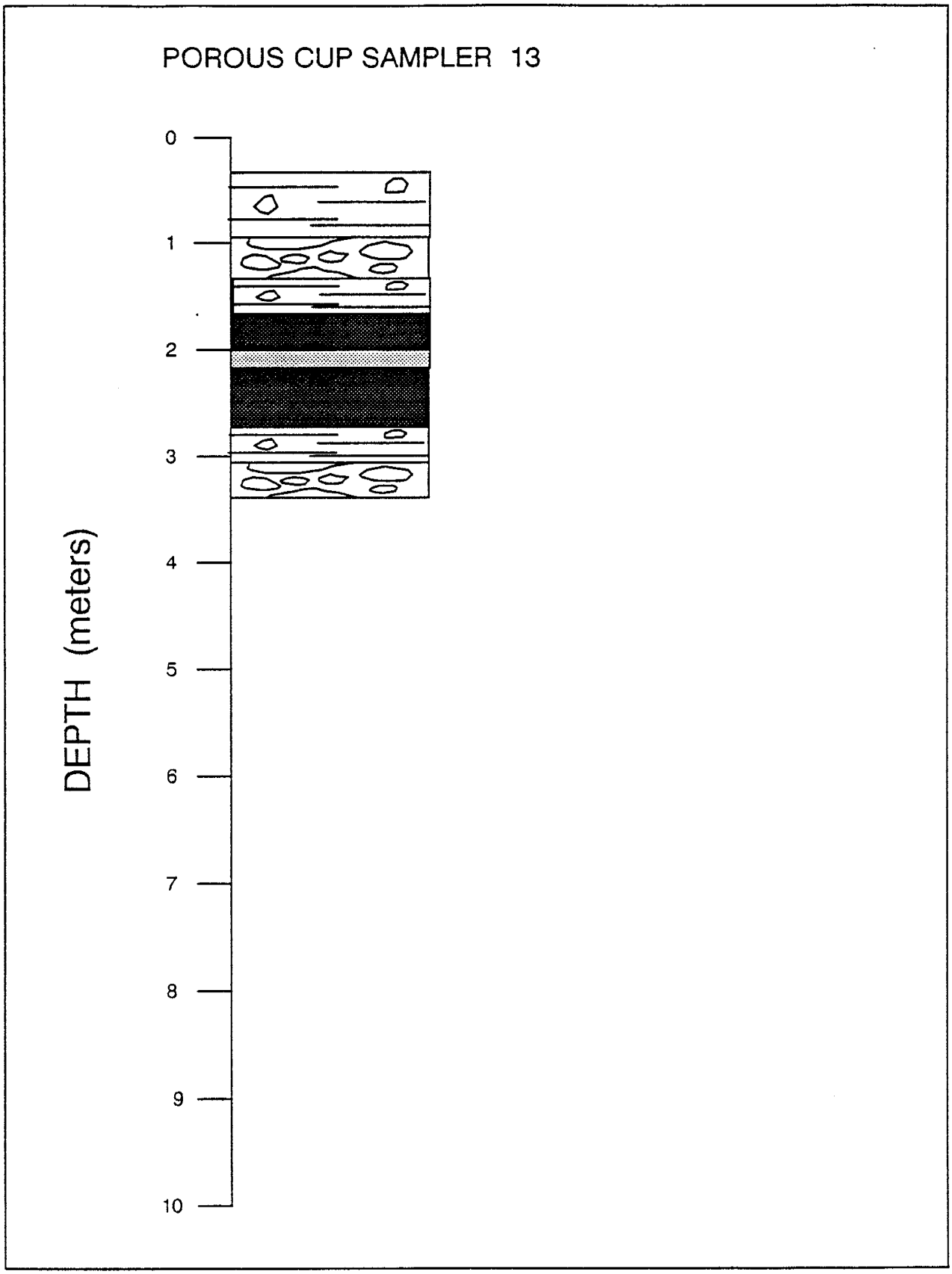
POROUS CUP SAMPLER 13
DEPTH (meters)
0
1
2
3
4
5
6
7
8
9
10

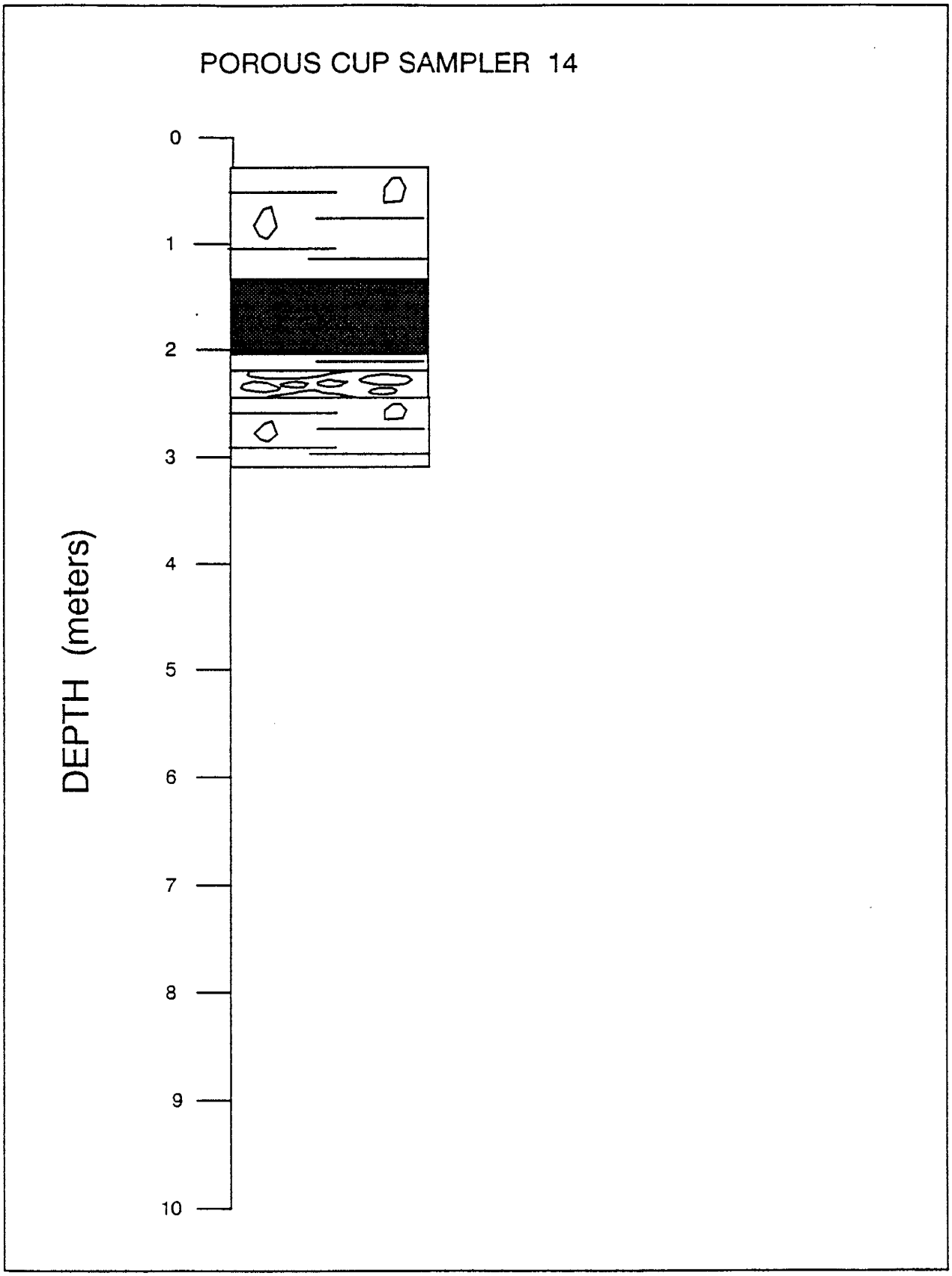
POROUS CUP SAMPLER 14
DEPTH (meters)
0
1
2
3
4
5
6
7
8
9
10

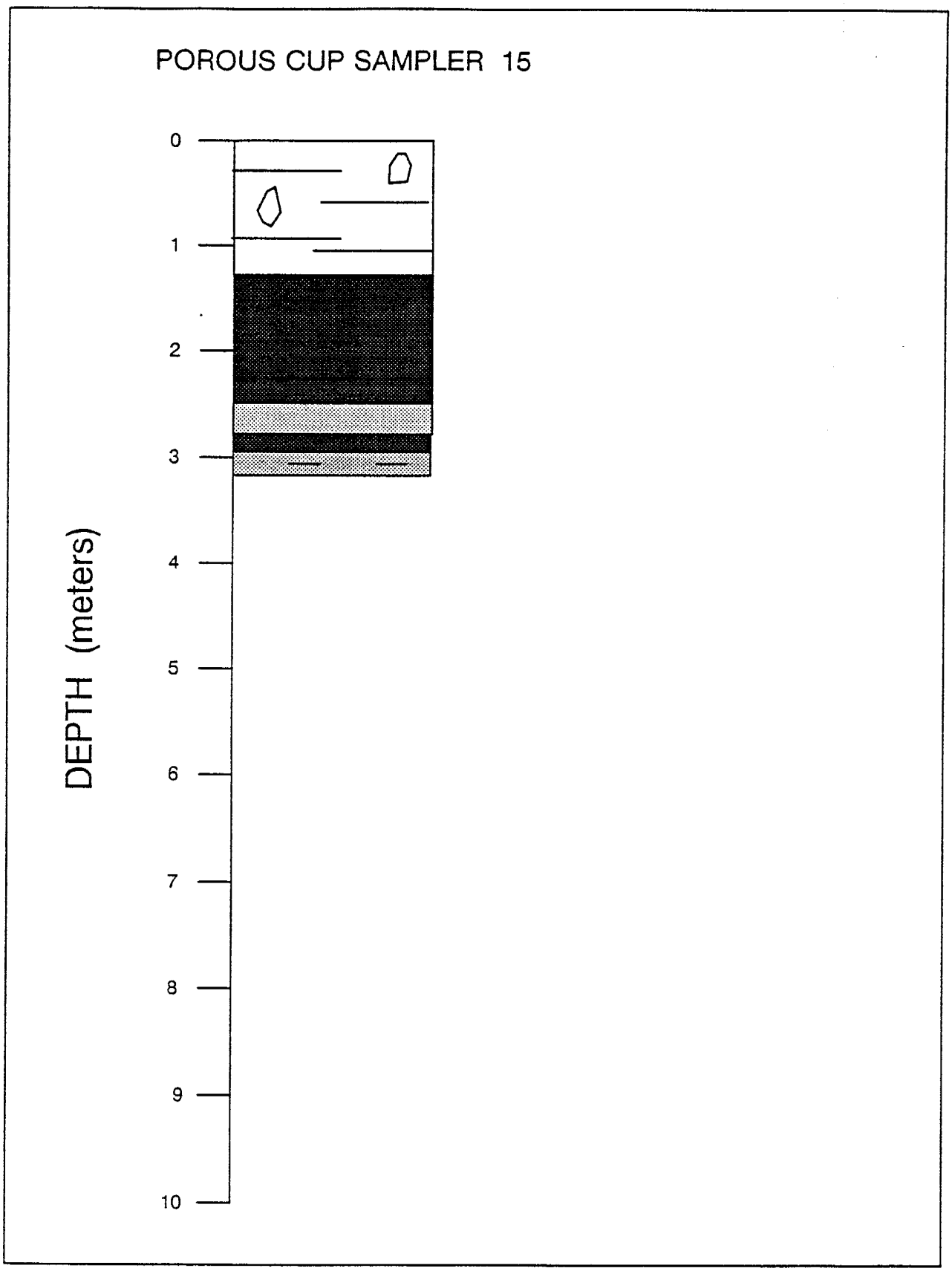
POROUS CUP SAMPLER 15
DEPTH (meters)
0
1
2
3
4
5
6
7
8
9
10

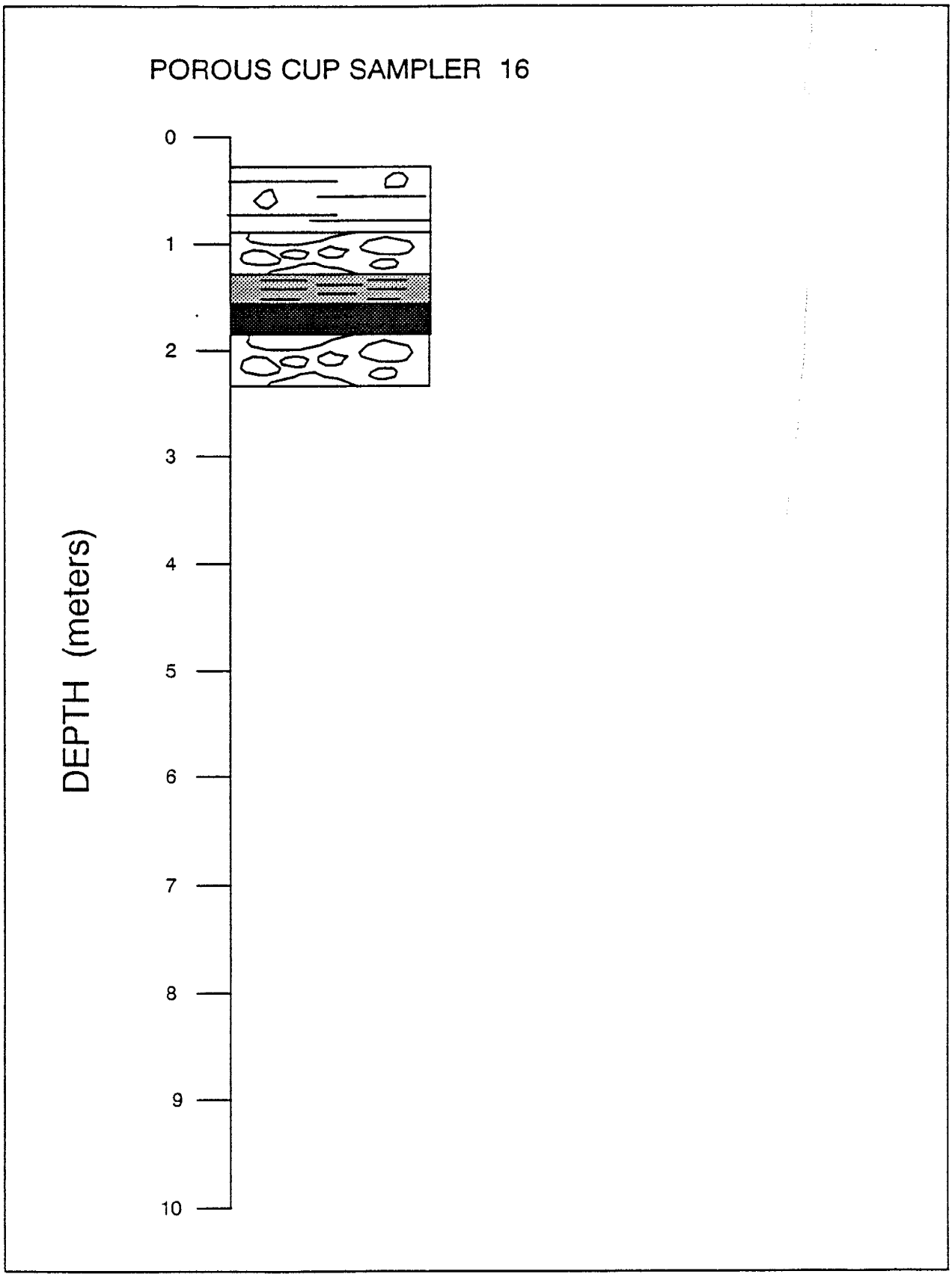
POROUS CUP SAMPLER 16
DEPTH (meters)
0
1
2
3
4
5
6
7
8
9
10

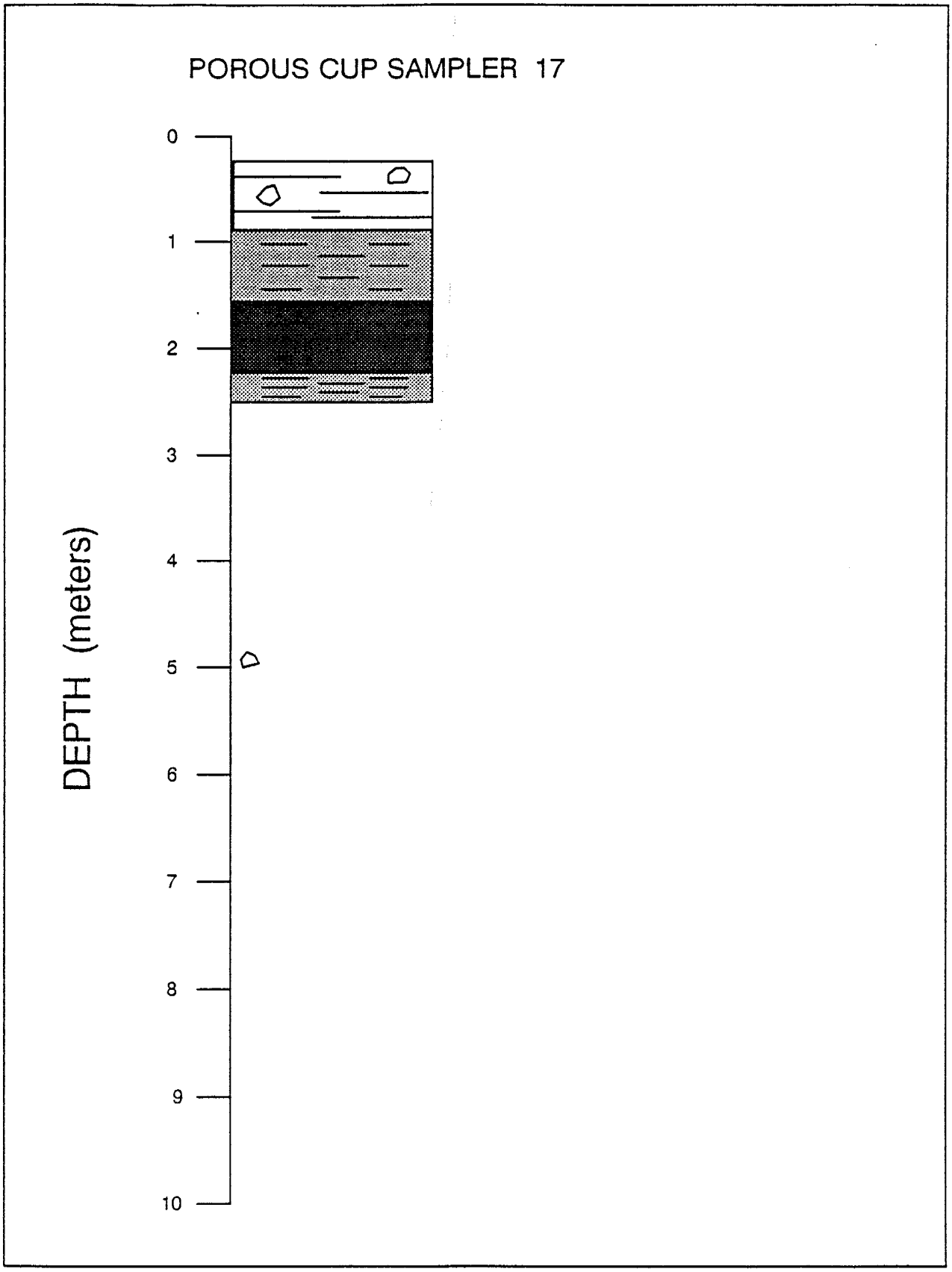
POROUS CUP SAMPLER 17
DEPTH (meters)
0
1
2
3
4
5
6
7
8
9
10

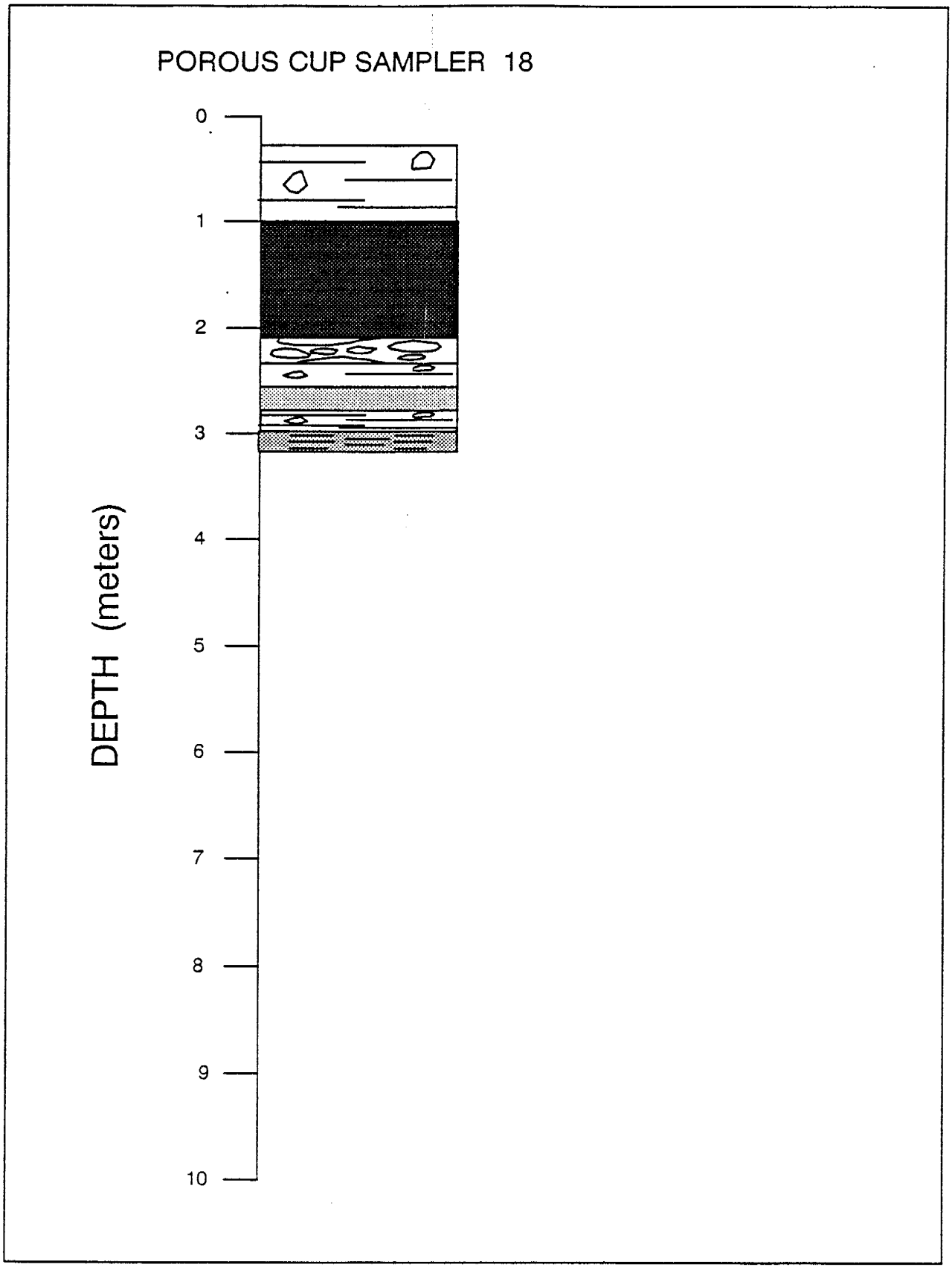
POROUS CUP SAMPLER 18
DEPTH (meters)
0
1
2
3
4
5
6
7
8
9
10

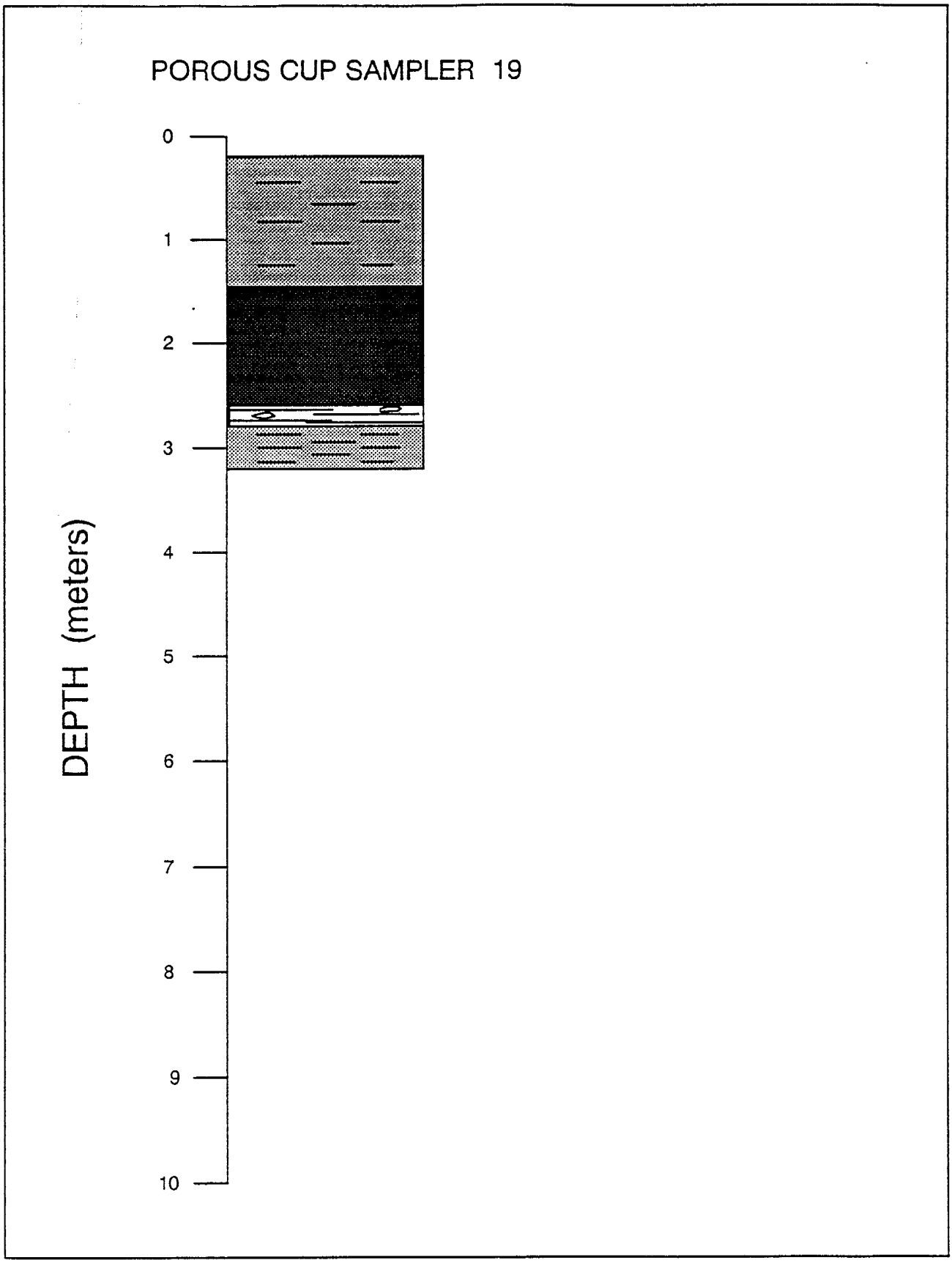
POROUS CUP SAMPLER 19
DEPTH (meters)
0
1
2
3
4
5
6
7
8
9
10

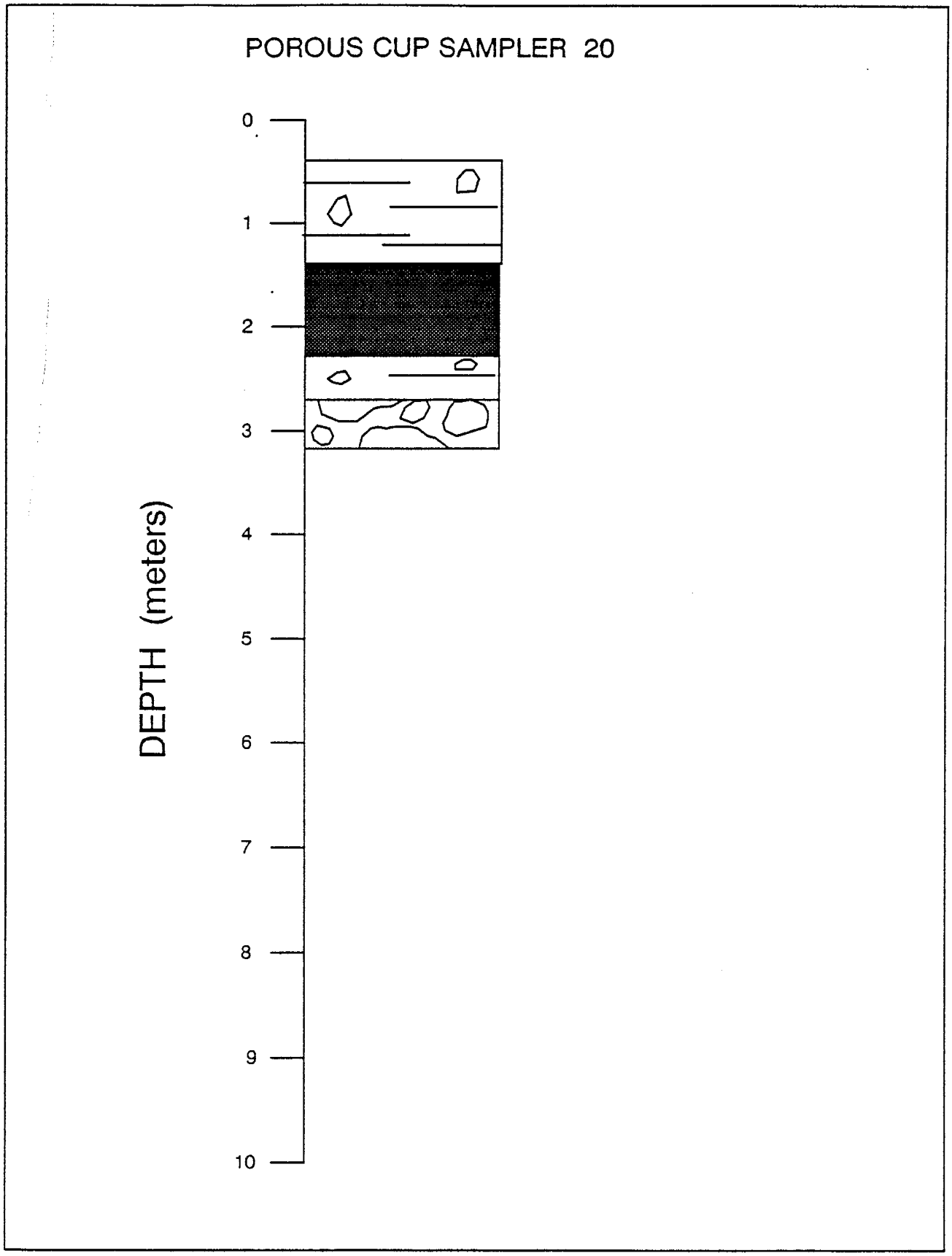
POROUS CUP SAMPLER 20
DEPTH (meters)
0
1
2
3
4
5
6
7
8
9
10

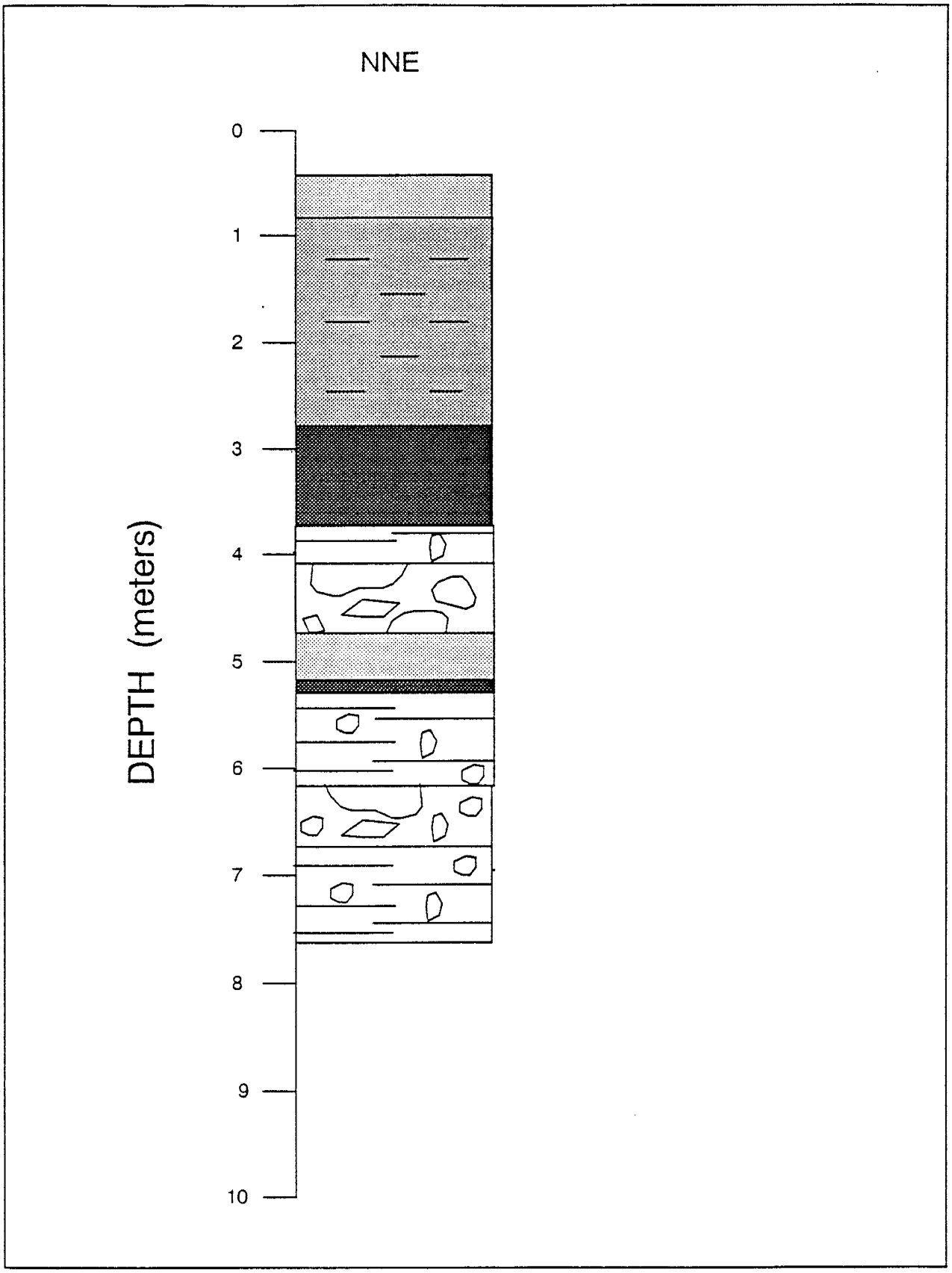
NNE
DEPTH (meters)
0
1
2
3
4
5
6
7
8
9
10

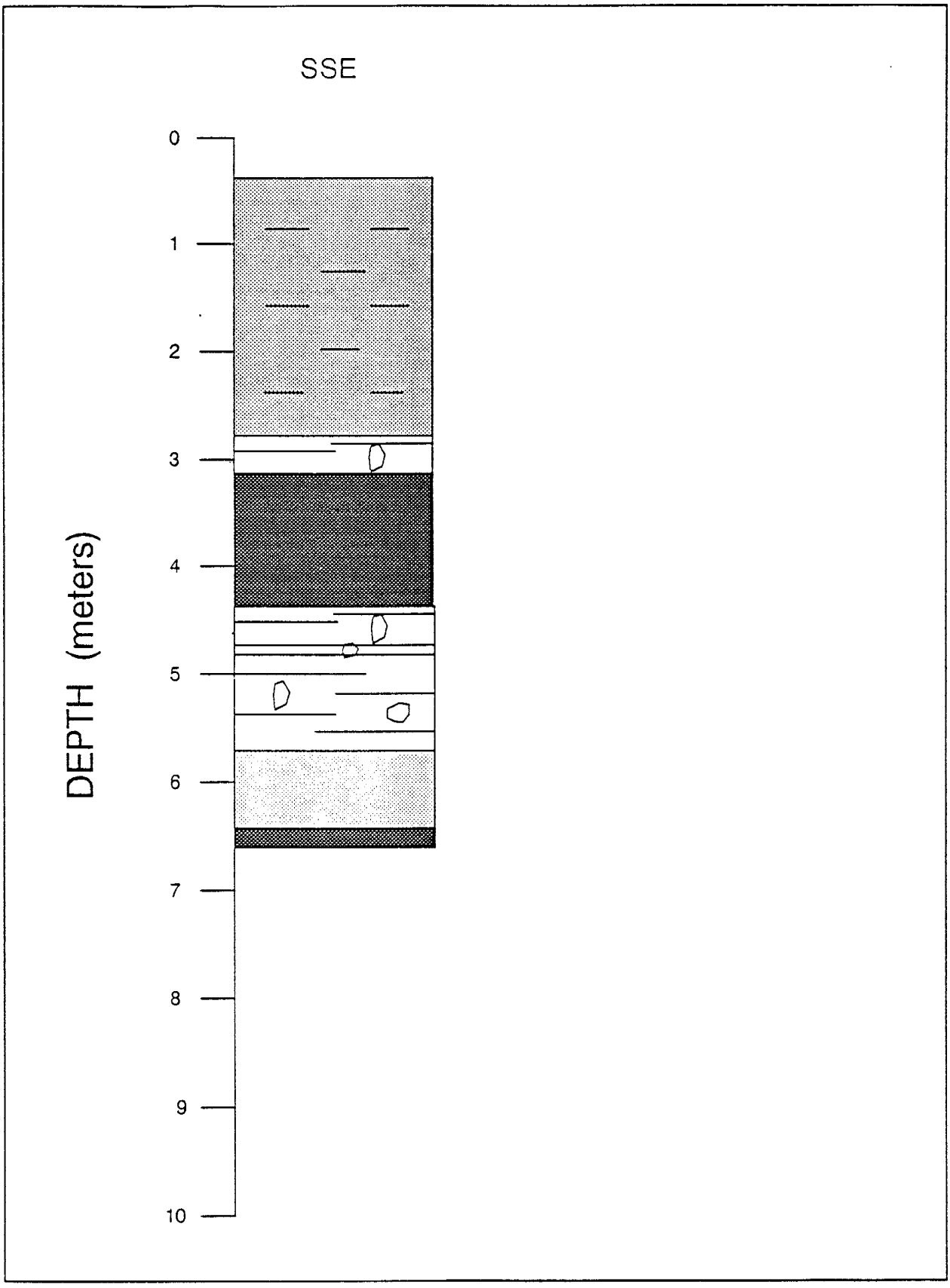
SSE
DEPTH (meters)
0
1
2
3
4
5
6
7
8
9
10

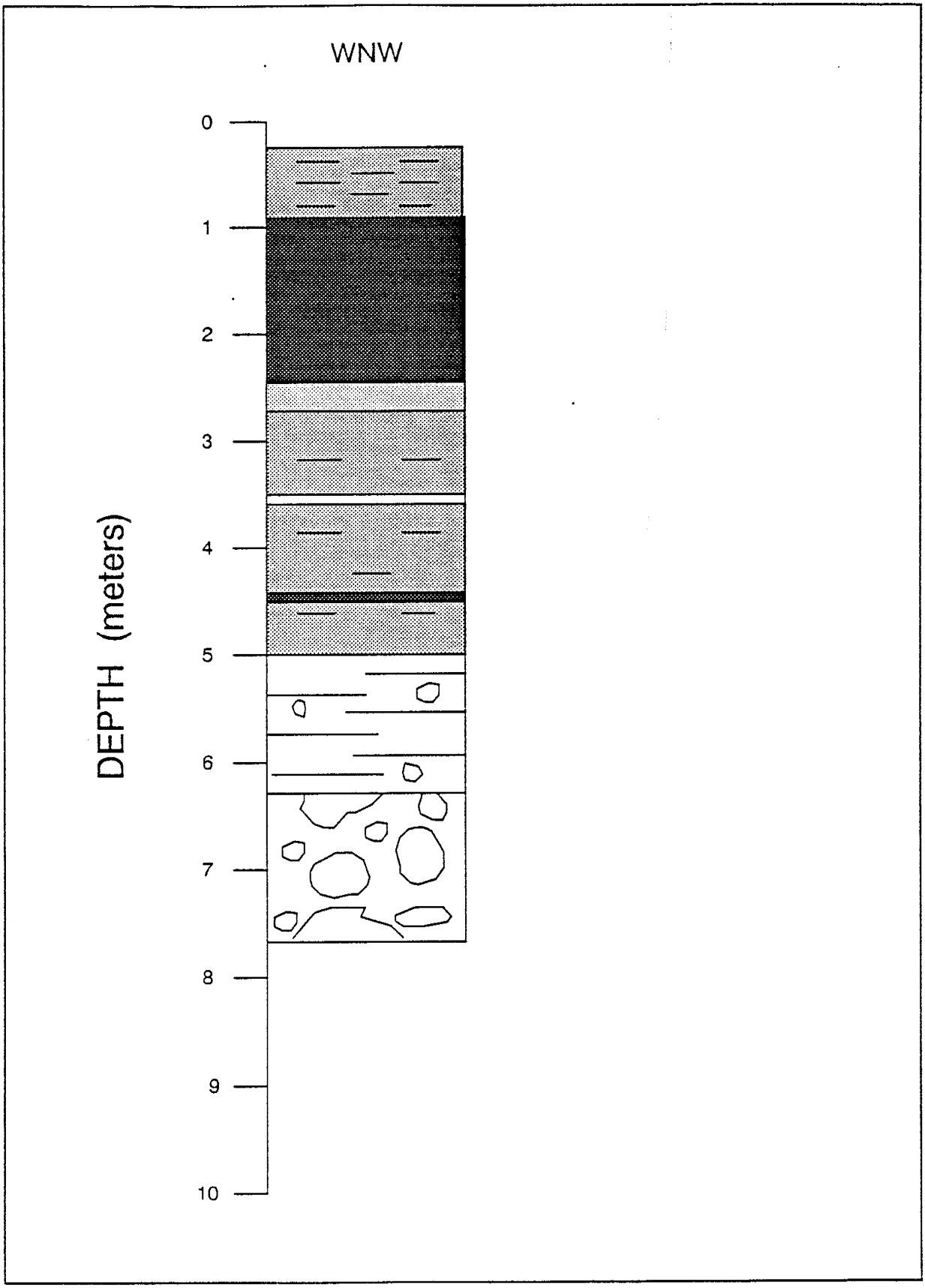
WNW
DEPTH (meters)
0
1
2
3
4
5
6
7
8
9
10

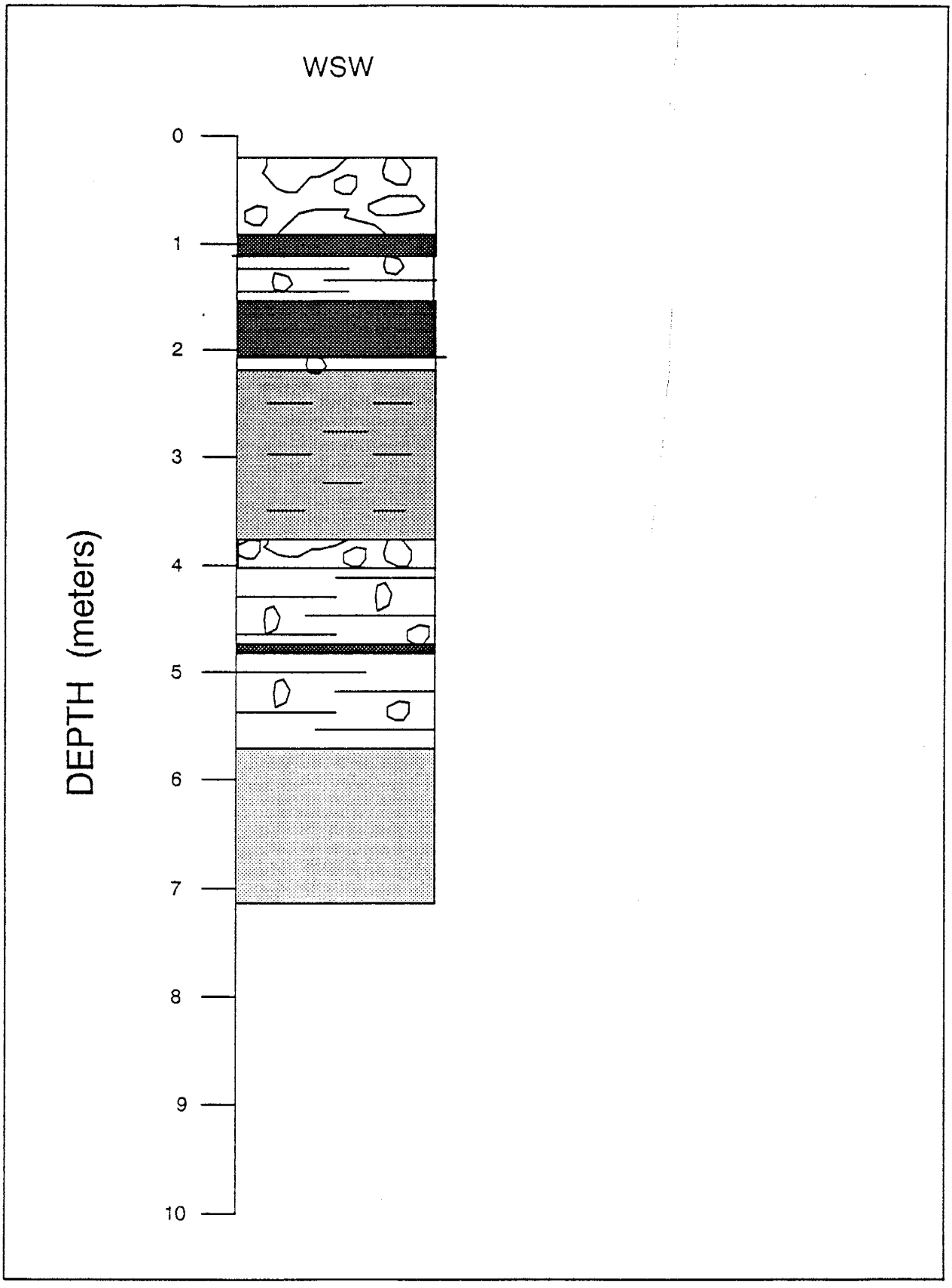
WSW
DEPTH (meters)
0
1
2
3
4
5
6
7
8
9
10

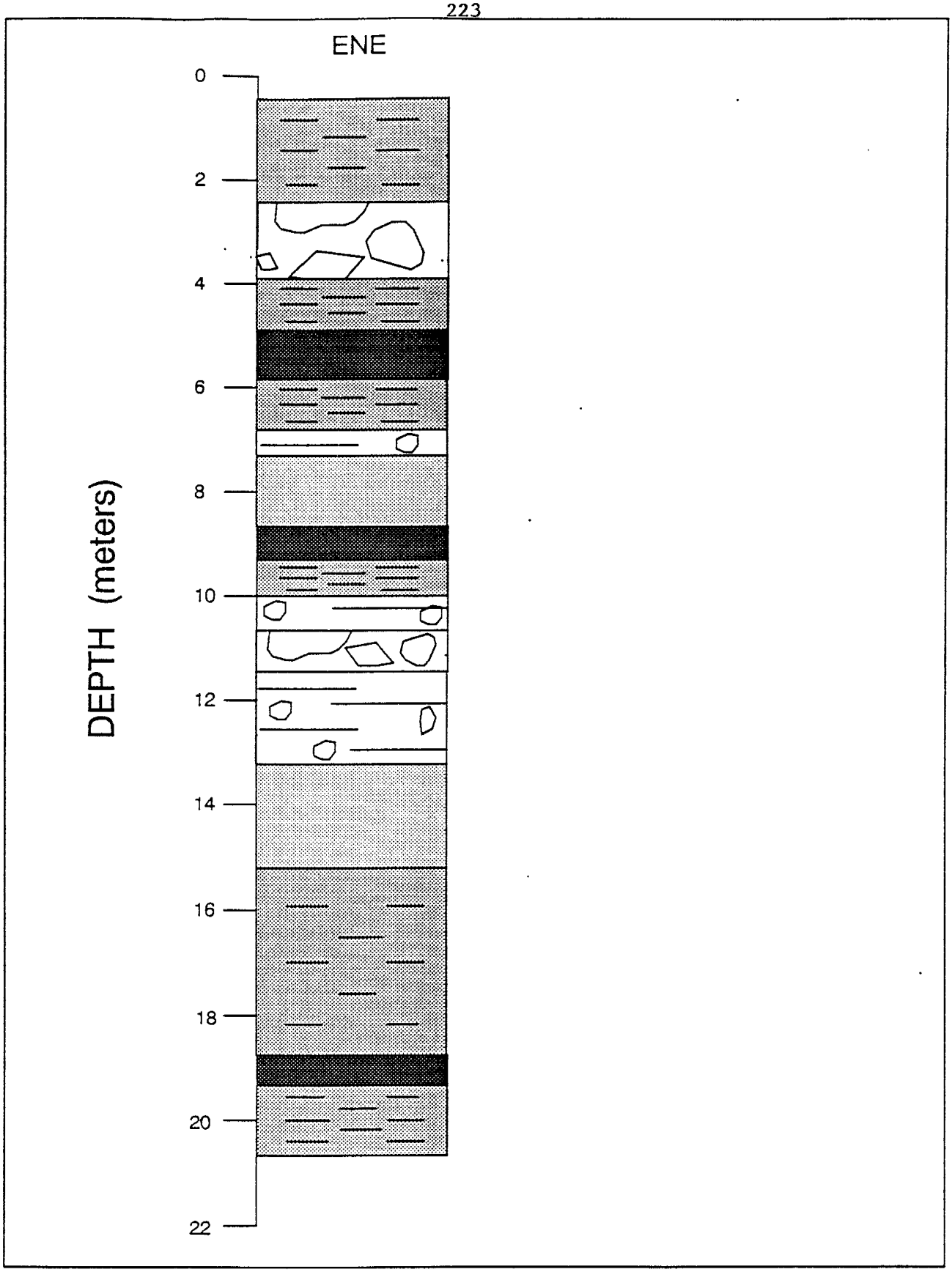
ENE
DEPTH (meters)
0
2
4
6
8
10
12
14
16
18
20
22

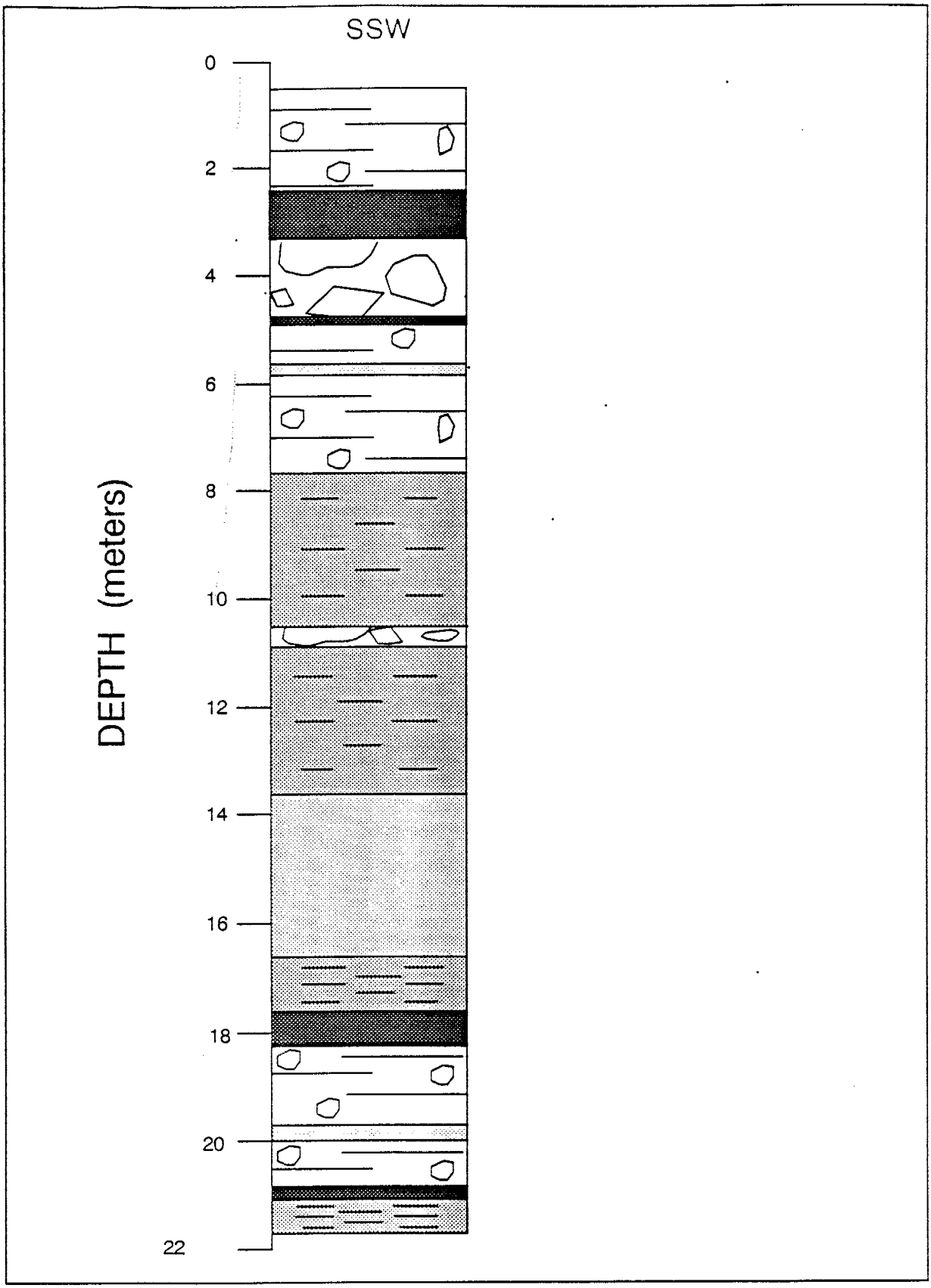
SSW
DEPTH (meters)
0
2
4
6
8
10
12
14
16
18
20
22

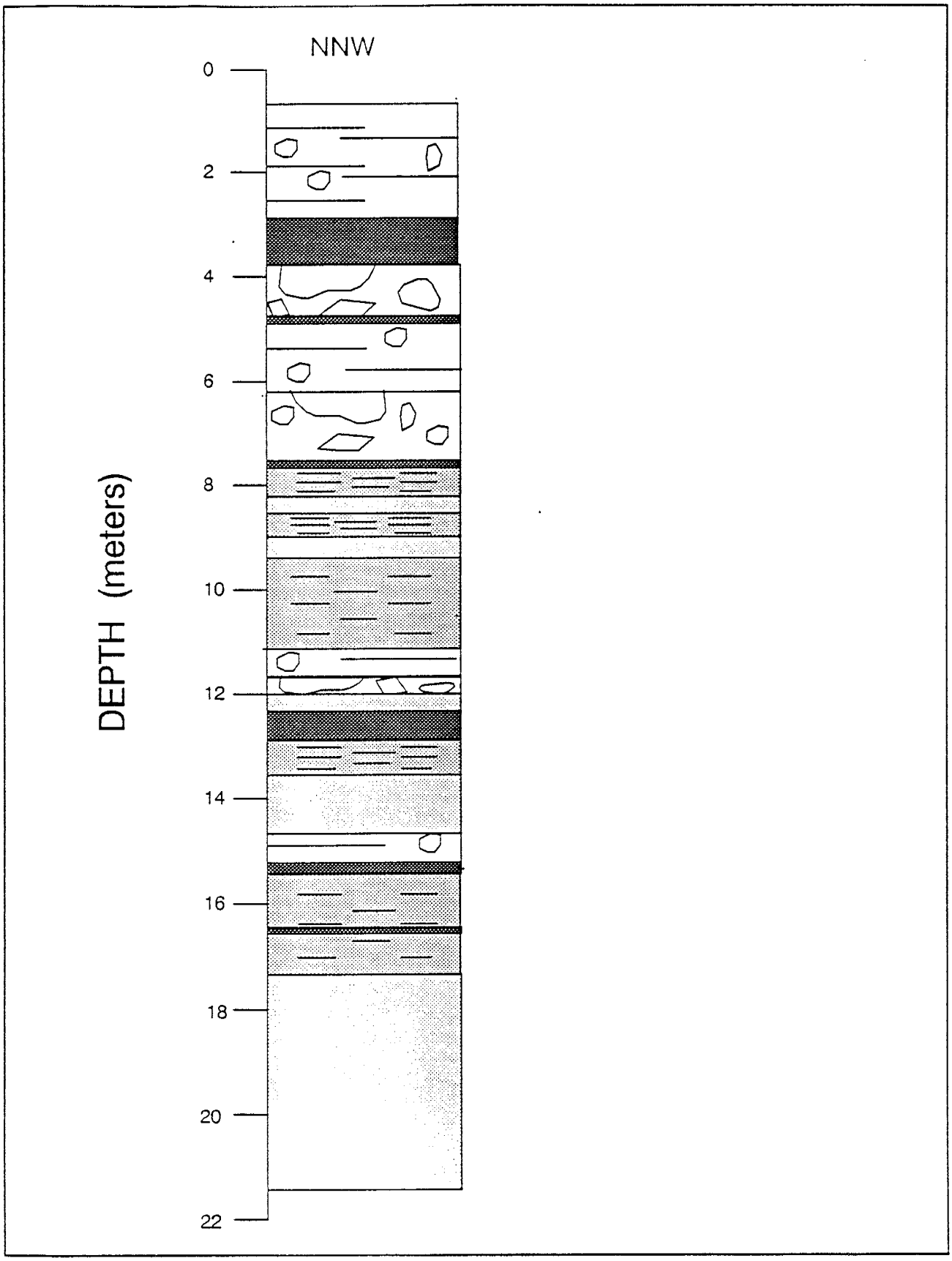
NNW
DEPTH (meters)
0
2
4
6
8
10
12
14
16
18
20
22

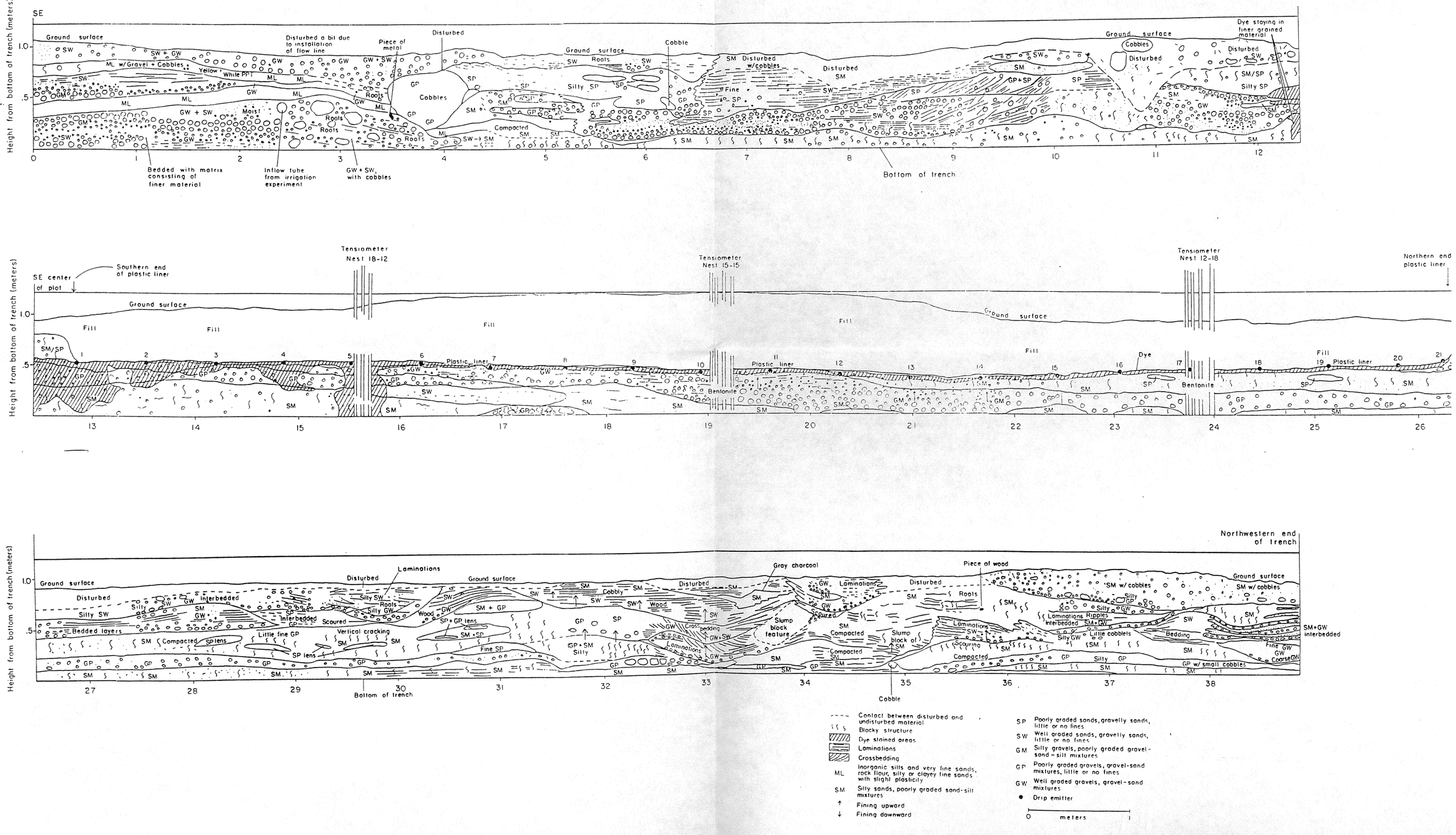
SE
Height from bottom of trench (meters)
1.0
.5
0
Ground surface
Disturbed a bit due to installation of flow line
Piece of metal
Disturbed
Cobble
Ground surface
Dye staying in finer grained material
Cobbles
Disturbed
Disturbed w/cobbles
Disturbed
Fine
Silty SP
Roots
Cobbles
Compacted
Mois!
Bedded with matrix consisting of finer material
Inflow tube from irrigation experiment
GW + SW, with cobbles
Bottom of trench
Southern end of plastic liner
SE center of plot
Tensiometer Nest 18-12
Tensiometer Nest 15-15
Tensiometer Nest 12-18
Northern end plastic liner
Fill
Plastic liner
Bentonite
Dye
Northwestern end of trench
Laminations
Gray charcoal
Piece of wood
Slump block feature
Slump block of
Cobble
Bedded layers
Compacted
Little fine GP
Vertical cracking
Scoured
Interbedded
Wood
Cross bedding
Bedding
Contact between disturbed and undisturbed material
Blocky structure
Dye stained areas
Laminations
Crossbedding
ML Inorganic silts and very fine sands, rock flour, silty or clayey fine sands with slight plasticity
SM Silty sands, poorly graded sand-silt mixtures
↑ Fining upward
↓ Fining downward
SP Poorly graded sands, gravelly sands, little or no fines
SW Well graded sands, gravelly sands, little or no fines
GM Silty gravels, poorly graded gravel-sand-silt mixtures
GP Poorly graded gravels, gravel-sand mixtures, little or no fines
GW Well graded gravels, gravel-sand mixtures
Drip emitter
0 meters 1